Setting the stage for lignin deposition: spatial distribution of enzymes directing lignification in *Arabidopsis thaliana*

by

Natalie Hoffmann

B.Sc., The University of Toronto, 2017

A THESIS SUBMITTED IN PARTIAL FULFILLMENT OF THE REQUIREMENTS FOR THE DEGREE OF

MASTER OF SCIENCE

in
The Faculty of Graduate and Postdoctoral Studies
(Botany)

THE UNIVERSITY OF BRITISH COLUMBIA
(Vancouver)
August 2019

The following individuals certify that they have read, and recommend to the Faculty of Graduate and Postdoctoral Studies for acceptance, a thesis entitled:

"Setting the stage for lignin deposition: spatial distribution and functional characterization of enzymes directing lignification in *Arabidopsis thaliana*"

---

submitted by Natalie Hoffmann in partial fulfillment of the requirements for

the degree of Master of Science

in Botany

Examining Committee:

Dr. Lacey Samuels

Supervisor

Dr. Shawn Mansfield

Supervisory Committee Member

Dr. Mathias Schuetz

Supervisory Committee Member

Dr. Harry Brumer

Additional Examiner

Abstract

Lignin is a critical phenolic polymer that reinforces secondary cell walls of plant cells. Lignin confers structural strength in fiber cells and enables water transportation in xylem vessel elements. Secreted enzymes, laccases (LACs) and peroxidases (PRXs), facilitate lignin polymerization by oxidizing lignin monomers called monolignols. In *Arabidopsis thaliana*, there are 17 LACs and 73 PRXs and the isoenzymes involved in lignification and their spatial distributions in plant tissues are poorly characterized. This study tested the hypotheses that LACs and PRXs occupy distinctive cell wall domains, and that the activity of these enzymes could enable deposition of lignin to different regions during development.

Putative lignin-associated LACs and PRXs, *AtLAC4*, *AtLAC10*, *AtLAC17*, *AtPRX42*, *AtPRX52*, *AtPRX71*, and *AtPRX72*, were identified using publicly-available mutant and bioinformatics data. Enzymes were fluorescently tagged with an mCherry label and co-localized with lignin, visible as UV autofluorescence. AtLAC4, AtLAC17, and AtPRX72 localized to xylan-rich secondary cell walls of xylem vessel elements and fibers while AtLAC4, AtPRX64, AtPRX71, and AtLAC10 localized to the pectin-rich middle lamella in fibers. AtLAC10, AtPRX42, AtPRX52, and AtPRX71 localized to non-lignified tissues.

Enzyme localization may be due to a combination of mobility in the cell wall and timing of expression. Expressing fluorescently-tagged *AtLAC4*, *AtLAC17*, and *AtPRX64* under the promoter of the secondary cell wall-specific gene *AtCESA7* resulted in similar cell wall localization patterns for all three enzymes in roots, indicating that changing the timing of expression was sufficient to alter localization. However, transgenes were transcriptionally silenced in stem tissue.

Stem histochemistry demonstrated that both LAC and PRX oxidative activity was restricted to lignifying cells throughout development. Production of apoplastic reactive oxygen species, such as H_2O_2 for PRX activity, was also found exclusively in lignifying tissue and differed temporally between lignified cell types. Taken together, these results indicate that characteristic sets of oxidative enzymes localize to specific cell types and regions of the lignified cell wall. The location of oxidative enzymes and production of oxidative substrates, such as H_2O_2, could ultimately dictate lignin deposition spatially and temporally throughout stem growth.

Lay summary

Wood, primarily composed of cellulose- and lignin-rich secondary walls, is a near-ubiquitous material in building, pulping, and paper industries and is a promising source of biofuel. Lignin is polymerized in secondary walls by secreted oxidative enzymes called laccases and peroxidases. I tested the hypothesis that laccases and peroxidases have unique distributions in secondary walls, which could control where lignin is deposited. I compared the localization of eight fluorescently-tagged laccases and peroxidases in the flowering stem of *Arabidopsis thaliana* to the presence of lignin. Each enzyme showed a specific distribution in different cell types and regions of the cell wall throughout plant growth. Six enzymes localized to lignified cell walls and thus may be involved in lignification, while other enzymes may be involved in diverse biological processes. Mapping the localization of these enzymes provides insight into how plants control lignification and could aid in optimizing woody tissue for industrial use.

Preface

prLAC4::LAC4-mCherry, *prLAC17::LAC17-mCherry*, *prUBQ10::LAC4-mCherry* and *prUBQ10::sec-mCherry* seeds were provided by Dr. Mathias Schuetz and Eva Chou (Chou et al., 2018; Schuetz et al., 2014). *prPRX64::PRX64-mCherry* seeds (Lee et al., 2013) were provided by Dr. Niko Geldner (University of Lausanne, Switzerland). The double *lac4-2/lac17* mutants (Berthet et al., 2011) were provided from Dr. Richard Sibout (French National Institute for Agricultural Research, France) and *prx64* null mutants (SALK_203548) were provided from Dr. Qiao Zhao (Tsinghua University, China).

For chapter 3, I was responsible for cloning and imaging *prLAC10::LAC10-mCherry, prPRX42::PRX42-mCherry*, *prPRX52::prPRX52-mCherry*, *prPRX71::PRX71-mCherry*, *prPRX72::PRX72-mCherry*, *prCESA7::LAC4-mCherry*, *prCESA7::LAC17-mCherry*, and *prCESA7::PRX64-mCherry* plants. I also imaged existing *prLAC4::LAC4-mCherry*, *prLAC17::LAC17-mCherry*, *prPRX64::PRX64-mCherry*, *prUBQ10::LAC4-mCherry*, and *prUBQ10::sec-mCherry* plant lines (Chou et al., 2018; Lee et al., 2013; Schuetz et al., 2014). I was responsible for examination of publicly-available bioinformatics data, quantitative analyses and statistics involved in functional characterization of *prx64* null plants, and RT-qPCR expression analyses.

For chapter 4, I was responsible for all imaging, immunolabeling, fluorescence intensity quantification, H_2O_2 quantification, and statistics.

Table of Contents

List of Tables

List of Figures

List of Abbreviations

Arabidopsis – *Arabidopsis thaliana*

CESAs – cellulose synthase

Col-0 – Columbia-0

DAF – 2,7-diaminofluorene

DPI – diphenyleneiodonium chloride

ER – Endoplasmic reticulum

FRAP – fluorescence recovery after photobleaching

G-unit – guaiacyl lignin subunit

HRP – horseradish peroxidase

H-unit – *p*-hydroxyphenyl lignin subunit

H_2DCF – 2',7'-dichlorodihydrofluorescein diacetate

H_2O_2 – hydrogen peroxide

LAC – laccase

miRNA – microRNA

n.d. – no data

n.s. – not significant

$^1O_2$ – singlet oxygen

O_2^- – superoxide anion

OH· – hydroxy radical

PCW – primary cell wall

PI – propidium iodide

PM – plasma membrane

prCESA7 – promoter sequence of *AtCESA7*

PRX – peroxidase

RBOH – respiratory burst oxidase homolog

ROS – reactive oxygen species

RT-qPCR – real-time quantitative polymerase chain reaction

SCW – secondary cell wall

SD – standard deviation

SE – standard error

SHAM – salicylhydroxamic acid

SOD – superoxide dismutase

S-unit – syringyl lignin subunit

TMB – 3,3’,5,5’-tetramethylbenzidine

UV – ultraviolet

Acknowledgements

I would like to sincerely thank my supervisor, Dr. Lacey Samuels, for her mentorship during the past two years - I have learned so much and will always remember my time at UBC fondly. I would also like to thank my supervisory committee members, Dr. Mathias Schuetz and Dr. Shawn Mansfield, for their guidance and advice.

I am very grateful for the help and encouragement from the members of the Samuels lab, both past and present. Additionally, I would like to thank my colleagues in the UBC Botany and Forestry departments, including Laryssa Halat, Yaseen Mottiar, and Kresimir Sola, for their technical and moral support throughout this project.

Finally, I would like to thank the UBC Bioimaging Facility for their assistance and training on the electron and confocal microscopes. Funding for this work was provided from NSERC and UBC Affiliated Fellowship scholarships.

Chapter 1: Introduction

1.1 Overview

Lignin is a critical phenolic biopolymer deposited in secondary cell walls of plant cells that provides strength for plants to grow upright and rigidity to withstand negative pressure from water transport. Wood, which is composed primarily of secondary cell walls, is an economically-important material in the pulping and paper and biofuel industries. In addition, lignin itself is recognized as a valuable potential source of bioproducts. A thorough understanding of lignin biosynthesis and deposition in secondary cell walls is therefore of importance, both for its role in plant development and for economic purposes. Nevertheless, the mechanisms by which plant cells deposit lignin in secondary cell walls during development remain elusive.

The final stage of lignin polymerization in secondary cell walls requires oxidation of lignin monomers by secreted enzymes, laccases and peroxidases. Identifying the roles of specific oxidative enzymes in lignification has been hindered by the large gene families of these enzymes and potential functional redundancy. In *Arabidopsis thaliana* (Arabidopsis), there are 17 laccases and 73 peroxidases, and a comprehensive analysis of these gene families has not been performed. The aim of this project is to elucidate the tissue and cellular distribution of oxidative enzymes with putative roles in lignification in Arabidopsis. Using a combination of molecular biology, confocal microscopy, immunolocalizations and histochemical staining, I will test the hypothesis that laccases and peroxidases occupy distinct cell wall domains throughout development of the lignified inflorescence stem and that this spatial separation may reflect non-redundant functional roles. The results of this study can ultimately be used to determine which laccases and peroxidases are important for lignification in Arabidopsis and uncover mechanisms involved in lignin deposition of secondary cell walls throughout development.

1.2 Plant cell walls

Plant cells are surrounded by an extracellular cell wall, which provides mechanical strength and structure (Keegstra, 2010). Cell walls are involved in critical processes such as cell-to-cell

adhesion, growth, defense against pathogens, and communication (Lampugnani et al., 2018). In addition, the composition of the cell wall matrix varies between tissues and developmental stages, which allows different cell types to perform specialized functions (Burton et al., 2010).

1.2.1 Primary and secondary cell walls

All plant cells are surrounded by a primary cell wall (PCW), which is laid down following initial cell division early in development (Keegstra, 2010). Between adjacent PCWs is a region called the middle lamella, which is essential for cell adhesion and structural support during growth (Zamil & Geitmann, 2017). PCWs consist predominantly of the polysaccharides cellulose, hemicellulose, and pectin, as well as structural proteins. PCWs undergo continual remodelling during development, which facilitates cell communication and growth through cell expansion (Keegstra, 2010). Consequently, the structure of the PCW needs to provide sufficient mechanical support yet be adaptable to undergo morphogenesis and respond to environmental stresses.

In contrast, secondary cell walls (SCWs) are laid down following cessation of growth, and mainly consist of cellulose, hemicellulose, and the phenolic polymer lignin (Růžička et al., 2015). The evolution of SCWs was essential for colonization of land, enabling efficient water transportation and providing structural strength for terrestrial plants to grow upright (Weng & Chapple, 2010; Zhong & Ye, 2015). SCWs are deposited adjacent to the plasma membrane (PM) within the PCW and provide extra support for a cell's specialized function (Zhong & Ye, 2015).

1.2.2 Cell wall polymers: Cellulose, hemicellulose, pectin, and lignin

Both PCWs and SCWs consist predominantly of cellulose, a linear chain of β-1,4-glucans (Somerville, 2006). Cellulose chains form numerous non-covalent interactions through inter- and intramolecular hydrogen bonding and thus contribute to a complex cellulose network within the cell wall (Nishiyama, 2009). Cellulose microfibrils are synthesized by PM-bound cellulose synthase enzymes (CESAs), which form multi-protein complexes called cellulose synthase complexes (CSCs; McFarlane et al., 2014). Different CESAs are involved in the production of cellulose in PCWs and SCWs, resulting in altered structural properties of the polysaccharide matrix in each cell wall type (Lampugnani et al., 2018).

Hemicelluloses include xyloglucan, glucuronoxylan (xylan), glucomannans, and galactoglucomannans, which consist of a β-1,4-linked sugar backbone decorated with glucuronic acid, acetyl, and 4-O-methylglucuronic acid side chains (Scheller & Ulvskov, 2010). Hemicelluloses make up approximately 10-40% of the cell wall dry weight (Bajpai, 2018). In eudicots, the predominant hemicellulose in PCWs is xyloglucan, while the most abundant SCW hemicellulose is xylan (Rennie & Scheller, 2014). Hemicelluloses are thought to provide additional structural support to cell walls by stabilizing cellulose polymers through hydrogen bond interactions (Henriksson & Gatenholm, 2001).

Pectins include diverse polysaccharides such as homogalacturonan, rhamnogalacturonan I and rhamnogalacturonan II (Harholt et al., 2010). Pectin is composed of a sugar backbone of α-1,4-D-galacturonic acid for homogalacturonan or alternating α-1,2-L-rhamnose and α-1,4-D-galacturonic units for rhamnogalacturonan, with side chain modifications (Harholt et al., 2010). Pectin is thought to play a major role in maintaining structural integrity of the PCW and middle lamella (Willats et al., 2001). During plant growth, the composition of pectins changes between tissue types and regions of the cell wall, leading to altered structural properties and functions (Freshour et al., 1996; Pelloux et al., 2007). For example, pectin modifications such as methylesterification have been implicated in numerous different developmental processes including cell wall extension or stiffening, cell abscission, seed germination, root tip elongation, fruit ripening, and dehiscence (Al-Qsous et al., 2004; Brummell et al., 2004; Ferrandiz, 2002; Moustacas et al., 2015; Pelloux et al., 2007; Pilling et al., 2004; Ren & Kermode, 2002).

In contrast, SCWs contain the phenolic heteropolymer lignin. Lignin constitutes up to 18-35% of the overall plant biomass and provides immense structural strength and hydrophobicity to the cell wall (Sarkanen & Ludwig, 1971). Lignin is formed by oxidative cross-linking of lignin monomers, called monolignols, which are produced in the cytoplasm and exported to the cell wall. The three most abundant monolignols are *p*-coumaryl alcohol, coniferyl alcohol, and sinapyl alcohol (Vanholme et al., 2010). Following polymerization into lignin, these monolignols are referred to as *p*-hydroxyphenyl (H), guaiacyl (G) or syringyl (S) units, respectively (Bonawitz & Chapple, 2010). The fraction of H-, G-, and S-units varies among cell types within the same plant and between species (Santos et al., 2012). Specific plant taxa, such as monocots, often

incorporate non-canonical units and produce a lignin polymer rich in ferulates, coniferylaldehydes, and modified monolignols containing acetate, *p*-coumarate, or *p*-hydroxybenzoate moieties (Hatfield et al., 2017; Jacquet et al., 1995; Ralph et al., 2004). Further details about the biosynthesis of monolignols, export to the cell wall, and oxidative polymerization can be found in section 1.3 below. Recent nuclear magnetic resonance (NMR) analysis in maize indicated close electrostatic interactions between lignin and xylan (Kang et al., 2019). In addition, monocot lignin can covalently bond with hemicelluloses through ferulate-arabinoxylan interactions, which provides additional structural strength for SCWs (Ralph et al., 2004).

The final structural component of cell walls are secreted proteins, making up approximately 5-10% of the cell wall by dry weight (Cassab, 1998). Secreted proteins are thought to be involved in diverse processes, including providing structural support, modifying cell wall components, and acting in defense or stress responses (Boudart et al., 2005). In this thesis, two classes of cell wall proteins are explored: laccases and peroxidases, which are required for monolignol oxidation and lignin polymer formation.

1.2.3 Secretion of cell wall components via Golgi vesicles

Cell wall composition in different cell types and during development is thought to be controlled by transcription of biosynthetic genes and modulation of the secretory system (van de Meene et al., 2017). The endoplasmic reticulum (ER) and Golgi play fundamental roles in production, modification, and delivery of polysaccharides and proteins to the cell wall (Meents et al., 2018).

Biosynthesis of the polysaccharides pectin and hemicellulose occurs in the Golgi, where Golgi-resident proteins are involved in production of the sugar backbone and chain modifications (Scheller & Ulvskov, 2010; Willats et al., 2001). For cellulose biosynthesis, membrane-bound CESAs form multi-protein CSC complexes in the Golgi and are subsequently transported to the PM to synthesize cellulose microfibrils (McFarlane et al., 2014). Most proteins destined for the cell wall are also secreted through the Golgi. In the default secretory pathway, proteins with a N-terminal signal sequence are synthesized in the ER and transported to the Golgi where they

undergo post-translational modifications such as glycosylation (van de Meene et al., 2017). Golgi-derived secretory vesicles containing polysaccharides, CSCs, and cell wall proteins are transported to the PM and the contents of the vesicles are released into the cell wall by exocytosis (Scheller & Ulvskov, 2010; van de Meene et al., 2017; Willats et al., 2001).

Increasing evidence indicates that cell wall formation is dependent on proper functioning of the secretory pathway. For example, Golgi vesicle targeting to the PM can be facilitated by the presence of an octomeric exocyst complex, which aids in vesicle tethering at the PM (Zhang et al., 2010). Golgi-derived vesicles containing CSCs and xylan were mis-localized when an exocyst subunit was absent, demonstrating that SCW formation requires a functional exocyst complex (Vukašinović et al., 2017). However, it is currently unknown whether polysaccharides and proteins destined for the cell wall are secreted in the same Golgi vesicles. One study that examined secretion of pectin and cell wall proteins in seeds found that loss of a trans-Golgi protein (*ECHIDNA*) resulted in mistargeting of polysaccharides to the vacuole and proteins to intracellular multilamellar bodies (McFarlane et al., 2013). The spatial separation of different cell wall components in this system suggested that cell wall polysaccharides and proteins may be found in separate secretory vesicles.

During SCW formation, polysaccharide biosynthesis in the Golgi and subsequent secretion occurs simultaneously with the production of monolignols for lignin polymerization. However, biosynthesis and export of monolignols occurs through distinctive mechanisms separate from polysaccharide biosynthesis.

1.3 Lignin

Lignin is a complex, branched phenolic polymer found in SCWs. Lignin is only found in vascular plants and is absent from non-vascular species like mosses and green algae (Weng & Chapple, 2010). As outlined in the sections below, monolignol biosynthesis occurs in the cytoplasm, where lignin monomers called monolignols are synthesized from the amino acid phenylalanine. Monolignols are then exported to the cell wall and oxidized by secreted enzymes called laccases and peroxidases. Oxidation of monolignols produces an unstable radical form which will then covalently bond with another monolignol radical or radicalized polymer. Ultimately,

combinatorial cross-linking of monolignols forms a high-order lignin polymer that completely impregnates the polysaccharide matrix of the middle lamella and SCW.

1.3.1 Monolignol biosynthesis and export to the cell wall

Monolignol biosynthesis is a multi-step process requiring coordination of several enzymes (Vanholme et al., 2010). These enzymes are divided into two main pathways, including the general phenylpropanoid pathway and the monolignol-specific pathway. In the general phenylpropanoid pathway, the amino acid phenylalanine is first diverted from primary metabolism in the shikimate pathway to produce *p*-coumaryl-CoA. Biosynthesis of other phenolic compounds, such as suberin, sporopollenin, cutin, flavonoids, hydroxycinnamic acids, tannins, and lignans branches from this early step (Dixon & Paiva, 1995). The monolignol-specific pathway continues with a series of chemical reactions starting with *p*-coumaryl-CoA, including hydroxylation of the aromatic ring, methylation of the hydroxyl groups, two rounds of reductions of the side chain, and conversion of the carboxyl acid-group to an aldehyde and then to a monolignol alcohol (Boerjan et al., 2003). Due to the localization of monolignol biosynthetic enzymes on the surface of the ER as well as in the cytoplasm, monolignol biosynthesis occurs in the cytoplasm in close association with the ER (Gou et al., 2018; Schuetz et al., 2014).

Ultimately, the three most abundant monolignols, *p*-coumaryl alcohol, coniferyl alcohol, and sinapyl alcohol, are formed (Vanholme et al., 2010). Once incorporated into the lignin polymer, these monolignols are referred to as *p*-hydroxyphenyl (H), guaiacyl (G) or syringyl (S) units, respectively. Analyses of plants with mutations in lignin biosynthetic genes have demonstrated that lignin polymerization is a highly flexible process, with mutant backgrounds showing incorporation of different ratios of monolignols or non-canonical subunits with a range of impacts on phenotype (Sederoff et al., 1999). For example, loss of function in *AtF5H* (*fah1*) in Arabidopsis resulted in SCWs rich in G-units and almost completely devoid of S-units; however, these mutants had no major defects in growth or development (Chapple et al., 1992). Other non-canonical compounds can also be incorporated into lignin, including ferulic acid (Leple et al., 2007), dihydroconiferyl alcohol (Ralph et al., 1997), and 5-hydroxyconiferyl alcohol (Marita et al., 2003).

Once synthesized in the cytoplasm, monolignols can either be exported to the cell wall or glycosylated and sequestered in the vacuole. The mechanisms by which monolignols are exported to the cell wall are unknown (Perkins et al., 2019). Microautoradiography analyses following labeled phenylalanine in lodgepole pine indicated that monolignols were not being secreted in Golgi-derived vesicles (Kaneda et al., 2008). Currently, the two predominant theories include passive diffusion through the PM or active transport through ATP-dependent ABC transporters (Perkins et al., 2019). Support for ABC transporters has mainly come from *in-vitro* studies; for instance, the ABC transporter AtABCG29 from Arabidopsis has been shown to transport *p*-coumaryl alcohol *in-vitro* (Alejandro et al., 2012). However, it is unclear whether this is a common mechanism *in-planta* for all monolignols, cell types, or plant species. Further work is therefore required to elucidate how monolignols are transported from the site of synthesis in the cytoplasm to the cell wall.

1.3.2 Oxidative coupling and radical transfer

Following export into the cell wall, monolignols undergo random cross-linking to form the lignin polymer. Erdtman (1933) originally proposed that lignin polymerization in the cell wall occurred through an oxidation (dehydrogenation) reaction involving radical intermediates (Erdtman, 1933). Further fundamental work by Freudenberg (1965) showed that following single-electron oxidation, monolignol radicals are estimated to have a half-life of approximately 45 seconds, as measured by electron spin resonance (Freudenberg, 1965). The high reactivity and short half-life of these radicals promotes bimolecular radical coupling, in which two radicals will covalently bond together. The lignin polymer thus increases in size via combination of two monolignol radicals, a monolignol radical and a radicalized growing end of a polymer (end-wise polymerization), or bulk polymerization of two radicalized polymers (Demont-Caulet et al., 2010; Ralph et al., 2004; Syrjänen & Brunow, 2000; Tobimatsu & Schuetz, 2019). Bond formation will quench both radicals, and depending on the structure, the resulting end groups may be radicalized again for further cross-linking.

In addition to cross-coupling with other monolignols or the lignin polymer, monolignol radicals can also react with other phenols or hydroxy groups of sugars in the cell wall

(Freudenberg, 1965). In monocots, lignin is covalently bound to the hemicellulose xylan through ferulate linkages, thus increasing the complexity of the SCW matrix (Terrett & Dupree, 2019). In addition, monocot lignin contains the flavonoid tricin, which can act as a nucleation site for lignin chain branching (Lan et al., 2015). However, as eudicots do not naturally incorporate ferulate or tricin into the cell wall, it is unclear to what degree lignin is linked to flavonoids or polysaccharides in other species (Hatfield et al., 2017).

Oxidation of monolignols or the lignin polymer could occur through two different mechanisms: either through direct oxidation by a laccase or peroxidase or through a non-enzymatic redox shuttle mechanism, in which the radical is transferred between compounds in the cell wall (Hatfield et al., 2008; Onnerud, 2002; Ralph et al., 2004; Ros-Barceló et al., 2006). Radical transfer is a spontaneous reaction that comes about from the differences in the oxidation-reduction potential of each monolignol or oligomer in the cell wall (Ros-Barceló et al., 2006). Various radical carriers have been proposed to facilitate a redox shuttle, such as Ca^{2+} (Westermark, 1982) or Mn^{2+} (Onnerud, 2002). However, *in-planta* evidence for electron shuttling via Ca^{2+} or Mn^{2+} is lacking. Therefore, the relative contribution of direct oxidation by enzymes or through a redox shuttle mechanism is unknown.

1.4 Laccases and peroxidases

Laccases (LACs; EC 1.10.3.2) are secreted, glycosylated, multi-copper oxidoreductases that oxidize phenolic compounds through the reduction of molecular oxygen to water (Figure 1.1; Mayer & Harel, 1979). Class III secreted peroxidases (PRXs; EC 1.11.1.7) are glycosylated, heme-containing oxidoreductases that oxidize phenolic compounds using hydrogen peroxide (H_2O_2) as an electron acceptor (Figure 1.1; Shigeto & Tsutsumi, 2016). Historically, both LACs and PRXs were thought to be involved in lignification, due to the ability of each enzyme to form a similar lignin-like dehydrogenation polymer (DHP) from monolignols *in-vitro* (Freudenberg, 1959). Later histochemical analyses by Harkin and Obst (1973) in angiosperm and gymnosperm wood samples found that a phenolic compound called syringaldazine was not oxidized unless exogenous H_2O_2 was added, leading to the hypothesis that PRXs were exclusively involved in lignification *in-planta* and not LACs (Harkin & Obst, 1973). LAC involvement in lignification was later revived following

evidence that extracted LACs from loblolly pine and in sycamore maple suspension cultures could oxidize monolignols (Bao et al., 1993; Sterjiades et al., 1992). Currently, there are numerous studies demonstrating LAC and PRX involvement in lignification; however, very little is known about the specific enzymes involved or their spatial distribution in lignifying tissues (Christensen et al., 1998; Herrero et al., 2013; Novo-Uzal et al., 2013; Turlapati et al., 2011; Warinowski et al., 2016).

Figure 1.1. Oxidation of monolignols to radical forms (blue circle) by LACs and PRXs.

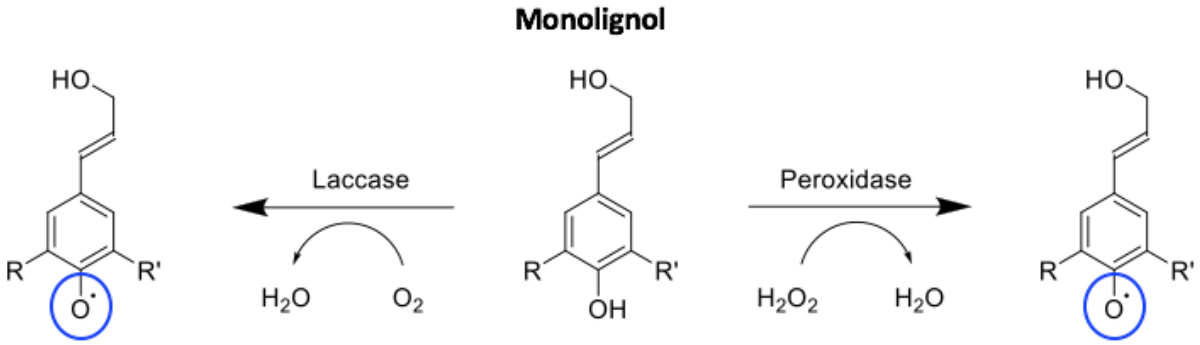

1.4.1 LAC and PRX enzyme structures, phylogenies, and biological roles

PRXs are found in all green plants and form large multigenic families due to genome duplication events (Passardi et al., 2004). For example, there are 73 PRXs in Arabidopsis, 138 PRXs in *Oryza sativa*, and at least 93 PRXs in *Populus trichocarpa* (Passardi et al., 2004; Ren et al., 2014). The three-dimensional structure of plant PRXs is highly conserved, with an N-terminal signal peptide, heme and Ca^{2+} binding sites, and four disulfide bridges (Lüthje & Martinez-Cortes, 2018). PRXs are glycosylated, which is required for proper folding, protein stability, enzymatic activity and substrate binding (Gabaldón et al., 2007; Lige et al., 2001). Specific PRXs have additional structural modifications that may alter their subcellular localization or activity (Welinder et al., 2002). For example, a C-terminal extension found on a *Catharanthus roseus* PRX is required to localize it to the vacuole where it is involved in alkaloid metabolism (Costa et al., 2008).

LACs also comprise large gene families, with 17 LACs in Arabidopsis, 30 LACs in *Oryza sativa*, 49 LACs in *Populus trichocarpa*, and 29 LACs in *Brachypodium distachyon* (Hu et al., 2018; Lu et al., 2013; Turlapati et al., 2011; Wang et al., 2015). Each LAC contains a highly conserved

Cu-binding domain (McCaig et al., 2005; Turlapati et al., 2011). In addition, most LACs have a predicted N-terminal signal sequence to target it to the secretory pathway (Turlapati et al., 2011). The average size of LACs range from 60-130kDa, with Arabidopsis LACs estimated to be 60-70kDa prior to glycosylation (Wang et al., 2015). Glycosylation on LACs is required for Cu retention, proper secretion, protein stability, and enzymatic activity (Maestre-Reyna et al., 2015). In addition, LAC activity is highly regulated at the transcriptional and post-transcriptional level, with modulation by antisense transcripts, histone and DNA methylation, and microRNAs (miRNA; Turlapati et al., 2011). Post-transcriptional regulation of LAC expression by miRNA targeting appears to be a common feature among plant lineages; for example, 7 of 17 Arabidopsis LACs, 29 of 49 *Populus trichocarpa* LACs, and 22 of 44 cotton LACs were predicted to have miRNA target sites (Abdel-Ghany & Pilon, 2008; Balasubramanian et al., 2016; Lu et al., 2013).

Despite functioning in a fundamental step in lignin polymerization, identifying and functionally characterizing the specific LACs and PRXs involved in lignification has been hindered by large gene families of these enzymes, overlapping expression profiles, broad substrate specificities, and functional redundancy (Cosio & Dunand, 2009; Duroux & Welinder, 2003; Shigeto & Tsutsumi, 2016; Turlapati et al., 2011). *In-vitro*, LACs and PRXs show broad substrate specificity towards numerous phenolics, which makes it difficult to determine what substrate a given isoenzyme is acting on *in-vivo* (Gumiero et al., 2010). In addition, LACs and PRXs have been shown to be involved in diverse cellular processes. For example, PRXs have been implicated in response to abiotic and biotic stresses, cell elongation, cell stiffening, auxin metabolism, seed coat mucilage extrusion, and lignification (Cosio & Dunand, 2009; Gabaldón et al., 2006; Shigeto & Tsutsumi, 2016). The complex and diverse roles that LACs and PRXs play in development could therefore be a combination of substrate specificity and availability, catalytic cycle, and spatiotemporal expression patterns. Consequently, the precise LACs and PRXs involved in developmental lignification are largely unknown.

1.4.2 Finding LACs and PRXs involved in lignification

Putative LACs and PRXs involved in lignification can be identified using diverse resources, including analysis of mutant phenotypes, homology to oxidative enzymes in other species,

expression profiles, and co-expression networks. Functional characterization of a specific lignin-associated LAC or PRX generally involves experiments demonstrating the ability to oxidize monolignols *in-vitro*, localization to lignified cell walls, and alterations in lignin content or structure following reduction of gene/enzyme function (Cosio & Dunand, 2009; Sato et al., 2006).

Several research groups have tried to elucidate potential lignin-associated LACs and PRXs based on single-, double-, and triple-knockout mutant analyses in the model species Arabidopsis and scoring structural and lignin-associated phenotypic alterations (Tables 1.1-1.3). A limitation of this method is the presence of functionally redundant members in the large gene families, resulting in a non-observable or minor phenotype for most single mutants (Tables 1.1-1.2). LAC involvement in lignification of Arabidopsis was first demonstrated by identification of an irregular xylem phenotype in plants with a mutation in *LACCASE4 (AtLAC4/AtIRX12;* Brown et al., 2005). Berthet *et al.* (2011) later demonstrated that simultaneous deletion of Arabidopsis *AtLAC4* and *AtLAC17* decreased lignin content by 40% and led to a severe irregular xylem phenotype in mutant plants (Berthet et al., 2011). Additionally, Arabidopsis triple *lac4-2/lac11/lac17* mutants were dwarfed and had decreased lignin content in stems and roots, providing strong genetic evidence for *AtLAC4*, *AtLAC11*, and *AtLAC17* in lignification (Table 1.3). Mutation in *AtLAC15/AtTT10* resulted in delayed browning of seed coats, suggesting that other LACs are involved in diverse processes outside lignification in different tissue types (Pourcel et al., 2005).

From genetic studies, the best characterized example of an Arabidopsis PRX involved in lignification is *PEROXIDASE64* (*AtPRX64*), which is required for lignification of the Casparian strip in roots (Lee et al., 2013). Several other PRXs in Arabidopsis have been implicated in lignification, including *AtPRX2*, *AtPRX4*, *AtPRX17*, *AtPRX25*, *AtPRX52*, *AtPRX71*, and *AtPRX72*, as mutation of these genes resulted in alterations to stem lignin content or composition (Tables 1.2-1.3; Cosio et al., 2017; Fernández-Pérez et al., 2015, 2015a, 2015b; Herrero et al., 2013; Shigeto et al., 2014, 2015). However, unlike the *lac* mutants, studies involving *prx* mutants lack strong evidence for roles in lignification of stem tissue. These studies report large variation in lignin reduction in mutant plants, ranging from a 10% reduction in stem lignin in *prx25* mutants, a 35% reduction in *prx72* stem lignin, or an 58% reduction in stem lignin in *prx17* mutants (Table 1.2). This is in contrast to the comparably modest 3.5-11% reduction in stem lignin consistently observed in

single *lac* mutants (Table 1.1). *prx* mutants also show diverse phenotypic alterations not related to lignification, such as increased epidermal cell size in leaves for *prx71* mutants (Raggi et al., 2015), so the precise function of a given enzyme and its involvement in lignification is unclear. Therefore, additional evidence is required to assess which of the 73 PRXs may be involved in lignification.

Interestingly, the root Casparian strip was still lignified in triple *lac4-2/lac11/lac17* mutants, indicating that LACs and PRXs are non-redundant in lignified tissues (Zhao et al., 2013). Tagging of Arabidopsis AtLAC4 and AtPRX64 with fluorescent proteins provided further evidence for the non-overlapping role of these enzymes during lignification. In lignifying inflorescence stems, AtLAC4-mCherry localized to the cellulose-rich lignified SCW while AtPRX64-mCherry localized to the lignified cell corner and middle lamella between adjacent cells (Chou et al., 2018). The spatial separation of these two enzymes to different regions of the cell wall could indicate different roles of LACs and PRXs during lignification. However, it is unknown whether other LAC or PRX proteins show spatial and/or temporal separation to lignifying tissues during development. An additional explanation for the non-redundancy of LACs and PRXs could be different substrate specificities or acting during different temporal stages during lignification (Laitinen et al., 2017; Sterjiades et al., 1993). Using a combination of lignin analyses from mutant lines and *in-vitro* tests using monolignol-like compounds, monolignol specificities have been suggested for LACs and PRXs *in-planta* (Table 1.4).

Another commonly-used tool to identify lignin-associated LACs or PRXs is finding Arabidopsis homologs of well-characterized LACs and PRXs involved in lignification in other species, such as *Zinnia elegans, Populus,* or tobacco (Blee et al., 2003; Herrero et al., 2013; Shigeto et al., 2013). Similarity in amino acid sequences and gene expression patterns could indicate conserved biological function between species (Patel et al., 2012). Numerous putative lignin-related PRXs from Arabidopsis have been identified using homology-based searches, such as AtPRX52, which shows high amino acid similarity to the lignin peroxidase ZePRX in *Zinnia elegans* (Fernández-Pérez et al., 2015b) or AtPRX71, which is homologous to the lignin peroxidase CWPO-C in poplar (Sasaki et al., 2006; Shigeto et al., 2013). However, experimental validation is still required to connect homologous LACs or PRXs with lignification in Arabidopsis.

Finally, LACs and PRXs involved in lignification may be identified through expression and co-expression analyses, such as selecting LACs or PRXs that are co-expressed with SCW cellulose, hemicellulose, or monolignol biosynthetic genes (Brown et al., 2005; Ruprecht et al., 2011). Significant co-expression of SCW biosynthetic genes and a given LAC or PRX could implicate involvement in similar biological processes (Ruprecht et al., 2011). For example, *AtLAC4* was first identified as playing a role in lignification due to significant co-expression with the SCW cellulose synthase gene *AtCESA7* (Brown et al., 2005). However, *in-silico* approaches are not sufficient to prove involvement in lignification and thus the biochemical activity of the enzyme and the spatial distribution in lignifying tissues needs to be confirmed.

Table 1.1. Arabidopsis *LACCASE* single T-DNA insertion line mutants and associated lignin-related phenotypes.

Gene	Loci	Mutant name/allele	T-DNA Insertion Site	RT-PCR Confirmation	Phenotype	Methods used	Reference
AtLAC2	At2g29130	*lac2*	Exon	Knockout	Reduced root elongation under dehydration stress	RT-qPCR; salt and dehydration stress treatment	Cai et al., 2006
AtLAC3	At2g30210	*lac3*	Exon	Knockout	No observable phenotype	RT-qPCR; salt and dehydration stress treatment	Cai et al., 2006
AtLAC4	At2g38080	*lac4-1/irx12*	Promoter	Knockdown	Decreased lignin (92% of wild type); weak irregular xylem phenotype	RT-qPCR; phloroglucinol/Mäule/toluidine blue staining; Klason/thioacidolysis analyses; determination of stem soluble phenolic compounds by HPLC; saccharification	Brown et al., 2005; Berthet et al., 2011
		lac4-2	Exon	Knockout	Decreased lignin (91% of wild type); irregular xylem phenotype under continuous light; increased S:G ratio; increased saccharification		
AtLAC5	At2g40370	*lac5*	Exon	Knockout	No observable phenotype	RT-qPCR; salt and dehydration stress treatment	Cai et al., 2006
AtLAC6	At2g46570	*lac6*	Exon	Knockout	No observable phenotype	Klason/thioacidolysis analyses, saccharification	Berthet et al., 2012
AtLAC7	At3g09220	*lac7*	Exon	Knockout	No observable phenotype	Klason/thioacidolysis analyses, saccharification	Berthet et al., 2012
AtLAC8	At5g01040	*lac8*	Exon	Knockout	Early flowering	RT-qPCR; salt and dehydration stress treatment	Cai et al., 2006
AtLAC9	At5g01050	*lac9*	Exon	Knockout	No observable phenotype	RT-qPCR; salt and dehydration stress treatment	Cai et al., 2006
AtLAC10	At5g01190	*lac10*	Exon	Knockout	No observable phenotype	Klason/thioacidolysis analyses, saccharification	Berthet et al., 2012
AtLAC11	At5g03260	*lac11*	Exon	Knockout	No observable phenotype	RT-qPCR; phloroglucinol/Mäule staining; thioacidolysis; determination of stem soluble phenolic compounds by HPLC	Berthet et al., 2012; Zhao et al., 2013
AtLAC12	At5g05390	*lac12*	Exon	Knockout	Decreased lignin (96.5% of wild type)	RT-qPCR; Klason analysis	Berthet et al., 2012
AtLAC13	At5g07130	*lac13*	Exon	Knockout	No observable phenotype	RT-qPCR; salt and dehydration stress treatment	Cai et al., 2006
AtLAC14	At5g09360	*lac14*	Exon	Knockout	No observable phenotype	RT-qPCR; salt and dehydration stress treatment	Cai et al., 2006
AtLAC15	At5g48100	*transparent testa10-2*	Intron	Knockout	Delayed browning of seed coat	RT-qPCR; salt and dehydration stress treatment; flavonoid histochemistry and identification by LC-MS	Pourcel et al., 2005; Cai et al., 2006
AtLAC16	At5g58910	*lac16*	Intron	Knockout	No observable phenotype	RT-qPCR; salt and dehydration stress treatment	Cai et al., 2006
AtLAC17	At5g60020	*lac17*	Promoter	Knockout	Decreased lignin (89% of wild type); increased S:G ratio	RT-qPCR; phloroglucinol/Mäule staining; Klason/thioacidolysis analysis; determination of stem soluble phenolic compounds by HPLC; saccharification	Berthet et al., 2011

Table 1.2. Arabidopsis *PEROXIDASE* single T-DNA insertion line mutants and associated lignin-related phenotypes.

Gene	Loci	Mutant name/allele	T-DNA Insertion Site	RT-PCR Confirmation	Phenotype	Methods used	Reference
AtPRX2	At1g05250	*atprx2*	Exon	Knockout	Reduced dry weight; reduced lignin (86% of wild type); increased S:G ratio; reduced fiber cell wall thickness	RT-qPCR; toluidine blue staining; acetyl bromide/derivatization followed by reductive cleavage analyses	Shigeto et al., 2013
AtPRX4	At1g14540	*atprx4*	Exon	Knockout	Decreased S:G ratio under long-day conditions; reduced lignin in long-day conditions (63% of wild type)	RT-qPCR; acetyl bromide/thioacidolysis/Fourier transform infrared spectroscopy analyses; TEM; toluidine blue/phloroglucinol/Mäule staining	Fernández-Pérez et al., 2015
AtPRX17	At2g22420	*atprx17-1*	Exon	Knockout	Delayed bolting, reduced elongation of stems; reduced lignin in leaves (58% of wild type), base of stem (76% of wild type), top of stem (42% of wild type) and siliques (19% of wild type)	RT-qPCR; thioacidolysis analysis; lignin deposition under UV light; immunolocalization of xylan	Cosio et al., 2017
AtPRX25	At2g41480	*atprx25*	Exon	Knockout	Reduced plant dry weight; reduced lignin (90% of wild type); increased S:G ratio; reduced fiber cell wall thickness	RT-qPCR; toluidine blue staining; acetyl bromide/derivatization followed by reductive cleavage analyses	Shigeto et al., 2013
AtPRX52	At5g05340	*atprx52-1*	Exon	Not reported	Earlier bolting; reduced lignin (69% of wild type); decreased S:G ratio in mature stems	RT-qPCR; toluidine blue/phloroglucinol/Mäule staining; TEM; acetyl bromide/ alkaline nitrobenzene oxidation/ thioacidolysis/Fourier transform infrared spectroscopy analyses	Fernández-Pérez et al., 2015b
AtPRX64	At5g42180		Endodermis-specific miRNA	Not reported	Inhibited Casparian root lignification	Propidium iodide uptake in roots	Lee et al., 2013
AtPRX71	At5g64120	*atprx71 (SALK_091561)*	Intron	Knockout	Increased S:G ratio in stems	RT-qPCR; toluidine blue staining; acetyl bromide/derivatization followed by reductive cleavage analyses	Shigeto et al., 2013
		atprx71-1 (SALK_123643)	Exon	Knockout	Increased rosette size, increased hypocotyl length, increased leaf epidermal cell area	RT-qPCR; measuring rosette and hypocotyl size, cell length, dry weight; peroxidase assay (oxidation of guaiacol); oxidative burst assay	Raggi et al., 2015
AtPRX72	At5g66390	*atprx72-1*	Exon	Not reported	Delayed and reduced growth; altered leaf morphology; reduced lignin (65% of wild type); decreased S-units; minor irregular xylem phenotype	Acetyl bromide/nitrobenzene oxidation/thioacidolysis analyses; toluidine blue/phloroglucinol/Mäule staining; Fourier transform infrared spectroscopy analyses	Herrero et al., 2013
		atprx72-2	5'UTR	Not reported	Thinner interfascicular fiber cell wall thickness; decreased S:G ratio	RT-qPCR; SEM/TEM; acetyl bromide/thioacidolysis/Fourier transform infrared spectroscopy analyses	Fernández-Pérez et al., 2015a

Table 1.3. Arabidopsis *LACCASE* and *PEROXIDASE* double and triple mutants and associated lignin-related phenotypes.

Mutant	Phenotype	Methods used to assess phenotype	Reference
lac4-2/lac11	Reduced lignin (87% of wild type)	RT-qPCR; toluidine blue staining; acetyl bromide/thioacidolysis analyses; metabolite extraction and analysis by HPLC	Zhao et al., 2013
lac4-1/lac17	Reduced lignin (83% of wild type) under continuous light	RT-qPCR; phloroglucinol/Mäule staining; Klason/thioacidolysis analysis; determination of stem soluble phenolic compounds by HPLC; saccharification	Berthet et al., 2011
lac4-2/lac17	Semi-dwarf under continuous light; irregular xylem phenotype; reduced lignin (60% of wild type); increased S:G ratio; increased saccharification	RT-qPCR; phloroglucinol/Mäule staining; Klason/thioacidolysis analysis; determination of stem soluble phenolic compounds by HPLC; saccharification	Berthet et al., 2011
lac11/lac17	Reduced lignin (88% of wild type)	RT-qPCR; toluidine blue staining; acetyl bromide/thioacidolysis analyses; metabolite extraction and analysis by HPLC	Zhao et al., 2013
lac12/lac17	Decreased lignin (84% of wild type); increased S:G ratio; increased saccharification	Klason/thioacidolysis analyses; saccharification	Berthet et al., 2012
lac4-2/lac11/lac17	Dwarf phenotype; decreased lignin histochemistry; indehiscent anthers; vascular development arrest; decreased root diameter; altered soluble phenolics	RT-qPCR; toluidine blue/phloroglucinol staining; acetyl bromide/thioacidolysis analyses; metabolite extraction and analysis by HPLC	Zhao et al., 2013
prx2/prx25	Reduced stem dry weight; reduced fiber cell wall thickness; reduced lignin (75% of wild type); increased S:G ratio; increased saccharification	RT-qPCR; toluidine blue/Mäule staining; acetyl bromide/derivatization followed by reductive cleavage analyses; saccharification	Shigeto et al., 2015
prx2/prx71	Reduced stem dry weight; reduced fiber cell wall thickness; reduced lignin (85% of wild type); increased S:G ratio; increased saccharification	RT-qPCR; toluidine blue/Mäule staining; acetyl bromide/derivatization followed by reductive cleavage analyses; saccharification	Shigeto et al., 2015
prx25/prx71	Reduced stem dry weight; reduced fiber cell wall thickness; reduced lignin (83% of wild type); increased S:G ratio; increased saccharification	RT-qPCR; toluidine blue/Mäule staining; acetyl bromide/derivatization followed by reductive cleavage analyses; saccharification	Shigeto et al., 2015

Table 1.4. Putative monolignol specificities of LACs and PRXs based on mutant analyses and *in-vitro* tests. *n.d. indicates no data. Syringaldazine and 2,6-dimethoxyphenol (2,6-DMP) are analogs for sinapyl alcohol (S-units) and guaiacol is an analog for coniferyl alcohol (G-units).

Enzyme	Species	Proposed Specificity	Evidence		Reference
			***In-vitro* oxidative assay**	**Mutant lignin analysis**	
AtLAC4	Arabidopsis	Coniferyl alcohol	n.d.	Decreased G-units with no change to S- or H-units in *lac4-2/lac17* mutants	Berthet et al., 2013
AtLAC15	Arabidopsis	Flavanols	n.d.	Decreased quercetin rhamnoside dimers (flavan-3-ols) in *tt10-2* mutants	Pourcel et al., 2005
AtLAC17	Arabidopsis	Coniferyl alcohol	n.d.	Decreased G-units with no change to S- or H-units in *lac4-2/lac17* mutants	Berthet et al., 2011
AtPRX2	Arabidopsis	Sinapyl and coniferyl alcohols	Syringaldazine>>2,6-DMP>Guaiacol; cytochrome c	Increased S-units and an increased S:G ratio in *prx2* mutants	Shigeto et al., 2013; 2014
AtPRX4	Arabidopsis	Sinapyl alcohol	n.d.	Decreased S:G ratio in *prx4* mutants	Fernández-Pérez et al., 2015
AtPRX25	Arabidopsis	Sinapyl and coniferyl alcohols	Syringaldazine=Guaiacol>2,6-DMP; cytochrome c	Increased S- and G-units and an increased S:G ratio in *prx25* mutants	Shigeto et al., 2013; 2014
AtPRX52	Arabidopsis	Sinapyl alcohol	n.d.	Decreased S:G ratio in *prx52* mutants	Fernández-Pérez et al., 2015b
AtPRX53	Arabidopsis	Coniferyl alcohol	Guaiacol	n.d.	Shigeto et al., 2013
AtPRX71	Arabidopsis	Sinapyl and coniferyl alcohols	Syringaldazine>2,6-DMP>Guaiacol; cytochrome c	Increased S- and G-units and an increased S:G ratio in *prx71* mutants	Shigeto et al., 2013; 2014
AtPRX72	Arabidopsis	Sinapyl alcohol	n.d.	Decreased S-units in *prx72* mutants	Herrero et al., 2013; Fernández-Pérez et al., 2015a
CWPO-C	*Populus alba*	Sinapyl and coniferyl alcohols	Syringaldazine>>2,6-DMP>Guaiacol; cytochrome c	n.d.	Sasaki et al., 2006; Shigeto et al., 2013
HRP-C	*Armoracia rusticana*	Coniferyl alcohol	Guaiacol>syringaldazine>2,6-DMP	n.d.	Shigeto et al., 2013

1.5 Development of Arabidopsis floral stems

Lignification of SCWs is controlled in space and time throughout growth, with only specific cell types becoming lignified while neighboring cells remain unlignified (Altamura et al., 2001; Hall et al., 2013). Currently, the cellular mechanisms directing specific patterns of lignin deposition are unknown, but one hypothesis is that plant cells control where lignin is deposited by specifying when and where LACs and PRXs involved in lignin formation are found (Schuetz et al., 2014). However, in addition to knowing very little about the specific LACs and PRXs involved in lignification, few studies have tested where these enzymes are spatially distributed. Due to the large number of LAC and PRX enzymes, different oxidative enzymes could be coordinating lignification in different cell types or during alternative stages of growth. Therefore, it is important to consider lignification and LAC or PRX activity within the broader context of plant development. The following sections will outline major developmental stages of stem growth and lignification in the model species Arabidopsis.

At the cellular level, plant cells undergo rapid developmental changes which are coordinated with modifications to cell wall composition and structure (Hall et al., 2013; Minic et al., 2009). Formation of lignified cells involves a series of biological processes, including cell division, cell elongation, cell function specification and differentiation, SCW deposition and lignification, and cell death. These stages are tightly controlled on a spatial and temporal level. In addition, plants must strictly regulate the number and types of cells undergoing SCW formation and lignification, as it is a metabolically expensive process that requires large amounts of carbon. Since plants are not able to digest lignin, any carbon invested in lignin polymerization is non-recoverable (Lewis & Yamamoto, 1990).

1.5.1 Main growth stages: Cell division, cell elongation, and cell differentiation

In the inflorescence stem of Arabidopsis, transcriptomic analyses have indicated that gene expression networks are closely linked to the age of the stem and major developmental stages (Minic et al., 2009). In early stages of growth, cells first undergo a period of cell division at the stem apical meristem. This is followed by a period of rapid cell elongation, with cells expanding axially up to 87-fold in length (Suh et al., 2005). Concurrently with cessation of

elongation, cells terminally differentiate into specialized tissue types and begin to lay down components of the SCW (Ye, 2002). These developmental transitions are not rigidly defined but rather overlap with one another within a given time period (Hall et al., 2013).

During the transition from cell elongation, cessation of elongation, and terminal differentiation, cell walls undergo distinct structural changes, which may be dependent on pH and the composition of PCWs and the middle lamella (Roberts & Haigler, 1994). Immunolocalization of xyloglucan and pectin in Arabidopsis seedlings and stems demonstrated that PCW polysaccharide composition changed dynamically in different cell types and regions of the cell wall throughout development (Freshour et al., 1996; Hall et al., 2013). Structural changes to inhibit cell expansion could include cross-linking of extensins and modifications to pectin, such as cross-linking with Ca^{2+} (Roberts & Haigler, 1994; Zamil & Geitmann, 2017). Following or concurrently with cessation of expansion, cells terminally differentiate into a given specialized cell type. For lignified cell types, cessation of elongation corresponds with initiation of SCW formation and deposition of SCW cellulose and hemicellulose (Ye, 2002; Zhong et al., 2001). After polysaccharides have been deposited in the SCW, lignification occurs (Donaldson, 2001; Terashima et al., 2012).

Increasing evidence has supported the role of reactive oxygen species (ROS) in cell development, signaling, and differentiation (Cheeseman, 2007). ROS are produced as part of cell metabolism and include singlet oxygen ($^1O_2$), superoxide anion (O_2^-), hydroxy radical (OH·), and H_2O_2. Specific ROS have been implicated in different development processes, ranging from expansion of root hairs, cell wall loosening and cross-linking, and lignification by PRXs (Dunand et al., 2007; Foreman et al., 2003; Liszkay et al., 2004; Pesquet et al., 2013; Ros Barceló, 1998). In addition, ROS production is induced upon wounding and plays an essential role in defense against pathogens (Bolwell, 1999).

Extracellular ROS is produced by NADPH oxidases (Respiratory Burst Oxidase Homologs [RBOH] in plants), which are highly conserved membrane-bound enzymes found in animal, plant, and fungal lineages (Torres & Dangl, 2005). NADPH oxidases produce O_2^- which is converted into H_2O_2 spontaneously or through the enzyme superoxide dismutase (SOD; Alscher et al., 2002). NADPH oxidase isoforms show divergent gene expression profiles throughout plant

development, indicating that production of ROS is highly controlled to certain tissues during growth (Morales et al., 2016). In addition to NADPH oxidases, extracellular ROS could also be generated by PRXs, polyamine oxidases, and oxalate oxidases in the cell wall (Allan & Fluhr, 1997). Despite its importance in plant development, very little is known about the amount and type of ROS produced in different tissues and the specific roles ROS play in altering cell wall structure during growth.

1.5.2 Spatial patterning of lignin during development: Tissue level and region of the cell wall

The spatial deposition of lignin in SCWs is highly regulated during development. At the tissue level, lignin is only found in specialized cell types, such as tracheary elements for water transportation and fibers for structural support (Esau, 1965). Additionally, lignin content and composition differs between regions of the cell wall (Donaldson, 2001).

The vascular tissue of Arabidopsis is organized in discrete bundles around the circumference of the stem, each of which consists of phloem (photosynthate-conducting) and xylem (water-conducting) tissues. Xylem tissue is made up of three cell types, including tracheary elements, xylary fibers, and xylem parenchyma (Smith et al., 2013). In angiosperms, tracheary elements include protoxylem and metaxylem vessel elements, which are derived from procambium tissues. Protoxylem are found in young, rapidly elongating tissues and have annular lignified SCWs separated by PCWs to support axial growth (Esau, 1965). Metaxylem develop following cessation of elongation and deposit lignified SCWs in a reticulate or pitted pattern for additional structural strength (Schuetz et al., 2013). Metaxylem make up the majority of xylem vessel elements later in development and functionally replace protoxylem (Růžička et al., 2015). In vessel elements, cells initiate lignification and undergo programmed cell death shortly after polysaccharides are deposited in the SCW, and the hollow cell walls act as channels for water transportation throughout the plant (Pesquet et al., 2013; Smith et al., 2017).

In addition to xylem vessel elements, xylem tissue is also made up of xylary fibers and xylem parenchyma. Xylary fibers develop lignified SCWs and provide additional mechanical strength to vascular bundles and the stem (Růžička et al., 2015). Unlike neighboring xylem vessel elements, xylary fibers are long-lived (Bollhöner et al., 2012). Xylem parenchyma cells are non-

lignifying cells that neighbour xylem vessel elements in vascular bundles. They are highly connected to xylem vessel elements via lateral pits through their cell wall and provide nutrients, water, hormones, sugar, and lipids for the xylem vessel elements (Spicer, 2014). Xylem parenchyma also act as "good neighbours" towards adjacent lignifying xylem vessel elements by providing monolignols and H_2O_2 to facilitate lignification of xylem vessel elements following cell death (Pesquet et al., 2013; Smith et al., 2013).

In contrast to xylem vessel elements, interfascicular fibers develop from ground meristem tissue and are found connecting vascular bundles around the stem circumference (Lev-Yadun & Flaishman, 2001). Morphologically, fibers are axially long (>300μm) with tapered ends (Lev-Yadun, 1997). Fibers are necessary for stem mechanical strength, as Arabidopsis *ifl1* mutants that do not form fibers have a pendent shoot phenotype where stems are unable to grow upright (Zhong et al., 1997). Interfascicular fiber cells are long-lived and are autonomous for production of monolignols and lignification (Smith et al., 2013; 2017).

Lignin composition is also remarkably diverse between cell types, regions of the cell wall, and developmental stage (Joseleau & Ruel, 1997; Terashima et al., 2012; Vanholme et al., 2010; Voxeur et al., 2015). In the earliest stage following cessation of cell elongation but before SCW formation, lignin is initially deposited in the cell corners and the middle lamella between adjacent cells (Fukushima & Terashima, 1991; Terashima & Fukushima, 1988). The lignin deposited in the cell corners and middle lamella is rich in G- and H-units (Donaldson, 2001; Joseleau & Ruel, 1997). Following deposition of cellulose and hemicellulose, lignin is polymerized within the SCW polysaccharide matrix (Donaldson, 2001). Angiosperm lignin is composed primarily of G- and S-units, with SCWs of xylem vessel elements being rich in G-units and the SCWs of fibers being rich in both G- and S-units (Chapple et al., 1992; Donaldson, 2001; Joseleau & Ruel, 1997).

1.6 Problem statement and research objectives

Accumulating evidence from several species has indicated that lignin composition and deposition to cell types and regions of the cell wall is precisely coordinated during growth; however, the cellular mechanisms directing specific patterns of lignification are currently unknown. Several possibilities for localized regions of lignin polymerization include polarized

biosynthesis of monolignols in regions of the cell, specifically-localized monolignol transporters on the PM, or spatially-regulated distribution of oxidative enzymes in the cell wall. Fluorescent tagging of the monolignol biosynthetic gene *AtC4H* and putative monolignol transporter *AtABCG29* localized these proteins to the ER and PM, respectively, but did not show preferential localization to regions of lignifying protoxylem cell walls (Schuetz et al., 2014). These results provide evidence that lignin deposition in specific regions of the SCW is not controlled by spatial positioning of biosynthetic enzymes or putative monolignol transporters (Schuetz et al., 2014).

However, fluorescently tagged AtLAC4 and AtLAC17 localized specifically to lignifying SCWs and were not found in non-lignifying PCWs (Schuetz et al., 2014). Therefore, the cells themselves may control where lignin is deposited by specifying when and where different oxidative enzymes involved in lignin formation are found (Schuetz et al., 2014). Although there is abundant evidence for LAC and PRX activity in lignifying cell walls (Czaninski et al., 1993; Goldberg et al., 1985; Ros Barceló, 1998), there is little information about the particular isoforms that are found in lignifying tissue and their spatial and temporal localization throughout development. This research project aims to test the hypothesis that lignin-associated LACs and PRXs have specific and differential distributions in the inflorescence stem of Arabidopsis and that these localization patterns could determine lignin deposition in time and space during development.

I had the following research questions for experimental testing:

1. Which cell types or regions of the cell wall do lignin-associated LACs and PRXs localize to in the inflorescence stem of Arabidopsis?
2. What cellular mechanisms dictate cell wall localization?
3. Do the distributions of LACs and PRXs correlate with developmental lignification of the stem?
4. How does cell wall structure, LAC and PRX enzymatic activity, and substrate availability change during stem growth?

To address these questions, I had the following research objectives:

Objective 1: Identify putative lignin-associated LACs and PRXs using bioinformatic tools and map the spatial distribution of selected LACs and PRXs in Arabidopsis stems (Chapter 3).

Objective 2: Test whether timing of expression plays a role in determining protein localization in the SCW (Chapter 3).

Objective 3: Characterize if and how the distributions of LACs and PRXs change in lignifying cell types throughout stem development and test whether localization patterns correlate with lignin deposition, cell wall structure, LAC and PRX enzymatic activity, or H_2O_2 production (Chapter 4).

For objectives 1 and 2, I used bioinformatic tools (phylogenetic tree building, expression and co-expression analyses) to identify putative lignin-associated LACs and PRXs in Arabidopsis. I tagged *AtLAC10*, *AtPRX42*, *AtPRX52*, *AtPRX71*, and *AtPRX72* under the respective native promoter with a -mCherry fluorescent tag and studied their localization patterns in stem cross-sections along with previously-made *prLAC4::LAC4-mCherry*, *prLAC17::LAC17-mCherry*, and *prPRX64::PRX64-mCherry* plants (Lee et al., 2013; Schuetz et al., 2014). I used UV autofluorescence to visualize lignin deposition in different cell types and regions of the cell wall and tested whether tagged LAC or PRX enzymes co-localized with lignin. To determine whether timing of expression plays a role in determining protein localization in the SCW, I fused the coding sequence of *AtLAC4*, *AtLAC17*, and *AtPRX64* to the promoter of the cellulose synthase gene *AtCESA7* and tagged these constructs with an -mCherry fluorescent marker. I compared the distribution of *prCESA7::LAC4-mCherry*, *prCESA7::LAC17-mCherry*, and *prCESA7::PRX64-mCherry* in stem cross-sections and primary roots to the native localization of these enzymes under their endogenous promoter and to the presence of lignin UV autofluorescence.

For objective 3, I used a combination of UV autofluorescence and lignin histochemical stains to visualize and quantify lignin deposition to different cell types and regions of the cell wall throughout development of the inflorescence stem. Using the tagged LAC and PRX enzymes under their native promoter from Objective (1), I localized these proteins during different stages of stem development and compared it to UV lignin autofluorescence. To study changes in cell wall structure, I used immunolabeling techniques to localize xylan and pectin in stem cross-sections. I also used the histochemical substrates 3,3',5,5'-tetramethylbenzidine (TMB) and 2,7-diaminofluorene (DAF) to visualize LAC and PRX oxidative activity throughout stem development.

Finally, to quantify H_2O_2 production in stem tissues throughout growth, I used TMB and the fluorescent dye 2',7'-dichlorodihydrofluorescein diacetate (H_2DCF).

Chapter 2: Materials and Methods

2.1 Plant material and growth conditions

All plants employed in this study are from *Arabidopsis thaliana* (Arabidopsis), background Columbia-0 (Col-0). *prLAC4::LAC4-mCherry*, *prLAC17::LAC17-mCherry*, *prUBQ10::LAC4-mCherry* and *prUBQ10::sec-mCherry* seeds were provided by Dr. Mathias Schuetz and Eva Chou (Chou et al., 2018; Schuetz et al., 2014). *prPRX64::PRX64-mCherry* seeds (Lee et al., 2013) were provided by Dr. Niko Geldner (University of Lausanne, Switzerland). The double *lac4-2/lac17* mutants (Berthet et al., 2011) and *prx64* null mutants (SALK_203548) were provided from Dr. Richard Sibout (French National Institute for Agricultural Research, France) and Dr. Qiao Zhao (Tsinghua University, China), respectively.

Seeds were surface-sterilized using chlorine gas and plated on germination media (GM; 1X Murashige-Skoog (MS), 1% Sucrose, 1X Gamborg's Vitamin mix, 0.05% MES, at pH 5.8) and 0.75% (w/v) agar. Following sterilization, seeds were vernalized for 3-4 days at 4°C in the dark. Seeds were transferred to 21°C under 24-hour light for 7 days before being transferred to soil (Sungro Sunshine Mix 4). Seedlings on soil were grown at 21°C for 18-hour light cycles.

2.2 Plant DNA extraction

Plant genomic DNA was extracted from 1-week-old Col-0 seedlings. Approximately 4-5 seedlings were ground in extraction buffer (200mM Tris-HCl pH 7.5, 250mM NaCl, 25mM Na_2EDTA, 0.5% SDS) and centrifuged. DNA was precipitated from the supernatant using isopropanol and pelleted. The pelleted DNA precipitate was washed twice with 70% ethanol, air-dried for 10 minutes, and resuspended in H_2O. DNA was quantified using a NanoDrop8000 spectrophotometer (ThermoFisher Scientific) and stored at -20°C.

2.3 Cloning LACs and PRXs under the respective native promoter and ectopically under prCESA7

For endogenous localization experiments, the open reading frame and approximately 2kb of the upstream putative promoter sequence for *AtLAC10* (At5g01190), *AtPRX42* (At4g21960), *AtPRX52* (At5g05340), *AtPRX71* (At5g64120), and *AtPRX72* (At5g66390) was amplified from genomic DNA using KAPA HiFi Hotstart ReadyMix® (Kapa Biosystems™). For expression under the

promoter of *AtCESA7* (prCESA7; At5g17420), the coding sequence (CDS) of *AtLAC4* (At2g38080), *AtLAC17* (At5g60020), and *AtPRX64* (At5g42180) was amplified from genomic DNA using KAPA HiFi Hotstart ReadyMix® (Kapa Biosystems™). Invitrogen™ Gateway® attB adaptor sequences with a modified stop codon (NSC) were added to gene products for addition of a C-terminal fusion protein. Amplified products were purified using the Qiagen™ QIAquick PCR Purification® Kit according to manufacturer's instructions. Genomic DNA (gDNA) primers and attB adaptors for the native promoter and promoter swap experiments are listed in Tables 2.1 and 2.2 below, respectively. gDNA primers were designed using Primer3 (Kõressaar et al., 2018).

Table 2.1. List of primers used for genomic and attB adaptor PCRs for endogenous localization. AttB adaptor is underlined.

Primer	Sequence (5'→3')
prLAC10:::LAC10 gDNA FW	ACAAACAATCGAGCAAACAAGC
prLAC10::LAC10 gDNA RV	TGACATTGCACCTACTCATTCA
prLAC10::LAC10 attB1 FW	GGGGACAAGTTTGTACAAAAAAGCAGGCTCACTACTCAACCATTCGTT
prLAC10::LAC10 attB2 NSC RV	GGGGACCACTTTGTACAAGAAAGCTGGGTCACATTTGGGAAGATCACTT
prPRX42::PRX42 gDNA FW	CGGTGGTCACAGTTCATTCA
prPRX42::PRX42 gDNA RV	CTTGTGGCCCGTTTCTCTTA
prPRX42::PRX42 attB1 FW	GGGGACAAGTTTGTACAAAAAAGCAGGCTGGAAAATCCAAATATCC
prPRX42::PRX42 attB2 NSC RV	GGGGACCACTTTGTACAAGAAAGCTGGGTCATGGTTCTTGTTTGCGAGA
prPRX52::PRX52 gDNA FW	TGTTCAAATGGCCCAATAACAA
prPRX52::PRX52 gDNA RV	GAAATCTCTCCCGCTTCAAAGA
prPRX52::PRX52 attB1 FW	GGGGACAAGTTTGTACAAAAAAGCAGGCTCATGTAAAGTAGTCAGTT
prPRX52::PRX52 attB2 NSC RV	GGGGACCACTTTGTACAAGAAAGCTGGGTCGTTGGTCCTCCCGCAAACC
prPRX71::PRX71 gDNA FW	CCCACTAATTGCCGGATTCC
prPRX71::PRX71 gDNA RV	ACCACACTCGAAACAAGTACT
prPRX71::PRX71 attB1 FW	GGGGACAAGTTTGTACAAAAAAGCAGGCTGGGCAGTCTGTTATCGACTCTTC
prPRX71::PRX71 attB2 NSC RV	GGGGACCACTTTGTACAAGAAAGCTGGGTCATTAACCGCAGAGCAAACC
prPRX72::PRX72 gDNA FW	GATACGGAACTGGTGGTGGT
prPRX72::PRX72 gDNA RV	AGTAGATGGAAGATTCGCCGT
prPRX72::PRX72 attB1 FW	GGGGACAAGTTTGTACAAAAAAGCAGGCTCGTATAACAGGAGGATGATGGACA
prPRX72::PRX72 attB2 NSC RV	GGGGACCACTTTGTACAAGAAAGCTGGGTAATAAGCATGGTTAACCCTCCGA

Table 2.2. List of primers used for genomic and attB adaptor PCRs for expression under prCESA7. AttB adaptor is underlined.

Primer	Sequence (5'→3')	Reference
AtLAC4 CDS gDNA FW	TCTTGGGTTTGGTCAGAGAGA	
AtLAC4 CDS gDNA RV	ACCGAACCTTTTGCTTTGCT	
AtLAC4 CDS attB1 FW	GGGGACAAGTTTGTACAAAAAAGCAGGCTTCGAGAGGGAGATGGGGTCT	
AtLAC4 CDS attB2 NSC RV	GGGGACCACTTTGTACAAGAAAGCTGGGTCGCACTTGGGAAGATCCTT	
AtLAC17 CDS gDNA FW	TTCACCTAAAAGGTGGCTAGTT	Schuetz et al., 2014
AtLAC17 CDS gDNA RV	CAGAAAACAGAGCTGTGCAA	Schuetz et al., 2014
AtLAC17 CDS attB1 FW	GGGGACAAGTTTGTACAAAAAAGCAGGCTGCCACTTTACTACGTAGTAATTG	Schuetz et al., 2014
AtLAC17 CDS attB2 NSC RV	GGGGACCACTTTGTACAAGAAAGCTGGGTCGCATTTGGGCAAGTCT	Schuetz et al., 2014
AtPRX64 CDS gDNA FW	TCCACCACAACCAAAATTAAACG	
AtPRX64 CDS gDNA RV	AGACCTAGGTTGCTGTCATGT	
AtPRX64 CDS attB1 FW	GGGGACAAGTTTGTACAAAAAAGCAGGCTTCGATCCATTCTTCATCACA	
AtPRX64 CDS attB2 NSC RV	GGGGACCACTTTGTACAAGAAAGCTGGGTCTTTGCGAACCCTTCTGCAGT	

2.4 Transformation of Arabidopsis with fluorescently tagged LACs and PRXs

Antibiotics used for selection during cloning were zeocin (50µg/mL), kanamycin (50µg/mL), gentamicin (50µg/mL), and hygromycin (25µg/mL).

2.4.1 Transformation of constructs into *E. coli*

Genomic DNA with attB adaptor fragments were cloned into the Invitrogen™ Gateway® pDONR-zeo vector using Invitrogen™ Gateway® BP cloning technology (Curtis, 2003). pDONR-zeo vectors were transformed into Invitrogen™ One Shot® TOP10 Chemically Competent *Escherichia coli* (*E. coli*) using a heat-shock protocol at 42°C for 30 seconds. Transformed *E. coli* were plated on Luria-Bertani (LB) broth plus 0.75% agar containing zeocin and grown overnight at 37°C. Resistant colonies were grown overnight in liquid LB broth containing zeocin. Vectors were purified using the Qiagen™ QIAprep Spin Miniprep® Kit and sequenced using GenScript® DNA sequencing services according to manufacturer's instructions.

For endogenous localization, confirmed pDONR transformants were then used in Gateway® LR cloning reactions and cloned into a modified pMDC111-mCherry vector (Schuetz et

al., 2014). For expression of *AtLAC4*, *AtLAC17*, and *AtPRX64* under prCESA7, confirmed pDONR transformants were cloned into a modified pMDC111-mCherry vector with a 1.1kb fragment of the upstream putative promoter of *AtCESA7* (Dr. Mathias Schuetz, unpublished). LR reactions were transformed into One Shot® TOP10 Chemically Competent *E. coli* using a heat-shock protocol at 42°C for 30 seconds. Transformed *E. coli* were grown on LB agar plates containing kanamycin overnight at 37°C. Resistant colonies were grown overnight in liquid LB broth containing kanamycin. Vectors were purified using the Qiagen™ QIAprep Spin Miniprep® Kit and sequenced using GenScript® DNA sequencing services according to manufacturer's instructions. Sequencing confirmed that the vectors showed no mutations and that the C-terminal mCherry fusion protein was in-frame.

2.4.2 Transformation of constructs into *Agrobacterium tumefaciens*

Selected pMDC111 vectors were transformed into *Agrobacterium tumefaciens* (Agrobacterium) strain GV3101 using electroporation. Electroporated cells were immediately transferred to chilled Super Optimal broth with Catabolite repression (SOC) media. Transformed Agrobacterium cells were then incubated at 28°C for a 4-6 hours at 200 rpm. Cells were plated on LB agar plates containing kanamycin and gentamicin antibiotics and incubated for 24-48 hours at 30°C. Resistant colonies were selected to transform into Arabidopsis.

2.4.3 Transformation of constructs into Arabidopsis

Selected Agrobacterium colonies transformed with the given destination vector were cultured in Yeast Extract Beef (YEB) broth containing kanamycin and gentamicin antibiotics at 28°C for 48 hours at 200 rpm. After 48 hours, cultures were transferred to fresh YEB broth without antibiotics and incubated at 200 rpm at 28°C for 8 hours. Before dipping, 0.02% Silwet L-77® (GE Silicones™) was added to the cultures. Arabidopsis Col-0 plants with young flowers (approximately 4-5 weeks old) were transformed using the floral dip method (Clough & Bent, 1998). Plants were kept overnight at room temperature in a dark, humid environment before being returned to growth chambers.

2.4.4 Screening transformed plant lines

T1-generation transformed seeds were surface sterilized, vernalized for 3-4 days at 4°C and grown on GM plates containing hygromycin. Resistant seedlings were transferred to soil after 1 week. Screening for presence of -mCherry was performed using hand sections of T1-generation stems on a Leica DMR compound microscope equipped with an EBQ 100 Isolated mercury lamp with a filter cube for RFP (excitation 540-560nm/emission 595nm). T2-generation seeds from confirmed T1-generation plants were collected. All subsequent microscopy and quantitative analyses were performed on T2-generation lines. Results were consistent for at least 3 independent lines for each construct.

2.5 Stem sampling protocol

For developmental analyses, inflorescence stems from the T2-generation were sampled at a height of 16-18cm, approximately 5 weeks after germination. Stems were divided into 2cm pieces (starting measurement from the apical tip of the stem) for a total of 8 developmental stages. Stem hand cross-sections from each developmental stage were cut using a double-edged razor in a drop of water under a dissecting scope. For analysis of mature stems, 10-week-old/approximately 35-40cm tall T2-generation plants were sampled at the base of the stem. Mature stem hand cross-sections were cut and processed as per developmental analyses.

Stem cross-sections were fixed in a solution of 4% (w/v) paraformaldehyde buffered in 1X PME (0.5M PIPES pH 7.4, 0.05M $MgSO_4$, 0.05M EGTA pH 7.5) for 1 hour at room temperature. Stem sections were rinsed three times in 1X TBST (10mM Tris pH 7.0, 0.25M NaCl, 0.1% Tween20) and stored in 1X TBST at 4°C for up to a month.

2.6 Lignin histochemistry of Arabidopsis stems

2.6.1 UV autofluorescence

Location of lignin was performed using lignin UV autofluorescence of stem cross-sections under the 405/UV laser (excitation 405nm, emission 440-510nm) on the spinning disk confocal microscope. To compare lignin deposition at different developmental stages, images were taken

maintaining the same microscope conditions (exposure time, sensitivity, and beam intensity) for all developmental stages and between biological replicates in the same plant line.

2.6.2 Phloroglucinol-HCl staining

Arabidopsis stem cross-sections were incubated in 10% (w/v) phloroglucinol (Fisher Scientific Canada) dissolved in 95% ethanol for 1 minute. A drop of concentrated hydrochloric acid was added to the solution and immediately imaged using a Leica DMR compound microscope.

2.6.3 Safranin-O/astra blue dual staining

Stem hand cross-sections were stained for 1 minute in a 1% (w/v) solution of safranin-O (MCB) and rinsed three times in H_2O. Stems were then stained with 1% (w/v) solution of astra blue (Sigma) dissolved in 2% (v/v) aqueous tartaric acid for 1 minute. Stems were rinsed three times in H_2O, and imaged on the Leica DMR compound microscope equipped with an EBQ 100 isolated mercury lamp. UV light (excitation 340-380 nm, 400nm emission) was used to visualize relative lignin concentration.

2.7 Immunolocalization of pectin and xylan

2.7.1 Fixation, embedding, and sectioning stem tissue

16-18cm Arabidopsis Col-0 stems were sampled and divided into 2cm long segments, as per developmental analyses. Developmental stages corresponding to 4cm, 6cm, 8cm, 10cm, and the base of the stem were fixed in a 4% paraformaldehyde solution buffered with 1X PME overnight at 4°C. Stem samples were rinsed three times in 1X TBST and dehydrated using a graded ethanol series. Samples were slowly infiltrated with increasing amounts of London Resin (LR) white (Electron Microscopy Sciences) resin over 4 days and embedded in sealed Beem capsules at 60°C for 72 hours. 1µm-thick samples were sectioned using a Leica UCT microtome and mounted on clean glass slides coated with poly-L-lysine (1mg/mL). Fixation and embedding was repeated for three biological replicates.

2.7.2 Immunolabeling of pectin and xylan in stem cross-sections

For immunolabeling of xylan and pectin, sections were first blocked in 5% (w/v) non-fat dry milk in 1X TBST for 20 minutes. Sections were briefly rinsed in 1X TBST and then incubated in a 1:50 dilution of primary antibodies in 1X TBST for 1 hour at room temperature. The primary antibodies used include LM10 for xylan (McCartney et al., 2005) or JIM7 for methylesterifed pectin (Knox et al., 1990). Slides were rinsed twice in 1X TBST for 10 minutes each. Sections were then incubated in a 1:100 dilution of the secondary antibody goat anti-rat IgG labeled with Alexa488 (Molecular Probes) in 1X TBST for 1 hour at room temperature in the dark. Slides were rinsed twice in 1X TBST for 10 minutes each before being mounted in glycerol and stored at 4°C in the dark until imaged on the Perkin Elmer spinning disk confocal. The 488-GFP filter (excitation 488nm, emission 525nm) was used to image Alexa488 labeled antibodies. Negative control samples were incubated with no secondary antibody and were instead replaced with the same amount of 1X TBST.

2.8 Methanol treatment to remove soluble phenolics

16-18cm tall Col-0 stems were hand-sectioned as per developmental analyses. Half of the stem cross-sections for a given developmental stage were incubated in 1mL of 100% methanol for 1 hour, while gently shaking. The other half of the stem cross-sections were mock-treated in 1mL of H_2O for one hour. Stem cross-sections were rinsed twice before fixation in 4% paraformaldehyde solution buffered with 1X PME for 1 hour at room temperature. Stem samples were rinsed and stored in 1X TBST. For quantification of UV lignin autofluorescence between control and methanol-treated stem samples, images were taken on the Perkin Elmer spinning disk confocal under the 405/UV laser (excitation 405nm, emission 440-510nm) while maintaining the same microscope conditions (exposure time, sensitivity, and beam intensity) for all developmental stages and between treatments. Data is representative of three biological replicates per treatment for two independent experiments.

2.9 LAC and PRX histochemistry

2.9.1 TMB histochemistry

To visualize PRX activity, 16-18cm tall Col-0 stems were sampled as per developmental analyses and incubated in 100µM 3,3',5,5'-tetramethylbenzidine (TMB; Acros Organics) for 1 hour in the dark, with gentle shaking. For TMB + H_2O_2 analysis, stem cross-sections were incubated in a solution of 100µM TMB and 100µM H_2O_2 for 1 hour in the dark, with gentle shaking. PRX enzymatic activity could be visualized by formation of a blue precipitate on stem samples. Stem sections were rinsed twice in H_2O and imaged on the Leica DMR compound microscope. Treatments were repeated for 5 biological replicates.

2.9.2 Controls for TMB histochemistry

To test for involvement of proteins, stem cross-sections were boiled in a 100°C water bath for 10 minutes, then incubated in TMB, as outlined above. To inhibit PRXs, stem cross-sections were pre-treated in 100mM salicylhydroxamic acid (SHAM; Sigma-Aldrich) for 1 hour with shaking, then incubated in TMB. To remove endogenous H_2O_2, stem cross-sections were incubated in 300U/mL bovine liver catalase (Sigma) for 2 hours with shaking, then incubated with TMB. All control experiments were repeated for at least three biological replicates with consistent results.

2.9.3 DAF histochemistry

To visualize LAC and PRX activity, 16-18cm tall Col-0 stems sampled as per developmental analyses were incubated in a 0.68mM solution of 2,7-diaminofluorene (DAF; Sigma-Aldrich) in 20mM BisTris pH 5.9 for 30 minutes in the dark, with gentle shaking. LAC and PRX enzymatic activity could be visualized by formation of a purple precipitate on stem samples. To compare DAF oxidation in stems with significantly reduced LAC enzymatic activity, 16-18cm tall *lac4-2/lac17* double mutant stems (Berthet et al., 2011) were incubated as per Col-0. Stem sections were rinsed twice in H_2O and imaged on the Leica DMR compound microscope. Treatments were repeated for 5 biological replicates per background.

2.10 Localization of ROS in stem cross-sections

2.10.1 H_2DCF staining

16-18cm tall Col-0 stems were sectioned as per developmental analysis and incubated in H_2O for approximately 24 hours at room temperature to reduce wound response. For collapsed interfascicular fiber phenotyping, stem cross-sections from the base of mature 10-week-old *prCESA7::PRX64-mCherry* T2-generation stems were incubated in H_2O for approximately 24 hours at room temperature to reduce wound response. A 10mM stock solution of 2',7'-dichlorodihydrofluorescein diacetate (H_2DCF; Thermo Fisher Scientific) was prepared in dimethylsulfoxide (DMSO) and stored at -20°C in the dark. Stem sections were incubated in a working stock of 50µM solution of H_2DCF in 50mM NaH_2PO_4, pH 6.0 for 15 minutes in the dark. Staining solution was made fresh the day-of use. The 488-GFP filter (excitation 488nm, emission 525nm) on the spinning disk confocal was used to image H_2DCF fluorescence. For quantification of H_2DCF fluorescence intensity, the same microscope conditions (exposure time, sensitivity, and beam intensity) were used for all developmental stages. Data is representative of three biological replicates for four independent experiments.

2.10.2 Controls for H_2DCF staining

All controls for H_2DCF staining were performed on stem cross-sections from the base of 17cm-tall Col-0 plants. To test for ROS-induced wounding response, stem cross-sections were hand sectioned and immediately placed in H_2DCF solution for 15 minutes in the dark and imaged. All other control experiments were first incubated in H_2O for 24 hours to reduce wound response. To inhibit PRXs, stem cross-sections were pre-treated in 100mM SHAM for 1 hour while shaking, then incubated in H_2DCF as described above. To inhibit NADPH oxidases, stem cross-sections were pre-treated in 1mM diphenyleneiodonium chloride (DPI; Sigma-Aldrich) for 2 hours while shaking, then incubated in H_2DCF. To remove endogenous H_2O_2, stem cross-sections were incubated in 300U/mL bovine liver catalase for 2 hours while shaking, then incubated in H_2DCF. The 488-GFP filter (excitation 488nm, emission 525nm) on the Perkin Elmer spinning disk confocal was used to image H_2DCF fluorescence. Data is representative of three biological replicates for four independent experiments.

2.11 Quantification of total stem H_2O_2

The H_2O_2 quantification protocol was adapted from Šola *et al.* (2019). Col-0 stems were sampled and sectioned into 2cm sections, as per developmental analyses. The fresh weight of the stem sections was measured and immediately frozen in liquid nitrogen. Stems were homogenized in 100mg polyvinylpyrrolidone (PVP; Sigma-Aldrich) in liquid nitrogen for 1 minute. 750µL of 0.1% (w/v) trichloroacetic acid was added and samples were homogenized for an additional 30 seconds. Solutions were centrifuged for 15 minutes at 12,000 *x g* at 4°C. 20µL of supernatant was added to 80µL of assay solution containing 50mM NaH_2PO_4 pH 6.0, 1U/mL horseradish peroxidase (HRP; Cedarlane Labs), and 100µM TMB. Absorbance at 562nm was immediately measured on a Synergy HT microplate reader (BioTek). Quantification was performed within the linear range (blue color). H_2O_2 concentration was calculated based on calibration curves of standards with known concentrations of H_2O_2 within a linear range. Control (H_2O) samples were loaded on the same 96-well plates in the same volumes as the stem extracts. All samples and standards were analysed in triplicates. Quantification was performed for eight biological replicates. Calibration curves were calculated from three replicates. Statistical differences between developmental stages were analyzed using a one-way ANOVA on Past3 (Hammer et al., 2001).

2.12 Localization of LACs and PRXs in root tissues

To study localization of LACs and PRXs in roots, surface sterilized seeds were plated on GM media and vernalized at 4°C for 2-3 days before being transferred to growth chambers. Seeds were grown vertically in 24-hour light conditions for 7 days before being mounted in H_2O and imaged on the Perkin-Elmer UltraView VoX spinning disk confocal. Root localization experiments were repeated at three independent times for each construct (3 lines/construct).

2.12.1 Mannitol plasmolysis

To study cell wall localization of *prCESA7::LAC4-mCherry*, *prCESA7::LAC17-mCherry*, and *prCESA7::PRX64-mCherry*, surface sterilized seeds were plated on GM media, vernalized at 4°C for 2-3 days before being transferred to growth chambers and grown vertically for 7 days in 24-

hour light conditions. Roots were plasmolyzed in 0.4M D-mannitol (Sigma-Aldrich) for 1 hour. Samples were mounted in 0.4M mannitol and imaged using the Perkin-Elmer UltraView VoX spinning disk confocal. Mannitol plasmolysis experiments were repeated three independent times.

2.12.2 Clearsee tissue clearing

To reduce intrinsic background autofluorescence of root tissues, samples were fixed and cleared in Clearsee solution according to the protocol outlined by Ursache *et al.* (2018). Root samples were fixed in a 4% paraformaldehyde solution buffered with 1X phosphate buffered saline (PBS; 0.137M NaCl, 2.7mM KCl, 10mM Na_2HPO_4, and 1.8mM KH_2PO_4; pH 7.4) for 1 hour at room temperature. Samples were washed twice in 1X PBS for 1 minute each before transferring into Clearsee solution containing 10% w/v xylitol (Sigma), 15% w/v sodium deoxycholate (Sigma-Aldrich), 25% w/v urea (Sigma) for up to one week. Clearsee solution was replaced every 2 days.

2.13 Real time-quantitative PCR (RT-qPCR) of Arabidopsis stems

50-100mg of plant tissue from the base of 16-18cm tall Arabidopsis stems was sampled and immediately frozen in liquid nitrogen. Samples were homogenized using a mortar and pestle and RNA was extracted using TRIzol™ (Life Technologies, USA) according to the manufacturer's instructions. RNA quantity was measured using a NanoDrop8000 spectrophotometer (ThermoFisher Scientific) and quality was assessed on a 1% agarose gel. RNA was stored at -80°C for up to one week. Genomic DNA was removed using DNaseI (NEB). Reverse transcription was performed with 5µg of total RNA with Superscript Reverse Transcriptase II (Invitrogen) using oligo-$(dT)_{12–18}$ primers, according to the manufacturer's instructions. cDNA was stored at -20°C.
Plant backgrounds used for RT-qPCR analysis include Col-0, *lac4-2/lac17*, *prx64* null, and two independent T2-generation lines each from *prCESA7::LAC4-mCherry*, *prCESA7::LAC17-mCherry*, and *prCESA7::PRX64-mCherry*. RNA extraction and cDNA synthesis were performed for four biological replicates from each background. RT-qPCR primers are listed in Table 2.2 below. *AtEF-1α* (At5g60390) was used as a reference gene due to stable expression in stem tissues (Czechowski et al., 2005).

Table 2.3. RT-qPCR primers used for expression analyses of promoter swap lines.

Primer	Sequence (5'→3')	Reference
AtLAC4 qPCR FW	TCCTTCAAGATACCGGCGTCA	Berthet et al., 2011
AtLAC4 qPCR RV	ACCGGATGGAACTCCGATTGT	Berthet et al., 2011
AtLAC17 qPCR FW	CGATAAACGGGCTTCCTGGTC	Berthet et al., 2011
AtLAC17 qPCR RV	AACCGTGTGATTTGCGATGCT	Berthet et al., 2011
AtPRX64 qPCR FW	GCCGACCACATTGTAACCAA	Li et al., 2018
AtPRX64 qPCR RV	TCTGACGAAACAGTCGTGGA	Li et al., 2018
AtEF-1α qPCR FW	CTGGAGGTTTTGAGGCTGGTAT	Berthet et al., 2011
AtEF-1α qPCR RV	CCAAGGGTGAAAGCAAGAAGA	Berthet et al., 2011

qPCR was performed on a Bio-Rad iQ5 thermal cycler using iQ SYBR Green (Bio-Rad) in a 10µl reaction mixture. Amplification was carried out as follows: initial denaturation step at 94°C for 2 minutes, 40 cycles at 95°C for 15 seconds, and 60°C for 1 minute. All reactions were performed for three technical replicates for three biological replicates. No-template (H_2O) controls were included in each run. The $2^{-\Delta\Delta Ct}$ relative quantification strategy (Livak & Schmittgen, 2001; Schmittgen & Livak, 2008) was used to calculate relative transcript levels compared to Col-0.

2.14 *prx64* null phenotyping

2.14.1 Genotyping for T-DNA insertion

prx64 null mutants (SALK_203548) were provided from Dr. Qiao Zhao (Tsinghua University, China). Plants were first confirmed to be homozygous for the T-DNA insert using the gene specific primers listed in Table 2.4 below and the T-DNA specific primer LBb1.3. Primers were designed using the SALK T-DNA Primer design tool (http://signal.salk.edu/tdnaprimers.2.html). The presence of a 1kb band indicated the presence of a wild-type gene copy, whereas the presence of an 500bp band indicated T-DNA insertion amplicons. Homozygous plants for the T-DNA insertion were used for further mutant phenotyping.

Table 2.4. T-DNA insertion primers used for genotyping *prx64* null plants.

Primer	Sequence (5'→3')
AtPRX64 gene specific FW	CCACACATATTATTGCTCTAGTC
AtPRX64 gene specific RV	TCCTGACTATAGTAACATCCAC
LBb1.3 FW	ATTTTGCCGATTTCGGAAC

2.14.2 RT-qPCR of *prx64* null stems

Quantification of gene expression for *prx64* null plants was performed as part of the RT-qPCR experiment for *prCESA7::PRX64-mCherry*, as described in Chapter 2.13.

2.14.3 Cell corner UV lignin autofluorescence quantification

UV lignin autofluorescence in the cell corners of interfascicular fibers was measured on stem cross-sections from the base of 17cm-tall Col-0 and *prx64* null plants. Cross-sections were fixed in a solution of 4% (w/v) paraformaldehyde buffered in 1X PME for 1 hour at room temperature. Stem sections were rinsed three times in 1X TBST and stored at 4°C for up to a month. Stem UV lignin autofluorescence was imaged using the 405/UV laser (excitation 405nm, emission 440-510nm) on the spinning disk confocal microscope. To compare lignin deposition between genotypes, images were taken maintaining the same microscope conditions (exposure time, sensitivity, and beam intensity) for all stages. Quantification was performed for 5 biological replicates per genotype for two independent experiments. Areas of interest (cell corners) were drawn by hand using FIJI. A student's t-test between genotypes conducted using Past3 (Hammer et al., 2001).

2.14.4 Propidium iodide uptake assay

To screen for a functional Casparian strip in *prx64* null mutants, a propidium iodide (PI) uptake assay was performed as described by Alassimone *et al.* (2010). 1-week-old roots were incubated in 15µM PI (Invitrogen) for 10 minutes in the dark. PI staining was imaged using the 561/RFP filter (excitation 561nm, emission 595-625nm) on the Perkin Elmer spinning disk confocal microscope. Results were consistent for five seedlings for *prx64* null and Col-0 for four independent experiments.

2.15 Calculation of corrected fluorescence

For quantification of UV lignin autofluorescence and mCherry-tagged enzymes, images were taken on the Perkin Elmer spinning disk confocal while maintaining the same microscope conditions (exposure time, sensitivity, and beam intensity) for all developmental stages and between biological replicates in the same plant line. Microscope conditions were optimized to minimize pixilated regions. Corrected fluorescence minus background signal was calculated from images using FIJI (Schindelin et al., 2012) according to the methodology of Bankhead (2014). Areas of interest (SCWs vs. cell corners) were drawn by hand. To calculate differences between developmental stages or genotypes, a student's t-test or ANOVA followed by a Tukey-Kramer *post-hoc* test were conducted using Past3 (Hammer et al., 2001).

2.16 Bioinformatics and phylogenetic tree construction

Tissue expression data for LACs and PRXs was collected from the BAR ePlant browser (bar.utoronto.ca/eplant; Waese et al., 2017) and the Genevestigator website (www.genevestigator.ethz.ch; Hruz et al., 2008). Lists of most significantly co-expressed genes was generated from Genevestigator and annotated using TAIR (Berardini et al., 2015).

Amino acid sequences for 17 LACs and 73 Class III PRXs from Arabidopsis were downloaded from TAIR10 (Berardini et al., 2015). Phylogenetic analysis and tree reconstruction was performed using MEGA7 (Kumar et al., 2016). Sequences were aligned using MUSCLE (Edgar, 2004) and phylogenetic trees were reconstructed using p-distances and the Neighbor Joining (NJ) method, with 1000 bootstrap replicates.

2.17 Brightfield microscopy and epifluorescence microscopy

Histochemistry treatments of Arabidopsis stem cross-sections were imaged using a Leica DMR compound microscope equipped with 10X and 63X objective lenses. Images were taken using the Qcapture digital camera (QImaging) and OpenLab imaging/Canon EOS Rebel T5 and EOSUtility software. All images were processed using FIJI (Schindelin et al., 2012).

Fluorescence imaging of -mCherry lines and lignin autofluorescence of Arabidopsis stem sections was performed using a Leica DMR compound microscope equipped with an EBQ 100

Isolated mercury lamp. UV (excitation 340-380 nm, 400nm emission) was used to detect lignin autofluorescence and the TX2 filter cube (excitation filter at 540-560 nm, 595 nm emission) was used to detect -mCherry. Images were taken using the Qcapture digital camera (QImaging) and OpenLab imaging/Canon EOS Rebel T5 and EOSUtility software. All images were processed using FIJI (Schindelin et al., 2012).

2.18 Spinning disk confocal microscopy

Arabidopsis plants were imaged using the Perkin-Elmer UltraView VoX spinning disk confocal mounted on a Leica DM16000 inverted microscope with a Hamamatsu 9100-02 CCD camera. The 405/UV filter (excitation 405nm, emission 440-510nm) was used to image lignin autofluorescence. The 488/GFP filter (excitation 488nm, emission 525nm) was used to image Alexa488-labeled antibodies and H_2DCF. The 561/RFP filter (excitation 561nm, emission 595-625nm) was used to image mCherry-tagged enzymes and the fluorescent dye PI. All images were processed using Volocity image analysis software (Improvision) and FIJI (Schindelin et al., 2012). Heatmaps to visualize fluorescence intensity were generated on FIJI by applying a LUT filter to a 32-bit image.

Chapter 3: LACs and PRXs localize to discrete cell types and regions of the cell wall

3.1 Introduction

Identification of LACs and PRXs specifically involved in lignification has been hindered due to large gene families, functional redundancy, and diverse roles in plant development (Passardi et al., 2005; Turlapati et al., 2011). Therefore, it is necessary to take a targeted approach to identify potential lignin-associated LACs and PRXs prior to *in-planta* functional characterization. Specific candidate genes can be isolated using previous phenotypic analyses of mutant plants and *in-silico* evidence for involvement in lignification. Bioinformatic data, such as abundant expression in the lignifying stem and co-expression patterns with other SCW genes, could suggest involvement of a particular LAC or PRX in lignification. Use of co-expression data is based on the rationale that genes with similar expression patterns could likely be involved in the same biological process (Persson et al., 2005; Wang et al., 2013).

However, to understand the role of a LAC or PRX in lignification it is necessary to demonstrate that the enzyme localizes to the cell wall of lignifying tissue. This can be achieved by attaching a fluorescent tag to the enzyme, studying its localization using confocal microscopy, and comparing it to the distribution of lignin. As a phenolic polymer, lignin naturally autofluoresces under ultraviolet (UV) light (Lin & Dence, 1992). Historically, this property has been used to identify location as well as relative concentration of lignin in cell walls (Donaldson, 2001; Fergus et al., 1969). Therefore, co-localization of a tagged putative lignin-associated LAC or PRX and UV lignin autofluorescence can provide additional evidence for a given enzyme's involvement in lignification.

Recent localization of AtLAC4-mCherry to the SCW of xylem vessel elements and fibers and AtPRX64-mCherry to the cell corners of fibers demonstrated that these oxidative enzymes localize to specific cell types and regions of the cell wall (Chou et al., 2018). Nevertheless, little is known about the localization of other LACs and PRXs hypothesized to be involved in lignification or the underlying cellular mechanisms that determine cell wall protein localization. Spatially distinct localizations of cell wall proteins could be due to differential expression, either in alternative cell types or during a different stage of development (Hatton et al., 1995; Pumplin et al., 2012). In addition, structural features of proteins, such as protein mobility or binding to cell

wall proteins or polysaccharides, may also impact protein localization to a particular region of the cell wall (Chou et al., 2018; Francoz et al., 2019; Lee et al., 2013). Previous work has shown that the timing of gene expression, based on the promoter sequence of a gene, was both necessary and sufficient to dictate when and where specific proteins localize during arbuscular mycorrhizal symbiosis in *Medicago truncatula* (Pumplin et al., 2012). However, it is unknown whether this is a common feature of secreted proteins. Therefore, identifying the location of different LACs and PRXs under their respective native promoter and a non-native promoter can not only suggest the specific function of an enzyme within a cell type or region of the cell wall, but will also provide a more thorough understanding of the mechanisms underlying protein localization in the cell wall.

Based on the published literature, I hypothesized that certain LAC and PRX isoforms are specifically involved in lignification and are co-expressed with SCW biosynthetic genes. I also predicted that these putative lignin-associated LACs and PRXs would localize to lignified SCWs.

I had the following three research objectives:

1) Identify putative lignin-associated LACs and PRXs in Arabidopsis using bioinformatic tools.
2) Spatially map the localization of putative lignin-associated LACs and PRXs in the inflorescence stem using native gene promoter regions.
3) Test whether AtLAC4, AtLAC17 and AtPRX64 localization is dependent on timing of expression.

In this chapter, I first used a combination of publicly-available literature and resources, such as mutant analyses, gene expression levels, and co-expression data, to identify a short-list of putative lignin-associated LACs and PRXs for further study. Enzymes were selected based on three criteria: (i) published literature reporting single-, double-, or triple-mutants with lignin-defect phenotypes; (ii) evidence of gene expression in the lignifying stem of Arabidopsis; and (iii) co-expression with SCW biosynthetic pathways. Putative lignin-associated LACs and PRXs were localized with a red fluorescent protein (-mCherry tag) and each showed a distinctive localization pattern, both to a given cell type as well as region of the cell wall. Interestingly, not all selected

LACs and PRXs localized to lignified tissues. To test whether timing of expression determines enzyme localization in the cell wall, I expressed *AtLAC4*, *AtLAC17*, and *AtPRX64* under the promoter of the cellulose synthase gene *AtCESA7*, which is highly expressed in cells forming SCWs (Brown et al., 2005; Smith et al., 2013). I show that changing the promoter sequence is sufficient to alter localization patterns in root and stem tissues. In the stem, ectopic expression of LACs and PRXs under the *AtCESA7* promoter resulted in abnormal SCW structure and lignification, suggesting that LAC and PRX expression and localization is highly regulated during growth.

3.2 Results

3.2.1 Identification of putative lignin-associated LACs and PRXs

To prioritize LACs and PRXs that are putatively involved in lignification, I first created a short-list of enzymes implicated in lignification from previous single-, double-, and triple- mutant analyses (Tables 1.1-1.3). I selected *AtLAC4*, *AtLAC11*, *AtLAC12*, and *AtLAC17,* and *AtPRX2*, *AtPRX4*, *AtPRX25*, *AtPRX52*, *AtPRX64*, *AtPRX71*, and *AtPRX72* as putative candidates for LAC or PRX-mediated cell wall lignification, respectively. In addition, I further refined this gene list using publicly-available bioinformatics tools. Using the rationale that LACs or PRXs involved in lignification should be highly expressed in lignified stem tissue, I evaluated gene expression levels in the stem of Arabidopsis using two independent expression datasets from previous microarray experiments (Figure 3.1; Hall & Ellis, 2013; Schmid et al., 2005). Finally, I evaluated co-expression networks of selected genes using Genevestigator, which uses clustering and bi-clustering algorithms to identify genes sharing similar expression patterns across RNA-sequencing arrays (Hruz et al., 2008; Laule et al., 2006). Co-expression gene lists were annotated using TAIR (Berardini et al., 2015) and were assessed for involvement in various biological processes. The combination of mutant phenotypes, transcript abundance in the stem, and co-expression network analyses therefore provided multiple lines of evidence for involvement in lignification for the selected LACs and PRXs.

Transcriptomic data showed moderate to high expression of *AtLAC4*, *AtLAC10*, *AtLAC11*, *AtLAC12*, and *AtLAC17* in the inflorescence stem (Figure 3.1a,c), and therefore these genes were good candidates for future study. In addition, co-expression analyses showed that these LACs

were significantly co-expressed with each other and SCW cellulose and xylan biosynthetic genes (Figure 3.2). *AtLAC4* is highly expressed in stem tissue and is co-expressed with *AtLAC11, AtLAC17*, and SCW polysaccharide biosynthetic genes (Figure 3.2a). Despite not showing a lignin phenotype in single mutant plants, *AtLAC10* is expressed in stem tissues and is co-expressed with SCW cellulose synthases and xylan biosynthetic genes (Table 1.1; Figure 3.2b). *AtLAC10* is also co-expressed with genes involved in defense responses and pectin biosynthesis (Figure 3.2b). *AtLAC11* is expressed in multiple tissues and is co-expressed with *AtLAC4*, *AtLAC17*, and SCW cellulose synthases (Figure 3.2c). *AtLAC12* is highly expressed in the stem and is co-expressed with *AtLAC2*, SCW cellulose synthases, and xylan biosynthetic genes (Figure 3.2d). Finally, *AtLAC17* is highly expressed in the stem and is significantly co-expressed with *AtLAC4*, *AtLAC11,* and SCW polysaccharide biosynthetic genes (Figure 3.2e). Phylogenetic analyses using amino acid sequences of the 17 Arabidopsis LACs showed that all identified putative lignin-associated LACs other than AtLAC12 cluster together, indicating high amino acid similarity and potential involvement in similar biological roles (asterisks, Figure 3.2f). Along with their strong co-expression patterns with other SCW genes, these LACs formed a clear set of candidate genes with putative involvement in lignification.

In contrast, transcriptomic analysis of PRXs in Arabidopsis stem tissues revealed highly variable expression among genes, with most being expressed at very low levels (Figure 3.1b,d). Due to low expression of *AtPRX2*, *AtPRX4*, *AtPRX17*, and *AtPRX25* in stem tissues, I did not include them in further tests (Figure 3.1d). In contrast, *AtPRX42*, *AtPRX52*, *AtPRX64*, *AtPRX71*, and *AtPRX72* were consistently detected in Arabidopsis stems (Figure 3.1b,d) and therefore selected as putative lignin-associated PRXs for further study.

AtPRX42 was included in the list of putative lignin-associated PRXs due to abundant expression in stem tissue, despite not having any previous functional characterization in mutant plants (Figure 3.1b,d). Analysis of the eFP expression map and co-expression networks showed that *AtPRX42* is highly expressed in stem, root, leaf, and seed tissues, and co-expressed with genes involved in PCW cellulose and pectin biosynthesis or modification (Figure 3.3a). *AtPRX52* is not highly expressed in stem tissues on the eFP tissue map and is significantly co-expressed with cell wall signaling and defense genes (Figure 3.3b). *AtPRX52* was included in the list of

putative lignin-associated genes due to co-expression with *AtCCoAOMT*, a monolignol biosynthetic gene, and the significant decrease in lignin content in *prx52* mutants (Figure 3.3b; Fernández-Pérez et al., 2015). *AtPRX64* shows the highest expression of any PRX in stem tissues but is co-expressed with genes involved in root endodermis and Casparian strip development (Figure 3.1; 3.3c). *AtPRX71* has low to moderate expression in the stem and is also expressed in root, leaf, and flower tissues (Figure 3.3d). The co-expression network of *AtPRX71* is diverse and includes genes involved in response to biotic and abiotic stress as well as nutrient transport and metabolism (Figure 3.3d). *AtPRX72* has relatively low expression in stems and shows a similar endodermal-specific co-expression network as *AtPRX64* (Figures 3.1, 3.3e). It was included in the current study due to the reported irregular xylem phenotype in *prx72* mutant stems (Fernández-Pérez et al, 2015a; Herrero et al., 2013). Phylogenetic analysis of the amino acid sequences of the 73 Arabidopsis PRXs showed that none of the selected lignin-associated PRXs cluster together on a phylogenetic tree (asterisks; Figure 3.3f). Overall, the selected PRXs did not provide as clear co-expression and evolutionary relationships as the LAC genes. The bioinformatic analyses still provided useful information, *e.g.* to eliminate *AtPRX2*, *AtPRX4*, *AtPRX17*, and *AtPRX25* due to low gene expression in stems, despite reported phenotypes in mutants (Table 1.2).

In summary, I selected *AtLAC4*, *AtLAC10*, *AtLAC11*, *AtLAC12*, *AtLAC17, AtPRX42*, *AtPRX52*, *AtPRX64*, *AtPRX71*, and *AtPRX72* as putative lignin-associated LACs and PRXs. All selected LACs and PRXs have a connection to lignification, such as reduced lignin content in knockout mutants, high expression in the lignifying stem, or co-expression with SCW genes. Therefore, the combined use of bioinformatics and mutant data from the literature allowed identification of a subset of LACs and PRXs that may be involved in cell wall lignification for further analyses.

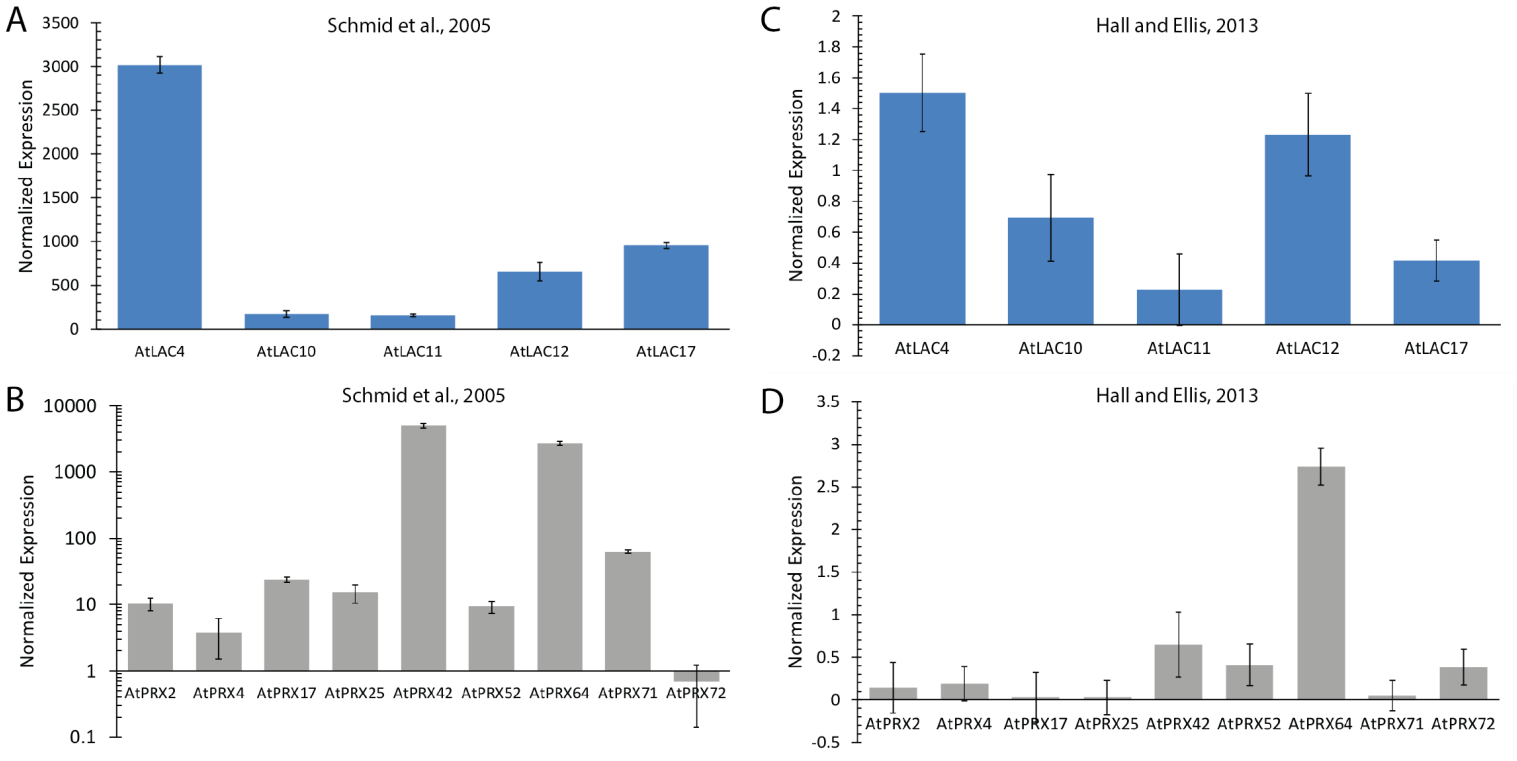

Figure 3.1. LACs and PRXs are differentially expressed in the inflorescence stem of Arabidopsis. A-B) Normalized gene expression values of Arabidopsis LACs and PRXs in stem tissue from the dataset of Schmid et al., (2005). Expression values are representative of three biological replicates. Bars are SD. A) Expression of putative lignin-associated LACs in stem tissues. B) Expression of putative lignin-associated PRXs in stem tissues. Normalized expression has a logarithmic scale for PRXs. C-D) Normalized gene expression values of Arabidopsis LACs and PRXs in stem tissue from the microarray dataset of Hall and Ellis (2013). Expression values were taken from the "cessation of growth" developmental stage and are representative of six biological replicates. Bars are SE. C) Expression of putative lignin-associated LACs in stem tissues. D) Expression of putative lignin-associated PRXs in stem tissues.

A AtGenExpress eFP: AT2G38080 / ATLMCO4, IRX12, LAC4, L

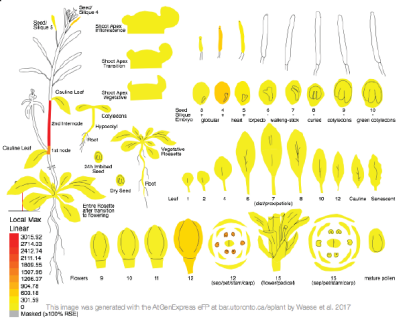

AtLAC4	
Gene	**Annotation**
CESA4	Cellulose synthase (SCW)
LAC17	LACCASE17
COBL4	COBRA-like protein4
CESA7	Cellulose synthase (SCW)
CESA8	Cellulose synthase (SCW)
LAC11	LACCASE11
XCP2	Xylem cysteine peptidase2
TED6	Tracheary element differentiation protein6
GDSL	Golgi esterase/lipase
GUX1	UDP-GlcA:xylan glucuronyltransferase
IRX9	IRREGULAR XYLEM9; xylan xylosyltransferase
XCP1	Xylem cysteine peptidase1

B AtGenExpress eFP: AT5G01190 / LAC10

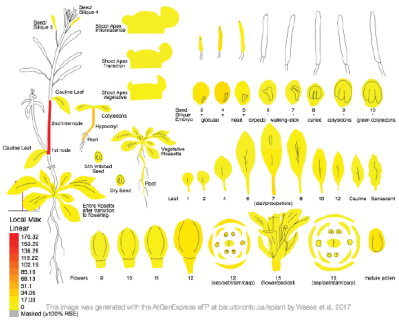

AtLAC10	
Gene	**Annotation**
GUX1	UDP-GlcA:xylan glucuronyltransferase
At5G38740	Probable LRR protein
IRX9	IRREGULAR XYLEM9; xylan xylosyltransferase
ARAC2	Rac-like GTP-binding protein
PME8	Pectin methylesterase8
MYB46	Transcription factor MYB46
NAC101	NAC domain-containing protein101
IRX10	IRREGULAR XYLEM10, beta-1,4-xylosyltransferase involved in xylan biosynthesis
At3G62160	HXXXD-type acyl-transferase family protein
RIC2	CRIB domain-containing protein RIC4
GAUT12	Galacturonosyltransferase; involved in pectin biosynthesis
CESA7	Cellulose synthase (SCW)
PLDε	Phospholipase Dε
IRX15	IRREGULAR XYLEM15; involved in xylan biosynthesis
CTL2	Chitinase-like protein2
AT5G30020	Pathogenesis related

C AtGenExpress eFP: AT5G03260 / LAC11

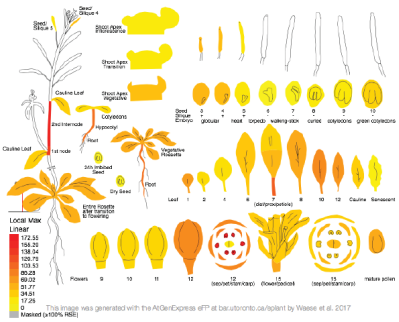

AtLAC11	
Gene	**Annotation**
LAC17	LACCASE17
XCP1	Xylem cysteine peptidase1
IRX12	LACCASE4
At5G40020	Pathogenesis related
RIC4	CRIB domain-containing protein RIC4
CESA4	Cellulose synthase (SCW)
TED6	Tracheary element differentiation protein6
GAUT12	Galacturonosyltransferase involved in pectin biosynthesis
COBL4	COBRA-like protein 4
CESA8	Cellulose synthase (SCW)
CESA7	Cellulose synthase (SCW)
MYB46	Transcription factor MYB46
At4G08160	Glycosyl hydrolase family

D AtGenExpress eFP: AT5G05390 / LAC12

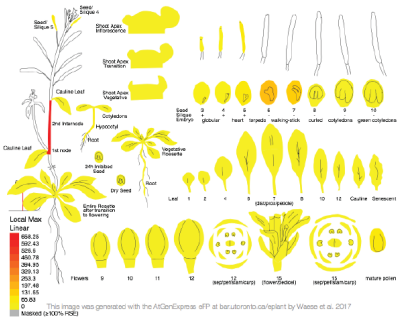

AtLAC12	
Gene	**Annotation**
LAC2	LACCASE2
At1G22480	Cupredoxin superfamily protein
IQD10	IQ-domain10
DICE1	DEFECT IN CELL ELONGATION1
COBL4	COBRA-like protein 4
NAC043	NAC domain-containing protein73
GXM1	GLUCURONOXYLAN METHYLTRANSFERASE1
AtMYB103	MYB domain protein 103
IRX15	IRREGULAR XYLEM15; involved in xylan biosynthesis
FAR6	fatty-acyl-CoA reducatase6
AtMYB52	MYB domain protein 53
GAUT12	Galacturonosyltransferase involved in pectin biosynthesis
CESA7	Cellulose synthase (SCW)
FLA12	Fasciclin-like arabinogalactan protein
CESA4	Cellulose synthase (SCW)

E AtGenExpress eFP: AT5G60020 / ATLAC17, LAC17

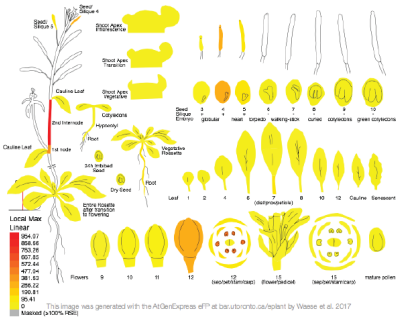

AtLAC17	
Gene	**Annotation**
CESA4	Cellulose synthase (SCW)
IRX12	LACCASE4
GAUT12	Galacturonosyltransferase involved in pectin biosynthesis
LAC11	LACCASE11
CESA8	Cellulose synthase (SCW)
RIC4	CRIB domain-containing protein RIC4
COBL4	COBRA-like protein 4
CESA7	Cellulose synthase (SCW)
GUX1	UDP-GlcA:xylan glucuronyltransferase
XCP1	Xylem cysteine peptidase1
XCP2	Xylem cysteine peptidase2
MYB46	Transcription factor MYB46
IRX9	IRREGULAR XYLEM9; xylan xylosyltransferase
TED6	Tracheary element differentiation protein6

F

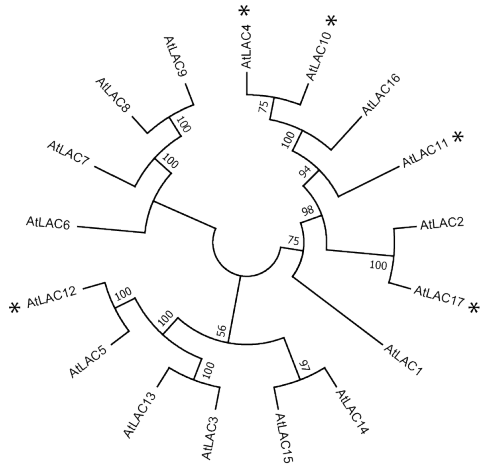

Figure 3.2. Putative lignin-associated LACs are identified through bioinformatics approaches. A-E) Tissue expression maps were generated using the eFP browser (Waese et al., 2017) and co-expression lists were generated using Genvestigator (Hruz et al., 2008). Gene lists were annotated using TAIR (Berardini et al., 2015). A) AtLAC4. B) AtLAC10. C) AtLAC11. D) AtLAC12. E) AtLAC17. F) Phylogenetic analysis of 17 Arabidopsis LAC peptide sequences. The tree was inferred using the Neighbour Joining (NJ) method, bootstrap replicates 1000, on MEGA7 (Kumar et al., 2016). Asterisks denote selected putative lignin-associated LACs selected in this study.

A AtGenExpress eFP: AT4G21960 / PRXR1

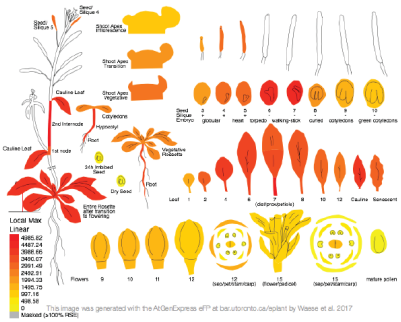

AtPRX42	
Gene	**Annotation**
CTL1	Chitinase-like protein1
TUBB5	Tubulin β-6 chain
DCD	DEVELOPMENTAL AND CELL DEATH domain protein
MES3	Methylesterase3
CYSD1	Bifunctional L-3-cyanoalanine synthase/cysteine synthaseD1
CBL	Cystathionine β-lyase
GLYR1	Glyoxylate/succinic semialdehyde reductase
PAE5	Pectin acetylesterase5
CESA3	Cellulose synthase (PCW)
TS2	Thronine synthase2
ENODL19	Early nodulin-like protein19
HSL1	Receptor-like protein kinase
EOL1	ETO1-like protein1
GAUT4	Galacturonosyltransferase4; involved in pectin biosynthesis

B AtGenExpress eFP: AT5G05340 / PRX52

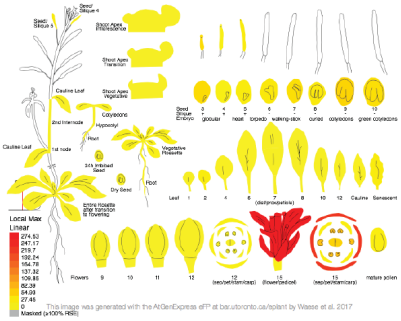

AtPRX52	
Gene	**Annotation**
IDA	INFLORESCENCE DEFICIENT IN ABSCISSION
PDF1.4	Defensin-like protein19
AtRLP22	Receptor-like protein22
WRKY28	Probable WRKY transcription factor28
DREB2E	Dehydration responsive element binding factor E
ATL41	E3 ubiquitin-protein ligase
WRKY8	Probable WRKY transcription factor8
WAKL10	Wall-associated receptor kinase-like10
CRRSP6	Cysteine-rich repeat secretory protein
WAKL7	Wall-associated receptor kinase-like7
GSTU3	Glutathione S-transferase U3
CCOAOMT	Caffeoyl-CoA methyltransferase
UGT91C1	UDP-glycosyltransferase91C1
VQ22	VQ motif-containing protein 22

C AtGenExpress eFP: AT5G42180 / PER64, PRX64

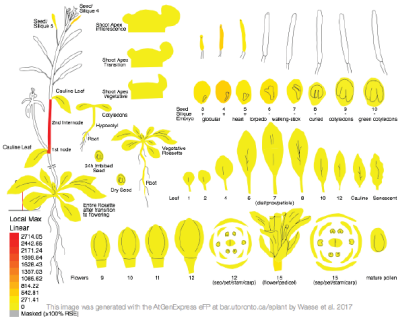

AtPRX64	
Gene	**Annotation**
MIF1	Mini zinc finger protein1
MYB63	MYB domain protein63; involved in monolignol biosynthesis
DIR9	Dirigent protein9
RABA6A	Ras-related protein
SOT5	Cytosolic sulfotransferase5
CASP1	Casparian strip membrane protein1
CASP3	Casparian strip membrane protein3
PRR1	Pinoresinol reductase1
CASP2	Casparian strip membrane protein2
MAP70.5	Microtubule-associated protein70-5
SOT8	Cytosolic sulfotransferase8
DIR6	Dirigent protein6
MYB43	MYB domain protein43
RALF1	Protein RALF-like1

D AtGenExpress eFP: AT5G64120 / AtPRX71, PRX71

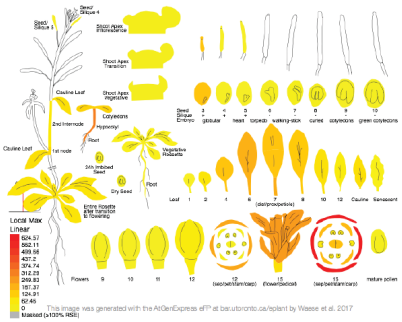

AtPRX71	
Gene	**Annotation**
PCR8	Plant cadium resistance8
HIR3	Hypersensitive-induced response protein
VSR7	Vacuolar-sorting receptor7
PCR2	Plant cadium resistance2
OCT5	Organic cation/carnitine transporter
CRK19	Cysteine-rich receptor-like protein kinase
CRRSP55	Cysteine-rich repeat secretory protein
AtNAC3	NAC domain containing protein3
GSL-OH	Probable 2-oxoacid dependent dioxygenase
ATL40	RING-H2 finger protein
ERD6	Sugar transporter
CYP71B6	Cytochrome P450 71B6
CSLE1	Cellulose synthase-like protein E1

E AtGenExpress eFP: AT5G66390 / PRX72

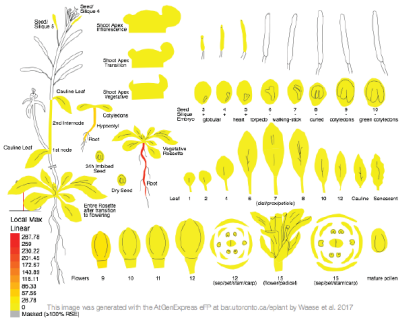

AtPRX72	
Gene	**Annotation**
DIR18	Dirigent protein18
UCC1	Uclacyanin1
DIR10	Dirigent protein10
CASP1	Casparian strip membrane protein1
LAC3	LACCASE3
CASP2	Casparian strip membrane protein2
DIR9	Dirigent protein9
NIC3	Nicotinamidase3
SOT8	Cytosolic sulfotransferase8
DIR23	Dirigent protein23
AHL23	AT-hook motif nuclear-localized protein
PRR2	Pinoresinol reductase2
CASP3	Casparian strip membrane protein3
MYB36	Endodermis-specific MYB domain protein36

F

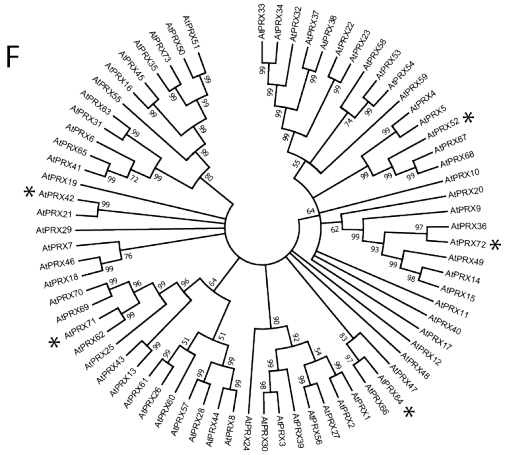

Figure 3.3. Putative lignin-associated PRXs are identified through bioinformatics approaches. A-E) Tissue expression maps were generated using the eFP browser (Waese et al., 2017) and co-expression lists were generated using Genvestigator (Hruz et al., 2008). Gene lists were annotated using TAIR (Berardini et al., 2015). A) AtPRX42. B) AtPRX52. C) AtPRX64. D) AtPRX71. E) AtPRX72. F) Phylogenetic analysis of 73 Arabidopsis class III PRX peptide sequences. The tree was inferred using the Neighbour Joining (NJ) method, bootstrap replicates 1000, on MEGA7 (Kumar et al., 2016). Asterisks denote selected putative lignin-associated PRXs selected in this study.

3.2.2 LACs and PRXs are secreted to specific cell types and regions of the cell wall in the inflorescence stem

To determine the localization of putative lignin-associated LACs and PRXs, I cloned the open reading frame for each selected LAC and PRX with its respective putative native promoter (encompassing approximately 2kb upsteam of the start codon). The native stop codon of the protein sequence was removed in order to facilitate translational fusion to a fluorescent -mCherry marker. mCherry is a monomeric protein modified from the red fluorescent protein (RFP) and was chosen for this study due to its stability in the acidic cell wall and brightness (Shaner et al., 2004). As all selected LAC and PRX proteins have a N-terminal signal sequence that targets them to the secretory pathway (Turlapati et al., 2011; Welinder et al., 2002), the -mCherry tag was attached to the C-terminal end of each protein. Fusion proteins were cloned into the wild-type Col-0 background of Arabidopsis. Stem tissue from independent T2-generation lines for *prLAC10::LAC10-mCherry*, *prPRX42::PRX42-mCherry*, *prPRX52::prPRX52-mCherry*, *prPRX71::PRX71-mCherry*, and *prPRX72::PRX72-mCherry* were analyzed for endogenous localization patterns in stem cross-sections using spinning disk confocal microscopy. Previously characterized lines of *prLAC4::LAC4-mCherry*, *prLAC17::LAC17-mCherry*, and *prPRX64::PRX64-mCherry* (Chou et al., 2018; Lee et al., 2013; Schuetz et al., 2014) were also imaged for comparison.

Tagged LACs and PRXs were categorized based on localization patterns to particular cell types (tissues) and subcellular localization to cell wall domains. In the mature Arabidopsis inflorescence stem, lignified cells are restricted to vascular bundles and interfascicular fibers. Within the vascular bundle, there are both lignified and non-lignified cell types (Figure 3.4a). Lignified cells include xylem vessel elements and xylary fibers, and unlignified cells include phloem cells and xylem parenchyma cells (Figure 3.4a). Lignified interfascicular fibers develop between the vascular bundles (Figure 3.4a). Within lignified cell walls there are two different regions, including the cellulose-rich SCW bordering the PM and the pectin-rich cell corner/middle lamella separating adjacent cell walls (Figure 3.4b). SCWs are made up of S1, S2, and S3 layers, each of which is deposited at a different period of development (Kerr & Bailey, 1934). To test whether the candidate lignin-associated LACs and PRXs localize to lignifying tissue, I compared

the localization of the mCherry-tagged proteins to UV lignin autofluorescence. Localization analyses were performed using stem cross-sections from the base of 5-week-old, 17cm-tall stems.

All eight tagged LACs and PRXs showed distinctive localizations to cell types and regions of the cell wall (Figures 3.5-3.8). As a control for evaluating protein localization, I re-analyzed the localization of AtLAC4-mCherry, which was previously shown to localize to the thick SCW of xylem vessel elements and fibers (Chou et al., 2018). Consistent with previous reports, AtLAC4-mCherry localized to the SCW of all lignifying cells and was not found in the middle lamella (Figure 3.5a). Evaluation of the other tagged LACs and PRXs found that AtLAC17-mCherry (Figure 3.5b) and AtPRX72-mCherry (Figure 3.5c) also localized to the SCW of xylem vessel elements and fibers. AtLAC4-mCherry, AtLAC17-mCherry, and AtPRX72-mCherry signals were all co-localized with lignin UV autofluorescence in the SCW and absent from the cell corners/middle lamella (Figure 3.5). Of the eight oxidative enzymes assessed, only AtLAC4, AtLAC17, and AtPRX72 were found within this region of lignified cell walls.

Other tagged LACs and PRXs localized to the cell corners of lignified cells (Figure 3.6). AtPRX64-mCherry localized specifically to the cell corners and middle lamella of fibers, confirming previous stem analysis (Figure 3.6a; Chou et al., 2018). AtPRX71-mCherry localized to the cell corners of both fibers and xylem vessel elements (Figure 3.6b). Within the interfascicular fibers, AtPRX71-mCherry showed highest concentration in the outer fiber cell layer near the endodermis, which is the cell layer bordering photosynthetic cortex cells (Figure 3.6b). Similarly, AtLAC10-mCherry localized to cell corners of interfascicular fibers but was restricted to the outer fiber cell layer adjacent to the endodermis (Figure 3.6c). Unlike the other cell corner PRXs, AtLAC10-mCherry did not localize to lignified cells in the vascular bundle (Figure 3.6c). These data demonstrated that both LACs and PRXs can be found in cell corners and that the outer-most fiber cell layer has a distinctive set of oxidative enzymes at the cell corner junctions.

Interestingly, several tagged LACs and PRXs localized to non-lignifying cell types, including epidermal cells and trichomes (Figure 3.7). In addition to localizing to the cell corners of lignified interfascicular fibers, AtLAC10-mCherry also localized to both the PCW of trichomes and the cell corners of epidermal cells (Figure 3.7a). AtPRX52-mCherry exclusively localized to the PCW of

trichomes (Figure 3.7b) and not apparent in any other cell type. AtPRX71-mCherry also localized to the cell corners of epidermal cells (Figure 3.7c), in addition to its localization in the cell corners of lignifying cell types. Unlike the other tagged LACs and PRXs, AtPRX42-mCherry localized to the cell corners of non-lignifying xylem parenchyma (Figure 3.8a) and phloem cells (Figure 3.8b) in the vascular bundle. AtPRX42-mCherry only localized to the PCW and was not seen in lignified xylem vessel elements or fibers (Figure 3.8). Therefore, these results suggest that certain enzymes can localize to both PCWs and SCWS (*e.g.* AtLAC10-mCherry and AtPRX71-mCherry) while other enzymes exclusively localize to PCWs (*e.g.* AtPRX42-mCherry and AtPRX52-mCherry).

The diverse localization patterns of the tagged LACs and PRXs is summarized in Figure 3.9. The localization of mCherry-tagged LACs and PRXs differed by tissue type, with AtLAC4, AtLAC17, AtPRX71, and AtPRX72 in lignified xylem vessel elements, and AtLAC4, AtLAC10, AtLAC17, AtPRX64, AtPRX71, and AtPRX72 in lignified fiber cells (Figure 3.9a). Within lignified cells, LACs and PRXs localized to different regions of the cell wall, with AtLAC4, AtLAC17, and AtPRX72 in the SCW and AtPRX64, AtPRX71, and AtLAC10 in the cell corners (Figure 3.9b). Other LACs and PRXs localized to non-lignifying cells, including AtLAC10, AtPRX42, AtPRX52, and AtPRX71 (Figure 3.9a).

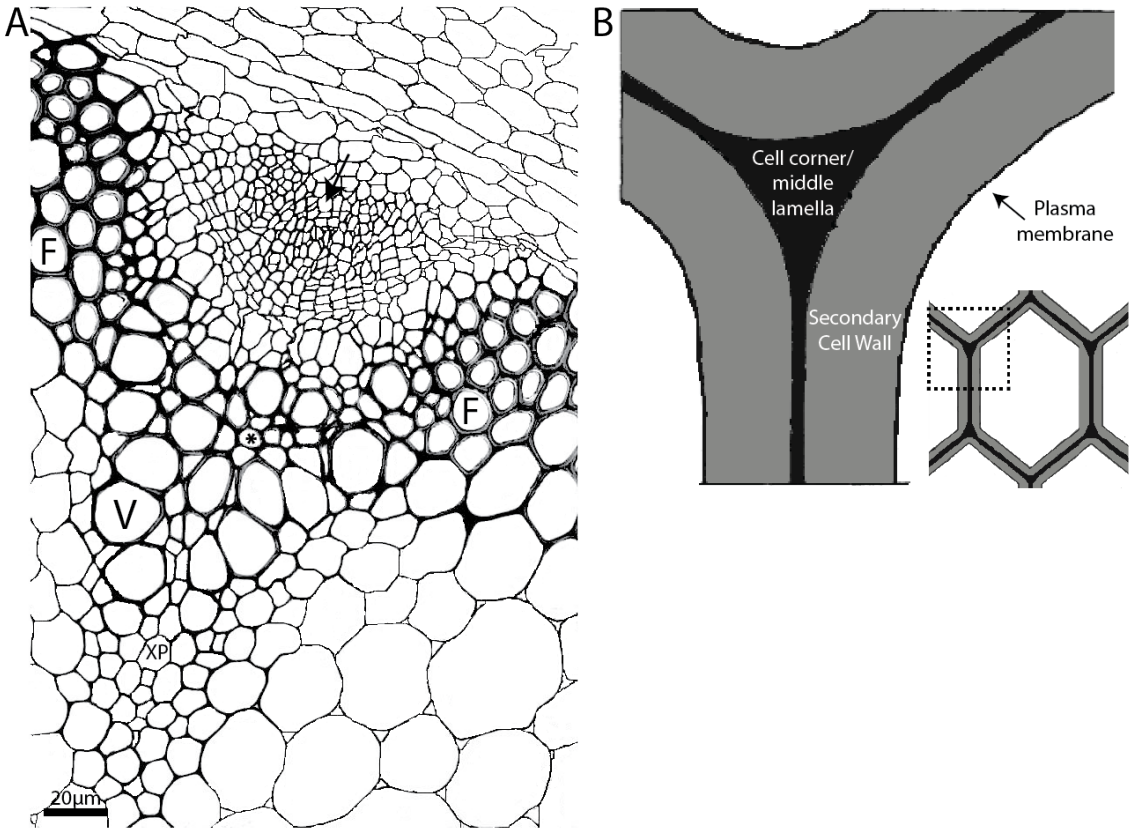

Figure 3.4. Anatomy of lignified and non-lignified cell types in the Arabidopsis inflorescence stem. A) Arabidopsis vascular bundles contain xylem and phloem tissues. Lignified xylem cells include xylem vessel elements (V) and xylary fibers (asterisk). Non-lignifying cell types include phloem cells (arrow) and xylem parenchyma (XP) cells that neighbour lignified xylem vessel elements. Lignified interfascicular fibers (F) connect vascular bundles. Image was derived from a toluidine blue-stained cross section from the base of a 17cm-tall stem. B) Lignified cells are sub-divided into different regions, including the cellulose-rich SCW adjacent to the plasma membrane and the pectin-rich cell corners/middle lamella separating adjacent cell walls. Imaged modified from Terashima and Fukushima (1988).

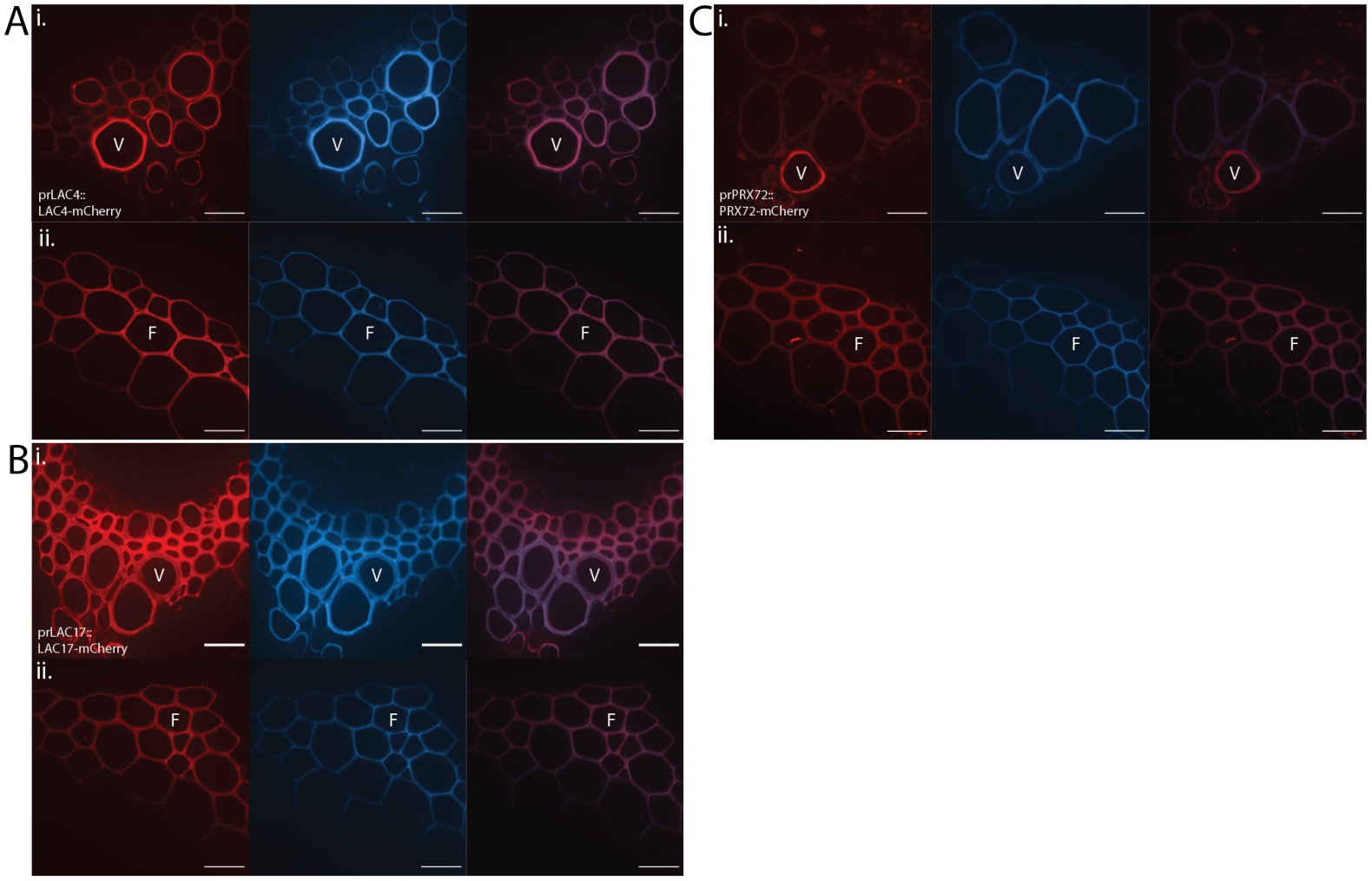

Figure 3.5. LACs and PRXs localize to the SCW in the inflorescence stem of Arabidopsis. Representative images depicting the tagged LAC or PRX under its native promoter (red), UV lignin autofluorescence (blue), and merged image. V=xylem vessel element; F=fiber. Scale bars are 20μm. A) AtLAC4-mCherry localizes to the SCW of xylem vessel elements (i) and fibers (ii). B) AtLAC17-mCherry localizes to the SCW of xylem vessel elements (i) and fibers (ii). C) AtPRX72-mCherry localizes to the SCW of xylem vessel elements (i) and fibers (ii).

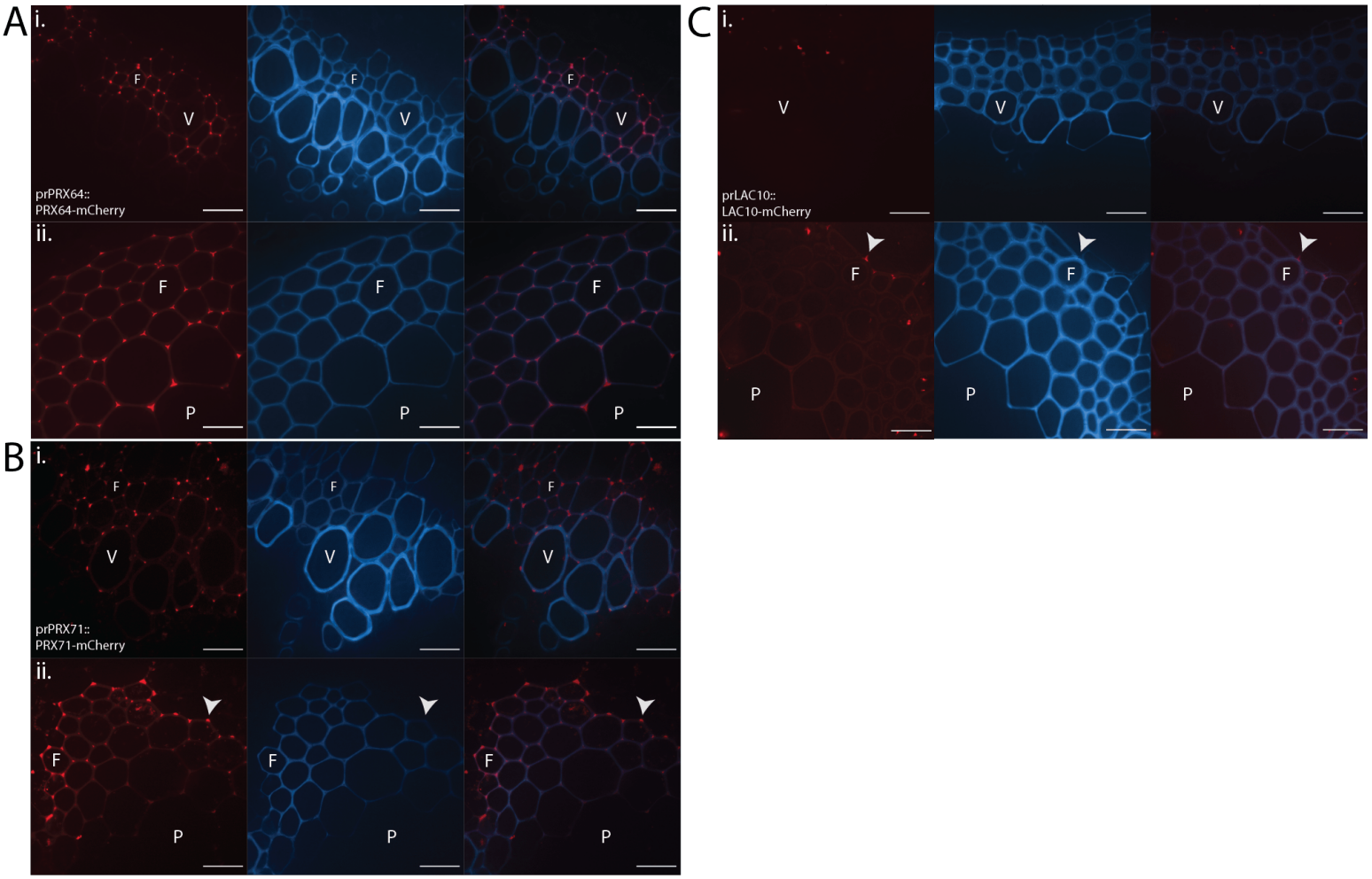

Figure 3.6. LACs and PRXs localize to lignifying cell corners in the inflorescence stem of Arabidopsis. Representative images depicting the tagged LAC or PRX under its native promoter (red), UV lignin autofluorescence (blue) and merged image. V=xylem vessel element; F=fiber, P=pith. Arrowhead indicates cell corner localization near endodermal layer. Scale bars are 20µm. A) AtPRX64-mCherry is absent from xylem vessel elements (i) but localizes to the cell corners of fibers (ii). B) AtPRX71-mCherry localizes to the cell corners of xylem vessel elements (i) and fibers (ii). C) AtLAC10-mCherry does not localize to xylem vessel elements (i) but localizes to the cell corners of the outer layer of fibers (ii).

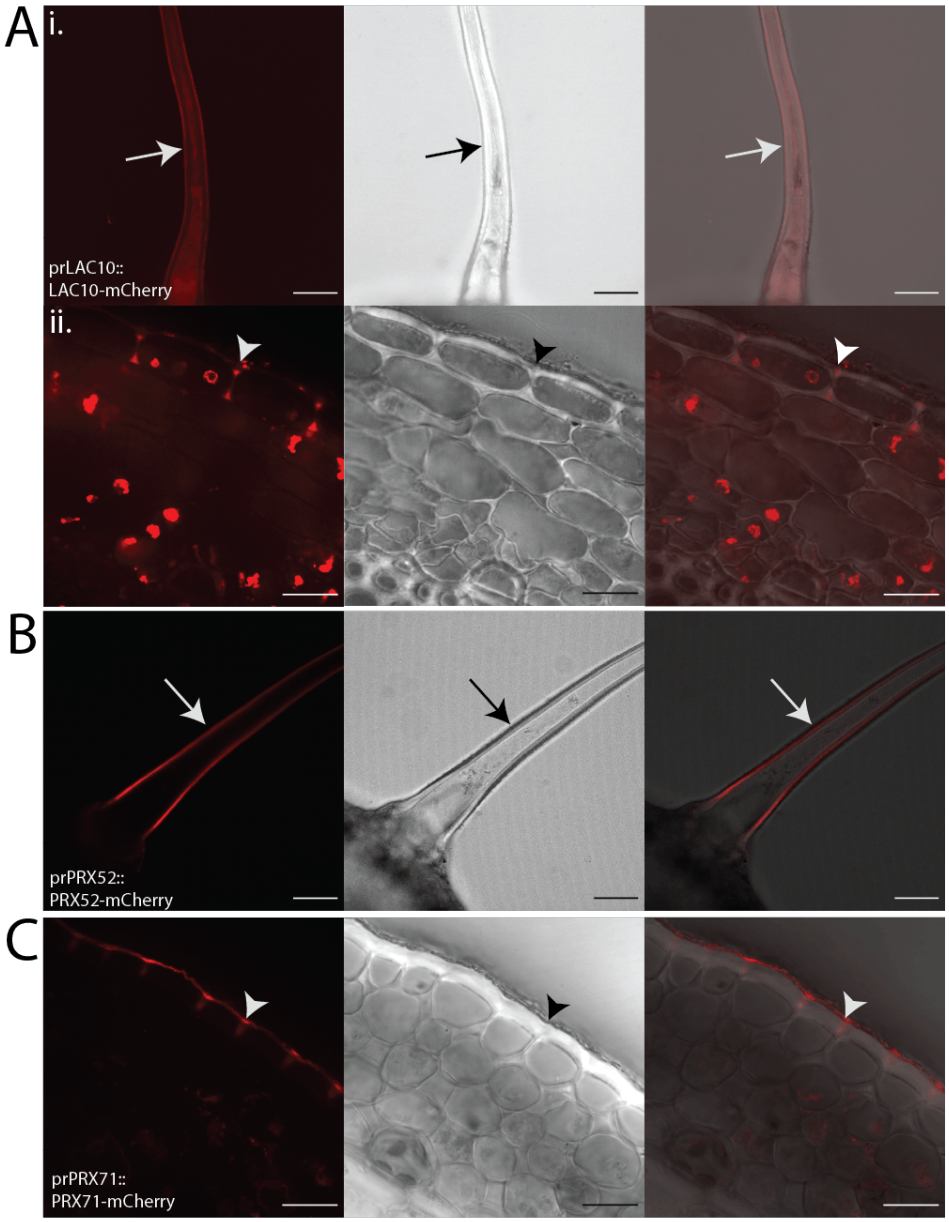

Figure 3.7. LACs and PRXs localize to trichomes and epidermal cells in the inflorescence stem of Arabidopsis. Representative images depicting the tagged LAC or PRX under its native promoter (red), brightfield, and merged image. Arrow=trichomes; arrowheads=epidermal cells. Scale bars are 50µm for Ai) and B) and 20µm for Aii) and C). A) AtLAC10-mCherry localizes to trichomes (i), and cell corners of epidermal cells (ii). B) AtPRX52-mCherry localizes to trichomes. C) AtPRX71-mCherry localizes to the cell corners of epidermal cells.

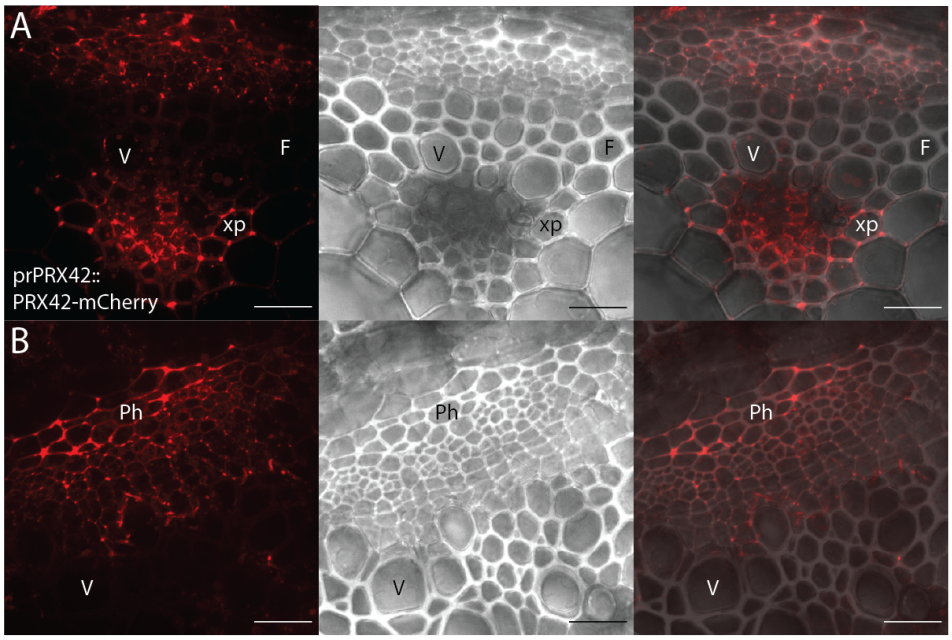

Figure 3.8. AtPRX42-mCherry localizes to xylem parenchyma and phloem cells in the inflorescence stem of Arabidopsis. Representative images depicting tagged AtPRX42 under its native promoter (red), brightfield, and merged image. V=xylem vessel element; F=fiber; xp=xylem parenchyma; Ph=phloem. Scale bars are 20µm. A) AtPRX42-mCherry localizes to the cell corners of non-lignifying xylem parenchyma cells. B) AtPRX42-mCherry localizes to the PCW of phloem cells.

A

Xylem Vessels	Fibers	Non-lignifying cells
AtLAC4 AtLAC17 AtPRX71 AtPRX72	AtLAC4 AtLAC10 AtLAC17 AtPRX64 AtPRX71 AtPRX72	AtLAC10 AtPRX42 AtPRX52 AtPRX71

B

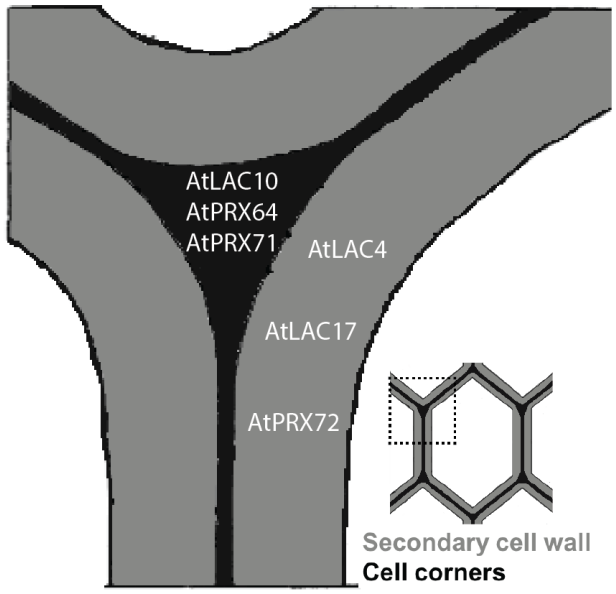

Figure 3.9. Summary of the endogenous localization patterns of tagged LACs and PRXs in the inflorescence stem of Arabidopsis. A) Tagged LACs and PRXs localize to both lignifying (xylem vessel elements and fibers) and non-lignifying cell types. B) Tagged LACs and PRXs localize to different regions of lignified cell walls. AtLAC4-mCherry, AtLAC17-mCherry, and AtPRX72-mCherry localize to the SCW. AtPRX64-mCherry, AtPRX71-mCherry, and AtLAC10-mCherry localize to cell corners. Imaged modified from Terashima and Fukushima (1988).

3.2.3 *prUBQ10::sec-mCherry* and *prUBQ10::LAC4-mCherry* localize to cell corners of lignifying and non-lignifying cell types

As tagged LACs and PRXs showed diverse co-expression networks (Figures 3.2-3.3) and were secreted to distinctive regions of the cell wall (Figures 3.5-3.8), I hypothesized that timing of expression may play a role in determining secretion patterns. LACs and PRXs are ER-targeted secreted glycoproteins, so they are predicted to be packaged in vesicles that traffic from the Golgi to the PM for exocytosis. Secretion early in development could deliver enzymes into the cell corners/middle lamella, while secretion during SCW biosynthesis could embed them into the thick SCW. Once in the SCW, the dense polysaccharide matrix may impede mobility and prevent diffusion to the cell corners (Chou et al., 2018). To study the secretion pattern of a small constitutively-expressed secreted protein, I analyzed the localization of *prUBQ10::sec-mCherry* (Chou et al., 2018), at the base of 17cm-tall stems. The promoter of *AtUBQ10* is highly-expressed in all cell types of Arabidopsis and is preferable for localization studies over the constitutive cauliflower mosaic virus *35S* promoter (Grefen et al., 2010). Consistent with previous reports, *prUBQ10::sec-mCherry* localized to trichomes and to the cell corners of fibers, xylem vessel elements, and epidermal cells (Figure 3.10a; Chou et al., 2018). Unlike tagged AtLAC4, *prUBQ10-sec-mCherry* was mobile in the SCW (Chou et al., 2018), so the observed localization patterns could reflect both targeted secretion to regions of the cell wall as well as remobilization during SCW formation.

To test whether timing of expression plays a role in localization of AtLAC4, I first examined stem cross-sections of *prUBQ10::LAC4-mCherry*, where *AtLAC4* is expressed under a constitutive promoter (Chou et al., 2018). Unlike native localization of AtLAC4-mCherry to the SCW, *prUBQ10-LAC4-mCherry* localized to the cell corners of lignified xylem vessel elements and fibers (Figure 3.10b). Therefore, changing the promoter sequence, which altered the timing of gene expression from SCW-specific to constitutive, was sufficient to alter the localization of tagged AtLAC4 from the SCW to the cell corners.

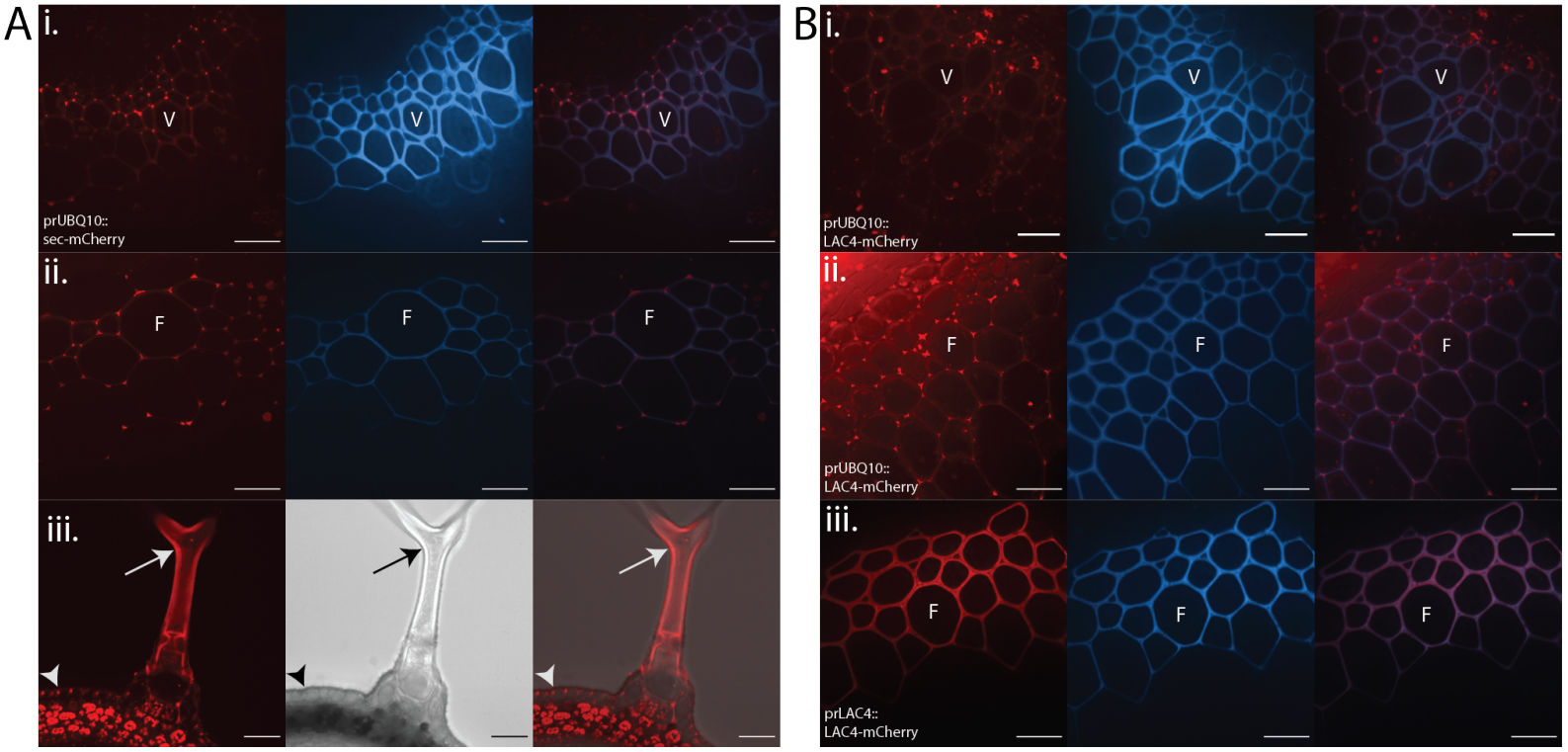

Figure 3.10. prUBQ10::sec-mCherry and prUBQ10::LAC4-mCherry localize to the cell corners of xylem vessel elements and fibers at the base of 17cm-tall Arabidopsis stems. Representative images depicting -mCherry fluorescence (red), UV lignin autofluorescence (blue), brightfield, and merged image. V=xylem vessel element; F=fiber; arrowhead=epidermal cell; arrow=trichome. Scale bars are 20µm for Ai)-Aii) and B), and 50µm for Aiii). A) prUBQ10::sec-mCherry, a small secreted protein (Chou et al., 2018) localizes to the cell corners of xylem vessel elements (i), fibers (ii), epidermal cells and trichomes (iii). B) prUBQ10::LAC4-mCherry localizes to the cell corners of xylem vessel elements (i) and fibers (ii). For comparison, prLAC4::LAC4-mCherry localizes the SCW of fibers (iii).

3.2.4 *prCESA7::LAC4-mCherry*, *prCESA7::LAC17-mCherry*, and *prCESA7::PRX64-mCherry* localize to PCWs and SCWs of lignified xylem in roots

As the constitutively-expressed *prUBQ10::sec-mCherry* and *prUBQ10::LAC4-mCherry* localized to cell corners, I next wanted to test whether changing the timing of expression to that of SCW polysaccharide biosynthesis was sufficient to localize proteins to the SCW. I therefore fused the open reading frame of *AtLAC4, AtLAC17* or *AtPRX64* to a 1.1kb putative promoter sequence of the SCW cellulose synthase gene *AtCESA7* (prCESA7) and labeled these constructs with a -mCherry tag. The promoter of *AtCESA7* was chosen as it is highly expressed in cells specifically producing SCWs in both roots and stems (Smith et al., 2013). Promoter-swap constructs were cloned into the Col-0 background of Arabidopsis. Stem and root tissue from independent T2-generation lines were analyzed for localization patterns using spinning disk confocal microscopy.

To test if driving gene expression with the *AtCESA7* promoter successfully embedded oxidative enzymes in SCW, I first studied the localization of *prCESA7::LAC4-mCherry*, *prCESA7::LAC17-mCherry*, and *prCESA7::PRX64-mCherry* in the primary root. Expression of *AtCESA7* in roots has been demonstrated to correspond with SCW production in lignified protoxylem and metaxylem (Brown et al., 2005). Due to the low amount of lignin and corresponding low UV lignin autofluorescence in the root, I mapped protein localization based on different tissue layers (Figure 3.11a; Péret et al., 2009). Under their respective native promoter, AtLAC4-mCherry (Figure 3.11b) and AtLAC17-mCherry (Figure 3.11c) both localized to lignified SCWs of protoxylem and metaxylem in stele tissues. AtPRX64-mCherry did not localize to lignified SCWs but instead localized to the PCW of the endodermis (Figure 3.11d), as was previously reported (Lee et al., 2013). In contrast to localization under their respective native promoters, *prCESA7::LAC4-mCherry*, *prCESA7::LAC17-mCherry*, and *prCESA7::PRX64-mCherry* all showed consistent localization to cell types and regions of the cell wall throughout root development (Figure 3.12). Surprisingly, this consistent pattern was not restricted to SCWs. Instead, *prCESA7::LAC4-mCherry*, *prCESA7::LAC17-mCherry*, and *prCESA7::PRX64-mCherry* localized to the PCW of young lignifying protoxylem near the root apical meristem and were not found in lignifying SCW bands (Figure 3.12a). In mature tissues, *prCESA7::LAC4-mCherry*,

prCESA7::LAC17-mCherry, and *prCESA7::PRX64-mCherry* disappeared from protoxylem PCWs and instead were only found in the SCW of lignified metaxylem (Figure 3.12b). The cell wall localization to both PCWs in young protoxylem and SCWs in metaxylem was confirmed with plasmolysis experiments, although intracellular signal was also detected for all three constructs in protoxylem and metaxylem (data not shown). These results indicated that changing the promoter sequence can change the cell wall localization of secreted proteins, as *prCESA7::LAC4-mCherry*, *prCESA7::LAC17-mCherry,* and *prCESA7::PRX64-mCherry* all showed the same localization patterns and had differential localizations compared with their respective native promoter (Figures 3.11-3.12).

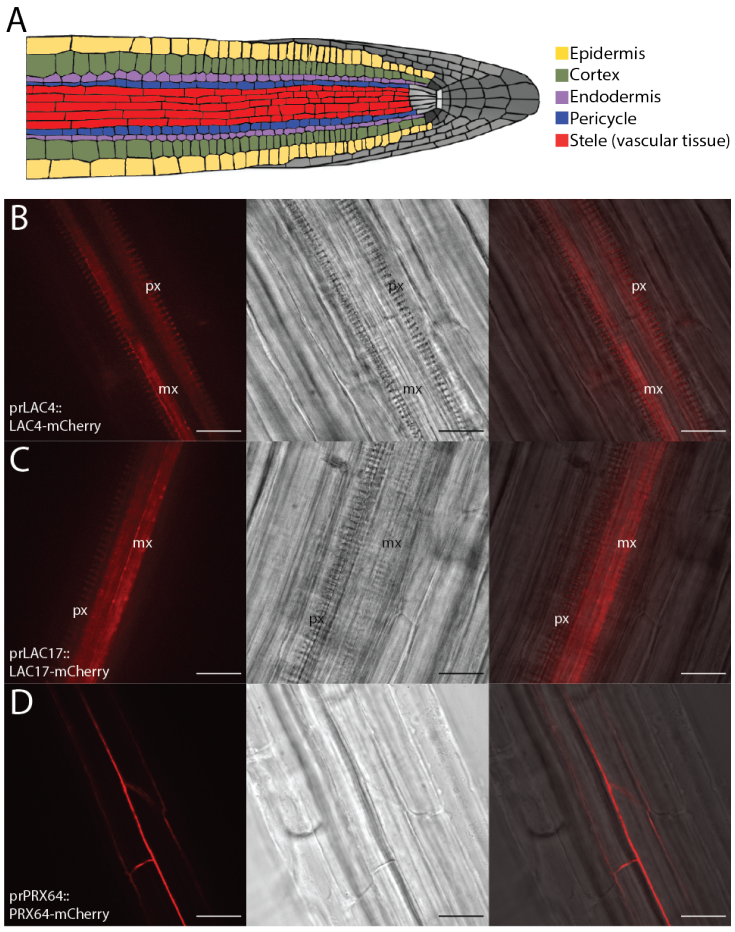

Figure 3.11. AtLAC4, AtLAC17, and AtPRX64 show distinct localization patterns in the primary root of Arabidopsis. Representative images depicting the tagged LAC or PRX under its native promoter (red), brightfield, and merged image. Px=protoxylem; Mx=metaxylem. Scale bars are 20µm. A) Map of the tissue layers in the Arabidopsis root. Image modified from Péret et al. (2009). B) AtLAC4-mCherry localizes to the SCW of protoxylem and metaxylem. C) AtLAC17-mCherry localizes to the SCW of protoxylem and metaxylem. D) AtPRX64-mCherry localizes to the PCW of the endodermis.

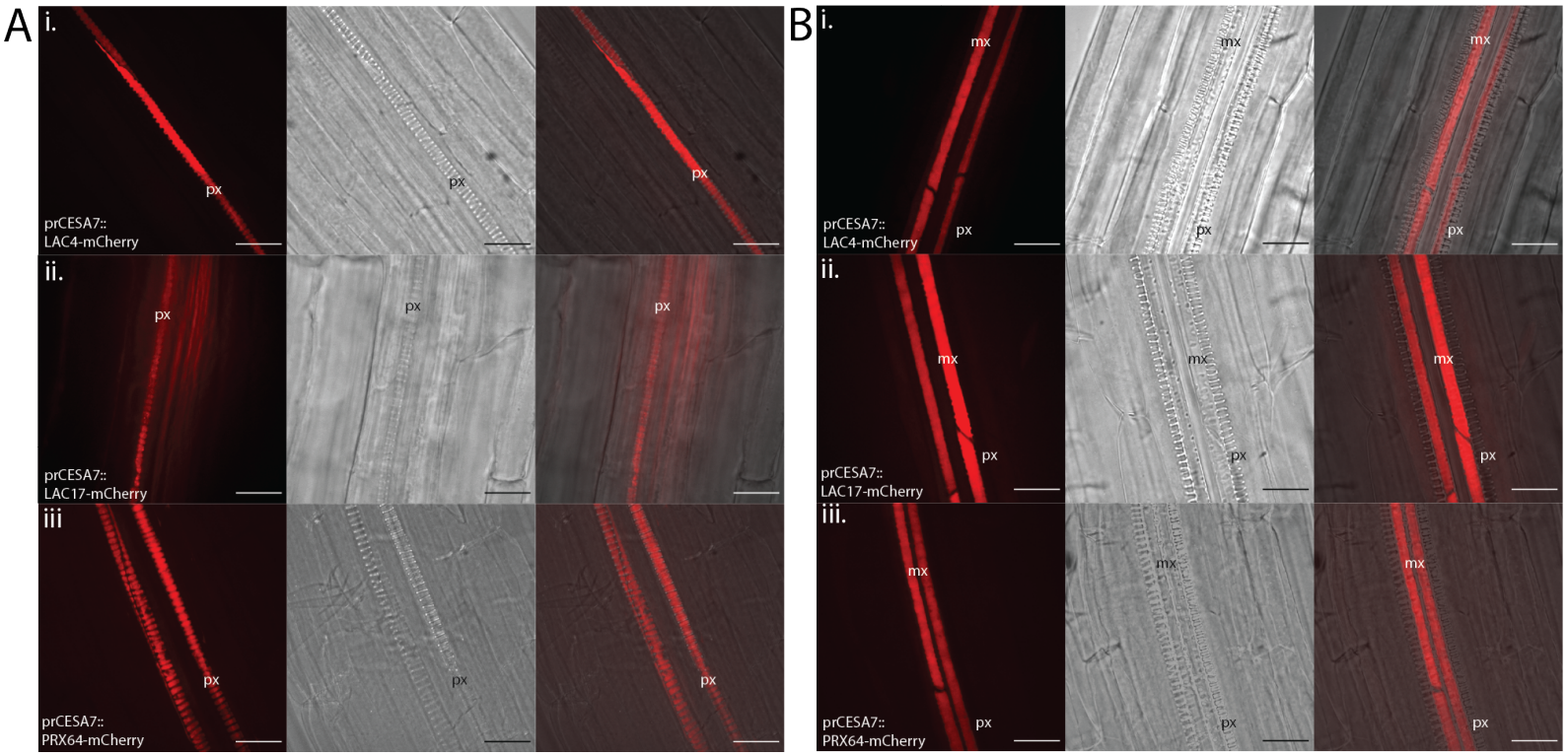

Figure 3.12. AtLAC4, AtLAC17, and AtPRX64 under the promoter of AtCESA7 localize to PCWs and lignified SCWs in Arabidopsis primary roots. Representative images depicting prCESA7::LAC4-mCherry, prCESA7::LAC17-mCherry, or prCESA7::PRX-64-mCherry (red), brightfield, and merged image. Px=protoxylem, Mx=metaxylem. Root tissue was first cleared in Clearsee buffer prior to imaging (Ursache et al., 2018). Scale bars are 20µm. A) prCESA7::LAC4-mCherry (i), prCESA7::LAC17-mCherry (ii), and prCESA7::PRX64-mCherry (iii) all localize to the PCW of protoxylem near the root apical meristem. B) In mature tissues, prCESA7::LAC4-mCherry (i), prCESA7::LAC17-mCherry (ii), and prCESA7::PRX64-mCherry (iii) are absent from protoxylem and instead localize to the SCW of metaxylem.

3.2.5 *prCESA7::LAC4-mCherry*, *prCESA7::LAC17-mCherry*, and *prCESA7::PRX64-mCherry* localize to lignified cell corners of xylem vessel elements in the stem but are transcriptionally silenced

To test if changing gene expression of *AtLAC4*, *AtLAC17*, and *AtPRX64* with the *AtCESA7* promoter altered localization in stem tissues, I analyzed cross-sections from the base of 17cm-tall Arabidopsis stems. Similar to roots, and unlike the patterns with their native promoters, *prCESA7::LAC4-mCherry*, *prCESA7::LAC17-mCherry*, and *prCESA7::PRX64-mCherry* consistently localized to the same cell type and region of the cell wall in stem tissues. All three constructs localized to cell corners of xylem vessel elements and were absent from fiber cell walls (Figure 3.13). However, localization to the cell corners was sporadic and not consistent between vascular bundles, replicates within a plant line, or independent plant lines. To test whether this inconsistent localization was due to alterations in transcription or transcript stability of the transgenes, I used real-time quantitative PCR (RT-qPCR) to quantify gene expression of *AtLAC4*, *AtLAC17*, and *AtPRX64* for two independent lines of *prCESA7::LAC4-mCherry*, *prCESA7::LAC17-mCherry*, and *prCESA7::PRX64-mCherry*, respectively. Compared to the Col-0 wild-type background, independent lines of *prCESA7::LAC4-mCherry*, *prCESA7::LAC17-mCherry*, and *prCESA7::PRX64-mCherry* all showed a reduction in gene expression for *AtLAC4*, *AtLAC17*, or *AtPRX64*, respectively, although this reduction was not always significant due to variation between biological replicates (Figure 3.13). Therefore, *AtLAC4*, *AtLAC17*, or *AtPRX64* may be transcriptionally silenced in stem tissue when their gene expression is driven by the *AtCESA7* promoter. However, residual expression and secretion of tagged AtLAC4, AtLAC17, and AtPRX64 produced consistent localization to regions of the cell wall that differed from the native localization of each of these proteins, indicating that changing the promoter sequence was sufficient to alter protein localization in the stem.

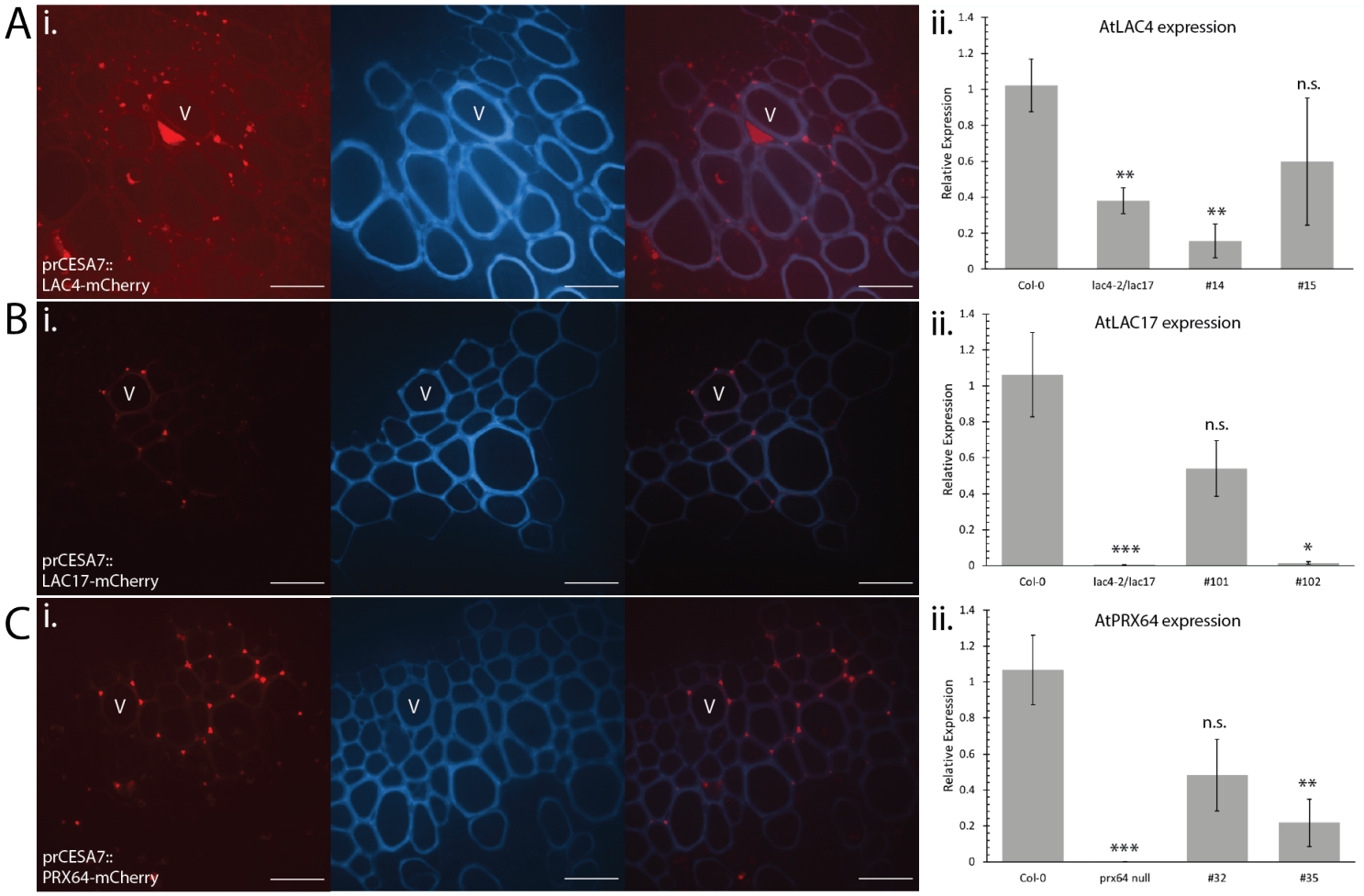

Figure 3.13. AtLAC4, AtLAC17, and AtPRX64 under the promoter of AtCESA7 localize to the cell corners of xylem vessel elements but are transcriptionally silenced in stem tissues. i) Representative images depicting prCESA7::LAC4-mCherry, prCESA7::LAC17-mCherry, or prCESA7::PRX64-mCherry (red), UV lignin autofluorescence (blue), and merged image. V=xylem vessel element. Scale bars are 20µm. ii) RT-qPCR expression quantification of gene expression from two independent prCESA7 lines (denoted by line number), Col-0, and the respective null mutant line. Data representative of three biological replicates/line. A 2-way t-test was used to determine differences between means; n.s.=not significant; *p<0.05; **p<0.01; ***p<0.001. Bars are SE. A) prCESA7::LAC4-mCherry localizes to cell corners of xylem vessels (i). prCESA7::LAC4-mCherry lines have reduced AtLAC4 expression in stem tissue (ii). B) prCESA7::LAC17-mCherry localizes to cell corners of xylem vessels (i). prCESA7::LAC17-mCherry lines have reduced AtLAC17 expression in stem tissues (ii). C) prCESA7::PRX64-mCherry localizes to cell corners of xylem vessels (i). prCESA7::PRX64-mCherry lines have reduced AtPRX64 expression in stem tissues (ii).

3.2.6 Expression of *AtLAC4*, *AtLAC17*, and *AtPRX64* under the *AtCESA7* promoter causes ectopic pith lignification and a reduction in fiber cell wall integrity

As previous localization analysis of the prCESA7 constructs was performed in relatively young 17cm-tall inflorescence stems, I imaged cross-sections from the base of mature 10-week-old (35-40cm tall) senescing stems. The localization of *prCESA7::LAC4-mCherry*, *prCESA7::LAC17-mCherry*, and *prCESA7::PRX64-mCherry* in mature stems was similar to younger stems, with sporadic accumulation in cell corners of xylem vessel elements (data not shown). Upon closer examination using UV autofluorescence, I noticed ectopic lignin deposition in PCWs of pith cells for all transgenic lines (arrowheads, Figure 3.14a). High magnification of lignified pith cells showed co-localization of tagged LACs and PRXs with UV lignin autofluorescence in the cell corners (Figure 3.14b; data not shown). In addition to ectopic pith lignification, sporadic interfascicular fiber cells accumulated *prCESA7::LAC4-mCherry*, *prCESA7::LAC17-mCherry*, or *prCESA7::PRX64-mCherry* in the cell corners and SCW (Figure 3.14c). Consistently accompanying LAC or PRX accumulation was a defect in SCW structure, loss of cell wall integrity, and cell wall collapse (arrows, Figure 3.14c). This is in contrast to neighboring cells that did not express *prCESA7::LAC4-mCherry*, *prCESA7::LAC17-mCherry*, or *prCESA7::PRX64-mCherry* and remained structurally intact (Figure 3.14c). Despite alterations in fiber cell walls, the overall growth of T2-generation transgenic plants were similar to wild type and showed no pendant stem phenotype characteristic of structurally-deficient fibers (data not shown; Muro-Villanueva et al., 2019; Smith et al., 2013; Zhong et al., 2006).

I hypothesized that the observed cell wall collapse in fibers could be due to reduced lignin content or from an altered oxidative environment in the SCW. To test whether collapsed fiber cell walls show abnormal or reduced lignin, I stained cross-sections of mature *prCESA7::PRX64-mCherry* stems with the dyes Safranin-O and astra blue, which can be used in combination to differentiate lignified and non-lignified tissues (Vazquez-Cooz & Meyer, 2002). Safranin-O is a non-specific stain for phenols and stains SCWs pink, while astra blue stains cellulose in PCWs blue (Lewis & Yamamoto, 1990). In addition, observation of the dual stain under UV light can infer phenolic concentration or composition (Vazquez-Cooz & Meyer, 2002). Similar to lignified xylem vessels and fibers in wild type Col-0 (Figure 3.15a), the collapsed fibers in *prCESA7::PRX64-*

mCherry lines stained pink with safranin-O/astra blue (Figure 3.15b). However, under UV light these regions were qualitatively less fluorescent compared with neighboring, structurally-intact SCWs (Figure 3.15b). Collapsed fiber cells and ectopically lignified pith cells also stained pink with the lignin-specific stain phloroglucinol-HCl (Figure 3.15c). Therefore, preliminary evidence suggested that collapsed fiber cells still contains lignin, although this amount may be reduced compared with neighbouring cells without accumulation of tagged AtLAC4, AtLAC17, or AtPRX64.

To test whether there is difference in the redox environment of the collapsed fibers, I stained cross-sections of mature *prCESA7::PRX64-mCherry* stems with the fluorescent dye 2',7'-dichlorodihydrofluorescein diacetate (H_2DCF), which forms a green fluorescent product upon reaction with ROS (Kalyanaraman et al., 2012). Observation of structurally-intact interfascicular fibers showed intense H_2DCF fluorescence in the SCW, while dead xylem vessel elements did not fluoresce with H_2DCF (Figure 3.15d). Compared to regions of structurally-intact interfascicular fibers, collapsed fibers with *prCESA7::PRX64-mCherry* accumulation qualitatively showed a decrease in H_2DCF fluorescence signal in the cell wall (Figure 3.15d). Therefore, H_2DCF staining indicated potential abnormal ROS production or accumulation in collapsed cell walls relative to structurally-intact fiber cell walls.

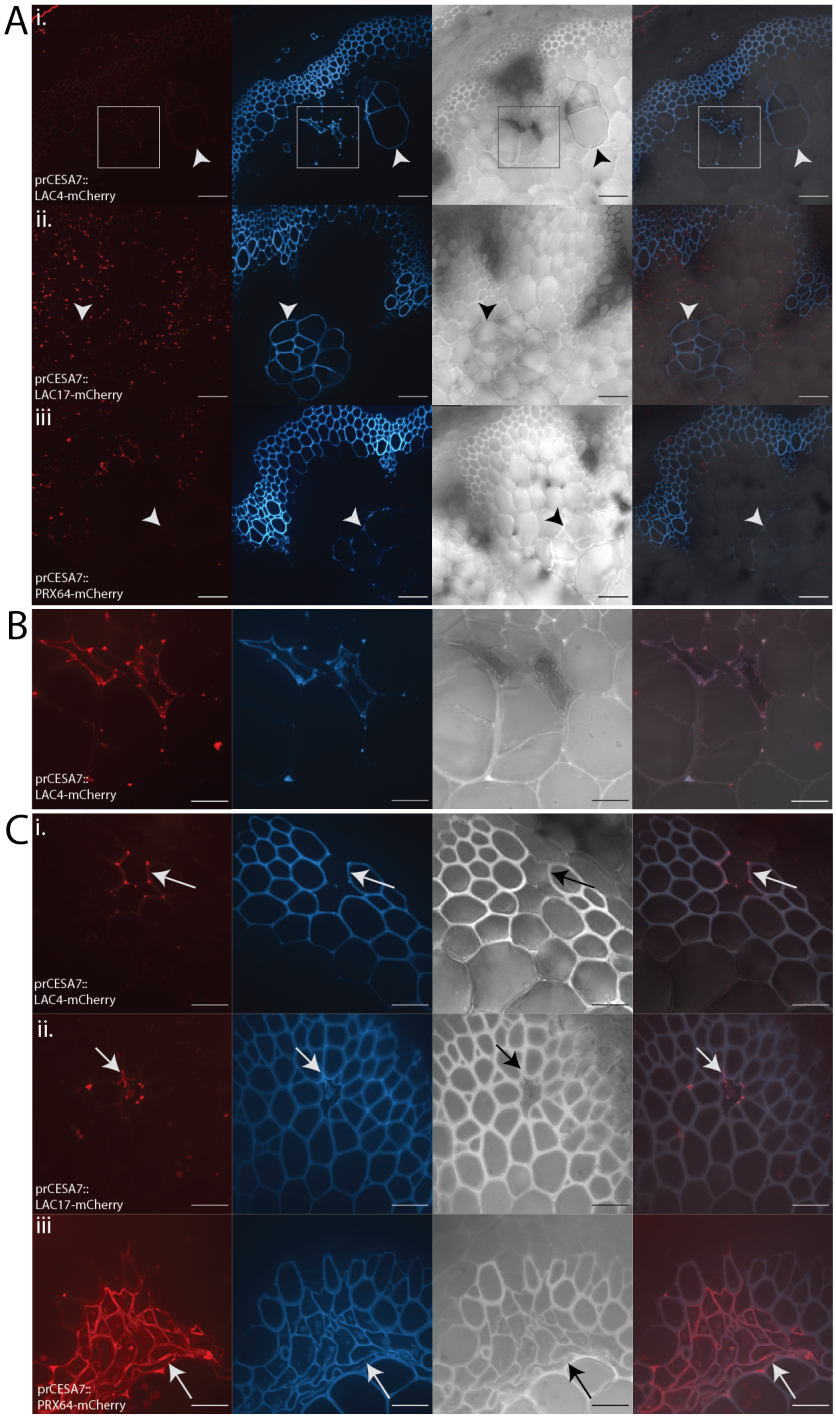

Figure 3.14. Ectopic expression of AtLAC4, AtLAC17, and AtPRX64 under the promoter of AtCESA7 results in ectopic pith lignification and loss of fiber cell wall integrity in mature stems. Representative images depicting prCESA7::LAC4-mCherry, prCESA7::LAC17-mCherry, or prCESA7::PRX64-mCherry (red), UV lignin autofluorescence (blue), brightfield, and merged image. Images are from the base of mature, 10-week-old plants. Arrowheads indicate regions of pith lignification and arrows indicate regions of SCW defect. Scale bars are 50µm for A) and 20µm for B-C) . A) Ectopic expression of AtLAC4, AtLAC17, or AtPRX64 under prCESA7 results in pith lignification. i) prCESA7::LAC4-mCherry, ii) prCESA7::LAC17-mCherry, iii) prCESA7::PRX64-mCherry. B) High magnification of pith lignification in box outlined in Ai) shows prCESA7::LAC4-mCherry localizes to lignified cell corners. C) Interfascicular fibers that accumulate tagged LAC or PRX expressed under prCESA7 have a collapsed cell wall structure in prCESA7::LAC4-mCherry (i), prCESA7::LAC17-mCherry (ii), or prCESA7::PRX64-mCherry (iii) lines.

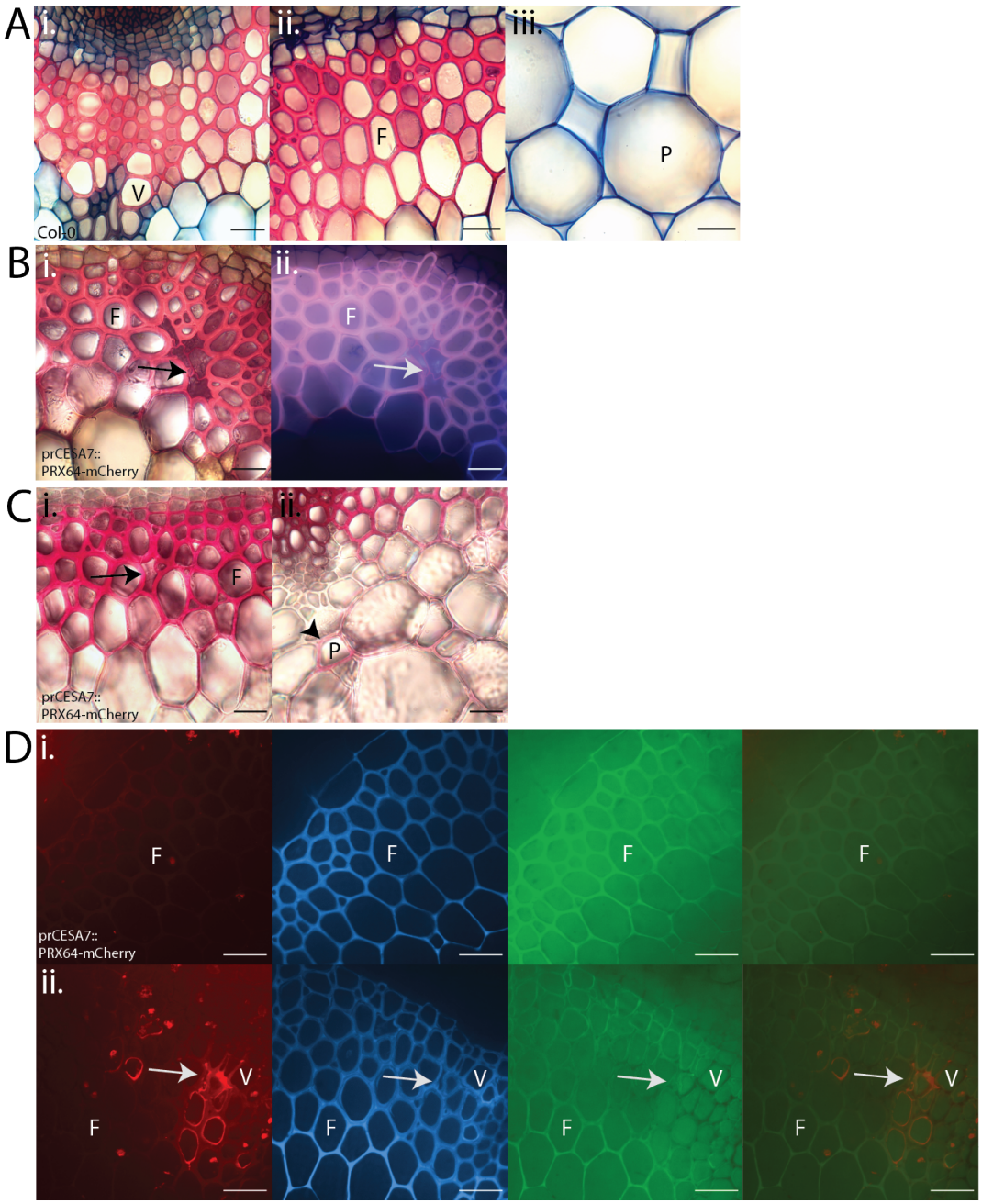

Figure 3.15. Loss of fiber integrity following prCESA7::PRX64-mCherry secretion to SCW could be due to altered cell wall structure or ROS production in mature stems. Images are from the base of mature, 10-week-old plants. A-B) Dual safranin-O/astra blue stains lignified SCWs pink and PCWs blue. A) Wild-type Col-0 has lignified xylem vessel elements (i) and fibers (ii) that stain pink while unlignified pith cells stain blue. B) prCESA7::PRX64-mCherry collapsed fibers have thin SCWs that stain pink (i) but show decreased UV fluorescence intensity (ii). C) Phloroglucinol stains collapsed fibers (i) and pith cells (ii) in prCESA7::PRX64-mCherry pink, indicating presence of lignin. D) H_2DCF staining of prCESA7::PRX64-mCherry shows production and accumulation of ROS in SCWs of intact interfascicular fibers (i) but reduced accumulation in collapsed fibers with prCESA7::PRX64-mCherry accumulation (ii). Lignin autofluorescence is in blue, H_2DCF is in green and prCESA7::PRX64-mCherry is in red. V=xylem vessel elements; F=fibers; P=pith; arrows indicate collapsed fiber cells. Scale bars are 20μm.

3.3 Discussion

Putative lignin-associated LACs and PRXs can be identified using mutant studies and bioinformatic tools

Due to large gene families, diverse expression patterns, and promiscuous substrate specificity, LACs and PRXs are involved in numerous diverse biological processes in addition to lignification (Passardi et al., 2005; Turlapati et al., 2011). To more precisely study the role of specific lignin-associated LACs and PRXs, I first selected candidate genes from the 17 LACs and 73 PRXs in the Arabidopsis genome based on reported lignin phenotypes in single-, double-, and triple-knockout mutant lines (Tables 1.1-1.3), gene expression in the lignifying stem (Figure 3.1), and co-expression networks (Figures 3.2-3.3). *AtLAC4*, *AtLAC10*, *AtLAC12*, *AtLAC11*, and *AtLAC17* were selected as strong candidates for involvement in lignification as they were all expressed in stem tissue, co-expressed with SCW biosynthetic genes, and generally clustered together on a phylogenetic tree (Figures 3.1-3.2).

Identification of putative lignin-associated PRXs was more complex, due to diverse phenotypes in mutant plants, varying expression levels in the stem, and broad co-expression networks. Many of the lignin-associated PRXs that were previously reported to have a mutant phenotype (*e.g. AtPRX2*, *AtPRX4*, *AtPRX17*, *AtPRX25*) had low expression in microarray experiments (Figure 3.1), calling into question whether a minimally-expressed oxidative enzyme can have a major role in lignification. I therefore updated the list of candidate PRXs to those that have detectable or high expression in the stem. However, PRXs have been implicated in numerous other processes along with lignification, including cell elongation, response to abiotic and biotic stress, and auxin catabolism (Shigeto & Tsutsumi, 2016), and therefore highly-expressed PRXs in the stem may not be specifically involved in lignification. My final short-list of putative lignin-associated PRXs included *AtPRX42*, *AtPRX52*, *AtPRX64*, *AtPRX71*, and *AtPRX72*, each of which has a lignin phenotype in mutant plants, is expressed in the stem, or is co-expressed with monolignol or SCW biosynthetic genes (Figure 3.3). Interestingly, the selected PRXs do not cluster on a phylogenetic tree (Figure 3.3f). This may be representative of broad substrate specificities or differential expression patterns (Jacobowitz et al., 2019; Tognolli et al., 2002).

Overall, co-expression analysis showed tight coordination of LACs with SCW biosynthetic genes while PRXs have more broad expression in tissues and diverse co-expression networks. The differences in expression patterns for LACs and PRXs across tissue types was also observed in a transcriptomic study of poplar secondary phloem, cambium and wood-forming tissues by Sundell *et al.* (2017), who hypothesized that LACs and PRXs are non-redundant in lignifying tissues due to non-overlapping expression domains (Sundell et al., 2017). In addition to different spatial distributions, both LACs and PRXs may be required for lignification due to distinctive substrate specificities for monolignols or varying availability of H_2O_2 for PRX activity during development (Sterjiades et al., 1992). However, the localization and substrate specificities for all Arabidopsis LACs and PRXs have not been extensively tested. This methodology for selecting putative lignin-associated LACs and PRXs therefore provides an excellent framework for testing the involvement of LACs and PRXs in lignification.

LACs and PRXs localize to different tissue types and regions of the cell wall

Prior to this work, the only oxidative enzymes that were localized in specific regions of lignifying cells were tagged AtPRX64 in cell corners and AtLAC4 in the thick SCW (Chou et al., 2018). The current work shows that each tagged LAC and PRX enzyme specifically localizes to a particular cell type and region of the cell wall. This spatial separation could denote a specialized function for a given LAC or PRX and could facilitate lignin deposition in a precise area during development.

AtLAC4-mCherry, AtLAC17-mCherry, and AtPRX72-mCherry all exclusively localized to lignified SCWs in xylem vessel elements and fibers, strongly supporting a role for these enzymes in lignification (Figure 3.5). Previous work localized AtLAC17-mCherry to the SCW bands of ectopically-produced protoxylem cells, but its localization in stems had not been confirmed (Schuetz et al., 2014). Similar localization of AtLAC4 and AtLAC17 suggests redundant functions, which is supported by mutant analyses where a significant defect in lignin content was only apparent in *lac4-2/lac17* double mutants but not in *lac4* or *lac17* single mutants (Tables 1.1, 1.3; Berthet et al., 2011). Interestingly, AtPRX72-mCherry is the first and only identified PRX to localize to the SCW in Arabidopsis. Despite showing low expression in the stem and not being significantly

co-expressed with SCW biosynthetic genes (Figure 3.2e), *prx72* mutants showed a significant reduction in stem lignin, a decrease in S-units, and a slight irregular xylem phenotype (Herrero et al., 2013). In addition, *AtPRX72* expression was increased in the *lac4-2/lac11/lac17* triple mutants, implying a possible functional linkage to AtLAC4, AtLAC11, and AtLAC17 (Zhao et al., 2013). However, increased *AtPRX72* expression in the *lac4-2/lac11/lac17* triple mutants was not sufficient to rescue the lignin defect. This could be due to different specificities of the enzymes, as AtLAC4 and AtLAC17 are reported to be specific for coniferyl alcohol and AtPRX72 is reported to be specific for sinapyl alcohol (Table 1.4). Therefore, LACs and PRXs may be involved in different processes related to lignification even within the same cell type and region of the cell wall. Future work could test whether AtLAC4, AtLAC17, and AtPRX72 play functionally redundant roles by creating double- or triple-knockout mutants of these genes and assessing lignin-related phenotypes.

AtLAC10-mCherry, AtPRX64-mCherry and AtPRX71-mCherry all localized to lignified cell corners (Figure 3.6), suggesting involvement in lignin polymerization of this region. The overlapping localization in cell corners may also indicate redundancy and explain the lack of a stem lignin phenotype in single knockout lines (Appendix; Tables 1.1-1.2). Cell corners are lignified early in development and are rich in G- and H-units (Donaldson, 2001; Fukushima & Terashima, 1991). The substrate specificities of AtLAC10 and AtPRX64 have not been determined, although the lignified Casparian strip for AtPRX64 was shown to consist of G- and H-units (Naseer et al., 2012). Despite being highly expressed in stem tissue, little is known about the functional role of AtPRX64 in the cell corners of fiber cells. UV lignin analysis of stem cross-sections between wild-type and *prx64* knockout lines found no significant difference in UV lignin autofluorescence intensity in fiber cell corners (Appendix), suggesting that the function of AtPRX64 is being masked by other LACs or PRXs localized in this region (*e.g.* AtLAC10 or AtPRX71). *In-vitro*, AtPRX71 showed specificity towards sinapyl alcohol over coniferyl alcohol substrates and could oxidize large substrates like cytochrome c (Table 1.4). However, *prx71* mutants showed no change to total lignin content but had increased numbers of G- and S-units (Table 1.2). Therefore, the specific role of AtPRX71 in lignification is unclear, although the localization data suggests a specialized function in cell corners.

AtLAC10-mCherry and AtPRX71-mCherry both concentrated in the outer cell layer of interfascicular fibers near the endodermis, suggesting a particular role for multiple oxidative enzymes in this region (Figure 3.6b-c). This is in contrast to the homogenous localization of AtPRX64-mCherry in cell corners of all cell layers (Figure 3.6a). Very little is known about the stem endodermal layer or its cell wall composition, although it was previously implicated in a gravitropic response (Fukaki et al., 1998) and was shown to have specific immunolabeling for structural proteins such as extensins and arabinogalactan proteins that were not present in cell walls of surrounding cortex or pith cells (Hall et al., 2013). Recently, AtPRX9 and AtPRX40 were shown to be involved in cross-linking of extensins to strengthen tapetum cell walls in Arabidopsis anthers (Jacobowitz et al., 2019), so it is possible that AtLAC10 and AtPRX71 are involved in extensin cross-linking or other cell wall stiffening processes besides lignification in these cell corners. Future work with *prx71* or *lac10* mutants could test whether there is a decrease in lignin content or change in cell wall composition specifically in fiber cell corners near the endodermal layer.

In addition to the cell corners of fibers, AtLAC10-mCherry and AtPRX71-mCherry also localized to non-lignifying epidermal cells (Figure 3.7). LACs and PRXs in the epidermal cell layer could be involved in defense responses; for example, AtPRX57 was previously shown to produce ROS in the leaf epidermis following pathogen attack (Survila et al., 2016). Alternatively, LACs and PRXs could be involved in maintaining cuticle structural integrity. The cuticle is a waterproof layer produced on top of epidermal cells and consists of cutin, waxes, and various phenolics (Hunt & Baker, 1980; Prats Mateu et al., 2016). Interestingly, impregnation of the cuticle with phenolics is hypothesized to predate the evolution of lignin (Renault et al., 2017). Involvement of AtPRX71 in cuticle structural integrity is supported by mutant studies, as plants over-expressing *AtPRX71* had an altered cuticle structure (Chassot et al., 2007). However, another study using *AtPRX71* over-expressor plants showed decreased cell size in rosette leaves and hypocotyls (Raggi et al., 2015), so the particular role AtPRX71 is playing in plant tissues remains unclear. Ultimately, due to promiscuous substrate binding *in-vitro* and broad expression patterns, these enzymes may play multiple functions in different tissues and at different developmental stages (Shigeto et al., 2014).

Surprisingly, tagged AtPRX42 and AtPRX52 did not localize to lignifying cell types, indicating they do not play a direct role in stem lignification (Figures 3.7, 3.8). The absence of AtPRX52-mCherry from lignifying cell types was unexpected, as *prx52* mutants were reported to have a reduction in total stem lignin and a decrease in S:G ratio (Fernández-Pérez et al., 2015b). However, histochemical analysis of stem cross-sections of *prx52* mutants showed no or minimal change to the structure of lignified SCWs (Fernández-Pérez et al., 2015). Instead, both AtPRX52-mCherry and AtLAC10-mCherry localized to the PCW of trichomes (Figure 3.7). The role of LACs and PRXs in trichome cell walls have not been studied extensively, although AtLAC10 and AtPRX52 could be involved in oxidizing sinapate esters and other phenolics found in trichome cuticles (Prats Mateu et al., 2016; Sinlapadech et al., 2007). *AtPRX52* expression was also highly up-regulated in cells at regions of organ abscission, denoting that AtPRX52 may play a specialized role in creating the lignin honeycomb pattern observed during separation of plant organs (Lee et al., 2018). Therefore, future work with AtPRX52-mCherry lines can test whether AtPRX52-mCherry localizes to regions of organ abscission or is involved in lignification of other tissues.

AtPRX42 is the one of the most highly-expressed PRXs in the Arabidopsis stem and localized to the PCWs of non-lignifying xylem parenchyma and phloem cells (Figures 3.1, 3.8). PRX activity in phloem tissues is well-documented in numerous species and is thought to be involved in response to biotic and abiotic stresses (Fleet, 1959; Singh et al., 2013; Walz et al., 2002). It is also possible that PRXs not found in lignifying cell walls could also play an indirect role in lignification. For example, *prPRX47:GUS* Arabidopsis lines also showed gene expression in xylem parenchyma cells, leading to the hypothesis that AtPRX47 may be acting as a "good neighbor" during lignification of neighboring xylem vessel elements (Smith et al., 2017). These PRXs could potentially act to polymerize low-order lignin oligomers or produce substrates like H_2O_2 for PRXs in neighboring lignifying cell walls (Pesquet et al., 2013; Smith et al., 2013). Further analysis of the substrate specificity of AtPRX42 is required to identify its particular biological role in these cell types.

Overall, each LAC and PRX showed a very specific localization pattern in stem tissues, both to cell types and regions of the cell wall (Figure 3.9). Tagged AtLAC4, AtLAC10, AtLAC17, AtPRX64, AtPRX71, and AtPRX72 localized to lignifying tissue, strongly suggesting a role in stem

lignification. The localization of these proteins to lignified cell types as well as their putative involvement in lignification is supported by mutant phenotypes, bioinformatics, and homology to lignin-associated LACs and PRXs in other species. AtLAC10 and AtPRX71 also localized to other non-lignifying cell types, suggesting multiple roles besides lignification. In addition, AtPRX42 and AtPRX52 did not localize to lignifying cells and thus may not play a direct role in stem lignification.

There are several limitations to these localization analyses, including not testing the functionality of the tagged enzyme and having a restricted promoter sequence. To ensure the fluorescently tagged protein is functional, *i.e.* it can perform the non-tagged enzymatic activity and is secreted to the same region as the wild-type protein, complementation tests are generally used. This involves transformation of the fluorescently-tagged protein into a mutant line to test whether the tagged protein can rescue the mutant phenotype. If a tagged protein is unable to complement or only partially complements the mutant phenotype, this could indicate that the fluorescent tag impedes protein function or localization (DeBlasio et al., 2010). This is especially relevant for the current study, as proper localization of tagged oxidative enzymes is necessary for spatial and temporal analysis in stems. Both AtLAC4-mCherry and AtLAC17-mCherry were previously shown to complement the irregular xylem phenotype of *lac4-2/lac17* mutants, confirming they are functional (Schuetz et al., 2014). However, many of the Arabidopsis LACs and PRXs selected for this study have no phenotypic changes or very minor alterations in knockout lines (Tables 1.1-1.2) and therefore it will be difficult to demonstrate experimentally that the tagged constructs are functional and are localized like the wild-type protein. In the current study, all constructs were cloned into the wild-type Col-0 background of Arabidopsis. As the functionality of these constructs have not been tested, the observed localization of the tagged proteins may not be representative of the wild-type enzyme.

Another limitation of this study is that the observed localizations could be accumulation of cleaved -mCherry protein in the apoplast and not representative of tagged enzymes. Cleavage of the fluorescent tag could occur following protein degradation by proteases in the cell wall (Boudart et al., 2005). To address this, I analyzed the localization of *prUBQ10::sec-mCherry*, which is predicted to target to the ER and be secreted through the default secretory pathway via Golgi vesicles (Chou et al., 2018). *prUBQ10::sec-mCherry* localized to the cell corners of epidermal

cells, xylem vessel elements, and fibers, as well as the PCW of trichomes (Figure 3.10). As many LACs and PRXs each show differential localization compared with that of *prUBQ10::sec-mCherry*, the fluorescence patterns observed most likely are reflective of unique enzyme positioning in the cell wall. To further confirm that each LAC and PRX is attached to the -mCherry tag, future work could estimate the size of tagged proteins using Western blots.

An additional potential caveat of this study is the use of a standard 2kb upstream putative promoter region to drive endogenous expression of the tagged LACs and PRXs. Cell-type expression and subsequent secretion of tagged proteins is dependent on specific cis-elements within promoter sequences (Hernandez-Garcia & Finer, 2014). For example, Hatton *et al.* (1995) demonstrated that certain AC elements in the promoter of *PAL2* in tobacco were necessary for tissue-specific expression in the xylem (Hatton et al., 1995). The included endogenous promoter sequence for all tagged LACs and PRXs in this study was approximately 2kb upstream of the start codon; however, trans-elements involved in expression of the gene may be located in different parts of the genome. Promoter:GUS expression constructs for *AtLAC4*, *AtLAC17*, and *AtPRX64* showed similar cell-type expression patterns as that of tagged AtLAC4, AtLAC17, and AtPRX64, suggesting that the 2kb upstream sequence was sufficient to drive gene expression in the native pattern (Koizumi et al., 2009; Turlapati et al., 2011). Similarly, promoter-GUS fusion constructs of *AtLAC10* reported expression in the cambium and cortical cells (Turlapati et al., 2011), which could correspond to observed tagged AtLAC10 near the epidermis and endodermal cell layer. Unexpectedly, GUS reporter lines for the promoter of *AtPRX42* showed high expression in all lignifying cell types and the cortex but was absent from the phloem and pith, where tagged AtPRX42 localized (Figure 3.8; Koizumi et al., 2009). Differences between the observed localizations could be due to the length of the promoter sequence included in the construct, as the *prPRX42::GUS* lines used a 3kb upstream promoter sequence (Koizumi et al., 2009). Alternatively, AtPRX42 mRNA was shown to be mobile between cells (Thieme et al., 2015), so expression patterns may not completely reflect protein localization. To provide further support to the localization of the other tagged PRXs, promoter:GUS constructs for *AtPRX52*, *AtPRX71*, and *AtPRX72* could be evaluated to see whether expression of the gene corresponds with the observed localization of tagged enzymes.

Cellular mechanisms underlying localization of cell wall proteins

There are several non-exclusive mechanisms that could impact cell wall localization of secreted proteins, including (i) direct binding to polysaccharide motifs or proteins in the cell wall; (ii) degradation of LACs and PRXs by proteases in specific regions of the cell wall; (iii) mobility in the cell wall; and (iv) timing of expression and secretion.

As LACs and PRXs show broad substrate specificity *in-vitro*, binding of a LAC or PRX to a polysaccharide or other protein in the cell wall would ensure it acts on a given target within a specific microdomain. In the root, AtPRX64 was shown to co-localize with a protein scaffold containing AtCASP1, a Casparian strip domain protein, and AtRbohF, a NADPH oxidase (Lee et al., 2013). This scaffold thus concentrates ROS production by NADPH oxidases and PRX enzymatic activity, which may facilitate lignin deposition to specific regions in the Casparian strip (Lee et al., 2013). Remarkably, when the scaffold was missing in *casp1/casp3* double mutants, lignification of the Casparian strip still occurred but in an abnormal, delocalized pattern (Lee et al., 2013). Thus, this protein scaffold is required for creating the specific lignin banding pattern of the Casparian strip. Another PRX, AtPRX36, was also shown to bind to specific motifs of demethylesterified pectin in PCWs of seed coats, providing a "platform" for restricted PRX activity in a given location (Francoz et al., 2019). Similarly, a motif of three basic amino acids on a PRX from zucchini facilitated attachment to Ca^{2+}-bound pectin (Carpin, 2001). However, it is unknown whether AtPRX64 or other lignin-associated LACs and PRXs bind to other proteins or polysaccharides in stem tissues. Interestingly, tagged AtLAC4 was immobile in the SCW even following reduction of xylan, cellulose, or lignin content (Chou et al., 2018); therefore, different LACs and PRXs may be bound to several components of the cell wall.

Extracellular proteases may also determine the presence or absence of cell wall proteins in a given domain (Boudart et al., 2005). For example, LACs and PRXs could be distributed homogenously in the SCW and middle lamella but be degraded from the SCW by proteases, thus restricting protein localization to cell corners. There have been several secreted proteases identified from both bioinformatic (Minic et al., 2009) and proteomic (Boudart et al., 2005; Tsai et al., 2017) studies of Arabidopsis cell walls. However, very little is known about the specificity or functional role of extracellular proteases, with studies indicating general involvement in

defense against pathogens and turnover of cell wall proteins (Jamet et al., 2008; Xia et al., 2004). Further work could elucidate the role of proteases in localization of putative lignin-associated LACs or PRXs, such as testing whether enzyme localization changes following chemical inhibition of proteases.

Alternatively, protein mobility in the cell wall may impact localization. Following secretion, proteins could diffuse from the PM to different regions, *e.g.* the SCW or cell corners. The mobility of enzymes can differ based on the structure of the protein as well as the composition of the surrounding polysaccharide matrix. Estimations of matrix pore size in PCWs suggested free diffusion of proteins below 40-50kDa, while larger proteins were expected to show reduced mobility (Baron-Epel et al., 1988; Carpita et al., 1979). As the pectin-rich middle lamella and PCW is more porous and heterogenous in structure than the compact lignified SCW, protein mobility in the SCW could be severely reduced (Donaldson, 1994). For example, estimates of pore size in mature wood of sweetgum and loblolly pine were estimated to be 1.2-3.8nm, which would restrict movement of proteins larger than approximately 20kDa (Blanchette et al., 1997; Flournoy et al., 1991). Experimental evidence for the SCW impeding protein movement was demonstrated using Fluorescence Recovery After Photobleaching (FRAP) experiments, where both *prUBQ10::sec-mCherry* and AtLAC4-mCherry were mobile in the PCW but had impaired or negligible mobility in the SCW, respectively (Chou et al., 2018). Arabidopsis PRXs are smaller in size than LACs (~30-40kDa for PRXs and ~60-70kDa for LACs; without glycosylation), so PRX movement through the SCW could be less restricted compared with LACs (Berardini et al., 2015). Therefore, the specific localization of putative lignin-associated LACs and PRXs may be due to high mobility or complete lack of diffusion to other regions of the cell wall following secretion. A potential caveat of this study is that I added on a ~28.8kDa -mCherry tag to selected LACs and PRXs and thus the mobility of the tagged enzymes and resulting cell wall localization may be impacted. However, both AtLAC4-mCherry and AtLAC17-mCherry were able to complement the mutant phenotype of *lac4-2/lac17* mutants, indicating functionality and proper localization despite the addition of the -mCherry tag (Schuetz et al., 2014).

Changing the promoter sequence is sufficient to alter localization of AtLAC4, AtLAC17, and AtPRX64

Additionally, the timing of gene expression and secretion during formation of the SCW may also impact enzyme localization. Co-expression analyses indicated that *AtLAC4* and *AtLAC17* were significantly co-expressed with SCW polysaccharide biosynthetic genes, including SCW *AtCESAs* and genes involved in production of the hemicellulose xylan (Figure 3.2a,e). Conversely, PRXs such as *AtPRX64* were differentially expressed compared to LACs and showed no consistent co-expression with SCW biosynthetic genes (Figure 3.3). Combined with the discrete localization of AtLAC4-mCherry and AtLAC17-mCherry to the SCW and AtPRX64-mCherry to the cell corners (Figures 3.5, 3.6), this led to the hypothesis that timing of expression and secretion could determine localization to regions of the cell wall. More specifically, packaging of LACs or PRXs in Golgi vesicles with components of the polysaccharide matrix could embed these proteins in a given cell wall domain. Therefore, the localization of AtLAC4-mCherry and AtLAC17-mCherry in the SCW may be due to expression and secretion at the same time as production of SCW polysaccharides. As *AtPRX64* is not expressed with biosynthetic enzymes for SCW polysaccharides, its localization to the cell corners and middle lamella could be due to differential timing of expression and secretion during development.

Localization of *prUBQ10-LAC4-mCherry* to the cell corners of SCWs indicated that changing the timing of expression was sufficient to alter localization and that there are no inherent structural features of AtLAC4 restricting it from the cell corner or middle lamella (Figure 3.10b). However, since *prUBQ10::LAC4-mCherry* did not localize to the lignified SCW, high constitutive expression does not lead to accumulation of proteins in all regions of the cell wall. Therefore, in order to localize to the SCW, proteins may need to be secreted at a specific time during development. I hypothesized that expressing *AtLAC4*, *AtLAC17*, or *AtPRX64* under the promoter of *AtCESA7* would alter the timing of expression and secretion to be the same as production of SCW cellulose, resulting in protein localization to the SCW. Alternatively, if timing of expression does not play a role in localization, each protein under prCESA7 would show similar localization as its respective native promoter.

Interestingly, the localization of *prCESA7::LAC4-mCherry*, *prCESA7::LAC17-mCherry*, and *prCESA7::PRX64-mCherry* differed from their respective native promoter and instead showed similar localization in both roots and stems. In the roots, *prCESA7::LAC4-mCherry*, *prCESA7::LAC17-mCherry*, and *prCESA7::PRX64-mCherry* unexpectedly first appeared in PCWs of protoxylem and not the lignifying SCW bands, where AtLAC4-mCherry and AtLAC17-mCherry normally localize (Figures 3.11, 3.12a; Schuetz et al., 2014). It could be that *AtCESA7* expression comes on earlier than bulk SCW cellulose deposition and endogenous LAC expression, thus leading to secretion to PCW domains. Later in development, *prCESA7::LAC4-mCherry*, *prCESA7::LAC17-mCherry*, and *prCESA7::PRX64-mCherry* disappeared from protoxylem and instead were secreted to the SCW of metaxylem, similar to the native localization of AtLAC4-mCherry and AtLAC17-mCherry (Figures 3.5b-c, 3.7b). Protoxylem and metaxylem differentiation are controlled by different up-stream master transcription factors, with AtVND6 controlling metaxylem formation and AtVND7 controlling protoxylem formation (Kubo et al., 2005). Differences in localization between these cell types could be due to variance in transcriptional hierarchies or timing of *AtCESA7* expression, thus leading to alterative localizations to regions of the cell wall. The observed loss of tagged enzyme signal from PCWs of protoxylem in mature tissues may be due to degradation by extracellular proteases.

The localization of *prCESA7::LAC4-mCherry*, *prCESA7::LAC17-mCherry*, and *prCESA7::PRX64-mCherry* in stem cross-sections from the base of 17cm-tall stems similarly produced unexpected results. *AtCESA7* is highly expressed in all cells with a SCW in stem tissues, including xylem vessel elements and fibers (Ohashi-Ito et al., 2010; Smith et al., 2013). *prCESA7::LAC4-mCherry*, *prCESA7::LAC17-mCherry*, and *prCESA7::PRX64-mCherry* did not localize to the SCW but were ectopically observed in the cell corners of xylem vessel elements (Figure 3.13). I hypothesized that the inconsistent localization may be due to altered transcription or transcript stability of the transgenes. Quantification of *AtLAC4*, *AtLAC17*, or *AtPRX64* expression using RT-qPCR confirmed transcriptional silencing in *prCESA7::LAC4-mCherry*, *prCESA7::LAC17-mCherry*, or *prCESA7::PRX64-mCherry* lines, respectively (Figure 3.13). Despite reduced expression, the consistent localization of *prCESA7::LAC4-mCherry*, *prCESA7::LAC17-mCherry*, and *prCESA7::PRX64-mCherry* to the cell corners of xylem vessel elements confirmed that timing of

localization plays a role in dictating cell wall localization in the stem. It is interesting to note that residual expression of *AtLAC4*, *AtLAC17*, or *AtPRX64* under prCESA7 led to accumulation of tagged enzyme in cell corners of xylem vessels, while it was not found in the SCW or any other cell types. Localization of proteins to the cell corners could represent a default secretory pathway, similar to cell corner localization observed in constitutively expressed *prUBQ10::sec-mCherry* and *prUBQ10::LAC4-mCherry* stems (Figure 3.10).

Transcriptional silencing during cloning is thought to arise if transcript levels of a transgene surpasses a certain level, specific to each gene (Schubert, 2004). Transcriptional silencing of *AtLAC4*, *AtLAC17*, and *AtPRX64* could occur through several different mechanisms, including histone modifications, DNA methylation, and miRNA binding (Turlapati et al., 2011). *In-planta* evidence of miRNA regulation of LACs was demonstrated by Wang *et al.* (2014), who showed that over-expression of *miR397b* significantly decreased *AtLAC2*, *AtLAC4*, and *AtLAC17* expression, reduced lignin content, and altered lignin composition in stems (Wang et al., 2014). Alternatively, targeted mutagenesis of *miR397b* prevented binding to *AtLAC4* transcripts and resulted in dwarfed plants with increased lignin content (Wang et al., 2014). Therefore, LAC expression is highly regulated by miRNAs during growth and this modulation is essential for proper development and lignification. There have been few studies on regulation of secreted PRXs, so it is unknown whether *AtPRX64* transcripts are also targeted by miRNAs or whether transcriptional silencing occurs through a different mechanism, such as methylation of DNA sequences (Schubert, 2004).

Another unexpected phenotype in mature stems expressing *prCESA7::LAC4-mCherry*, *prCESA7::LAC17-mCherry*, or *prCESA7::PRX64-mCherry* was ectopic pith lignification (Figure 3.14a-b). Pith cells are non-photosynthetic, non-lignifying cells in the center of the stem that function mainly in storage of water and nutrients (Zhong et al., 2000). In addition, sporadic interfascicular fiber cells showed SCW accumulation of *prCESA7::LAC4-mCherry*, *prCESA7::LAC17-mCherry*, or *prCESA7::PRX64-mCherry* and had reduced structural integrity (Figure 3.14c).

Similar to the accumulation of tagged AtLAC4, AtLAC17, or AtPRX64 in the cell corners of xylem vessels, residual expression in fiber cells may have led to secretion to cell corners and the SCW. However, it is unclear why there was such a dramatic alteration in fiber SCW structure

following LAC or PRX secretion. One hypothesis is that ectopic secretion and accumulation of tagged AtLAC4, AtLAC17, or AtPRX64 is causing SCW lignin digestion. While plant LACs and PRXs are involved in polymerizing lignin, fungal LACs and PRXs are involved in oxidative depolymerization of lignin (Lewis & Yamamoto, 1990). Given that both plant and fungal LACs share a common enzyme structure with a conserved Cu-binding active site, it is unknown how certain enzymes polymerize lignin while others break it down (Awasthi et al., 2015; Dwivedi et al., 2011). *In-vitro*, LACs from the fungus *Polyporus versicolor* and the tree species *Rhus vernicifera* were able to oxidize similar phenolic compounds (Benfield et al., 1964). However, these two enzymes had different pH optima, with a pH optima for fungal LACs between pH 3.6 and 5.2 and a pH optima for plant LACs between pH 6.8 and 7.4 (Benfield et al., 1964). Despite these differences, both fungal and plant LACs could oxidize phenolic compounds outside the pH optima range. This flexibility could thus act to differ the oxidative mechanism of LACs and PRXs in different environments (*e.g.* lignin synthesis or breakdown). Therefore, the specific microenvironment of the SCWs present when AtLAC4, AtLAC17, or AtPRX64 is ectopically expressed under prCESA7 and secreted to SCWs could be facilitating lignin depolymerization and leading to reduced cell wall integrity. In support of this hypothesis is the observation that loss of the monolignol biosynthetic gene *AtCCR1* in Arabidopsis *ccr1g* mutants resulted in significantly reduced lignin, altered SCW polysaccharide structure, and a similar loss of fiber cell wall integrity (Ruel et al., 2009).

Loss of cell wall integrity in fibers could also be due to cleavage of SCW polysaccharides. PRXs have dual catalytic cycle, including a peroxidative (H_2O_2 consumption) and an hydroxylic cycle (H_2O_2 production), and are thus able to both oxidize monolignols as well as produce ROS (Passardi et al., 2005). Similarly, fungal LACs can produce ROS to aid in lignin depolymerization (Wei et al., 2010). Importantly, ROS have been demonstrated to cleave cellulose, pectin, and xylan polysaccharide chains *in-vitro* (Fry, 1998; Miller, 1986). Therefore, ectopic expression and secretion of LACs and PRXs driven by the promoter of *AtCESA7* could result in altered enzymatic activity, preferential production of ROS, and subsequent breakdown of cell wall polysaccharides. Cleavage of integral polysaccharides like SCW cellulose could result in the observed loss of cell wall integrity, similar to the irregular xylem phenotype observed in *AtCESA7* (*irx3)* mutants with

reduced SCW cellulose content (Taylor et al., 1999). The control over whether a LAC or PRX oxidizes monolignols or produces ROS is most likely dependent on the microenvironment of the enzyme and cell wall, but the specific mechanisms have not been studied extensively (Passardi et al., 2004). To test whether the collapsed fiber phenotype is due to an alteration in the redox environment, I stained mature *prCESA7::PRX64-mCherry* stem cross-sections with H_2DCF, which forms a fluorescent product upon reaction with ROS (Kalyanaraman et al., 2012). Compared with structurally-intact fiber cells, there was a reduction in H_2DCF fluorescence intensity in collapsed fiber cell walls that had secreted *prCESA7::PRX64-mCherry* (Figure 3.15d). This reduction in fluorescence intensity suggests that ROS are being produced at lower levels in these regions or that ROS are being consumed at higher rates. This preliminary data therefore suggests there is some alteration in redox environment in collapsed fiber cells.

Defects in cellulose structure and cell wall integrity could also explain the ectopic pith lignification. Mutation of the PCW *AtCESA3* (*eli1*) impaired cell expansion, activated defense responses through hormone signaling, and caused ectopic pith lignification (Caño-Delgado et al., 2000). In *eli1* mutants, ectopic lignification was due to the activation of defense signaling rather than the defect in cellulose itself. Therefore, collapsed SCW fibers in transgenic lines may be activating a systemic wounding response that causes ectopic lignification of pith cells.

It is also possible that transformation of *prCESA7::LAC4-mCherry*, *prCESA7::LAC17-mCherry*, or *prCESA7::PRX64-mCherry* disrupted normal development and caused artifacts that are not representative of the true function or localization of the cloned genes. All constructs were transformed into a Col-0 wild-type background, so transgenic plants have an additional copy of the given LAC or PRX in the genome. Increasing gene dosage may alter normal lignification or localization of these enzymes to the cell wall. For instance, over-expression of *AtSND1*, a master transcriptional regulator of SCW formation in fibers, resulted in a pendant stem phenotype, ectopic lignification in non-lignifying cell types, and reduced cell wall thickness in fibers (Zhong et al., 2006). This and other studies suggest that ectopic or over-expression of lignin-related genes negatively impacts lignified tissue. However, previous cloning of *prLAC4::LAC4-mCherry*, *prLAC17::LAC17-mCherry*, and *prPRX64::PRX64-mCherry* were performed in the Col-0 background without noticeable differences to lignification or fiber cell morphology, so gene

dosage cannot completely explain the transcriptional silencing or abnormal lignin phenotypes (Lee et al., 2013; Schuetz et al., 2014). Currently, I have cloned *prCESA7::LAC4-mCherry*, *prCESA7::LAC17-mCherry*, and *prCESA7::PRX64-mCherry* into the respective knockout mutant background for these genes (*lac4-2/lac17* for *AtLAC4* and *AtLAC17*, and *prx64* null for *AtPRX64*, respectively) and future work can test whether localization patterns, ectopic pith lignification, and the collapsed fiber phenotypes are consistent.

3.4 Conclusions

The results of this chapter demonstrate that a combination of bioinformatics and mutant phenotypes can support identification of putative lignin-associated LACs and PRXs. Analyses of fluorescently-tagged LACs and PRXs expressed under their native respective promoter showed that AtLAC4, AtLAC17, and AtPRX72 co-localized with lignin in the SCW, which is consistent with their mutant phenotypes. A subset of the tagged LACs and PRXs, including AtPRX64, AtPRX71, and AtLAC10, localized to the cell corners and middle lamella of fiber cells. While tagged AtPRX64 was distributed throughout the interfascicular fiber cell layers, AtPRX71 and AtLAC10 localized to cell corners adjacent to the endodermis, suggesting that this cell wall domain may have specialized structural features. Overlap between regions of localization could indicate potential redundancy between enzymes and explain the lack of mutant phenotypes in single knockout lines. Other LACs and PRXs did not localize to lignified tissues and may be involved in other biological processes.

To test whether timing of gene expression could influence a protein's location in the cell wall, I expressed *AtLAC4*, *AtLAC17*, and *AtPRX64* under the promoter of *AtCESA7*. *prCESA7::LAC4-mCherry*, *prCESA7::LAC17-mCherry*, and *prCESA7::PRX64-mCherry* consistently localized to the same cell type and region of the cell wall in stems and roots, suggesting that timing of expression plays a role in protein localization and that no structural properties restrain these enzymes from a certain cell wall microenvironment. These experiments were confounded by transcriptional silencing in the stem, which is consistent with strong regulation over gene expression of oxidative enzymes throughout development. Further support for this was seen following ectopic LAC or PRX secretion in stem tissues, which led to pith lignification and a loss

of SCW structural integrity. Therefore, while timing of expression plays a role in localization, there are potentially multiple regulatory layers over transcription, translation, and localization of LACs and PRXs to ensure developmental lignification occurs at the right time and in the correct cell types.

Chapter 4: Differential localization of LACs and PRXs in developing Arabidopsis stems

4.1 Introduction

Lignin polymerization and SCW formation is highly controlled throughout development, both spatially to different cell types and regions of the cell wall, and temporally throughout growth (Altamura et al., 2001; Hall et al., 2013). During primary growth, procambial and ground tissue that will develop into xylem vessel elements and fiber cells undergo a period of division in the root or shoot apical meristem followed by elongation, terminal differentiation, SCW deposition, and cell death. Consequently, these cell types must coordinate lignification within the context of changing developmental cues (*e.g.* elongating organs and tissues) and cell wall structures. In this chapter, the inflorescence stem of Arabidopsis is used as a model for development of lignifying cell types. During growth of Arabidopsis stems, water-conducting xylem vessel elements are lignified early in development and fibers are lignified later to provide structural support. Earlier work on secondary growth in trees showed that lignin is first deposited in the pectin-rich middle lamella and later polymerized within the cellulose- and xylan-rich SCW (Donaldson, 2001; Terashima & Fukushima, 1988). Clearly, the amount, composition, and spatial distribution of lignin polymerization in different cell types and cell wall domains during stem development is tightly regulated. However, the cellular mechanisms that control the spatio-temporal deposition of lignin are poorly understood. Given that LACs and PRXs are involved in the final stage of lignin polymerization, coordinated lignin deposition to particular regions during development could be managed by dictating the specific localization of lignin-associated LACs and PRXs (Schuetz et al., 2014). To test this hypothesis, it is necessary to visualize where lignin-associated LACs and PRXs are located throughout development and document how their localization correspond to lignin deposition.

In addition to spatially controlling where lignin-associated LACs and PRXs are found in space and time, a further level of regulation over enzyme activity could occur by limiting access to oxidative substrates for lignification. As PRXs require H_2O_2 to oxidize monolignols, it is possible that plant cells modulate apoplastic H_2O_2 production to regulate PRX oxidative activity in cell walls (Córdoba-Pedregosa et al., 2003; Gabaldón et al., 2006; Lee et al., 2013; Ros Barceló, 1998,

2005). Therefore, identifying the location and quantity of apoplastic H_2O_2 throughout development may provide evidence as to whether PRX oxidative activity is limited spatially and/or temporally by H_2O_2 availability in the stem.

Based on the observed localizations of tagged putative lignin-associated LACs and PRXs from Chapter (3), I hypothesized that lignin deposition in a particular region of the cell wall during development would be accompanied by specific localization of multiple oxidative enzymes to that area. I also predicted that production of apoplastic H_2O_2 would be higher in lignifying cell walls compared with non-lignifying cell walls.

I had the following objectives:

1) Develop a reproducible method for detecting lignin deposition to cell types and regions of the cell wall throughout development of the Arabidopsis inflorescence stem.
2) Identify the cell types and regions of the cell wall which tagged LACs and PRXs are specifically secreted to during different stages of stem development.
3) Determine whether PRX localization to different regions of the cell wall is due to reduced mobility following deposition of SCW polysaccharides during development.
4) Determine the spatial distribution of apoplastic ROS production during stem development.

In this chapter I demonstrate that lignification of vascular bundle xylem vessel elements precedes lignification of xylary and interfascicular fibers. As stem development proceeded, a unique set of LACs and PRXs were specifically secreted to SCWs of xylem vessel elements and mature fibers (AtLAC4, AtLAC17, and AtPRX72), while the cell corners of lignifying fibers contained a different set of oxidative enzymes (AtPRX64 and AtPRX71). Similar with observed localization patterns of tagged enzymes, total LAC and PRX oxidative activity was limited to lignifying cell types throughout development. Whole stem H_2O_2 levels were not correlated with lignin deposition during growth, but histochemical staining showed higher apoplastic ROS production in xylem vessel elements early in development and higher ROS production in fibers in more mature tissues. In combination, these results demonstrate that distinct sets of oxidative

enzymes are turned on at specific developmental stages to control where lignin is deposited. PRX oxidative activity in specific regions of the cell wall could be controlled throughout development by modulation of apoplastic H_2O_2 production.

4.2 Results

4.2.1 Mapping lignin deposition during development of the inflorescence stem of Arabidopsis

Earlier studies have qualitatively recorded spatial distributions of lignin in Arabidopsis stems (Altamura et al., 2001; Ehlting et al., 2005; Hall et al., 2013). However, quantitative mapping of lignin deposition in specific cell types during stem development has not been performed. To quantify developmental lignin deposition in the stem, I sampled 17 cm-tall, 5-week-old Col-0 stems. Stems were divided into 2cm pieces, starting from the apical tip, for a total of eight developmental stages. Stem cross-sections were taken from each stage and analyzed for UV lignin autofluorescence using spinning disk confocal microscopy (Figure 4.1). At the apical tip of the stem (2cm-4cm), low lignin UV autofluorescence was detected in xylem vessel elements (Figure 4.1a-b). Towards the middle of the stem (6-8cm), lignin in xylem vessel elements increased and faint UV autofluorescence was evident in the cell walls of interfascicular fibers (Figure 4.1a). From 10cm to the base of the stem, UV lignin autofluorescence increased in both xylem vessel elements and fibers (Figure 4.1a-b), with greater intensity in the vascular bundles than the interfascicular fibers. At this stage of development, small lignified cells in the vascular bundles were observed, but it was not possible to classify these as small metaxylem vessels, tracheids, or xylary fibers. To establish how UV lignin autofluorescence specifically changed at the cellular level, I quantified the intensity of UV lignin autofluorescence in lignified xylem cells and interfascicular fibers from each of the developmental stages (4.1c-d). Similar to the qualitative evaluation, lignin UV autofluorescence in the lignified xylem cells was very low at the tip of the stem but significantly increased to greater intensities toward the base of the stem (Figure 4.1c). The UV lignin autofluorescence for fibers was negligible at the tip of the stem and first detected at approximately 6-10cm (Figure 4.1d). In more mature stages (12cm to the base of the stem), UV lignin autofluorescence in fibers significantly increased (Figure 4.1d). These data indicated that lignin deposition started in the vascular bundles, which continuously lignified as

new cells differentiated. Interfascicular fiber started lignification at a later developmental stage compared with the vascular bundles, with high lignin deposition in both xylem and fiber cells at the mature base of the stem.

After establishing lignin deposition throughout development, I chose three discrete developmental stages to focus on for further localization and histochemical analyses (Figure 4.2). To select these stages, I evaluated location and intensity of UV lignin autofluorescence as well as SCW deposition in different cell types. Stage 1 occurs early in development at the apical tip of the stem (2cm-4cm), when lignin is restricted to the SCW of xylem vessel elements (Figure 4.2a). At this stage, UV lignin fluorescence intensity in xylem vessel elements is very low (heatmap; Figure 4.2a). In addition, brightfield images show that undifferentiated fibers have a thin PCW and have not developed a thick SCW. Stage 2 is located towards the middle of the stem (6-8cm), where lignin fluorescence intensity increases in the SCW of xylem vessel elements and is first deposited in the cell corners and middle lamella of interfascicular fibers (Figure 4.2b). At this stage, fibers are in the initial stages of depositing a SCW and show a slightly increased thickness of their cell wall relative to neighboring non-lignified cell types (Figure 4.2b). Finally, Stage 3 is found in mature tissues (10cm to the base of the stem), where bulk lignin deposition occurs in the SCW of both xylem vessel elements and fibers (Figure 4.2c). The appearance of a thick SCW in both xylem cells and fibers is evident in brightfield images, as compared to the thin PCWs of neighbouring unlignified cell types (Figure 4.2c).

An additional experimental approach for localization of lignin is to treat stem cross-sections from each of the developmental stages with phloroglucinol-HCl, which stains hydroxycinnamyl aldehydes pink (Pomar et al., 2002). At Stage 1, xylem vessel elements stained pink but not fibers (Figure 4.2d). At Stage 2, xylem vessel elements turned pink and the early cell corners of fibers also turned a very faint pink (Figure 4.2d). During Stage 3 the SCW of both xylem cells and interfascicular fibers turned pink (Figure 4.2d). Therefore, the presence of lignin at each of the developmental stages may be determined using either UV lignin autofluorescence or the lignin-specific stain phloroglucinol-HCl. These stages consequently represent three major developmental time-points for lignin deposition in the stem, both to different cell types as well as regions of the cell wall.

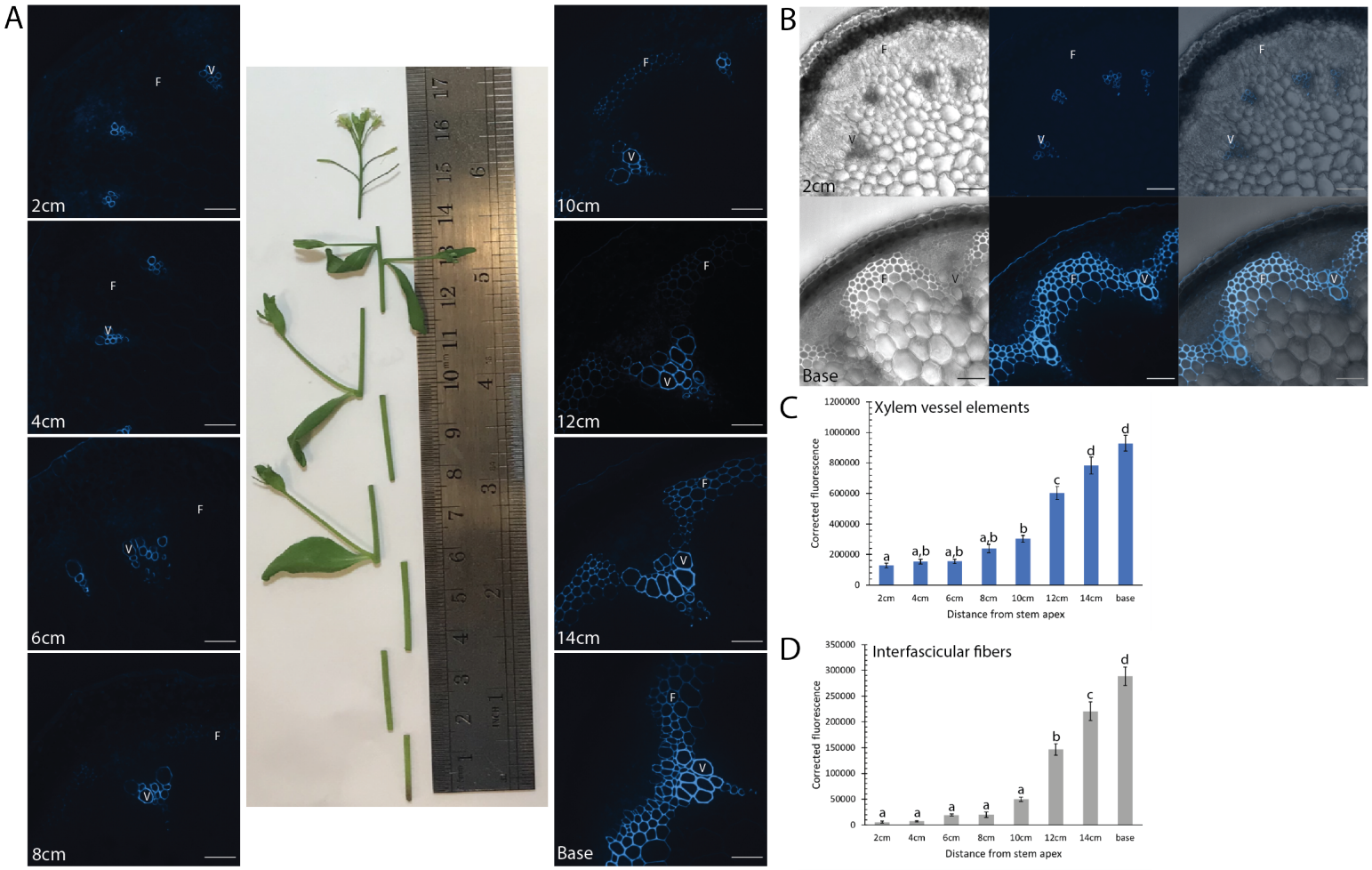

Figure 4.1. Lignin is deposited to different cell types and regions of the cell wall during development of the Arabidopsis floral stem. A) 17cm-tall Col-0 inflorescence stems were divided into 2cm pieces (starting measurement from the apical tip of the stem) for a total of 8 developmental stages. UV lignin autofluorescence (blue) was analyzed from stem cross-sections from each stage. V=xylem vessel elements; F=interfascicular fibers. Scale bars are 50µm. B) Brightfield images provide context for UV lignin autofluorescence in xylem vessel elements and fibers in stem cross-sections from 2cm and the base of the stem. C) Corrected lignin UV autofluorescence for xylem vessel elements increases throughout development. N>30 cells for each developmental stage; 1-way ANOVA; letters indicate significantly different values, $p<0.05$. D) Corrected lignin UV autofluorescence for fibers increases throughout development. N>30 cells for each developmental stage; 1-way ANOVA; letters indicate significantly different values, $p<0.0001$. Bars are SE.

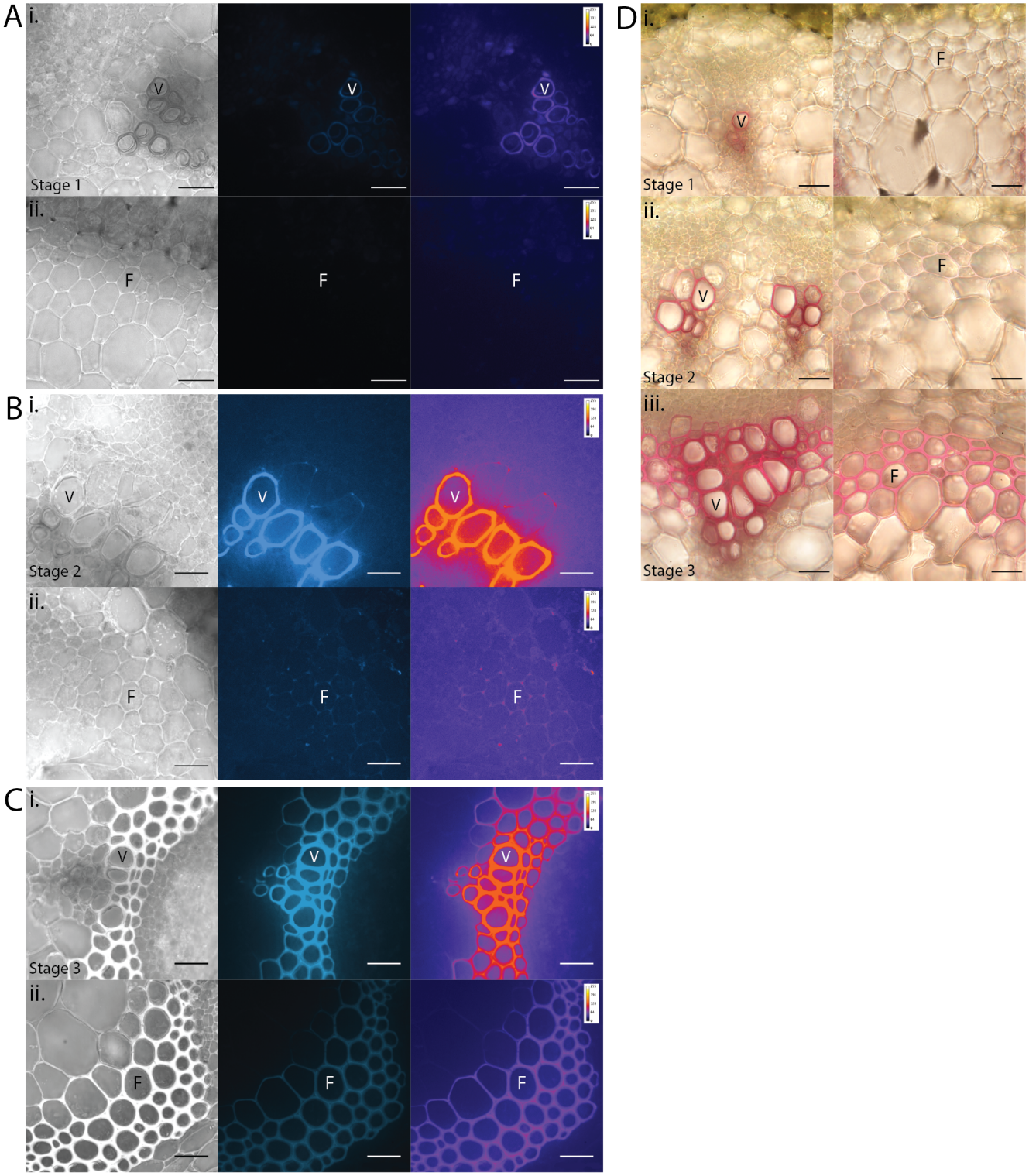

Figure 4.2. Defining three stages of developmental lignification in the Arabidopsis Col-0 stem. A-C) Representative images depicting brightfield, UV lignin autofluorescence (blue), and falsely-coloured heat map. V=xylem vessel element; F=fiber. Scale bars are 20µm. A) Stage 1 has lignin exclusively in the SCW of xylem vessel elements (i) and not in interfascicular fibers (ii). B) Stage 2 has lignin in the SCW of xylem vessel elements (i) and the cell corners of interfascicular fibers (ii). C) Stage 3 has lignin in the SCW of xylem vessel elements (i) and in the SCW of interfascicular fibers (ii). D) Phloroglucinol-HCl staining confirms presence of lignin in regions indicated by UV autofluorescence for Stage 1 (i), Stage 2 (ii) and Stage 3 (iii).

4.2.2 Polymerized lignin in the cell wall, not soluble phenolics, produce the dominant autofluorescent signal

In these stem analyses, UV lignin autofluorescence was used as a reporter for the presence and relative concentration of lignin in lignified cell walls. However, other phenolic compounds besides polymerized lignin in the SCW can also contribute to the observed UV autofluorescence signal. To test for the involvement of soluble phenolics, I incubated Col-0 stem cross-sections from each of the eight developmental stages in 100% methanol for 1 hour. I quantified the intensity of UV autofluorescence in xylem cells and interfasicular fibers at each of the developmental stages and compared it to UV autofluorescence of mock-treated (H_2O) Col-0 stem cross-sections (Figure 4.3). Qualitatively, there were no apparent differences in UV lignin autofluorescence at any of the three major developmental stages for either xylem vessel elements (Figure 4.3a) or fibers (Figure 4.3b). Quantification of UV autofluorescence in each of the cell types did find significant differences between control and methanol-treated stems, but only at particular developmental stages. In xylem vessel elements, there was a significant reduction in UV autofluorescence at 4cm and at the base of the stem following methanol treatment (Figure 4.3c). In interfascicular fibers, there was a significant reduction in UV autofluorescence intensity at 6cm and at the base of the stem (Figure 4.3d). Overall, the reductions in UV autofluorescence following methanol treatment were relatively minor, indicating that soluble phenolics did contribute to the UV autofluorescence signal but the majority represented polymerized lignin in the cell wall.

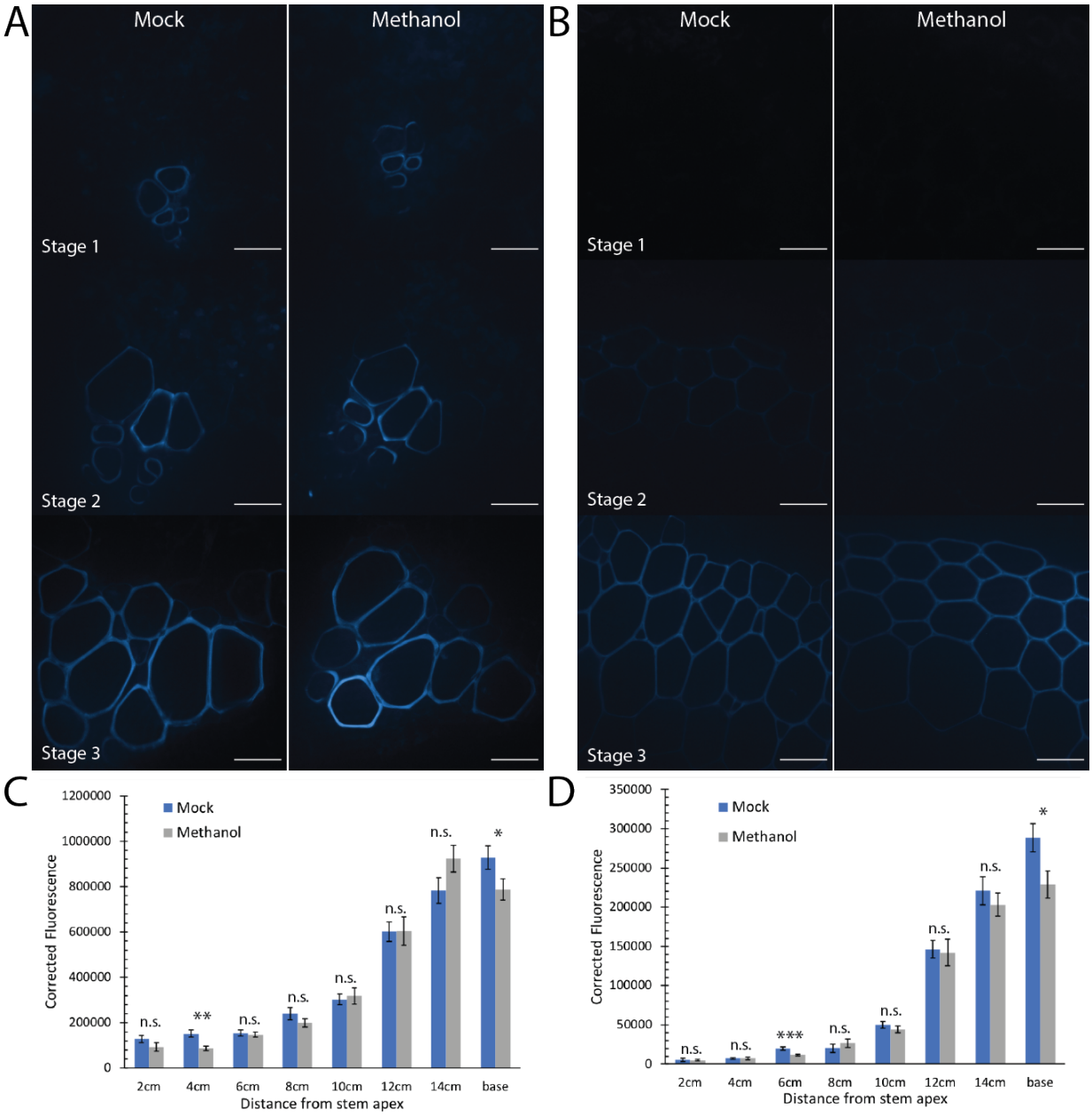

Figure 4.3. UV autofluorescence is from polymerized lignin in the cell wall with minor contribution from soluble phenolics. Stem cross-sections were treated with 100% methanol to remove soluble phenolics and imaged for UV lignin autofluroresecence (blue). Mock treatment was H_2O. Scale bars are 20µm. A) UV lignin autofluorescence in xylem vessel elements looks qualitatively the same between mock- and methanol-treated stems for the three major developmental stages. B) UV lignin autofluorescence in fibers looks qualitatively the same between mock and methanol-treated stems for the three major developmental stages. C) Quantification of UV lignin autofluorescence in xylem vessel elements indicate significant reduction of fluorescence intensity at 4cm and at the base of the stem. D) Quantification of UV lignin autofluorescence of fibers indicate significant reduction of fluorescence intensity at 6cm and at the base of the stem. UV lignin autofluorescence quantification was performed for N>30 cells from 3 biological replicates; 1-way ANOVA; letters indicate significantly different values, n.s.=not significant; *p<0.05; **p<0.01; ***p<0.001. Bars are SE.

4.2.3 Lignifying cell wall domains have distinct cell wall polysaccharide compositions

In addition to changes in lignin deposition, the PCW, SCW, and adjoining middle lamella also undergo major structural and compositional modifications during the three major developmental stages. To compare lignin patterns with changes in cell wall polysaccharides, I incubated LR white resin-embedded cross-sections of Arabidopsis stems with the primary antibody JIM7 and a secondary antibody conjugated with Alexa488 (Figure 4.4). JIM7 is specific for methylesterified pectin in the middle lamella (Knox et al., 1990). At Stage 1, JIM7 signal was found in the cell corners/middle lamella of all cell types but was not found in the SCW of lignified xylem vessel elements (Figure 4.4a). Undifferentiated fiber cell walls showed high fluorescence intensity and homogenous JIM7 labeling. At Stage 2, JIM7 signal was not found in the SCW of xylem vessel elements and the fluorescence intensity diminished within the middle lamella of interfascicular fibers (Figure 4.4b). Strong antibody labeling was still evident in the cell corners of non-lignifying cell types adjacent to interfascicular fibers. At Stage 3, JIM7 signal was absent from the SCW of lignified xylem vessel elements and fibers and was highly diminished from the cell corners of interfascicular fibers (Figure 4.4c). In contrast, JIM7 signal was still abundant in the cell corners of non-lignifying cells. Therefore, immunolocalization analyses indicated that these highly methylesterified pectin epitopes were restricted to cell corners/the middle lamella throughout development. In addition, pectin epitopes in the cell corners of lignifying cells may either be modified by cell wall proteins or masked during progressive lignification.

To immunolabel SCWs, I incubated resin-embedded cross-sections with the primary antibody LM10, which is specific for the SCW hemicellulose xylan (Figure 4.5; McCartney et al., 2005). At Stage 1 at the apical tip of the stem, LM10 signal was very low and only found in the lignified SCW of xylem vessel elements (Figure 4.5a). No signal was apparent in any region of the cell wall in interfascicular fibers (Figure 4.5a). During Stage 2, LM10 signal increased in the SCW of xylem vessel elements and was also observed in the SCW of interfascicular fibers at a low fluorescence intensity (Figure 4.5b). During Stage 3, LM10 signal had the highest fluorescence intensity and was found in the SCW of both lignified xylem vessel elements and fibers (Figure 3.5c). For all developmental stages, LM10 signal was only detected in the SCW and not in the cell corners or middle lamella. Immunolocalization using LM10 antibodies therefore demonstrated

that xylan was exclusively found in the SCW and increased through development. In addition, SCW xylan in interfascicular fibers was first deposited at approximately the same time as initial lignification of cell corners in Stage 2 and preceded bulk lignin deposition in the SCW during Stage 3.

To confirm the observed immunolocalization signal is from binding of the respective primary antibody, I incubated control cross-sections at the base of the stem with either JIM7 or LM10 primary antibodies but no secondary antibody conjugated to Alexa488. These control sections showed no signal using the GFP/Alexa488 filter on the confocal microscope (Figures 4.4d, 4.5d), confirming that the fluorescence signal observed was due to fluorescent labeling of primary antibodies.

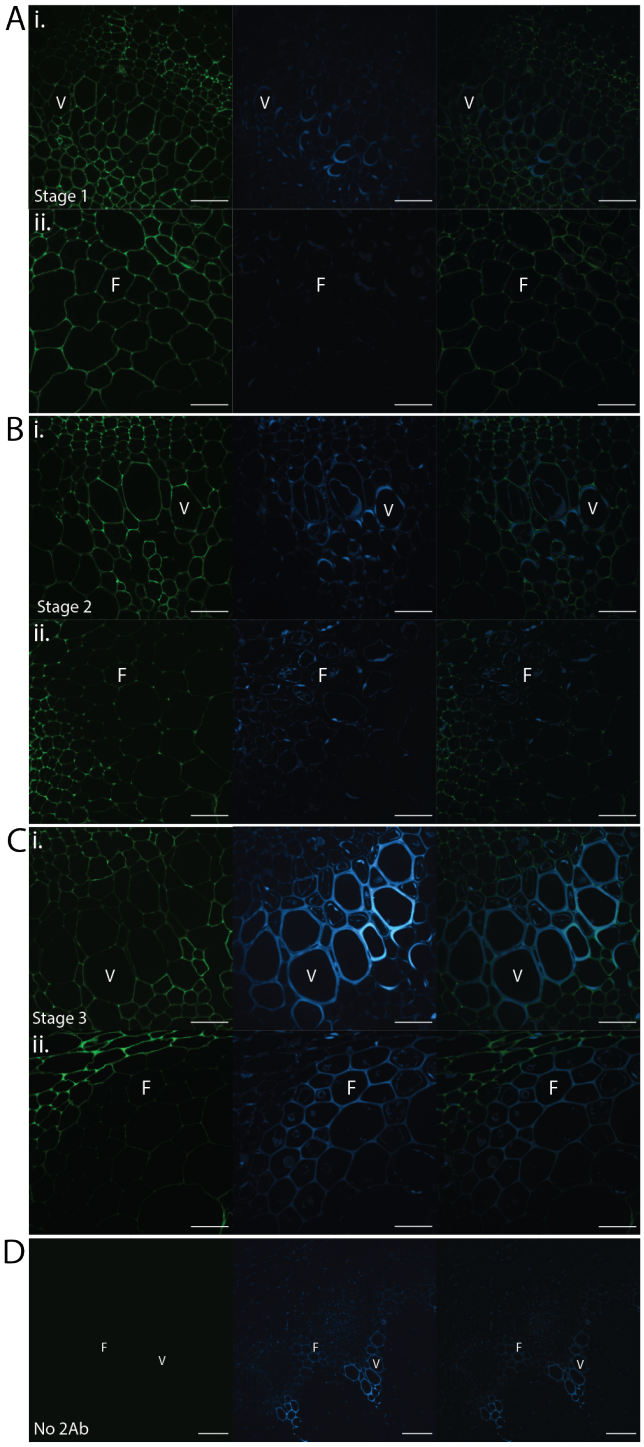

Figure 4.4. Immunolocalization of pectin shows dynamic changes to the composition of PCWs and the middle lamella throughout development of the Arabidopsis stem. Representative images depicting Alexa488-labeled JIM7 antibody (green), UV lignin autofluorescence (blue), and merged image. V=xylem vessel element; F=fiber. JIM7 is specific for methylesterified pectin. Scale bars are 20µm for A-C) and 50µm for D). A) In Stage 1, JIM7 labels the cell corners and PCWs of all cell types but is restricted from the SCW of xylem vessel elements (i). JIM7 signal is found in the cell corners of undifferentiated fibers (ii). B) In Stage 2, JIM7 labels the cell corners and PCWs of all cell types but is restricted from the SCW of xylem vessel elements (i). JIM7 signal is reduced in the cell corners of differentiating fibers (ii). C) In Stage 3, JIM7 labels the cell corners and PCWs of all cell types but is restricted from the SCW of xylem vessel elements (i). JIM7 signal is highly reduced/absent in the cell corners of undifferentiated fibers (ii). D) Control sections with no Alexa488 secondary antibody show no signal for JIM7.

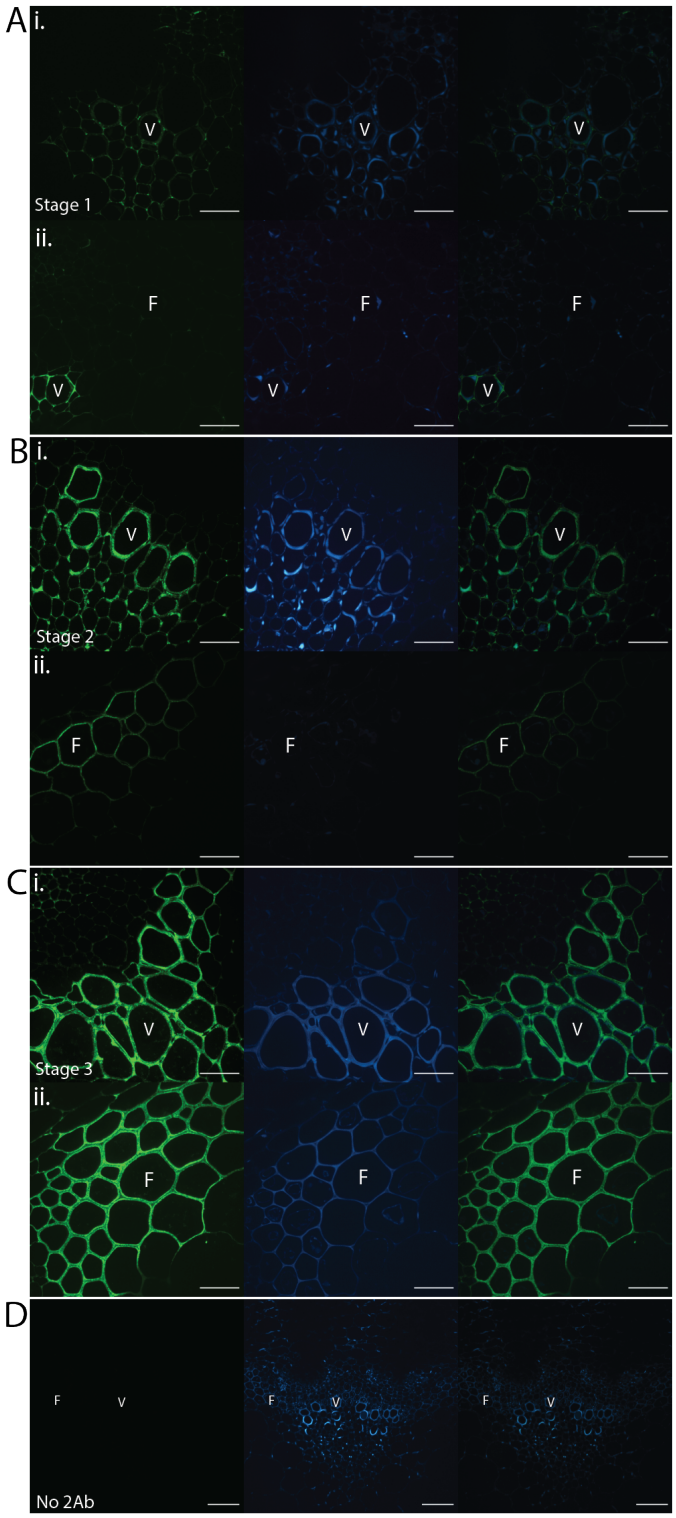

Figure 4.5. Immunolocalization of xylan shows dynamic changes to the composition of SCWs throughout development of the Arabidopsis stem. Representative images depicting Alexa488-labeled LM10 antibody (green), UV lignin autofluorescence (blue), and merged image. V=xylem vessel element; F=fiber. LM10 is specific for the SCW hemicellulose xylan. Scale bars are 20µm for A-C) and 50µm for D). A) In Stage 1, LM10 labels the SCW of xylem vessel elements (i) and is not seen in the cell walls of undifferentiated fibers (ii). B) In Stage 2, LM10 labels the SCW of xylem vessel elements (i) and first appears in the SCW of differentiating fibers (ii). C) In Stage 3, LM10 labels the SCW of xylem vessel elements and fibers (ii). D) Control sections with no secondary Alexa488 antibody show no signal for LM10.

4.2.4 Specific sets of LACs and PRXs localize to different SCW regions throughout stem development

Previous studies (Chapter 3; Chou et al., 2018) examined the localization of oxidative enzymes in mature Arabidopsis stems and showed that mCherry-tagged lignin-associated LACs and PRXs were found in specific cell types and wall domains. For example, interfascicular fibers had AtLAC4, AtLAC17, and AtPRX71 in the xylan-rich SCW, while AtLAC10, AtPRX64, and AtPRX71 were found in cell corners/middle lamella. Given the changes in lignin patterns over development (Figure 4.3), I hypothesized that the oxidative enzymes found in the cell corners would be deposited early in development while enzymes embedded in the SCW would appear later during SCW polysaccharide deposition. I analyzed the distribution of tagged LACs and PRXs under their respective native promoter from Chapter (3) in stem cross-sections from the three main developmental stages and tested whether enzymes co-localized with UV lignin autofluorescence. I focused on LACs and PRXs that were found in lignifying cells, including AtLAC4-mCherry, AtLAC17-mCherry, AtPRX64-mCherry, AtPRX71-mCherry, and AtPRX72-mCherry.

At Stage 1 at the apical tip of the stem, AtLAC4-mCherry (Figure 4.6a), AtLAC17-mCherry (Figure 4.6b), and AtPRX72-mCherry (Figure 4.6c) all localized to the SCW of lignified xylem vessel elements. Their distribution was analogous to mature stems, where they were embedded in the thick SCW. In contrast, AtPRX64-mCherry and AtPRX71-mCherry were not seen in any cell types at this stage (data not shown). At Stage 2, AtLAC4-mCherry, AtLAC17-mCherry, and AtPRX72-mCherry again localized to the thick SCW of xylem vessel elements (Figure 4.7a). Surprisingly, AtLAC4-mCherry (Figure 4.7a) also localized to the lignifying cell corners of interfascicular fibers, contrasting its observed localization in mature tissues. Localization of AtLAC4-mCherry to the SCW of xylem vessel elements and the cell corners of fibers was confirmed with higher magnification images (Figure 4.7b). As predicted from earlier findings, AtPRX64-mCherry (Figure 4.7c) and AtPRX71-mCherry (Figure 4.7c) localized to the lignifying cell corners of fibers at this stage. In contrast, AtLAC17-mCherry and AtPRX72-mCherry were not seen in any region of the cell wall of interfascicular fibers during this developmental stage (Figure 4.7a). As described in Chapter (3), AtLAC4-mCherry (Figure 4.8a), AtLAC17-mCherry (Figure 4.8b), and AtPRX72-mCherry (Figure 4.8c) localized to the SCW of both xylem vessel elements and fibers in mature

tissues during Stage 3. The AtLAC4-mCherry signal observed in the cell corners of interfascicular fibers from Stage 2 was absent. AtPRX64-mCherry was found in a continuous ring of both xylary and interfascicular fibers, but only in the cell corners (Figure 4.8d). AtPRX71-mCherry localized to the outer ring of fibers, with some signal in the cell corners of xylem vessel elements (Figure 4.8e). These data demonstrated that oxidative enzymes localized to the cell corners with the onset of SCW thickening, rather than deposition in the PCW early in development. Building on the data in Chapter 3, the specific set of oxidative enzymes found within a region of a cell wall is dependent on the developmental stage, with transient appearance of AtLAC4 in the cell corners of fibers and later localization exclusively in the thick SCW.

The observation that two PRXs (AtPRX71 and AtPRX72) localized to different regions of the cell wall in interfascicular fibers provided an opportunity to study how two members of the same gene family accumulate in fibers over development. The fluorescence intensity of AtPRX71-mCherry and AtPRX72-mCherry was quantified over the three developmental stages. AtPRX71-mCherry was not found in interfascicular fibers at Stage 1 but first appeared at very low fluorescence intensity in the lignified cell corners during Stage 2, corresponding to approximately 6-8cm from the apical tip of the stem (Figure 4.9a). AtPRX71-mCherry fluorescence signal in cell corners significantly increased from Stage 2 to Stage 3 (Figure 4.9a). These results indicated that AtPRX71-mCherry first localized to the cell corners early in lignification of fibers and was continually secreted to cell corners during lignification of the SCW at later stages of development. AtPRX72-mCherry was not detected in Stage 1 fibers and showed negligible signal at Stage 2 (Figure 4.9b). During Stage 3, AtPRX72-mCherry was first detected in the SCW, corresponding to about 8-10cm from the stem apex (Figure 4.9b). Quantification of the fluorescence intensity of AtPRX72-mCherry in the SCW showed significantly increased fluorescence signal from 10cm to the mature base of the stem (Figure 4.9b). Therefore, the fluorescence intensity of AtPRX71-mCherry in cell corners and AtPRX72-mCherry in the SCW both increased throughout developmental lignification, suggesting that different proteins could simultaneously localize to separate regions of the cell wall during progressive lignification.

In summary, the localization of tagged LACs and PRXs was highly regulated throughout stem growth and was correlated with lignin deposition to different cell type and region of the cell

wall. Tagged AtLAC4, AtLAC17, and AtPRX72 localized to the SCW of xylem vessel elements and fibers throughout development. Tagged AtPRX64 and AtPRX71 exclusively localized to cell corners of fibers and appeared at the developmental stage corresponding to initial fiber cell corner lignification. Unlike the other enzymes, AtLAC4 showed localization to both the SCW and cell corners in fibers, but the localization in cell corners was transient. In addition, enzymes were continually secreted to a given region of the cell wall throughout progressive lignification.

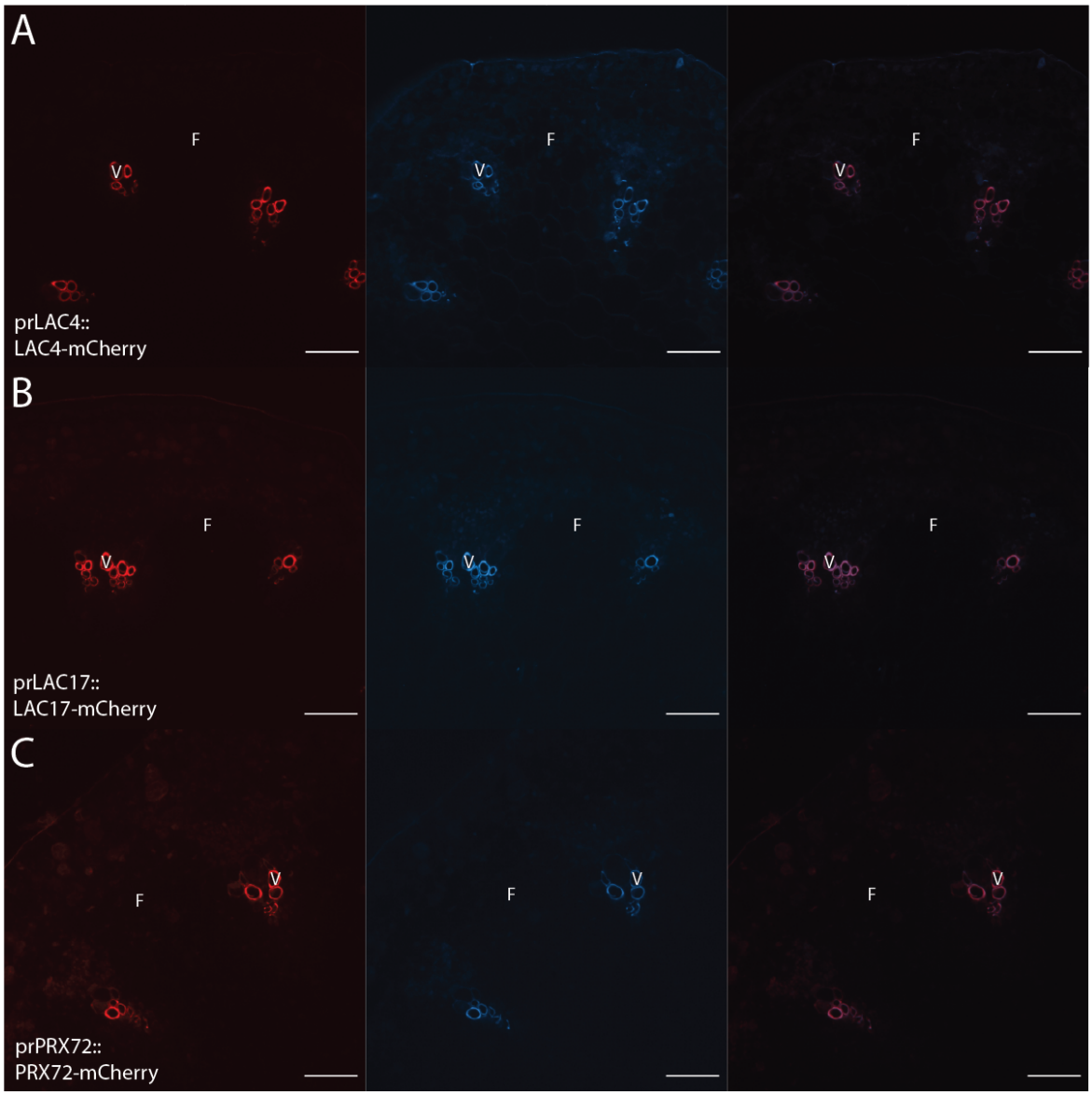

Figure 4.6. Putative lignin-associated LACs and PRXs localize to the SCW of xylem vessel elements during Stage 1 at the apical tip of the stem. Representative images depicting the tagged LAC or PRX under its respective native promoter (red), UV lignin autofluorescence (blue), and merged image. V=xylem vessel element; F=interfascicular fiber. At the tip of the stem (Stage 1), AtLAC4, AtLAC17, and AtPRX72 localize to the SCW of early lignifying xylem vessel elements. Scale bars are 50μm. A) AtLAC4-mCherry. B) AtLAC17-mCherry. C) AtPRX72-mCherry.

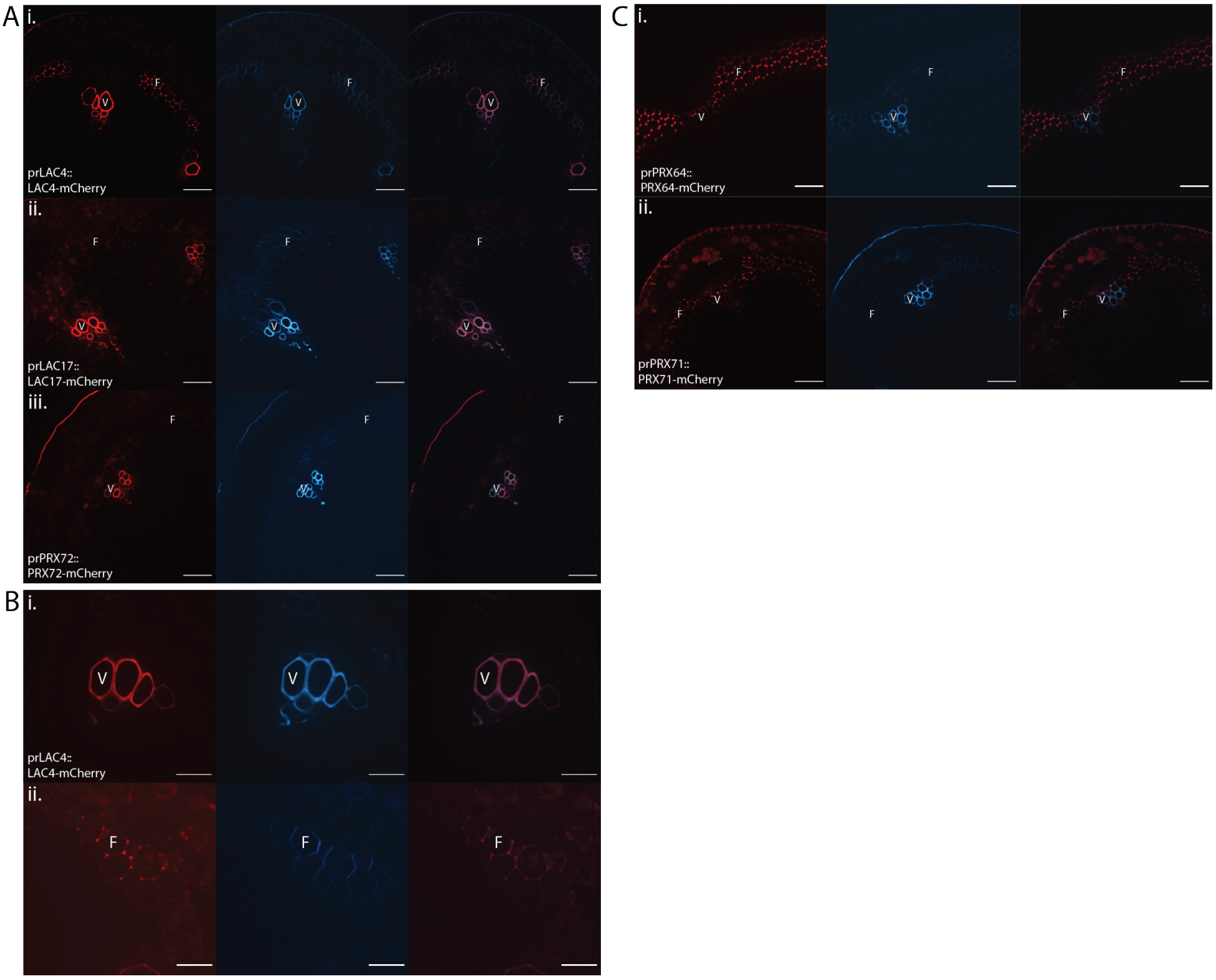

Figure 4.7. LACs and PRXs are secreted to early lignifying cell corners of fibers at Stage 2. Representative images depicting the tagged LAC or PRX under its respective native promoter (red), UV lignin autofluorescence (blue), and merged image. V=xylem vessel elements, F=interfascicular fibers. Scale bars are 50μm for A) and C) and 20μm for B). A) AtLAC4-mCherry (i), AtLAC17-mCherry (ii), and AtPRX72-mCherry (iii) localize to the SCW of lignifying xylem vessel elements. AtLAC4-mCherry also localizes to the cell corners of fibers. B) High magnification shows AtLAC4-mCherry localization to both the SCW of xylem vessels (i) and the cell corners of fibers (ii). C) AtPRX64-mCherry (i), and AtPRX71-mCherry (ii) localize to lignifying cell corners of fibers.

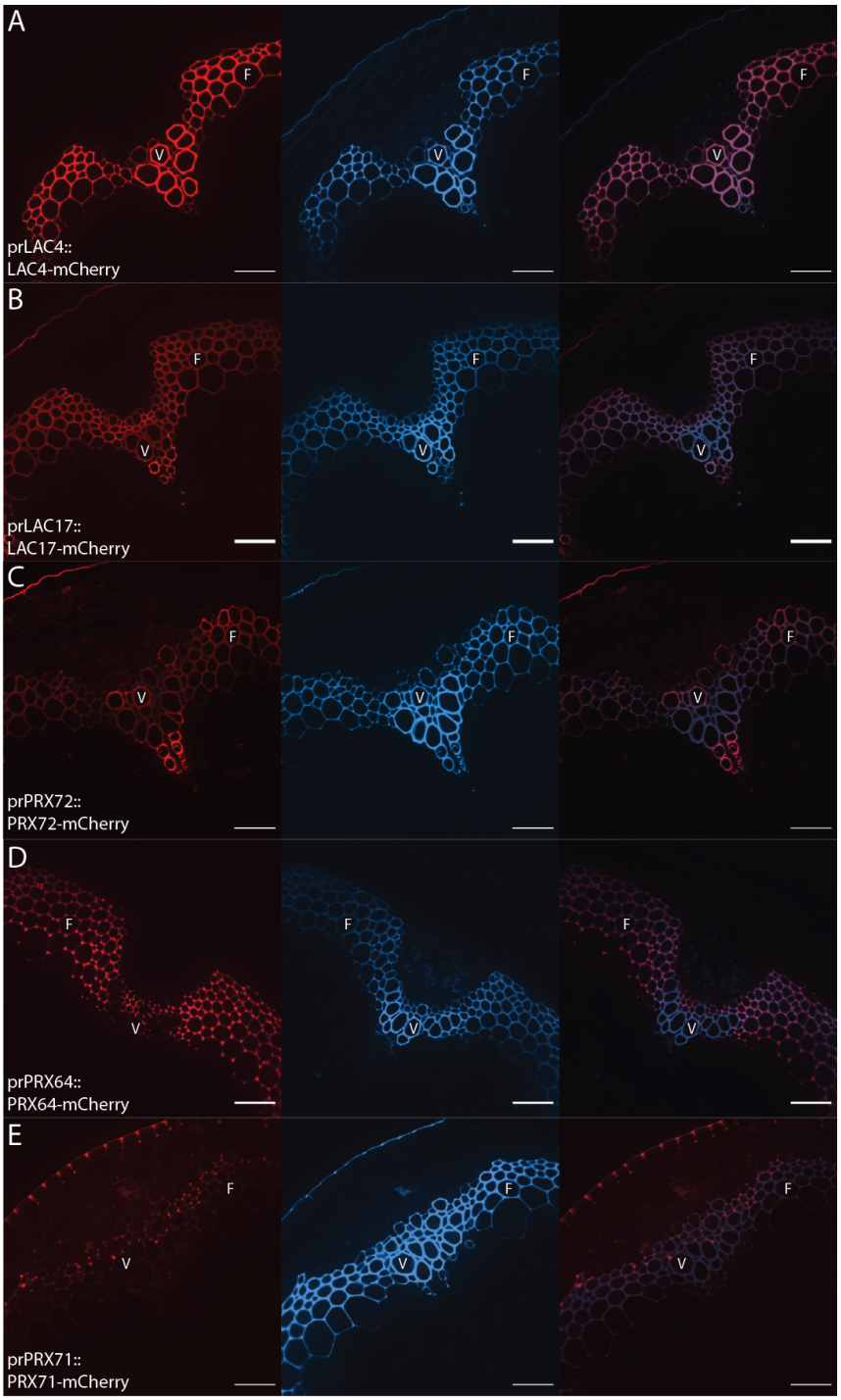

Figure 4.8. LACs and PRXs are secreted to both the SCW and cell corners of xylem vessel elements and fibers during Stage 3. Representative images depicting the tagged LAC or PRX under its respective native promoter (red), UV lignin autofluorescence (blue), and merged image. V=xylem vessel element; F=interfascicular fiber. Scale bars are 50µm. A) AtLAC4-mCherry localizes to the SCW of lignifying xylem vessel elements and fibers. B) AtLAC17-mCherry localizes to the SCW of lignifying xylem vessel elements and fibers. C) AtPRX72-mCherry localizes to the SCW of lignifying xylem vessel elements and fibers. D) AtPRX64-mCherry localizes to the cell corners of fibers. E) AtPRX71-mCherry localizes to cell corners of xylem vessel elements and fibers.

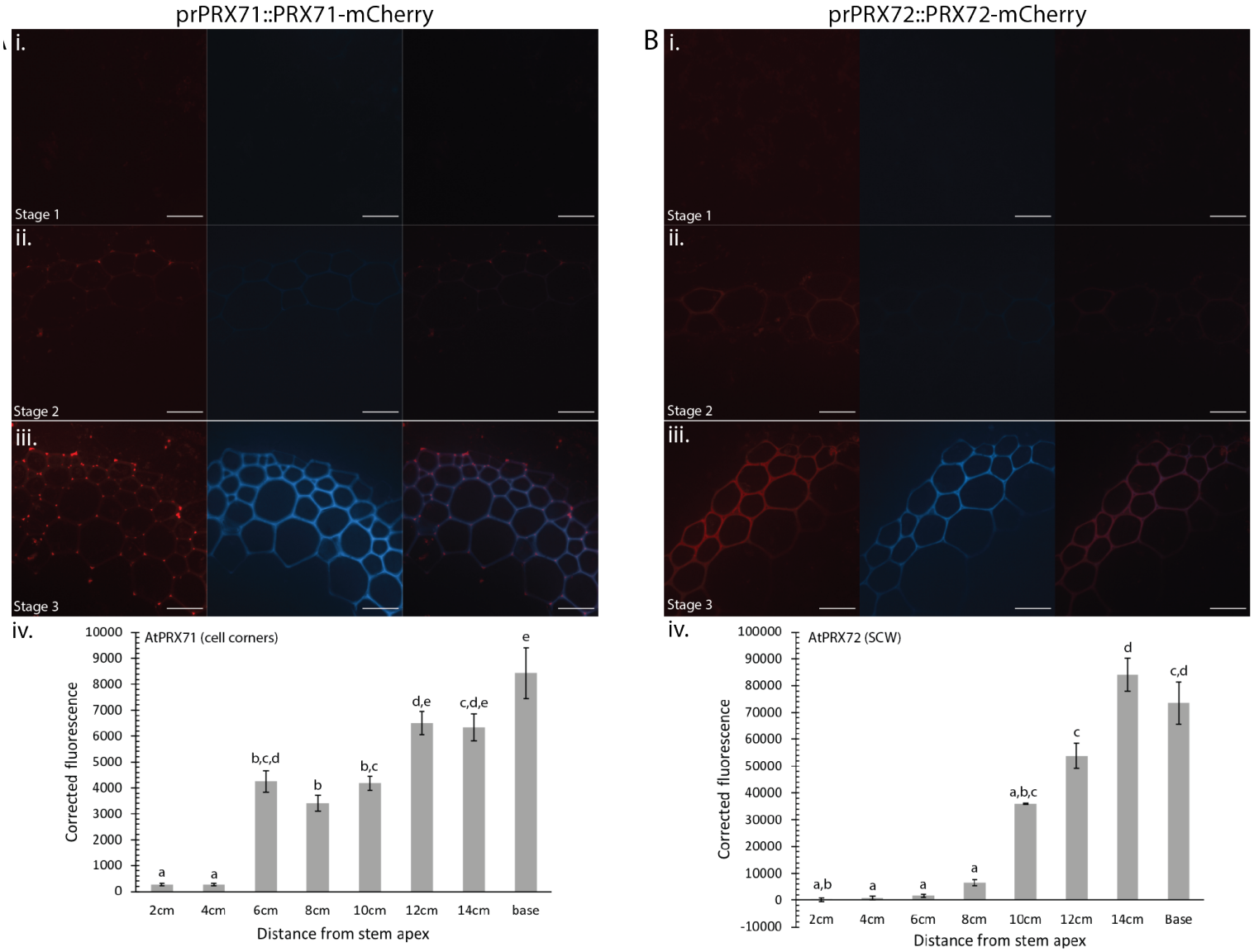

Figure 4.9. PRXs are secreted to different regions of the cell wall simultaneously. Representative images depicting tagged PRX under its respective native promoter (red), UV lignin autofluorescence (blue), and merged image. Scale bars are 20µm. A) AtPRX71-mCherry increases in fluorescence intensity in the cell corners of fibers in Stage 1 (i), Stage 2 (ii), and Stage 3 (iii) during stem development. Quantification of AtPRX71-mCherry cell corner fluorescence (iv). B) AtPRX72-mCherry increases in fluorescence intensity in the SCW of fibers in Stage 1 (i), Stage 2 (ii), and Stage 3 (iii) during stem development. Quantification of AtPRX72-mCherry SCW fluorescence (iv). Corrected fluorescence was measured for N>30 cells for each developmental stage; 1-way ANOVA; letters indicate significantly different values, $p<0.05$. Bars are SE.

4.2.5 TMB and DAF histochemistry shows LAC and PRX enzymatic activity during lignin deposition in developing Arabidopsis stems

As seen in the localization data above, the appearance of multiple oxidative enzymes was correlated with lignification in distinct cell types and cell wall regions during development. However, it was unclear whether these enzymes were active. To visualize where overall LAC and PRX oxidative enzymatic activity was occurring during stem growth, I incubated cross-sections of 17cm-tall Col-0 stems with either 3,3',5,5'-tetramethylbenzidine (TMB) or 2,7-diaminofluorene (DAF). TMB is oxidized by PRXs in the presence of H_2O_2 to form a blue precipitate (Ros Barceló, 1998), while DAF is oxidized by both LACs and PRXs to form a purple precipitate (Bao et al., 1993).

To study PRX-specific oxidative activity, I incubated Col-0 stem cross-sections from different developmental stages with TMB. For all developmental stages, a blue precipitate formed exclusively in regions of lignification (Figure 4.10a). At Stage 1 near the apical tip, a blue precipitate was apparent in the SCW of xylem vessel elements and in the PCWs of neighboring xylem parenchyma cells (Figure 4.10a). No precipitate was detected in the PCWs of undifferentiated fibers. At Stage 2, a blue precipitate formed in the SCWs of xylem vessel elements and PCWs of surrounding xylem parenchyma cells in the vascular bundle. TMB oxidation was also evident in the early lignifying cell corners and middle lamella of interfascicular fibers (Figure 4.10a). At Stage 3, a blue precipitate formed in both the middle lamella and SCWs of xylem vessel elements and fibers (Figure 4.10a). These results provided direct evidence for PRX oxidative activity in lignifying cell types in Arabidopsis. In addition, TMB histochemistry demonstrated that PRX oxidative activity closely matched the distribution of tagged PRXs and developmental lignification to cell types and regions of the cell wall.

To test for the presence and location of other PRXs in stem tissues, I incubated Col-0 stem cross-sections with a combination of TMB and exogenous H_2O_2 (Figure 4.10b). Addition of exogenous H_2O_2 provides information about the location of any PRX capable of oxidizing TMB. Following incubation in H_2O_2, a blue precipitate was detected in all regions of the cell wall for xylem, phloem, cortex, epidermal, pith, and trichome cells at every developmental stage (Figure 4.10b). TMB and H_2O_2 histochemistry therefore suggested that secreted PRXs are found in the

cell wall of all cell types, but the amount of apoplastic H_2O_2 may be limiting the oxidative activity of these enzymes under normal growth conditions.

To confirm that TMB was specific for PRX oxidative activity, I performed a series of control experiments in Col-0 cross-sections at the base of 17cm-tall stems. Firstly, I boiled stem sections and incubated them in TMB. There was no blue precipitate in boiled stem sections (Figure 4.10c), indicating that TMB oxidation requires functional enzymes. To test whether PRXs were required for TMB oxidation, I pre-incubated stem cross-sections in the PRX-inhibitor salicylhydroxamic acid (SHAM). In SHAM-treated cross-sections there was no blue precipitate (Figure 4.10c), indicating that inhibition of PRX activity prevented TMB oxidation. Finally, to test whether TMB oxidation by PRXs requires H_2O_2, I pre-incubated stem cross-sections in catalase to scavenge apoplastic H_2O_2. Again, treatment with catalase abolished formation of the blue TMB precipitate (Figure 4.10c), confirming that PRXs required H_2O_2 to oxidize TMB. Therefore, TMB control experiments showed that the blue precipitate formed in stem cross-sections required PRX activity and the presence of H_2O_2.

To visualize both LAC and PRX oxidative activity, I incubated Col-0 stem cross-sections from different developmental stages with DAF. When oxidized by endogenous LACs and PRXs, DAF forms an insoluble purple precipitate. Similar to localization of PRX activity by TMB staining, formation of the DAF purple precipitate was only observed in regions of lignification (Figure 4.11). At Stage 1, a DAF purple precipitate was formed in the SCW of xylem vessel elements and PCW of surrounding xylem parenchyma cells, but was absent from PCWs of undifferentiated fibers (Figure 4.11a). At Stage 2, a purple precipitate was formed in the SCW of xylem vessel elements as well as lignifying cell corners and middle lamella of interfascicular fibers (Figure 4.11a). At Stage 3, DAF precipitation was observed in the middle lamella and SCW of both xylem vessel elements and interfascicular fibers (Figure 4.11a).

Overall, TMB and DAF histochemistry demonstrated that the greatest LAC and PRX oxidative activity occurred in areas of the stem where the tagged oxidative enzymes were localized and where lignin deposition was active. To test the relative contribution of LAC or PRX enzymatic activity in DAF staining, I incubated cross-sections from the base of 17cm-tall *lac4-2/lac17* mutant stems in DAF. Similar to previous reports, *lac4-2/lac17* double mutants had

collapsed xylem vessel elements (Figure 4.11b; Berthet et al., 2011). Both lignified xylem vessel elements and fibers showed formation of the DAF purple precipitate in the SCW and middle lamella; however, the intensity of the purple precipitate in *lac4-2/lac17* stems was strongly reduced compared with Col-0 samples (Figure 4.11b). The reduction in purple precipitate was strongest in lignified interfascicular fibers (Figure 4.11b). Therefore, AtLAC4 and AtLAC17 clearly play a major role in oxidation of DAF in stem cross-sections but other LACs and PRXs contributed in both xylem vessel elements and fibers.

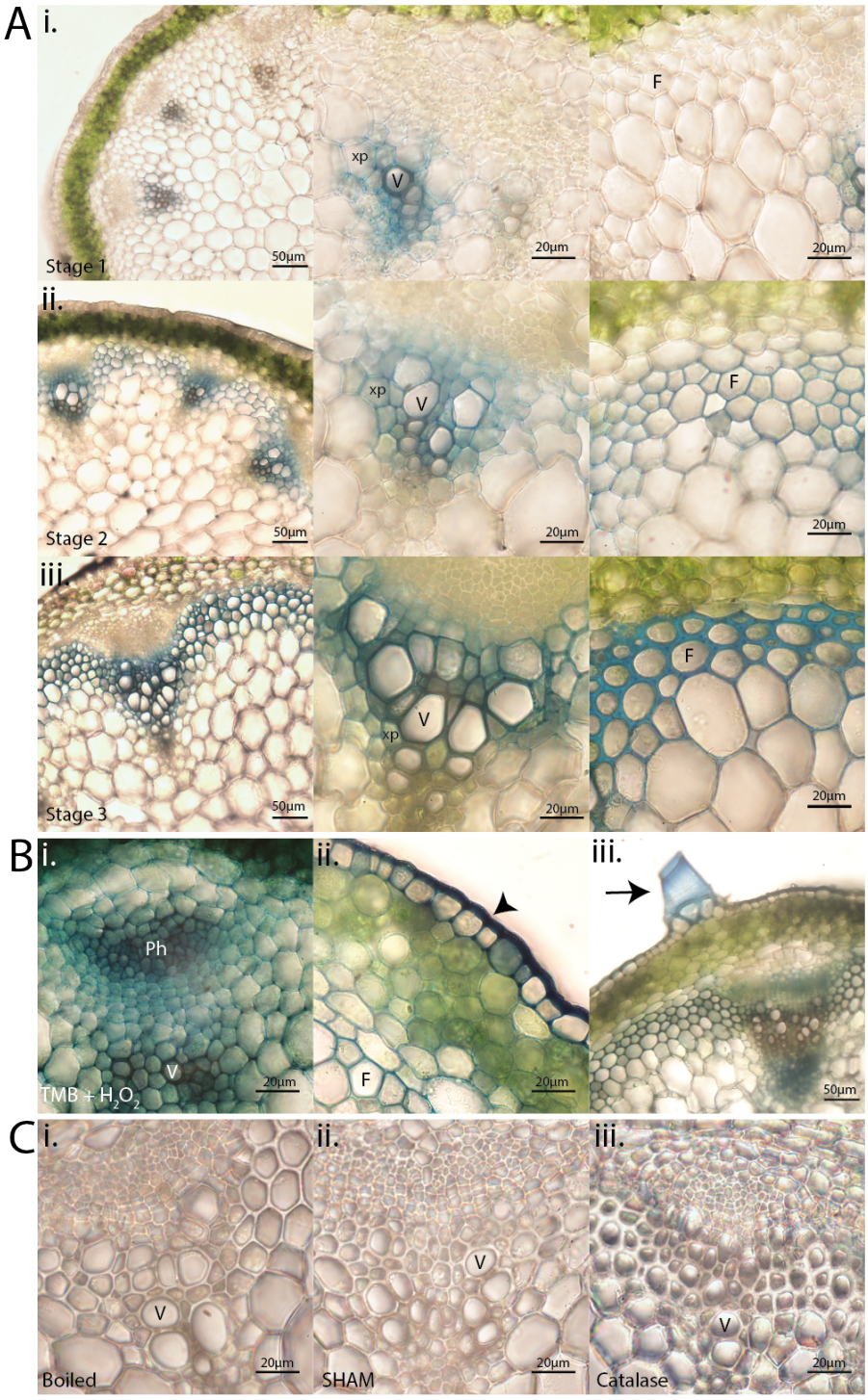

Figure 4.10. PRX histochemistry using the substrate TMB closely matches the observed patterns of lignin deposition and secretion of tagged PRXs. PRX oxidation of TMB results in a blue precipitate in Col-0 stems. V=xylem vessel elements; F=fibers; xp=xylem parenchyma; Ph=phloem; arrowhead=epidermis; arrow=trichome. A) PRX enzymatic activity localizes specifically to regions of lignin deposition in Stage 1 (i), Stage 2 (ii), and Stage 3 (iii) of stem development. B) Addition of H_2O_2 causes TMB oxidation in cell walls of both lignifying and non-lignifying cell types, including xylem and phloem cells (i), cortex and epidermal cells (ii), and trichomes (iii). C) PRX oxidation of TMB can be inhibited by boiling (i), treating with the PRX inhibitor SHAM (ii), and scavenging apoplastic H_2O_2 with catalase (iii).

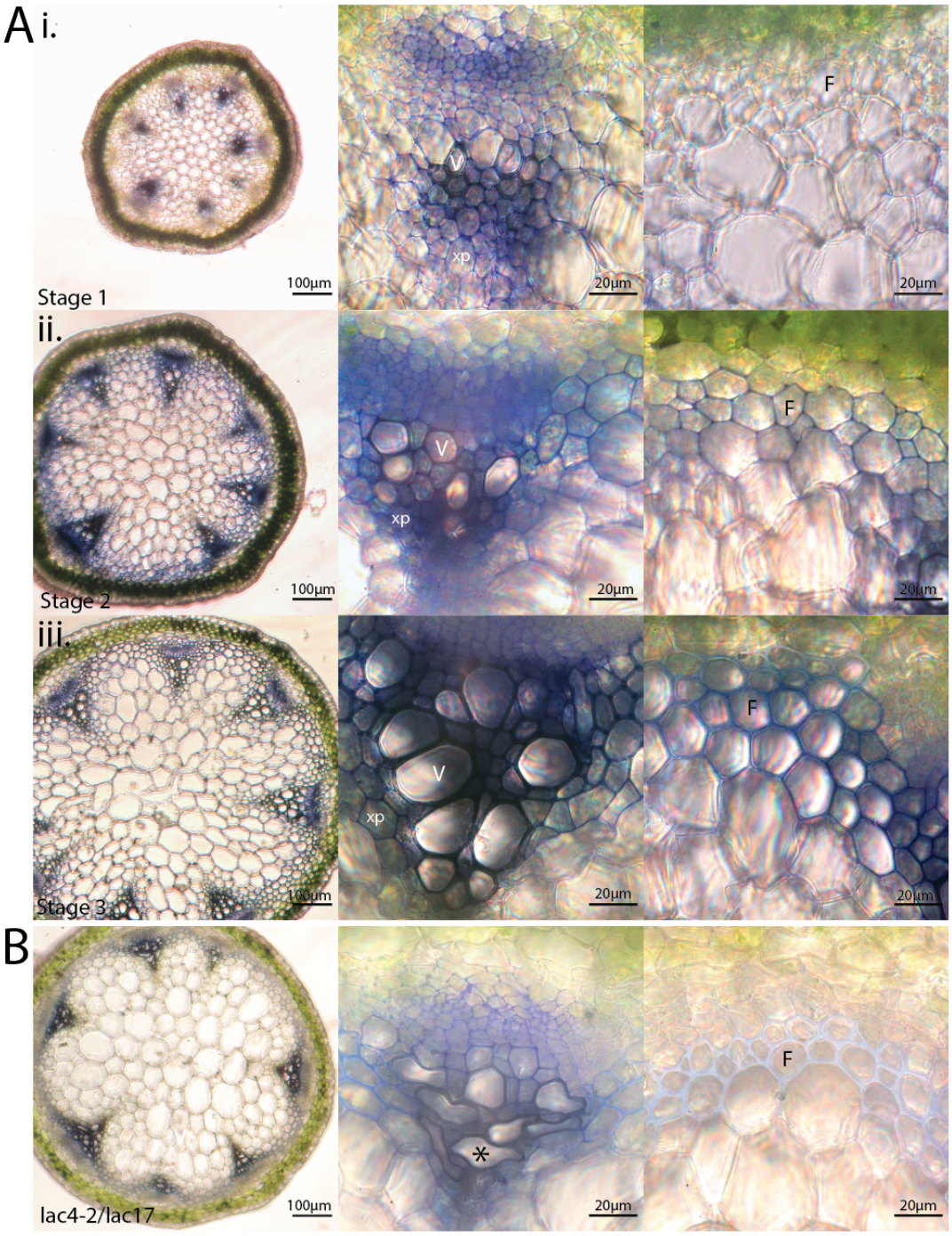

Figure 4.11. LAC and PRX histochemistry using the substrate DAF closely matches the observed patterns of lignin deposition and secretion of tagged LACs and PRXs. LAC and PRX oxidation of DAF results in a purple precipitate in Col-0 stems. V=xylem vessel elements; F=fibers; xp=xylem parenchyma. A) LAC and PRX enzymatic activity localizes specifically to regions of lignin deposition in Stage 1 (i), Stage 2 (ii), and Stage 3 (iii) of stem development. B) DAF oxidation is highly reduced in lac4-2/lac17 plants but is still seen in xylem vessel elements and fibers. Irregular xylem phenotype is indicated by an asterisk.

4.2.6 Total stem H_2O_2 levels are highly regulated during development and do not correlate with lignification

To test whether the amount of stem H_2O_2 increased with progressive lignin deposition, I quantified total (intracellular and apoplastic) stem H_2O_2 with a colorimetric assay using TMB and horseradish peroxidase (HRP). I first extracted H_2O_2 from 2cm developmental segments of 17cm-tall Col-0 stems, added H_2O_2 extracts to the TMB-HRP assay solution, and measured absorbance of the TMB reaction at 562nm on a spectrophotometer. There was no detected signal in the absence of either H_2O_2 or TMB. H_2O_2 concentrations were calculated from values on a standard curve. Analysis of the 8 developmental stages showed that total stem H_2O_2 was highest at the apical tip of the stem (2cm) and decreased to a lower, consistent level of approximately 2μmol/gram fresh weight (FW) for all remaining developmental stages (Figure 4.12). These results suggested that total tissue H_2O_2 is maintained at a consistent level for the majority of stem development and is not correlated with the observed increased lignin deposition during growth.

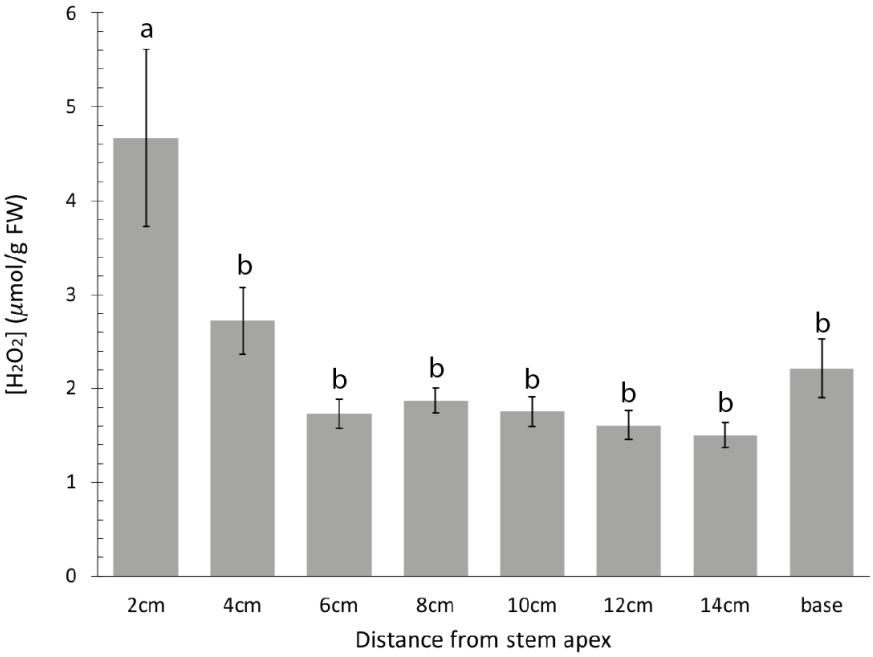

Figure 4.12. Total stem H_2O_2 concentration is not correlated with progressive stem lignification. Total H_2O_2 (intracellular and apoplastic) was extracted from 17cm-tall Col-0 stems at various developmental stages and quantified using a colorimetric TMB-HRP assay. Concentration of H_2O_2 was calculated from values on a standard curve and adjusted based on fresh weight (FW) of the stem sample. Quantification was repeated for 8 biological replicates. Different letters represent significantly different values using a one-way ANOVA; $p<0.05$. Bars are SE.

4.2.7 Apoplastic production of ROS is normally restricted to lignifying cell walls but is sensitive to wounding

Despite whole-tissue H_2O_2 concentrations not correlating with developmental lignification, I hypothesized apoplastic H_2O_2 production would be high specifically in lignifying cell walls. To visualize production of ROS in stems, I incubated stem cross-sections in the fluorescent dye 2',7'-dichlorodihydrofluorescein diacetate (H_2DCF). H_2DCF is a commonly-used probe for detecting presence of ROS and oxidative stress (Kalyanaraman et al., 2012). The non-fluorescent H_2DCF dye is permeable through the PM, where it is cleaved by esterases to a carboxylate anion. Oxidation of this product produces the fluorescent molecule dichlorofluorescein (DCF) which can be visualized using confocal microscopy (Jakubowski & Bartosz, 2000). Initial tests using H_2DCF on stem cross-sections immediately after sampling and sectioning resulted in a super-saturated, non-specific fluorescent signal in every cell type (Figure 4.13a), which may be due to ROS production following wounding. To minimize the wounding response, I cut cross-sections and incubated them in H_2O for 24 hours at room temperature. After 24 hours, overall H_2DCF fluorescence intensity was highly reduced. Certain regions, particularly lignifying cell walls and chloroplasts in photosynthetic cortex cells, showed high H_2DCF fluorescence intensity (Figure 4.13b). Therefore, reducing the wounding response following sectioning allowed identification of certain subcellular regions producing ROS.

To quantify ROS production or accumulation during stem development, I measured H_2DCF fluorescence intensity in the cell wall of xylem vessel elements and interfascicular fibers at each of the eight developmental stages (Figure 4.13c). Fluorescence intensity of xylem vessel elements was low early in development (2cm-4cm), but substantially increased to a maximum at 10cm before decreasing to lower levels in more mature tissues (Figure 4.13c). In contrast, interfascicular fibers had negligible fluorescence intensity in cell walls until 8-10cm from the stem apex, and continued to increase in more mature tissues to the base of the stem (Figure 4.13c). The fluorescence intensity of H_2DCF staining in the SCW of xylem vessel elements was significantly higher than fibers from 6cm-10cm, but at the mature base of the stem the fluorescence intensity of fibers was significantly higher than that of xylem vessel elements (Figure 4.13c). Therefore, H_2DCF staining showed that xylem vessel elements had highest accumulation

of ROS early in development and fibers showed highest accumulation of ROS later in development following SCW formation.

To test whether H_2DCF staining is specific to ROS and PRXs, I performed a series of chemical inhibitor tests on cross-sections from the base of 17cm-tall Col-0 stems. All stem cross-sections were first incubated in H_2O for 24 hours before chemical pre-treatment and H_2DCF staining. To test the involvement of PRXs, I pre-incubated stem cross-sections in the PRX inhibitor SHAM. The H_2DCF signal was highly reduced from stem cross-sections following SHAM treatment (Figure 4.14a). To determine whether NADPH oxidases were involved in producing ROS and the observed H_2DCF signal, I incubated stem cross-sections in the NADPH oxidase inhibitor diphenyleneiodonium chloride (DPI). Similar to SHAM treatment, incubation with DPI highly reduced the H_2DCF signal in stem cross-sections (Figure 4.14a). Finally, to test whether H_2O_2 was contributing to the H_2DCF signal, I treated stem cross-sections with the H_2O_2 scavenger catalase. Following pre-treatment with catalase, H_2DCF signal was decreased but not completely abolished (Figure 4.14a). To more accurately determine the relative impact of PRXs, NADPH oxidases, and H_2O_2 on the H_2DCF signal, I quantified the fluorescence intensity in mock and inhibitor-treated xylem vessel elements and fibers (Figures 4.14b-c). For both xylem vessel elements and fibers, the H_2DCF fluorescence intensity was significantly reduced for all inhibitor treatments compared with mock-treated stems (Figure 4.14b-c). Therefore, the observed H_2DCF signal required ROS production by NADPH oxidases, the enzymatic activity of PRXs, and H_2O_2.

In summary, total stem H_2O_2 levels were maintained at relatively consistent levels throughout growth. Nevertheless, ROS histochemical staining showed differences in apoplastic production during development, with xylem vessel elements showing higher ROS production early in development and fibers showing higher ROS production later in development.

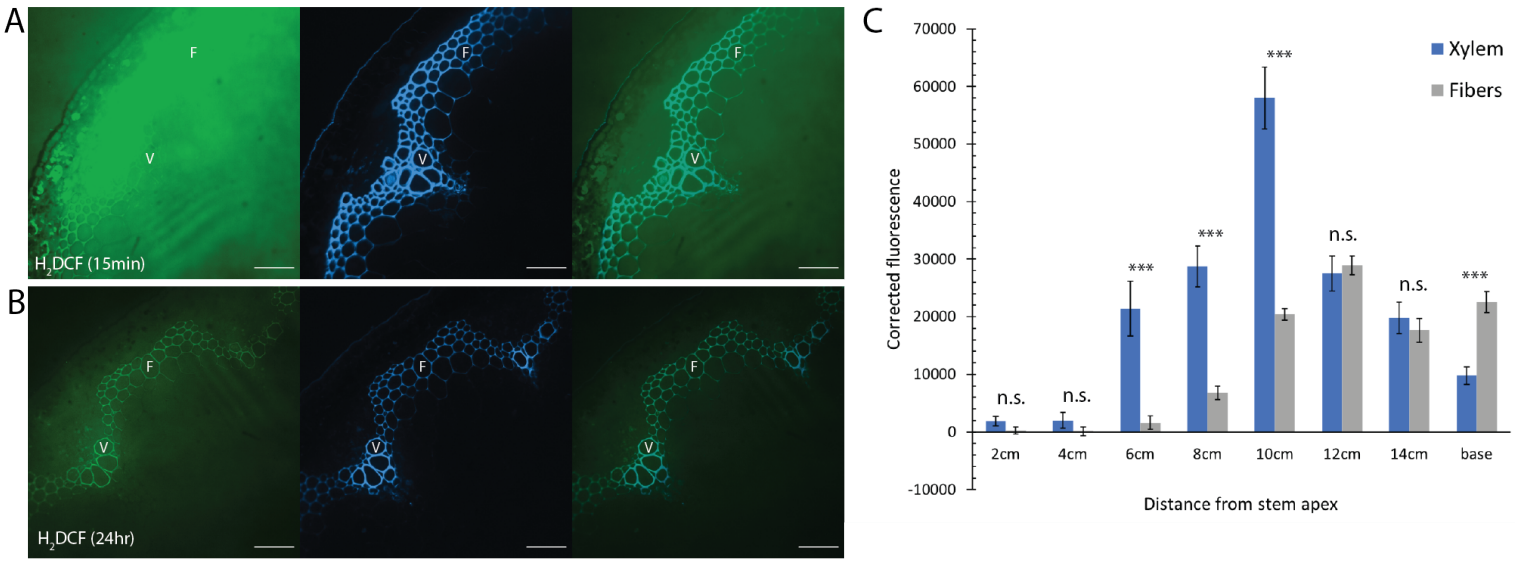

Figure 4.13. Xylem vessel elements and fibers have differential ROS accumulation during development. A-B) Representative images depicting H_2DCF (green), UV lignin autofluorescence (blue), and merged image. V=xylem vessel elements; F=fibers. Scale bars are 50µm. A) H_2DCF incubation of Col-0 stem sections immediately after sectioning causes wound-induced ROS production. B) Incubating Col-0 stem cross-sections in H_2O for 24 hours prior to incubation in H_2DCF reduces wound-induced ROS production. C) Quantification of H_2DCF fluorescence intensity in xylem vessel elements and fibers at different stages of stem development. A two-way t-test was used to compare xylem vessel elements and fibers for a given developmental stage; ***$p<0.001$, n.s.=not significant. N>20 cells for four biological replicates. Bars are SE.

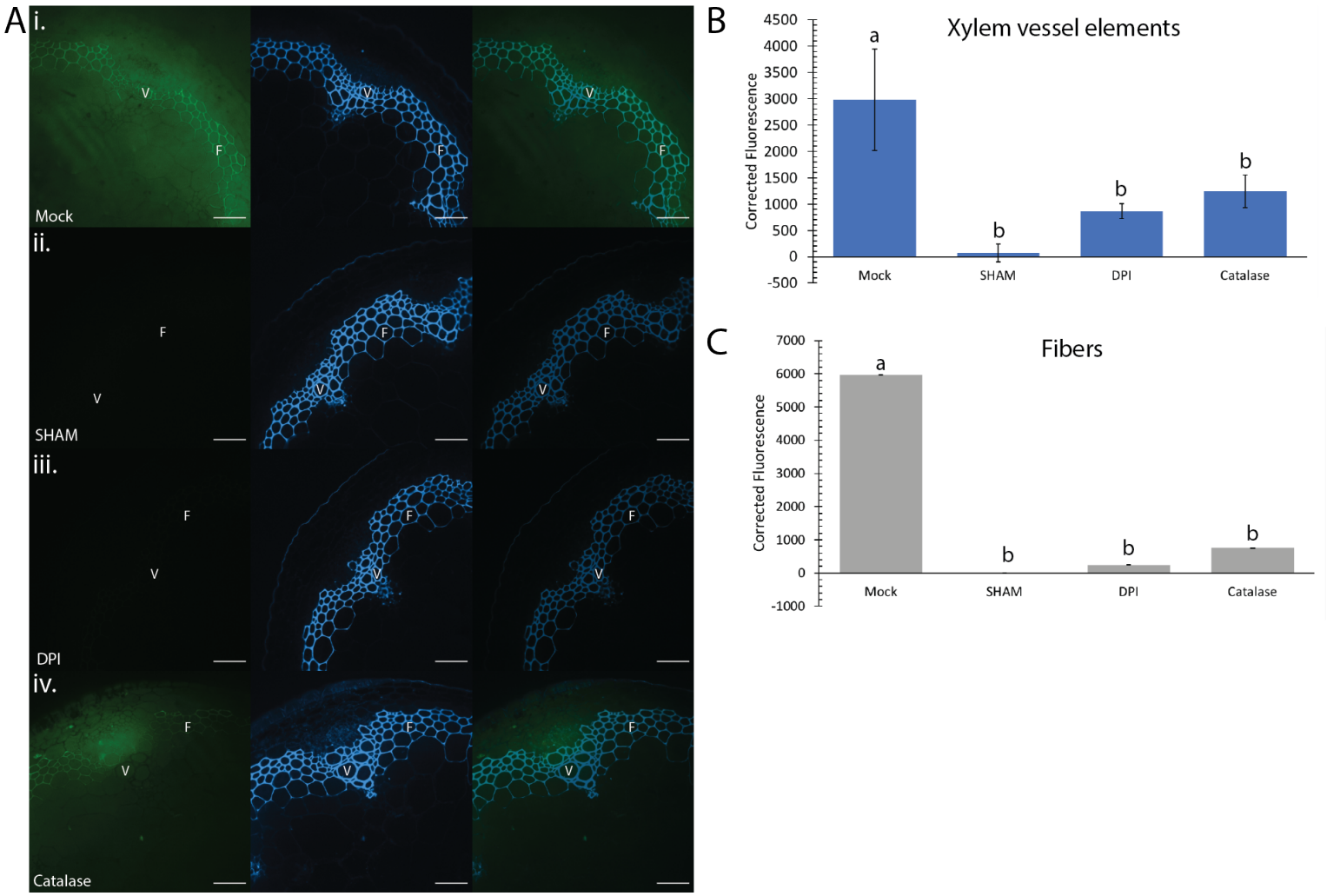

Figure 4.14. H_2DCF fluorescence signal in Arabidopsis stems is dependent on ROS, PRXs, and NADPH oxidases. Stem cross-sections from the base of 17cm-tall Col-0 stems were pre-treated with chemical inhibitors prior to incubation with H_2DCF. Representative images depicting H_2DCF (green), UV lignin autofluorescence (blue), and merged image. V=xylem vessel elements; F=fibers. Scale bars are 50µm. A) Stem cross-sections were treated with H_2O /mock (i), the PRX inhibitor SHAM (ii), the NADPH oxidase inhibitor DPI (iii) and the H_2O_2 scavenger enzyme catalase (iv). B) Quantification of the H_2DCF fluorescence intensity in xylem vessel elements following chemical treatement. C) Quantification of the H_2DCF fluorescence intensity in interfascicular fibers following chemical treatement. N>20 cells per treatment. Letters indicate significantly different values using a one-way ANOVA; $p<0.05$. Bars are SE.

4.3 Discussion

Mapping distinct subsets of LACs and PRXs to regions of lignin deposition in cell types and regions of the cell wall throughout development of the Arabidopsis stem

Despite previous microscopy and transcriptomics experiments examining qualitative developmental changes to lignin in Arabidopsis stems (Altamura et al., 2001; Ehlting et al., 2005; Hall & Ellis, 2012; Minic et al., 2009), there is little known about the roles of oxidative enzymes within regions of the cell wall throughout this process. The ultimate goal was to determine how the localization of oxidative enzymes changed over the development of the stem. The main results of this chapter are summarized in Figure 4.15. Across developmental stages, AtLAC4, AtLAC17, and AtPRX72 were found in the xylan-rich thick SCW in both xylem cells and interfascicular fibers. There was a dynamic change in the oxidative enzymes present in the pectin-rich cell corners and middle lamella, with AtLAC4 appearing transiently and AtPRX64 and AtPRX71 consistently localizing to this region following initiation of SCW biosynthesis. These results indicated that the localization of an oxidative enzyme, both to cell type and regions of the cell wall, is dependent on the developmental stage.

A

Stage 1	Lignin		Cell wall composition		Localization of tagged LACs and PRXs		Apoplastic ROS
	Location	UV autofluorescence	Pectin	Xylan	SCW	Cell corners	
Xylem vessel elements	SCW	Low	Middle lamella/cell corners	SCW	AtLAC4, AtLAC17, AtPRX72	-	Low
Fibers	-	Negligible	Middle lamella/cell corners	-	-	-	Negligible

B

Stage 2	Lignin		Cell wall composition		Localization of tagged LACs and PRXs		Apoplastic ROS
	Location	UV autofluorescence	Pectin	Xylan	SCW	Cell corners	
Xylem vessel elements	SCW	Mid	Middle lamella/cell corners	SCW	AtLAC4, AtLAC17, AtPRX72	AtPRX71	High
Fibers	Cell corners	Low	Middle lamella/cell corners (masked)	SCW	-	AtLAC4, AtPRX64, AtPRX71	Low

C

Stage 3	Lignin		Cell wall composition		Localization of tagged LACs and PRXs		Apoplastic ROS
	Location	UV autofluorescence	Pectin	Xylan	SCW	Cell corners	
Xylem vessel elements	SCW	High	Middle lamella/cell corners	SCW	AtLAC4, AtLAC17, AtPRX72	AtPRX71	Low
Fibers	SCW	Mid	Middle lamella/cell corners (masked)	SCW	AtLAC4, AtLAC17, AtPRX72	AtPRX64, AtPRX71	Mid

Figure 4.15. Summary of lignin, cell wall polysaccharide, tagged enzyme localization, and apoplastic ROS analyses during developmental lignification of Arabidopsis inflorescence stems. Lignin indicates the location and relative quantiy of UV lignin autofluorescence. Cell wall polysaccharide localization comes from pectin (JIM7) and xylan (LM10) immunolabeling. Localization of tagged LACs and PRXs under their respective native promoter for AtLAC4-mCherry, AtLAC17-mCherry, AtPRX64-mCherry, AtPRX71-mCherry, and AtPRX-72-mCherry. Apoplastic ROS indicates relative fluorescence intensity of H_2DCF histochemistry. A) Stage 1 of stem development. B) Stage 2 of stem development. C) Stage 3 of stem development.

Examination of UV lignin autofluorescence from each of the developmental stages showed gradual lignin deposition to different cell types throughout growth (Figure 4.1). To control for non-specific autofluorescence from other soluble phenolics in the cell wall, such as monolignols, lignans, soluble oligolignols, or other flavonoids (Cocuron et al., 2019), I tested whether there were differences in UV lignin autofluorescence following incubation of stem cross-sections in methanol. Polar molecules, such as free phenolic monolignols, are soluble in methanol (Cybulska et al., 2012; Horvath, 2005; Shukry et al., 2008). Previous methanol treatment of *Medicago truncatula* stem cross-sections showed no effect on lignin UV autofluorescence (Ha et al., 2016).

Following confirmation that UV autofluorescence primarily reflects insoluble lignin polymer, lignin deposition was mapped during three developmental stages, from earliest lignification of xylem vessel elements to the robust lignified vascular bundles and fibers in more mature tissues. Stage 1 is the earliest developmental stage and corresponds to 2-4cm from the apical tip of the stem. During this stage, cells undergo a period of cell division near the stem apical meristem followed by rapid elongation (Suh et al., 2005). Previous calculations found that lignin contributed to approximately 3% of the stem dry weight at this development stage (Ehlting et al., 2005), which is consistent with the observed weak UV lignin autofluorescence observed (Figures 4.1c, 4.2a). Stage 2 occurs approximately 6-8cm from the apical tip of the stem and is characterized by cessation of cell elongation (Hall & Ellis, 2012; Suh et al., 2005) and terminal differentiation of specialized cell types such as fibers (Didi et al., 2015). During this stage there was increased lignin deposition to SCWs of xylem vessel elements and initial lignin deposition in cell corners of interfascicular fibers (Figure 4.2c).

To study changes in the structure of both the middle lamella and SCW during the three major developmental stages, I used immunolocalization techniques to visualize the distribution of pectin and xylan. The primary antibody JIM7 is specific for methylesterified homogalacturonan (Knox et al., 1990) and was previously shown to bind to the middle lamella, cell corners, and PCWs in Arabidopsis stems (Hall et al., 2013; Verhertbruggen et al., 2009). This pectin-rich region of the cell wall had a distinct set of oxidative enzymes (AtPRX64 and AtPRX71) compared with other regions of the lignified cell wall. The observed thick SCW was rich in xylan, as demonstrated

by immunolabeling with the primary antibody LM10, which is specific for the xylan backbone (McCartney et al., 2005). LM10 was previously shown to bind exclusively to SCWs of xylem vessel elements and interfascicular fibers, but not to the cell corners or the middle lamella (Hall et al., 2013; Kim & Daniel, 2012). This xylan-rich region contained a different set of oxidative enzymes, including AtLAC4, AtLAC17, and AtPRX72. Therefore, LM10 and JIM7 immunolabeling experiments highlighted the different polysaccharide environments in which unique sets of oxidative enzymes are embedded.

During Stage 1 at the apical tip of the stem, tagged AtLAC4, AtLAC17, and AtPRX72 localized to the SCW of lignifying xylem vessel elements, strongly suggesting a role for these enzymes in the lignification of these cell types during early stem development (Figure 4.6). Interestingly, no tagged enzymes localized to the PCW of fibers at this stage (Figure 4.6), despite the fact that they are found in this domain of the cell wall at later developmental stages. This observation argues against a simple model where oxidative enzymes are co-secreted with the polysaccharides (*e.g.* pectin) in which they reside. During Stage 2, tagged AtLAC4, AtLAC17, and AtPRX72 localized to the SCW of xylem vessel elements and tagged AtLAC4, AtPRX64, and AtPRX71 first appeared in the lignifying cell corners of interfascicular fibers (Figure 4.7). During immunolocalization of PRXs in alfalfa, Wi *et al.* (2005) documented a substantial increase in PRX labeling in the middle lamella following initiation of lignification (Wi et al., 2005). This is consistent with the current study in Arabidopsis, as three tagged oxidative enzymes all localized to cell corners specifically at the onset of lignification.

The observation that tagged AtLAC4 was found in both the early cell corners of fibers and in the SCW of mature tissues suggested that it plays a role during early and later stages of fiber lignification. Using radiolabeled monolignol glucosides, Terashima and Fukushima (1988) documented two distinct periods of G-lignin incorporation in pine lignin: first in the cell corners and at a later period in the SCW (Terashima & Fukushima, 1988). These results correlate well with the initial cell corner and later SCW localization of tagged AtLAC4, which is thought to be specific for coniferyl alcohol (Table 1.4; Berthet et al., 2011). Therefore, AtLAC4 may be involved in lignification of both the cell corners and middle lamella during development, while other enzymes play a more specialized role within a certain region of the cell wall. For example,

AtPRX72 and AtLAC17 may play a specific role in lignification of the SCW, while AtPRX64 and AtPRX71 may play a particular role in lignification of the cell corners. The finding that AtPRX72 appears in SCWs of fibers later in development is supported by previous mutant studies, as *prx72* mutants only showed a decrease in lignin content and S-units in mature and not young stems (Fernández-Pérez et al., 2015). These data contribute to a refined model of SCW lignification, where individual LACs or PRXs contribute to lignification as part of a mixed set of oxidative enzymes embedded in specific polysaccharide environments.

In poplar, Sasaki *et al.* (2006) found that increased lignin UV autofluorescence throughout development was correlated with increased immunolabeling of the lignin-associated PRX CWPO-C (Sasaki et al., 2006). To test whether the amount of tagged PRXs in Arabidopsis also increased during progressive lignification, I studied the fluorescence intensity of AtPRX71-mCherry in cell corners and AtPRX72-mCherry in the SCW of fibers throughout stem development (Figure 4.9). Qualitative and quantitative analyses of fluorescence intensity at different developmental stages determined that both tagged AtPRX71 and AtPRX72 were continually secreted to their respective regions of the cell wall throughout progressive lignification of fibers (Figure 4.9). Remarkably, these results indicated that tagged AtPRX71 could diffuse through the lignified SCW to the cell corners. As shown by Chou *et al.*, (2018), FRAP experiments using tagged AtPRX71 could reveal the mobility of this protein within the cell wall. In contrast, tagged AtPRX72 was limited to the SCW. It would be interesting for future work to look at whether the localization of tagged AtPRX72 in the SCW is due to limited mobility or by some other mechanism (*e.g.* a binding motif in the SCW).

AtLAC4-mCherry localized to both the cell corners and the SCW at different stages of development. Timing of secretion during production of the SCW as well as differential mobility in separate polysaccharide microenvironments could explain the observed localizations. During Stage 2, initial lignification of cell corners preceded or occurred simultaneously with xylan deposition in the SCW (Figure 4.5b; Donaldson, 2001). Previous work determined that tagged AtLAC4 was mobile in the PCW and middle lamella (Chou et al., 2018); therefore, secretion of AtLAC4 in the early stages of SCW formation may allow it to diffuse to the cell corners. In later stages, when tagged AtLAC4 mobility is limited by the presence of cellulose, hemicellulose, and

lignin in the SCW (Chou et al., 2018), secreted AtLAC4 could be restricted to SCW domains. A similar mechanism might be trapping AtPRX72 and AtLAC17 in the SCW, as both these enzymes are secreted concurrently with bulk lignin deposition in SCWs later in development. Interestingly, the fluorescence signal of AtLAC4-mCherry disappeared from the cell corners immediately following first lignification of the thick SCW (Figure 4.8). The loss of tagged AtLAC4 in the cell corners could be due to degradation by cell wall proteases. Transcriptomic analysis found that extracellular proteases were differentially expressed during stem growth, suggesting cell wall protein turn-over by proteases is highly regulated during development (Minic et al., 2009).

Overall, putative lignin-associated LACs and PRXs consistently co-localized with the appearance of lignin in different cell types and regions of the cell wall throughout development, providing additional evidence that spatial and temporal control over the localization of oxidative enzymes could dictate when and where lignin is deposited in cell walls. With the exception of AtLAC4, which localized to both the cell corners and SCW, all other tagged enzymes localized exclusively to a single region of the cell wall. Specific localization in a region of the cell wall may be due to a combination of timing of secretion during development, mobility in alternating polysaccharide environments, and degradation by proteases.

LAC and PRX enzymatic activity is specific to lignifying tissues throughout stem development

A potential caveat of the observed localizations of tagged LACs and PRXs is that the presence of oxidative enzymes in lignifying cell walls does not necessarily indicate oxidative activity. I performed histochemical analyses using the substrates DAF and TMB to test whether LAC and PRX oxidation of these model substrates, which serves as a proxy for enzymatic activity, correlated with developmental lignification of Arabidopsis stems. The purple precipitate produced by oxidation of DAF was found only in lignifying tissues for every developmental stage in the stem, signifying abundant LAC and PRX activity in these regions (Figure 4.11a). Appearance of the DAF purple precipitate correlated not only with lignin deposition in both regions of the cell wall and cell type (Figure 4.11a) but also with the observed localization of tagged putative lignin-associated LACs and PRXs (Figures 4.6-4.8). Consequently, DAF histochemistry supports the

hypothesis that the localization and activity of LACs and PRXs dictates the spatial distribution of lignin (Schuetz et al., 2014).

To test the relative contribution of LACs and PRXs in DAF oxidation, I incubated *lac4-2/lac17* stem cross-sections in DAF. Previous enzymatic analysis of *lac4-2/lac17* double mutants found a 53% decrease in LAC activity (Berthet et al., 2011). The intensity of purple DAF oxidation was highly reduced in *lac4-2/lac17* stems, particularly in the interfascicular fibers, consistent with AtLAC4 and AtLAC17 playing a major role in stem lignification (Figure 4.11b; Berthet et al., 2011). However, there was still observed DAF oxidation in the SCW and middle lamella of fibers and xylem vessel elements, indicating that other LACs and PRXs were active and playing redundant roles with AtLAC4 and AtLAC17. In triple *lac4-2/lac11/lac17* mutants, stem lignification was highly reduced and plants were dwarfed, implicating AtLAC11 as another LAC involved in lignification (Zhao et al., 2013). The severe phenotype of the triple mutant ultimately led to the conclusion that PRXs played a minor or alternative role in stem lignification relative to AtLAC4, AtLAC11, and AtLAC17 (Zhao et al., 2013). As tagged AtPRX64, AtPRX71, and AtPRX72 localized to lignifying cell walls, it would be informative to use DAF histochemistry to visualize the residual amount of oxidative activity in lignifying cell types of *lac4-2/lac11/lac17* triple mutants, although this experiment would be challenging as they rarely survived to produce a flowering stem (Zhao et al., 2013). I made several attempts to transform *prLAC11::LAC11-mCherry* into wild-type Arabidopsis, but unfortunately there was strong silencing of the transgene in these plants (data not shown).

Although DAF histochemistry suggested that LACs play a major role, several putative lignin-associated PRXs were also highly expressed in the stem. To get a snapshot of PRX activity at the tissue level, I used TMB oxidation throughout stem development to identify the specific location and relative concentration of PRXs and H_2O_2. Upon oxidation by PRXs in the presence of H_2O_2, TMB is oxidized into an insoluble blue precipitate (Ros Barceló, 1998). Importantly, the precipitate does not diffuse within tissues and thus directly corresponds to the location of PRXs and H_2O_2 (Mesulam, 1978). Similar to DAF histochemistry, TMB oxidation correlated with lignin deposition to cell types and regions of the cell wall for every developmental stage (Figure 4.10a). As TMB oxidation was limited to regions of lignification, these results suggested that PRX

oxidative activity was spatially and temporally regulated during stem growth. Similar to the observed results in Arabidopsis, *Zinnia elegans* stems incubated with TMB also showed specific histochemical staining in lignified tissue (Ros Barceló, 1998).

Interestingly, both TMB and DAF oxidation was observed in non-lignifying PCWs of xylem parenchyma cells (Figures 4.10-4.11). These cells could be acting as "good neighbours" which produce monolignols and H_2O_2 for adjacent lignifying xylem vessels (Pesquet et al., 2013; Ros Barceló, 2005; Smith et al., 2013). In addition, Sasaki *et al.* (2006) proposed that neighboring parenchyma cells produce and secrete CWPO-C, a poplar lignin-associated PRX, into the cell corners and middle lamella of neighboring lignifying cells (Sasaki et al., 2006). It is unclear how these cell types have apoplastic PRX oxidative activity and produce monolignols and H_2O_2 but remain unlignified. It is possible that these PRXs have low substrate specificity for monolignols or only form low-order oligolignols for lignin polymerization in neighboring cells. TMB oxidation in the xylem parenchyma cells paralleled the observed localization of AtPRX42-mCherry (Figures 3.8, 4.10). Future work could therefore determine the specific biological role of AtPRX42 in these cells and test for involvement in lignification of neighboring xylem vessel elements.

Previous analyses indicated that approximately 62 PRXs were expressed in Arabidopsis stems (Valério et al., 2004), many of which are most likely playing different biological roles in separate tissue types. As fluorescent tagging only elucidated the localization of a limited number of PRXs, I hypothesized that incubating stem sections in a combination of TMB and H_2O_2 would provide all the substrates necessary for PRX oxidative activity and thus permit visualization of all secreted PRXs. Remarkably, the addition of exogenous H_2O_2 demonstrated that PRXs were found in every cell type and every region of the cell wall during development (Figure 4.10b). The ubiquitous localization of PRXs in cell walls was not unexpected, as PRXs have been implicated in numerous biological processes, including response to abiotic and biotic stresses, cell elongation, cell stiffening, auxin metabolism, and lignification (Cosio & Dunand, 2009; Gabaldón et al., 2006; Shigeto & Tsutsumi, 2016). In addition, detected PRX activity in the cell walls of phloem, trichomes, and epidermal cells provided additional support to the localization of tagged AtPRX42-mCherry, AtPRX52-mCherry, and AtPRX71-mCherry to these cell types (Figures 3.7-3.8, 4.10b).

Overall, TMB histochemistry indicated that PRXs are found distributed ubiquitously in all plant cell walls, but in the absence of wounding or pathogen attacks, only PRXs in lignifying cell walls normally have access to H_2O_2 (Figure 4.10a,b). Similarly, Dunand *et al.* (2007) demonstrated that while PRX enzymatic activity was distributed homogenously throughout the meristematic, cell elongation, and cell differentiation zones of Arabidopsis roots, there were different types and quantities of ROS within these regions (Dunand et al., 2007). Therefore, PRX oxidative activity during lignification could be regulated by access to apoplastic H_2O_2.

Total stem H_2O_2 does not correlate with lignification but apoplastic ROS production differs between lignifying cell types throughout development of the Arabidopsis stem

As PRXs but not LACs require H_2O_2 as an electron acceptor during oxidation reactions (Gabaldón et al., 2006; Ros Barceló, 2005), spatial and temporal control over PRX activity could be regulated by production of apoplastic H_2O_2 (Córdoba-Pedregosa et al., 2003; Lee et al., 2013). To assess total stem H_2O_2 levels, I performed a TMB-colorimetric assay at eight developmental stages in 17cm-tall Arabidopsis stems. Intriguingly, the highest level of H_2O_2 was at the apical tip of the stem (2cm) and decreased to steady-state levels for the remaining developmental stages (Figure 4.12). H_2O_2 has been associated in numerous biological processes, including cell development, signaling, and differentiation, so total amounts of H_2O_2 must be highly regulated throughout development (Cheeseman 2007). High intracellular H_2O_2 in the earliest developmental stage may be required to promote cell differentiation following cell division at the stem apical meristem (Zeng et al., 2017). At later stages, intracellular or apoplastic H_2O_2 may be involved in stomatal closure (Ge et al., 2015), cell wall expansion (Xiong et al., 2015), cell wall cross-linking (Dunand et al., 2007), promoting programmed cell death (Kaurilind et al., 2015) or xylem lignification (Ros-Barceló et al., 2002). Therefore, only a fraction of total stem H_2O_2 at any given developmental stage will be involved in lignification.

Despite total H_2O_2 concentrations not correlating with developmental lignification, I hypothesized that apoplastic levels of H_2O_2 in lignifying cell walls would be higher than in non-lignifying cell walls. Spatial restriction of H_2O_2 to specific cell types and locations during development may be a common mechanism to regulate activity of PRXs. One study showed that

the ability of maize root cells to produce H_2O_2 was transient and only occurred while cells were in the growing zone above the root apical meristem (Liszkay et al., 2004). Similarly, Arabidopsis root hairs had ROS accumulation specifically at the tip of the growing root hair, which was required for polar tip growth (Foreman et al., 2003) and H_2O_2 was located in discrete cell types and locations during abscission of floral organs in Arabidopsis (Lee et al., 2018). Therefore, differential H_2O_2 production in lignified cell walls could control PRX oxidative activity and lignification at different stages of stem growth.

To visualize ROS production in Arabidopsis stems, I incubated stem sections in the dye H_2DCF. Following incubation of stem cross-sections in H_2O for 24 hours to reduce immediate wound-induced ROS production, I observed that the appearance of H_2DCF fluorescence correlated with lignification of different cell types throughout stem development (Figure 4.13c). Xylem vessel elements showed highest ROS production in the middle of the stem but decreased in more mature tissues, which could correspond to programmed cell death of these cells (Yamaguchi et al., 2011). Similarly, actively-differentiating cells in inducible lignifying cell cultures of *Zinnia elegans* had high H_2DCF fluorescence within the cell wall but this signal decreased in older, more mature TEs (Karlsson et al., 2005). In contrast, fiber H_2DCF signal steadily increased towards the mature base of the stem. Unlike total UV lignin autofluorescence, H_2DCF fluorescence intensity in fibers was significantly higher than that of xylem vessel elements at the base of the stem (Figure 4.13c). Fibers, which are long-lived relative to xylem vessel elements, could take over the production and accumulation of ROS in later stages and act in combination with xylem parenchyma to produce H_2O_2 for post-mortem lignification of xylem vessel elements (Gómez Ros et al., 2006; Pesquet et al., 2013; Smith et al., 2013, 2017).

The observed localization of apoplastic ROS specifically in lignifying tissues of Arabidopsis is consistent with results from *Zinnia elegans*, *Populus alba*, *Populus euramericana*, *Citrus aurantium*, and *Eucalyptus camaldulensis* (Czaninski et al., 1993; Gómez Ros et al., 2006; Karlsson et al., 2005; Ros-Barceló et al., 2006). It is currently unknown how lignifying cells produce and accumulate large amounts of apoplastic ROS while neighboring cells do not. One hypothesis is that the specific accumulation of ROS in lignifying tissue is due to continual ROS production during lignification and an imbalance of H_2O_2-producing and H_2O_2-scavenging enzymes (Gómez

Ros et al., 2006). Interestingly, chemical inhibition of H_2DCF fluorescence using DPI provided direct evidence for NADPH oxidase activity in lignifying cell walls of stem tissue. Despite previous studies demonstrating the involvement of NADPH oxidases in lignification of the Arabidopsis Casparian strip (Lee et al., 2013) and *Zinnia elegans* stems (Ros Barcelo, 1998; Pesquet et al., 2013), NADPH oxidase involvement in Arabidopsis stem lignification has not been directly demonstrated. Future work could identify the specific NADPH oxidase isoforms in lignifying cells and test whether mutation or inhibition of NADPH oxidases impairs developmental lignification.

Overall, H_2O_2 quantification and ROS histochemistry demonstrated that H_2O_2 levels are highly controlled during development. In particular, xylem vessel elements produced high amounts of ROS in early stages, while fibers showed increased production of apoplastic ROS following xylem vessel element cell death. Within lignifying cell walls, production of apoplastic ROS by NADPH oxidases or PRXs could act to permit or limit PRX oxidative activity within specific regions. In cell walls with low apoplastic H_2O_2 concentrations, LAC activity could predominate over PRX activity. For example, AtLAC4 and AtLAC17 may be involved in early lignin deposition in the SCW of xylem vessel elements until apoplastic ROS is produced in high abundance towards the middle of the stem, when AtPRX72 would be active. Similarly, AtPRX72 localization to the SCW of interfascicular fibers was delayed until later stages, when ROS production in interfascicular fibers had significantly increased. Therefore, despite similar localization patterns to regions of the cell wall, LAC and PRX oxidative activity may be non-redundant during lignification due to temporal and spatial differences in production of H_2O_2.

There are several potential caveats involved in the H_2O_2 quantification and detection experiments. In the literature there are a wide range of reported H_2O_2 concentrations for different plant tissues between species, which could be the result of the numerous methods utilized for quantification (Cheeseman, 2007; Veljovic-Jovanovic et al., 2002). In addition, H_2O_2 is relatively unstable and has an estimated half-life ranging from 1 millisecond to 5 minutes (D'Autréaux & Toledano, 2007; Neill et al., 2002; Queval et al., 2008). It is therefore possible that the H_2O_2 quantification measurements may be underestimates of true H_2O_2 concentrations in tissues (Veljovic-Jovanovic et al., 2002). Despite this limitation, the calculated levels of H_2O_2 in Arabidopsis stem tissue were similar to that of Arabidopsis leaves as well as field-grown leaves

of mangrove and soybean, which were within the range of 1-5μm/gFW (Cheeseman, 2006; Karpinski et al., 2007). Therefore, the quantification analysis still provides useful information on relative amounts of H_2O_2 in stem tissues and how H_2O_2 levels change during different developmental stages.

Similarly, there are several limitations to quantifying or visualizing ROS using H_2DCF (Bonini et al., 2006; Chen et al., 2010; Kalyanaraman et al., 2012; Winterbourn, 2014). For example, other oxidants besides ROS could act on H_2DCF, including reactive nitrogen species and redox-active metals (*e.g.* Fe^{2+}). Heme-containing proteins such as cytochrome C and PRXs could also directly oxidize H_2DCF, leading to an increase of fluorescence from enzymatic activity (Chen et al., 2010). Importantly, the involvement of PRXs with ROS production or H_2DCF oxidation in the current study was demonstrated by treating stem cross-sections with the PRX inhibitor SHAM, which significantly reduced H_2DCF signal in lignifying cell types (Figure 4.14). Alternatively, it has been shown that free radicals alone can activate H_2DCF fluorescence (Winterbourn, 2014). For example, Szychowski *et al.* (2016) demonstrated that the compound TBBPA had free radical properties that could stimulate the conversion of H_2DCF to the fluorescent product DCF in a cell-free system (Szychowski et al., 2016). Therefore, H_2DCF quantification may represent a more general trend of oxidative potential or PRX activity in lignifying cell walls rather than indicative of ROS levels (Jakubowski & Bartosz, 2000). However, similar to the limitations of the quantification analyses, H_2DCF histochemistry still provides valuable information regarding alternative redox environments in different cell types and between developmental stages in lignifying Arabidopsis stems.

4.4 Conclusions

These results provide insight into the dynamic biosynthesis and remodelling of cell wall domains during development. Pectin-rich cell corners contained a unique set of putative lignin-associated enzymes, including AtPRX64 and AtPRX71, which specifically localized to this region during initial lignification of fiber cell corners. Xylan-rich SCWs contained AtLAC4, AtLAC17, and AtPRX72 and were produced early in development in xylem vessel elements and later in xylary and interfascicular fibers. Tagged AtLAC4 transiently appeared in the cell corners during initial

lignification of fibers and later localized to the SCW, suggesting it could participate in lignification of both regions of the cell wall. Despite increased deposition of xylan and lignin in the SCW in mature tissues, tagged AtPRX71 was mobile in the SCW and continually localized to cell corners. Other enzymes like AtLAC4 and potentially AtPRX72 and AtLAC17 were immobile in the compact SCW matrix, suggesting that spatial separation between enzymes in different regions of the cell wall may be primarily determined by timing of gene expression and mobility in the SCW. Oxidative enzymatic activity and production of ROS was restricted to lignifying regions throughout development, and correlated not only with localization of tagged oxidative enzymes but also with observed lignin deposition. The restricted production of ROS to lignifying tissues could act to coordinate PRX activity specifically in lignifying cell types throughout development, while regulation over LAC oxidative activity may be more heavily dependent on targeted secretion to certain cell types and immobilization in regions of the cell wall. In combination, these results support the hypothesis that the location of oxidative enzymes and availability of substrates, such as H_2O_2, dictate lignin deposition spatially and temporally throughout stem growth.

Chapter 5: Conclusions and future directions

5.1 Main conclusions

For my thesis, I was interested in examining the distribution of putative lignin-associated LACs and PRXs in the lignified inflorescence stem of Arabidopsis. As previous work had shown that AtLAC4 and AtPRX64 localize to different SCW domains, I also wanted to examine whether timing of expression determined the localization of a LAC or PRX in the cell wall, or if oxidative enzymes could move across the SCW into the middle lamella. Finally, I assessed the spatial distribution of H_2O_2, reasoning that a PRX may be present in a cell wall domain but would not be active without H_2O_2.

I had the following research questions:

1. Out of the 17 *AtLAC* and 73 *AtPRX* gene members in Arabidopsis, which LACs or PRXs are most likely to be lignin-associated based on mutant analyses from the literature and bioinformatic analyses?
2. What is the spatial distribution of putative lignin-associated LACs and PRXs in the inflorescence stem of Arabidopsis?
3. Does the timing of gene expression impact protein localization to discrete cell wall domains?
4. How do the localizations of LACs and PRXs change between cell types or regions of the lignified cell wall during stem development?
5. Could H_2O_2 availability explain PRX activity in particular cell types?

To select candidate LACs and PRXs that may be involved in lignification of Arabidopsis stem tissue, I first used previous *lac* and *prx* mutant analyses and publicly-available expression and co-expression data. To visualize selected enzymes, I tagged *AtLAC10*, *AtPRX42*, *AtPRX52*, *AtPRX71*, and *AtPRX72* under their respective native promoter with a -mCherry fluorescent protein and examined their localization in stem cross-sections relative to UV lignin autofluorescence. I also re-analyzed existing *prLAC4::LAC4-mCherry*, *prLAC17::LAC17-mCherry*, and *prPRX64::PRX64-mCherry* plants (Lee et al., 2013; Schuetz et al., 2014). Of the eight tagged

enzymes, six localized to lignifying tissues, with tagged AtLAC4, AtLAC17, and AtPRX72 in the SCWs of both xylem vessel elements and fibers, and AtLAC10, AtPRX64, and AtPRX71 in the lignified cell corners of fibers. The numerous LACs and PRXs in a given region of the cell wall or cell type could imply specialized roles during lignification or potential functional redundancy. AtLAC10 and AtPRX71 showed highest concentration in the cell corners adjacent to the endodermis, suggesting a specific structural role for this cell layer. AtLAC10, AtPRX42, AtPRX52, and AtPRX71 also localized to PCWs of non-lignifying tissues, denoting alternative biological roles besides lignification. Taken together, these results showed that each cell type and region of the cell wall has a characteristic set of oxidative enzymes. In addition, it supports the use of bioinformatic data and previous mutant analyses to identify LACs and PRXs that may be involved in lignification.

As previous localization data only provided a snapshot of LAC and PRX localization patterns in mature tissues, I analysed LAC and PRX secretion and oxidative activity during development of the stem. Consistent with mature tissues, tagged AtLAC4, AtLAC17 and AtPRX72 localized to the lignified xylan-rich SCW of lignifying xylem vessel elements at the apical tip of the stem. At this stage, unlignified pectin-rich PCWs of undifferentiated fibers had no tagged oxidative enzymes. However, AtLAC4, AtPRX64, and AtPRX71 specifically localized to fiber cell corners upon initial lignification of this region later in development. In mature tissues, bulk deposition of xylan and lignin in the SCW of interfascicular fibers was accompanied with AtLAC4, AtLAC17, and AtPRX72 localization to this region. Tagged AtLAC4 localized transiently to the cell corners of early lignifying fibers and ultimately to the SCW in mature tissues, suggesting that it is involved in lignification of both regions of the cell wall.

Despite evidence for ubiquitous PRX presence in every cell wall, oxidative activity of LACs and PRXs was restricted to lignifying regions throughout stem development. Therefore, in addition to the specific localization of putative lignin-associated oxidative enzymes, LAC and PRX oxidative activity and subsequent lignin deposition to certain regions could be restricted by limiting oxidative substrates required for lignification. Apoplastic ROS production was high in xylem vessel elements early in development but decreased in later stages, while ROS production was low in early lignifying fibers and increased in mature stems. Therefore, PRXs (*e.g.* AtPRX72)

could have discrete temporal periods of oxidative activity, with abundant activity while ROS production is high. During stages of low apoplastic ROS production, such as early lignification of xylem vessel elements at the tip of the stem or immediately following xylem vessel element cell death, LACs (*e.g.* AtLAC4 and AtLAC17) show predominant activity. These results support the hypothesis that LACs and PRXs may be non-redundant in regions of the cell wall or tissue types due to differential periods of activity during stem growth, dependent on apoplastic H_2O_2 production (Laitinen et al., 2017; Sterjiades et al., 1993).

Spatially discrete localizations in regions of the cell wall could be due to differential timing of expression and secretion during development or inhibited mobility within certain polysaccharide environments. For example, early diffusion of tagged AtLAC4 to the cell corners of fibers may prevented at later stages due to reduced mobility in the SCW (Chou et al., 2018). However, immobility of secreted LACs and PRXs in the SCW is not a universal feature, as tagged AtPRX71 accumulated in the cell corners throughout progressive lignification. To determine whether timing of expression influenced protein localization in lignified SCWs, I expressed *AtLAC4*, *AtLAC17*, and *AtPRX64* under the promoter of the cellulose synthase gene *AtCESA7* and tagged these constructs with an -mCherry marker. In both root and stem tissues, all three constructs localized to the same cell type and region of the cell wall, indicating that changing the timing of expression was sufficient to alter localization. In addition, it suggested that structural features had a limited impact on localization to a particular polysaccharide matrix, as each of these constructs could localize to pectin-rich PCWs and xylan-rich SCWs in roots. Mis-timing of expression of these enzymes in stem tissues resulted in transgene silencing, co-suppression of endogenous LAC or PRX expression, ectopic pith lignification, and collapsed interfascicular fibers. Therefore, while timing of expression does play a role in localization, there are multiple other regulatory factors that restrain LAC and PRX expression and localization.

Taken together, the results of this thesis show that characteristic sets of oxidative enzymes localize to a particular lignified cell type or region of the cell wall at a specific developmental stage. Localization of putative lignin-associated LACs or PRXs and oxidative activity in the cell wall was consistently coordinated with observed lignin deposition in that area. The distribution of secreted sets of oxidative enzymes could therefore “set the stage” for when

and where lignin is deposited during development. As LACs and PRXs show broad specificity *in-vitro*, lignin polymerization during stem growth may ultimately be coordinated by regulated secretion and localization of these enzymes and monolignol and/or H_2O_2 substrate availability.

5.2 Future directions

5.2.1 Test whether putative lignin-associated LACs and PRXs in the stem are involved in lignification of other tissues

Although this study has elucidated the localization of putative lignin-associated LACs and PRXs in stems, it is unknown whether these oxidative enzymes localize to cell walls of other tissue types. Many of the putative lignin-associated LACs and PRXs have diverse expression patterns; for example, promoter:GUS constructs showed *AtLAC4* expression in stems, anthers, roots, and seed coat columella (Turlapati et al., 2011), and eFP browser expression maps showed high expression of *AtPRX52* in flower tissue (Figure 3.3b). In addition to the vascular tissue of roots, hypocotyls, leaves, and stems, lignin is deposited in the root endodermis, seed coat, anthers, and siliques (Barros et al., 2015). Therefore, the identified putative lignin-associated LACs and PRXs could also be involved in lignification of other tissues. Alternatively, they may be involved in diverse biological processes.

Using the expression data of the putative-lignin LACs and PRXs (Figures 3.2-3.3), future work could take a targeted approach to studying the localization of the tagged LACs and PRXs in different tissue types. In particular, it would be interesting to test whether a given putative lignin-associated LAC or PRX may only be involved in lignification (*i.e.* only localizes to lignified SCWs) or is involved in multiple diverse biological processes (*i.e.* localizes to SCWs and PCWs in other tissues). Similarly, many of these genes have been implicated in response to biotic and abiotic stresses (Little et al., 2006; Mohr & Cahill, 2007; Turlapati et al., 2011), so future work could test whether localizations of these proteins change following wounding, pathogen attack, or drought conditions. These results would not only indicate whether specific LACs and PRXs are involved in lignification of other tissues, but could also provide information about the possible pleiotropic roles of these enzymes.

5.2.2 Use the localization data of LACs and PRXs to guide identification of lignin phenotypes in mutant plants and unravel enzyme redundancy

The current localization data demonstrated that each enzyme localized to a specific cell type and region of the cell wall, where it may play a specific role in maintaining cell wall structure or in lignin polymerization. Despite not showing overall reductions to stem lignin content or cell wall morphology, single *lac* and *prx* mutants may show a phenotype within the specific subdomain where the enzyme is found. Therefore, targeted phenotyping experiments within a particular cell type or region of the cell wall could provide information about the particular function of a given enzyme. For instance, localization of tagged AtPRX64 to the root endodermis identified its involvement with Casparian strip development (Appendix; Lee et al., 2013). However, loss of AtPRX64 did not impact cell corner lignification of fibers in stem tissues (Appendix), possibly due to redundancy with other oxidative enzymes in the cell corners like AtPRX71 or AtLAC10.

Zhao *et al.* (2013) hypothesized that LACs and PRXs were non-redundant in lignification due to differential expression patterns (Zhao et al., 2013). Similarly, other studies have suggested that LACs and PRXs are non-redundant due to alternative temporal activity during lignin polymerization, with LACs polymerizing low-order dilignols and oligolignols at early stages and PRXs polymerizing high-order oligolignols at later stages (Laitinen et al., 2017; Sterjiades et al., 1993). The results of this thesis have demonstrated that both LACs and PRXs localize within the same cell types or regions of the cell wall. Despite similar localization patterns, it is unclear whether LACs and PRXs play redundant functional roles within a given area. Future work could test if both LACs and PRXs are required for lignin polymerization or if there is redundancy between different LAC and PRX isoforms. Both *lac4-2* and *prx72* single mutants both showed a weak irregular xylem phenotype, which is consistent with their localization to the SCW of xylem cells (present work; Berthet et al., 2011; Herrero et al., 2013). It would be interesting to test whether double mutant lines of *lac4-2/prx72* show a more severe lignin phenotype, similar to double *lac4-2/lac17* mutants (Berthet et al., 2011). Alternatively, a triple mutant of *lac10/prx64/prx71* could indicate whether deleting three enzymes in fiber cell corners could alter cell corner lignification or morphology. The use of the current localization data could therefore

not only guide single mutant phenotyping efforts to particular cell types, but could also reveal whether LAC and PRX play unique or redundant roles within the same subdomain of the cell wall.

5.2.3 Visualize LAC and PRX secretion in Golgi-derived vesicles

Live-cell imaging during protoxylem differentiation found that Golgi bodies often temporarily paused at regions of lignifying SCW bands (Wightman & Turner, 2008) which could act to deliver xylan to the cell wall and AtCesAs to the PM, respectively. Schuetz *et al.* (2014) hypothesized that these vesicles could also contain AtLAC4 or AtLAC17, which would position these enzymes exclusively in the SCW (Schuetz et al., 2014). Despite this observation, there is little experimental evidence demonstrating that SCW components are secreted in the same Golgi-derived vesicles as LACs and PRXs. Interestingly, mutation in the exocyst complex gene *AtEXO70A1* resulted in mis-localization of Golgi-derived vesicles containing AtCesAs and xylan but did not impact the localization of tagged AtLAC17 to the SCW (Vukašinović et al., 2017). Similarly, mutation of *AtCESA7* (*baculites*) inhibited cellulose formation in protoxylem SCWs but did not impact xylan or lignin deposition (Takenaka et al., 2018). Therefore, LAC and PRX biosynthesis and secretion may occur independently of other SCW components.

Identification of the cellular mechanisms underlying LAC and PRX secretion have been hindered by the lack of intracellular signal for tagged enzymes. This could be due to rapid secretion of tagged proteins following synthesis and modification in the ER and Golgi. Remarkably, expression of *AtLAC4*, *AtLAC17*, and *AtPRX64* under the promoter of *AtCESA7* resulted in an increase in the intracellular signal of these proteins, which was never seen under the respective native promoter. Therefore, despite the limitation of changing endogenous timing of expression, analysis of the intracellular signal in *prCESA7::LAC4-mCherry*, *prCESA7::LAC17-mCherry*, or *prCESA7::PRX64-mCherry* plant lines could provide additional information about Golgi-derived vesicles containing LACs and PRXs. To facilitate live-cell imaging, I have cloned *prCESA7::LAC4-mCherry*, *prCESA7::LAC17-mCherry* and *prCESA7::PRX64-mCherry* into the *pr35S:VND7-VP16-GR* background, which forms ectopic protoxylem elements in all cell types following induction by the hormone dexamethasone (Yamaguchi et al., 2010). Future work could

study whether Golgi vesicles containing LACs or PRXs are secreted directly to SCW bands or if LACs and PRXs co-localize in Golgi vesicles with AtCesAs or xylan biosynthetic enzymes.

5.2.4 Test whether timing of expression is sufficient and necessary to determine protein localization in the cell wall

The consistent localization of *AtLAC4*, *AtLAC17*, and *AtPRX64* under the promoter of *AtCESA7* demonstrated that changing the promoter sequence was sufficient to alter protein localization in the cell wall. However, I had originally hypothesized that changing the timing of gene expression to that of SCW cellulose production would result in secretion of LACs and PRXs to the SCW. This prediction was based off of co-expression data, as *AtLAC4* is highly co-expressed with *AtCESA7* (Brown et al., 2005). Instead, *prCESA7::LAC4-mCherry*, *prCESA7::LAC17-mCherry*, and *prCESA7::PRX64-mCherry* localized to the PCW of protoxylem in the root (Figure 3.12a), the SCW of metaxylem in the root (Figure 3.12b), and the cell corners of xylem vessel elements in the stem (Figure 3.13). In addition, observed localization patterns in the stem were likely confounded by transcriptional silencing (Figure 3.13).

To further evaluate if and how timing of expression impacts LAC and PRX localization in different regions of the SCW, it is essential to perform a more specific promoter-swap experiment, such as expressing *AtPRX64* under the promoter of *AtLAC4* (*prLAC4::PRX64-mCherry*) to test whether changing the timing of expression to that of *AtLAC4* is sufficient to localize AtPRX64 to the SCW. Similarly, expressing *AtLAC4* under the promoter of *AtPRX64* (*prPRX64::LAC4-mCherry*) could determine whether changing the timing of expression to that of *AtPRX64* could localize AtLAC4 exclusively to the cell corners of fibers. Ultimately, these experiments would provide a more thorough understanding on how timing of gene expression impacts protein localization to cell types and regions of the cell wall.

5.2.5 Characterize LAC and PRX function in tree species

The results of this project can ultimately be applied to species of economic importance, such as Norway spruce or poplar, which also require LACs and PRXs for lignified wood formation (Fagerstedt et al., 2010; Ranocha et al., 2002). Previous studies in multiple species have

demonstrated that down-regulation or mutation of LACs or PRXs can reduce lignin biomass or alter lignin composition (Berthet et al., 2012; Blee et al., 2003; Li et al., 2003; Lu et al., 2013). This is relevant for the biofuel industry, as efficient processing of wood is currently hindered by the presence of lignin, which is largely resistant to enzymatic and chemical degradation. Consequently, identification and functional characterization of lignin-associated LACs and PRXs in tree species could support targeted genetic modification of wood tissue for improved downstream processing and aid in development of renewable biofuels. In particular, modifications to the amount, structure, or composition of lignin by modulating LAC or PRX activity could make it more amendable to degradation or suitable for valorization (Mahon & Mansfield, 2019; Mottiar et al., 2016).

Similar to Arabidopsis, poplar has numerous diverse LACs and PRXs, with 49 LACs and 93 PRXs (Lu et al., 2013; Ren et al., 2014) but the specific enzymes involved in lignification have not been extensively identified (Ranocha et al., 2002). Putative lignin-associated LACs and PRXs in poplar can be identified using similar bioinformatics techniques as those outlined in Chapter (3) for Arabidopsis, including high expression in lignifying tissue and co-expression with SCW genes. Following identification, selected LACs and PRXs can be fluorescently labeled and analyzed for localization patterns. Previous immunolocalization of CWPO-C, a lignin-associated PRX in *Populus alba*, detected labeling primarily in the cell corners and middle lamella of fibers and xylem (Sasaki et al., 2006), suggesting that lignin-associated LACs and PRXs in other species also show distinctive localizations to cell types and regions of the cell wall.

To characterize the functional roles of these enzymes during lignification, future experiments can use gene silencing techniques to test whether the absence of specific LACs or PRXs results in reduced lignification. Given that enzymes involved in lignification are required for proper development of water-conducting tissues, gene silencing often comes at a cost to plant growth and biomass. For example, Arabidopsis triple *lac4-2/lac11/lac17* mutants are dwarfed and sterile (Zhao et al., 2013). To minimize these effects, these experiments can take a targeted approach by silencing lignin-related LACs and PRXs in specific cell types, *e.g.* decrease lignin in fibers, but not in the water-conducting vessels. Specific silencing of poplar LACs or PRXs in lignified fiber cells could generate transgenic trees with altered SCW structure and lignin while

minimizing negative growth defects. This method was successfully demonstrated in Arabidopsis, as a fiber-specific promoter fused to a gene-silencing construct against the lignin biosynthetic gene *AtCCR1* reduced lignification specifically in fibers without impacting xylem tissue (Smith et al., 2017). Transgenic poplar lines can be examined for alterations in lignin content or composition, as well as other traits important for industrial treatment, such as saccharification. Therefore, identification and functional characterization of putative lignin-associated LACs and PRXs in woody species will not only lead to a better understanding of the biological role of oxidative enzymes in other species, but could also guide the production of genetically engineered trees with either decreased lignin content so it is more amenable to efficient industrial processing or increased lignin to make valuable bioproducts (Mansfield, 2009).

Bibliography

Abdel-Ghany, S. E., & Pilon, M. (2008). MicroRNA-mediated systemic down-regulation of copper protein expression in response to low copper availability in Arabidopsis. *Journal of Biological Chemistry*, *283*(23), 15932–15945. https://doi.org/10.1074/jbc.M801406200

Al-Qsous, S., Carpentier, E., Klein-Eude, D., Burel, C., Mareck, A., Dauchel, H., … Balangé, A. P. (2004). Identification and isolation of a pectin methylesterase isoform that could be involved in flax cell wall stiffening. *Planta*, *219*(2), 369–378. https://doi.org/10.1007/s00425-004-1246-1

Alassimone, J., Naseer, S., & Geldner, N. (2010). A developmental framework for endodermal differentiation and polarity. *Proceedings of the National Academy of Sciences*, *107*(11), 5214–5219. https://doi.org/10.1073/pnas.0910772107

Alejandro, S., Lee, Y., Tohge, T., Sudre, D., Osorio, S., Park, J., … Martinoia, E. (2012). AtABCG29 is a monolignol transporter involved in lignin biosynthesis. *Current Biology*, *22*(13), 1207–1212. https://doi.org/10.1016/j.cub.2012.04.064

Allan, A. C., & Fluhr, R. (1997). Two Distinct Sources of Elicited Reactive Oxygen Species in Tobacco Epidermal Cells. *The Plant Cell*, *9*, 1559–1572. https://doi.org/10.2307/3870443

Alscher, R. G., Erturk, N., & Heath, L. S. (2002). Role of superoxide dismutases (SODs) in controlling oxidative stress in plants. *Journal of Experimental Botany*, *53*(372), 1331–1341. https://doi.org/10.1093/jxb/53.372.1331

Altamura, M. M., Possenti, M., Matteucci, A., Baima, S., Ruberti, I., & Morelli, G. (2001). Development of the vascular system in the inflorescence stem of Arabidopsis. *New Phytologist*, *151*(2), 381–389. https://doi.org/10.1046/j.0028-646x.2001.00188.x

Awasthi, M., Jaiswal, N., Singh, S., Pandey, V. P., & Dwivedi, U. N. (2015). Molecular docking and dynamics simulation analyses unraveling the differential enzymatic catalysis by plant and fungal laccases with respect to lignin biosynthesis and degradation. In *Journal of Biomolecular Structure and Dynamics* (Third, Vol. 33, pp. 1835–1849). https://doi.org/10.1080/07391102.2014.975282

Bajpai, P. (2018). Chapter 2 - Wood and Fiber Fundamentals. In P. B. T.-B. H. of P. and P. (Third E. Bajpai (Ed.), *Biermann's Handbook of Pulp and Paper* (3rd ed., pp. 19–74). Elsevier.

https://doi.org/https://doi.org/10.1016/B978-0-12-814240-0.00002-1

Balasubramanian, V. K., Rai, K. M., Thu, S. W., Hii, M. M., & Mendu, V. (2016). Genome-wide identification of multifunctional laccase gene family in cotton (Gossypium spp.); expression and biochemical analysis during fiber development. *Scientific Reports*, *6*(34309). https://doi.org/10.1038/srep34309

Bankhead, P. (2014). Analyzing fluorescence microscopy images with ImageJ. *ImageJ*. Nikon Imaging Center; Heidelberg University, Queen's University Belfast. https://doi.org/10.1109/NER.2015.7146654

Bao, W., O'Malley, D. M., Whetten, R., & Sederoff, R. R. (1993). A Laccase Associated with Lignification in Loblolly Pine Xylem. *Science*, *260*(5108), 672–674. https://doi.org/10.1126/science.260.5108.672

Barberon, M. (2017). The endodermis as a checkpoint for nutrients. *New Phytologist*, *213*(1561), 1604–1610. https://doi.org/10.1111/nph.14140

Baron-Epel, O., Gharyal, P. K., & Schindler, M. (1988). Pectins as mediators of wall porosity in soybean cells. *Planta*, *175*(3), 389–395. https://doi.org/10.1007/BF00396345

Barros, J., Serk, H., Granlund, I., & Pesquet, E. (2015). The cell biology of lignification in higher plants. *Annals of Botany*, *115*(7), 1053–1074. https://doi.org/10.1093/aob/mcv046

Benfield, G., Bocks, S. M., Bromley, K., & Brown, B. R. (1964). Studies of fungal and plant laccases. *Phytochemistry*, *3*(1), 79–88. https://doi.org/10.1016/S0031-9422(00)83998-9

Berardini, T. Z., Reiser, L., Li, D., Mezheritsky, Y., Muller, R., Strait, E., & Huala, E. (2015). The Arabidopsis information resource: Making and mining the "gold standard" annotated reference plant genome. *Genesis*, *53*(8), 474–485. https://doi.org/10.1002/dvg.22877

Berthet, S., Demont-Caulet, N., Pollet, B., Bidzinski, P., Cezard, L., Le Bris, P., … Jouanin, L. (2011). Disruption of LACCASE4 and 17 Results in Tissue-Specific Alterations to Lignification of Arabidopsis thaliana stems. *The Plant Cell*, *23*(3), 1124–1137. https://doi.org/10.1105/tpc.110.082792

Berthet, S., Thevenin, J., Baratiny, D., Demont-Caulet, N., Debeaujon, I., Bidzinski, P., … Gomez, L.-D. (2012). Chapter 5 - Role of Plant Laccases in Lignin Polymerization. In L. Jouanin & C. Lapierre (Eds.), *Lignins: Biosynthesis, Biodegradation and Bioengineering* (Vol. 61, pp. 145–

172). Academic Press Inc. https://doi.org/10.1016/B978-0-12-416023-1.00005-7

Blanchette, R. A., Krueger, E. W., Haight, J. E., Akhtar, M., & Akin, D. E. (1997). Cell wall alterations in loblolly pine wood decayed by the white-rot fungus, Ceriporiopsis subvermispora. *Journal of Biotechnology*, *53*(2–3), 203–213. https://doi.org/10.1016/S0168-1656(97)01674-X

Blee, K. A., Choib, J. W., O'Connella, A. P., Schuchc, W., Lewis, N. G., & Bolwell, G. P. (2003). A lignin-specific peroxidase in tobacco whose antisense suppression leads to vascular tissue modification. *Phytochemistry*, *64*(1), 163–176. https://doi.org/10.1016/S0031-9422(03)00212-7

Boerjan, W., Ralph, J., & Baucher, M. (2003). Lignin biosynthesis. *Annual Review of Plant Biology*, *54*, 519–546. https://doi.org/10.1146/annurev.arplant.54.031902.134938

Bollhöner, B., Prestele, J., & Tuominen, H. (2012). Xylem cell death: Emerging understanding of regulation and function. *Journal of Experimental Botany*, *63*(3), 1081–1094. https://doi.org/10.1093/jxb/err438

Bolwell, G. P. (1999). Role of active oxygen species and NO in plant defence responses. *Current Opinion in Plant Biology*, *2*(4), 287–294. https://doi.org/10.1016/S1369-5266(99)80051-X

Bonawitz, N. D., & Chapple, C. (2010). The Genetics of Lignin Biosynthesis: Connecting Genotype to Phenotype. *Annual Review of Genetics*, *44*(1), 337–363. https://doi.org/10.1146/annurev-genet-102209-163508

Bonini, M. G., Rota, C., Tomasi, A., & Mason, R. P. (2006). The oxidation of 2',7'-dichlorofluorescin to reactive oxygen species: A self-fulfilling prophesy? *Free Radical Biology and Medicine*, *40*(6), 968–975. https://doi.org/10.1016/j.freeradbiomed.2005.10.042

Boudart, G., Jamet, E., Rossignol, M., Lafitte, C., Borderies, G., Jauneau, A., … Pont-Lezica, R. (2005). Cell wall proteins in apoplastic fluids of Arabidopsis thaliana rosettes: Identification by mass spectrometry and bioinformatics. *Proteomics*, *5*(1), 212–221. https://doi.org/10.1002/pmic.200400882

Brown, D. M., Zeef, L. A. H., Ellis, J., Goodacre, R., & Turner, S. R. (2005). Identification of Novel Genes in Arabidopsis Involved in Secondary Cell Wall Formation Using Expression Profiling

and Reverse Genetics. *The Plant Cell*, *17*(8), 2281–2295. https://doi.org/10.1105/tpc.105.031542

Brummell, D. A., Dal Cin, V., Crisosto, C. H., & Labavitch, J. M. (2004). Cell wall metabolism during maturation, ripening and senescence of peach fruit. *Journal of Experimental Botany*, *55*(405), 2029–2039. https://doi.org/10.1093/jxb/erh227

Burton, R. A., Gidley, M. J., & Fincher, G. B. (2010). Heterogeneity in the chemistry, structure and function of plant cell walls. *Nature Chemical Biology*, *6*(10), 724–732. https://doi.org/10.1038/nchembio.439

Cai, X., Davis, E. J., Ballif, J., Liang, M., Bushman, E., Haroldsen, V., … Wu, Y. (2006). Mutant identification and characterization of the laccase gene family in Arabidopsis. *Journal of Experimental Botany*, *57*(11), 2563–2569. https://doi.org/10.1093/jxb/erl022

Caño-Delgado, A. I., Metzlaff, K., & Bevan, M. W. (2000). The eli1 mutation reveals a link between cell expansion and secondary cell wall formation in Arabidopsis thaliana. *Development*, *127*(15), 3395–2405.

Carpin, S. (2001). Identification of a Ca2+-Pectate Binding Site on an Apoplastic Peroxidase. *The Plant Cell*, *13*(3), 511–520. https://doi.org/10.1105/tpc.13.3.511

Carpita, N., Sabularse, D., Montezinos, D., & Delmer, D. P. (1979). Determination of the pore size of cell walls of living plant cells. *Science*, *205*(4411), 1144–1147. https://doi.org/10.1126/science.205.4411.1144

Cassab, G. I. (1998). Plant Cell Wall Proteins. *Annual Review of Plant Physiology and Plant Molecular Biology*, *49*, 281–309. https://doi.org/10.1146/annurev.arplant.49.1.281

Chapple, C. C. S., Vogt, T., Ellis, B. E., & Somerville, C. R. (1992). An Arabidopsis Mutant Defective in the General Phenylpropanoid Pathway. *The Plant Cell*, *4*(11), 1413. https://doi.org/10.2307/3869512

Chassot, C., Nawrath, C., & Métraux, J. P. (2007). Cuticular defects lead to full immunity to a major plant pathogen. *The Plant Journal*, *49*(6), 972–980. https://doi.org/10.1111/j.1365-313X.2006.03017.x

Cheeseman, J. M. (2006). Hydrogen peroxide concentrations in leaves under natural conditions. *Journal of Experimental Botany*, *57*(10), 2435–2444. https://doi.org/10.1093/jxb/erl004

Cheeseman, J. M. (2007). Hydrogen Peroxide and Plant Stress : A Challenging Relationship. *Plant Stress*, *1*(1), 4–15.

Chen, X., Zhong, Z., Xu, Z., Chen, L., & Wang, Y. (2010). 2′,7′-Dichlorodihydrofluorescein as a fluorescent probe for reactive oxygen species measurement: Forty years of application and controversy. *Free Radical Research*, *44*(6), 587–604. https://doi.org/10.3109/10715761003709802

Chou, E. Y., Schuetz, M., Hoffmann, N., Watanabe, Y., Sibout, R., & Samuels, A. L. (2018). Distribution, Mobility and Anchoring of Lignin-Related Oxidative Enzymes in Secondary Cell Walls. *Journal of Experimental Botany*, *9*(8), 1849–1859. https://doi.org/https://doi.org/10.1093/jxb/ery067

Christensen, J. H., Bauw, G., Welinder, K. G., Montagu, M. V., & Boerjan, W. (1998). Purification and characterization of peroxidases correlated with lignification in poplar xylem. *Plant Physiology*, *118*(1), 125–135. https://doi.org/10.1104/pp.118.1.125

Clough, S. J., & Bent, A. F. (1998). Floral dip: A simplified method for Agrobacterium-mediated transformation of Arabidopsis thaliana. *The Plant Journal*, *16*(6), 735–743. https://doi.org/10.1046/j.1365-313X.1998.00343.x

Cocuron, J. C., Casas, M. I., Yang, F., Grotewold, E., & Alonso, A. P. (2019). Beyond the wall: High-throughput quantification of plant soluble and cell-wall bound phenolics by liquid chromatography tandem mass spectrometry. *Journal of Chromatography A*, *1589*, 93–104. https://doi.org/10.1016/j.chroma.2018.12.059

Córdoba-Pedregosa, M. D. C., Córdoba, F., Manuel Villalba, J., & González-Reyes, J. A. (2003). Differential distribution of ascorbic acid, peroxidase activity, and hydrogen peroxide along the root axis in Allium cepa L. and its possible relationship with cell growth and differentiation. *Protoplasma*, *221*(1–2), 57–65. https://doi.org/10.1007/s00709-002-0069-9

Cosio, C., & Dunand, C. (2009). Specific functions of individual class III peroxidase genes. *Journal of Experimental Botany*, *60*(2), 391–408. https://doi.org/10.1093/jxb/ern318

Cosio, C., Ranocha, P., Francoz, E., Burlat, V., Zheng, Y., Perry, S. E., … Dunand, C. (2017). The class III peroxidase PRX17 is a direct target of the MADS-box transcription factor

AGAMOUS-LIKE15 (AGL15) and participates in lignified tissue formation. *New Phytologist*, *213*(1), 250–263. https://doi.org/10.1111/nph.14127

Costa, M. M. R., Hilliou, F., Duarte, P., Pereira, L. G., Almeida, I., Leech, M., … Sottomayor, M. (2008). Molecular Cloning and Characterization of a Vacuolar Class III Peroxidase Involved in the Metabolism of Anticancer Alkaloids in Catharanthus roseus. *Plant Physiology*, *146*, 403–417. https://doi.org/10.1104/pp.107.107060

Curtis, M. D. (2003). A Gateway Cloning Vector Set for High-Throughput Functional Analysis of Genes in Planta. *Plant Physiology*, *133*(2), 462–469. https://doi.org/10.1104/pp.103.027979

Cybulska, I., Brudecki, G., Rosentrater, K., Julson, J. L., & Lei, H. (2012). Comparative study of organosolv lignin extracted from prairie cordgrass, switchgrass and corn stover. *Bioresource Technology*, *118*, 30–36. https://doi.org/10.1016/j.biortech.2012.05.073

Czaninski, Y., Sachot, R. M., & Catesson, A. M. (1993). Cytochemical localization of hydrogen peroxide in lignifying cell walls. *Annals of Botany*, *72*(6), 547–550. https://doi.org/10.1006/anbo.1993.1143

Czechowski, T., Stitt, M., Altmann, T., Udvardi, M. K., & Scheible, W.-R. (2005). Genome-Wide Identification and Testing of Superior Reference Genes for Transcript Normalization in Arabidopsis. *Plant Physiology*, *139*, 5–17. https://doi.org/10.1104/pp.105.063743

D'Autréaux, B., & Toledano, M. B. (2007). ROS as signalling molecules: Mechanisms that generate specificity in ROS homeostasis. *Nature Reviews Molecular Cell Biology*, *8*(10), 813–824. https://doi.org/10.1038/nrm2256

DeBlasio, S. L., Sylvester, A. W., & Jackson, D. (2010). Illuminating plant biology: using fluorescent proteins for high-throughput analysis of protein localization and function in plants. *Briefings in Functional Genomics*, *9*(2), 129–138. https://doi.org/10.1093/bfgp/elp060

Demont-Caulet, N., Lapierre, C., Jouanin, L., Baumberger, S., & Méchin, V. (2010). Arabidopsis peroxidase-catalyzed copolymerization of coniferyl and sinapyl alcohols: Kinetics of an endwise process. *Phytochemistry*, *71*, 1673–1683. https://doi.org/10.1016/j.phytochem.2010.06.011

Didi, V., Jackson, P., & Hejátko, J. (2015). Hormonal regulation of secondary cell wall formation. *Journal of Experimental Botany*, *66*(16), 5015–5027. https://doi.org/10.1093/jxb/erv222

Dixon, R. A., & Paiva, N. L. (1995). Stress-Induced Phenylpropanoid Metabolism. *The Plant Cell*, *7*, 1085–1097. https://doi.org/10.2307/3870059

Donaldson, L. A. (1994). Mechanical constraints on lignin deposition during lignification. *Wood Science and Technology*, *28*(2), 111–118. https://doi.org/10.1007/BF00192690

Donaldson, L. A. (2001). Lignification and lignin topochemistry — an ultrastructural view. *Phytochemistry*, *57*(6), 859–873. https://doi.org/10.1016/S0031-9422(01)00049-8

Dunand, C., Crèvecoeur, M., & Penel, C. (2007). Distribution of superoxide and hydrogen peroxide in Arabidopsis root and their influence on root development: Possible interaction with peroxidases. *New Phytologist*, *174*(2), 332–341. https://doi.org/10.1111/j.1469-8137.2007.01995.x

Duroux, L., & Welinder, K. G. (2003). The Peroxidase Gene Family in Plants: A Phylogenetic Overview. *Journal of Molecular Evolution*, *57*(4), 397–407. https://doi.org/10.1007/s00239-003-2489-3

Dwivedi, U. N., Singh, P., Pandey, V. P., & Kumar, A. (2011). Structure-function relationship among bacterial, fungal and plant laccases. *Journal of Molecular Catalysis B: Enzymatic*, *68*(2), 117–128. https://doi.org/10.1016/j.molcatb.2010.11.002

Edgar, R. C. (2004). MUSCLE: Multiple sequence alignment with high accuracy and high throughput. *Nucleic Acids Research*, *32*(5), 1792–1797. https://doi.org/10.1093/nar/gkh340

Ehlting, J., Mattheus, N., Aeschliman, D. S., Li, E., Hamberger, B., Cullis, I. F., … Douglas, C. J. (2005). Global transcript profiling of primary stems from Arabidopsis thaliana identifies candidate genes for missing links in lignin biosynthesis and transcriptional regulators of fiber differentiation. *The Plant Journal*, *42*(5), 618–640. https://doi.org/10.1111/j.1365-313X.2005.02403.x

Erdtman, H. (1933). Dehydrierungen in der Coniferylreihe. II. Dehydrodi-isoeugenol. *Justus Liebigs Annalen Der Chemie*, *503*(1), 283–294. https://doi.org/10.1002/jlac.19335030116

Esau, K. (1965). *Vascular Differentiation in Plants*. New York: Holt, Rinehart & Winston.

Fagerstedt, K. V, Kukkola, E. M., Koistinen, V. V. T., Takahashi, J., & Marjamaa, K. (2010). Cell Wall Lignin is Polymerised by Class III Secretable Plant Peroxidases in Norway Spruce. *Journal of Integrative Plant Biology*, *52*(2), 186–194. https://doi.org/10.1111/j.1744-7909.2010.00928.x

Fergus, B. J., Procter, A. R., Scott, J. A. N., & Goring, D. A. I. (1969). The distribution of lignin in sprucewood as determined by ultraviolet microscopy. *Wood Science and Technology*, *3*(2), 117–138. https://doi.org/10.1007/BF00639636

Fernández-Pérez, F., Pomar, F., Pedreño, M. A., & Novo-Uzal, E. (2015a). Suppression of Arabidopsis peroxidase 72 alters cell wall and phenylpropanoid metabolism. *Plant Science*, *239*, 192–199. https://doi.org/10.1016/j.plantsci.2015.08.001

Fernández-Pérez, F., Pomar, F., Pedreño, M. A., & Novo-Uzal, E. (2015b). The suppression of AtPrx52 affects fibers but not xylem lignification in Arabidopsis by altering the proportion of syringyl units. *Physiologia Plantarum*, *154*(3), 395–406. https://doi.org/10.1111/ppl.12310

Fernández-Pérez, F., Vivar, T., Pomar, F., Pedreño, M. A., & Novo-Uzal, E. (2015). Peroxidase 4 is involved in syringyl lignin formation in Arabidopsis thaliana. *Journal of Plant Physiology*, *175*, 86–94. https://doi.org/10.1016/j.jplph.2014.11.006

Ferrándiz, C. (2002). Regulation of fruit dehiscence in Arabidopsis. *Journal of Experimental Botany*, *53*(377), 2031–2038. https://doi.org/10.1093/jxb/erf082

Fleet, D. S. Van. (1959). Analysis of the histochemical localization of peroxidase related to the differentiation of plant tissues. *Canadian Journal of Botany*, *37*(3), 449–458. https://doi.org/10.1139/b59-036

Flournoy, D. S., Kirk, K., & Highley, T. L. (1991). Wood decay by brown-rot fungi: changes in pore structure and cell wall volume. *Holzforschung*, *45*(5), 383–388. https://doi.org/10.1515/hfsg.1991.45.5.383

Foreman, J., Demidchik, V., Bothwell, J. H. F., Mylona, P., Miedema, H., Angel Torres, M., … Dolan, L. (2003). Reactive oxygen species produced by NADPH oxidase regulate plant cell growth. *Nature*, *422*(6930), 442–446. https://doi.org/10.1038/nature01485

Francoz, E., Ranocha, P., Le Ru, A., Martinez, Y., Fourquaux, I., Jauneau, A., … Burlat, V. (2019).

Pectin Demethylesterification Generates Platforms that Anchor Peroxidases to Remodel Plant Cell Wall Domains. *Developmental Cell*, *48*(2), 261–276. https://doi.org/10.1016/j.devcel.2018.11.016

Freshour, G., Clay, R. P., Fuller, M. S., Albersheim, P., Darvill, A. G., & Hahn, M. G. (1996). Developmental and Tissue-Specific Structural Alterations of the Cell-Wall Polysaccharides of Arabidopsis thaliana Roots. *Plant Physiology*, *110*(4), 1413–1429.

Freudenberg, K. (1959). Biosynthesis and constitution of lignin. *Nature*, *183*, 1152–1155. https://doi.org/10.1038/1831152a0

Freudenberg, K. (1965). Lignin: Its constitution and formation from p-hydroxycinnamyl alcohols. *Science*, *148*(3670), 595–600. https://doi.org/10.1126/science.148.3670.595

Fry, S. C. (1998). Oxidative scission of plant cell wall polysaccharides by ascorbate-induced hydroxyl radicals. *Biochemical Journal*, *332*, 507–515. https://doi.org/10.1042/bj3320507

Fukaki, H., Wysocka-Diller, J., Kato, T., Fujisawa, H., Benfey, P. N., & Tasaka, M. (1998). Genetic evidence that the endodermis is essential for shoot gravitropism in Arabidopsis thaliana. *The Plant Journal*, *14*(4), 425–430. https://doi.org/10.1046/j.1365-313X.1998.00137.x

Fukushima, K., & Terashima, N. (1991). Heterogeneity in formation of lignin - Part XV: Formation and structure of lignin in compression wood of Pinus thunbergii studied by microautoradiography. *Wood Science and Technology*, *25*(5), 371–381. https://doi.org/10.1007/BF00226177

Gabaldón, C., Gómez-Ros, L. V., Núñez-Flores, M. J. L., Esteban-Carrasco, A., & Barcelo, A. R. (2007). Post-translational modifications of the basic peroxidase isoenzyme from Zinnia elegans. *Plant Molecular Biology*, *65*, 43–61. https://doi.org/10.1007/s11103-007-9197-0

Gabaldón, C., López-Serrano, M., Pomar, F., Merino, F., Cuello, J., Pedreño, M. A., & Barceló, A. R. (2006). Characterization of the last step of lignin biosynthesis in Zinnia elegans suspension cell cultures. *FEBS Letters*, *580*(18), 4311–4316. https://doi.org/https://doi.org/10.1016/j.febslet.2006.06.088

Ge, X. M., Cai, H. L., Lei, X., Zhou, X., Yue, M., & He, J. M. (2015). Heterotrimeric G protein mediates ethylene-induced stomatal closure via hydrogen peroxide synthesis in Arabidopsis. *The Plant Journal*, *82*(1), 138–150. https://doi.org/10.1111/tpj.12799

Goldberg, R., Lê, T., & Catesson, A. M. (1985). Localization and properties of cell wall enzyme activities related to the final stages of lignin biosynthesis. *Journal of Experimental Botany*, *36*(3), 503–510. https://doi.org/10.1093/jxb/36.3.503

Gómez Ros, L. V., Paradiso, A., Gabaldón, C., Pedreño, M. A., De Gara, L., & Ros Barceló, A. (2006). Two distinct cell sources of H2O2 in the lignifying Zinnia elegans cell culture system. *Protoplasma*, *227*(2–4), 175–183. https://doi.org/10.1007/s00709-005-0128-0

Gou, M., Ran, X., Martin, D. W., & Liu, C. J. (2018). The scaffold proteins of lignin biosynthetic cytochrome P450 enzymes. *Nature Plants*, *4*, 299–310. https://doi.org/10.1038/s41477-018-0142-9

Grefen, C., Donald, N., Hashimoto, K., Kudla, J., Schumacher, K., & Blatt, M. R. (2010). A ubiquitin-10 promoter-based vector set for fluorescent protein tagging facilitates temporal stability and native protein distribution in transient and stable expression studies. *Plant Journal*, *64*(2), 355–365. https://doi.org/10.1111/j.1365-313X.2010.04322.x

Gumiero, A., Murphy, E. J., Metcalfe, C. L., Moody, P. C. E., & Raven, E. L. (2010). An analysis of substrate binding interactions in the heme peroxidase enzymes: A structural perspective. *Archives of Biochemistry and Biophysics*, *500*(1), 13–20. https://doi.org/10.1016/j.abb.2010.02.015

Ha, C. M., Escamilla-Trevino, L., Yarce, J. C. S., Kim, H., Ralph, J., Chen, F., & Dixon, R. A. (2016). An essential role of caffeoyl shikimate esterase in monolignol biosynthesis in Medicago truncatula. *The Plant Journal*, *86*(5), 363–375. https://doi.org/10.1111/tpj.13177

Hall, H. C., Cheung, J., & Ellis, B. E. (2013). Immunoprofiling reveals unique cell-specific patterns of wall epitopes in the expanding Arabidopsis stem. *The Plant Journal*, *74*(1), 134–147. https://doi.org/10.1111/tpj.12111

Hall, H., & Ellis, B. (2012). Developmentally equivalent tissue sampling based on growth kinematic profiling of Arabidopsis inflorescence stems. *New Phytologist*, *194*(1), 287–296. https://doi.org/10.1111/j.1469-8137.2012.04060.x

Hall, H., & Ellis, B. (2013). Transcriptional programming during cell wall maturation in the expanding Arabidopsis stem. *BMC Plant Biology*, *13*(14). https://doi.org/10.1186/1471-2229-13-14

Hammer, Ø., Harper, D. A. T., & Ryan, P. D. (2001). PAST: Paleontological Statistics Software Package for Education and Data Analysis. *Palaeontologia Electronica*, *4*(1), 1–9. https://doi.org/10.1016/j.bcp.2008.05.025

Harholt, J., Suttangkakul, A., & Vibe Scheller, H. (2010). Biosynthesis of Pectin. *Plant Physiology*, *153*(2), 384–395. https://doi.org/10.1104/pp.110.156588

Harkin, J. M., & Obst, J. R. (1973). Lignification in Trees: Indication of Exclusive Peroxidase Participation. *Science*, *180*(4083), 296–298. https://doi.org/10.1126/science.180.4083.296

Hatfield, R. D., Rancour, D. M., & Marita, J. M. (2017). Grass Cell Walls: A Story of Cross-Linking. *Frontiers in Plant Science*, *7*(2056). https://doi.org/10.3389/fpls.2016.02056

Hatfield, R., Ralph, J., & Grabber, J. H. (2008). A potential role for sinapyl p-coumarate as a radical transfer mechanism in grass lignin formation. *Planta*, *228*(6), 919–928. https://doi.org/10.1007/s00425-008-0791-4

Hatton, D., Sablowski, R., Yung, M. -H, Smith, C., Schuch, W., & Bevan, M. (1995). Two classes of cis sequences contribute to tissue-specific expression of a PAL2 promoter in transgenic tobacco. *The Plant Journal*, *7*(6), 859–876. https://doi.org/10.1046/j.1365-313X.1995.07060859.x

Henriksson, A., & Gatenholm, P. (2001). Controlled assembly of glucuronoxylans onto cellulose fibres. *Holzforschung*, *55*(5), 494–502. https://doi.org/10.1515/HF.2001.081

Hernandez-Garcia, C. M., & Finer, J. J. (2014). Identification and validation of promoters and cis-acting regulatory elements. *Plant Science*, *217*, 109–119. https://doi.org/10.1016/j.plantsci.2013.12.007

Herrero, J., Esteban-Carrasco, A., & Zapata, J. M. (2013). Looking for Arabidopsis thaliana peroxidases involved in lignin biosynthesis. *Plant Physiology and Biochemistry*, *67*, 77–86. https://doi.org/10.1016/j.plaphy.2013.02.019

Herrero, J., Fernández-Pérez, F., Yebra, T., Novo-Uzal, E., Pomar, F., Pedreño, M. Á., … Zapata, J. M. (2013). Bioinformatic and functional characterization of the basic peroxidase 72 from Arabidopsis thaliana involved in lignin biosynthesis. *Planta*, *237*(6), 1599–1612. https://doi.org/10.1007/s00425-013-1865-5

Horvath, A. L. (2005). Solubility of Structurally Complicated Materials: I. Wood. *Journal of*

Physical and Chemical Reference Data, *35*(1), 77–92. https://doi.org/10.1063/1.2035708

Hruz, T., Laule, O., Szabo, G., Wessendorp, F., Bleuler, S., Oertle, L., … Zimmermann, P. (2008). Genevestigator V3: A Reference Expression Database for the Meta-Analysis of Transcriptomes. *Advances in Bioinformatics*, *2008*, 1–5. https://doi.org/10.1155/2008/420747

Hu, Q., Min, L., Yang, X., Jin, S., Zhang, L., Li, Y., … Zhang, X. (2018). Laccase GhLac1 Modulates Broad-Spectrum Biotic Stress Tolerance via Manipulating Phenylpropanoid Pathway and Jasmonic Acid Synthesis. *Plant Physiology*, *176*(2), 1808–1823. https://doi.org/10.1104/pp.17.01628

Hunt, G. M., & Baker, E. A. (1980). Phenolic constituents of tomato fruit cuticles. *Phytochemistry*, *19*(7), 1415–1419. https://doi.org/10.1016/0031-9422(80)80185-3

Jacobowitz, J. R., Doyle, W. C., & Weng, J.-K. (2019). PRX9 and PRX40 are extensin peroxidases essential for maintaining tapetum and microspore cell wall integrity during Arabidopsis anther development. *The Plant Cell*, *31*, 848–861. https://doi.org/10.1105/tpc.18.00907

Jacquet, G., Pollet, B., Lapierre, C., Mhamdi, F., & Rolando, C. (1995). New Ether-Linked Ferulic Acid-Coniferyl Alcohol Dimers Identified in Grass Straws. *Journal of Agricultural and Food Chemistry*, *43*(10), 2746–2751. https://doi.org/10.1021/jf00058a037

Jakubowski, W., & Bartosz, G. (2000). 2,7-dichlorofluorescin oxidation and reactive oxygen species: What does it measure? *Cell Biology International*, *24*(10), 757–760. https://doi.org/10.1006/cbir.2000.0556

Jamet, E., Albenne, C., Boudart, G., Irshad, M., Canut, H., & Pont-Lezica, R. (2008). Recent advances in plant cell wall proteomics. *Proteomics*, *8*(4), 893–908. https://doi.org/10.1002/pmic.200700938

Joseleau, J.-P., & Ruel, K. (1997). Study of Lignification by Noninvasive Techniques in Growing Maize Internodes. *Plant Mol Biol*, *114*(3), 1123–1233. https://doi.org/http://dx.doi.org/10.1104/pp.114.3.1123

Kalyanaraman, B., Darley-Usmar, V., Davies, K. J. A., Dennery, P. A., Forman, H. J., Grisham, M. B., … Ischiropoulos, H. (2012). Measuring reactive oxygen and nitrogen species with fluorescent probes: Challenges and limitations. *Free Radical Biology and Medicine*, *52*(1),

1–6. https://doi.org/10.1016/j.freeradbiomed.2011.09.030

Kaneda, M., Rensing, K. H., Wong, J. C. T., Banno, B., Mansfield, S. D., & Samuels, A. L. (2008). Tracking Monolignols during Wood Development in Lodgepole Pine. *Plant Physiology*, *147*, 1750–1760. https://doi.org/10.1104/pp.108.121533

Kang, X., Kirui, A., Dickwella Widanage, M. C., Mentink-Vigier, F., Cosgrove, D. J., & Wang, T. (2019). Lignin-polysaccharide interactions in plant secondary cell walls revealed by solid-state NMR. *Nature Communications*, *10*(1), 347. https://doi.org/10.1038/s41467-018-08252-0

Karlsson, M., Melzer, M., Prokhorenko, I., Johansson, T., & Wingsle, G. (2005). Hydrogen peroxide and expression of hipl-superoxide dismutase are associated with the development of secondary cell walls in Zinnia elegans. *Journal of Experimental Botany*, *56*(418), 2085–2093. https://doi.org/10.1093/jxb/eri207

Karpinski, S., Escobar, C., Karpinska, B., Creissen, G., & Mullineaux, P. M. (2007). Photosynthetic Electron Transport Regulates the Expression of Cytosolic Ascorbate Peroxidase Genes in Arabidopsis during Excess Light Stress. *The Plant Cell*, *9*, 627–640. https://doi.org/10.2307/3870512

Kaurilind, E., Xu, E., & Brosché, M. (2015). A genetic framework for H2O2 induced cell death in Arabidopsis thaliana. *BMC Genomics*, *16*(837). https://doi.org/10.1186/s12864-015-1964-8

Keegstra, K. (2010). Plant Cell Walls. *Plant Physiology*, *154*(2), 483–486. https://doi.org/10.1104/pp.110.161240

Kerr, T., & Bailey, I. W. (1934). The cambium and its derivative tissues: X. Structure, optical properties and chemical composition of the so-called middle lamella. *Journal of the Arnold Arboretum*, *15*(4), 327–349. Retrieved from http://www.jstor.org/stable/43782261

Kim, J. S., & Daniel, G. (2012). Immunolocalization of hemicelluloses in Arabidopsis thaliana stem. Part I: Temporal and spatial distribution of xylans. *Planta*, *236*(4), 1275–1288. https://doi.org/10.1007/s00425-012-1686-y

Knox, J. P., Linstead, P. J., King, J., Cooper, C., & Roberts, K. (1990). Pectin esterification is spatially regulated both within cell walls and between developing tissues of root apices. *Planta*, *181*(4), 512–521. https://doi.org/10.1007/BF00193004

Koizumi, K., Yokoyama, R., & Nishitani, K. (2009). Mechanical load induces upregulation of transcripts for a set of genes implicated in secondary wall formation in the supporting tissue of Arabidopsis thaliana. *Journal of Plant Research*, *122*(6), 651–659. https://doi.org/10.1007/s10265-009-0251-7

Kõressaar, T., Lepamets, M., Kaplinski, L., Raime, K., Andreson, R., & Remm, M. (2018). Primer3-masker: Integrating masking of template sequence with primer design software. *Bioinformatics*, *34*(11), 1937–1938. https://doi.org/10.1093/bioinformatics/bty036

Kubo, M., Udagawa, M., Nishikubo, N., Horiguchi, G., Yamaguchi, M., Ito, J., … Demura, T. (2005). Transcription switches for protoxylem and metaxylem vessel formation. *Genes and Development*, *19*(16), 1855–1860. https://doi.org/10.1101/gad.1331305

Kumar, S., Stecher, G., & Tamura, K. (2016). MEGA7: Molecular Evolutionary Genetics Analysis Version 7.0 for Bigger Datasets. *Molecular Biology and Evolution*, *33*(7), 1870–1874. https://doi.org/10.1093/molbev/msw054

Laitinen, T., Morreel, K., Delhomme, N., Gauthier, A., Schiffthaler, B., Nickolov, K., … Kärkönen, A. (2017). A Key Role for Apoplastic H 2 O 2 in Norway Spruce Phenolic Metabolism. *Plant Physiology*, *174*(3), 1449–1475. https://doi.org/10.1104/pp.17.00085

Lampugnani, E. R., Khan, G. A., Somssich, M., & Persson, S. (2018). Building a plant cell wall at a glance. *Journal of Cell Science*, *131*. https://doi.org/10.1242/jcs.207373

Lan, W., Lu, F., Regner, M., Zhu, Y., Rencoret, J., Ralph, S. A., … Ralph, J. (2015). Tricin, a Flavonoid Monomer in Monocot Lignification. *Plant Physiology*, *167*, 1284–1295. https://doi.org/10.1104/pp.114.253757

Laule, O., Hirsch-Hoffmann, M., Hruz, T., Gruissem, W., & Zimmermann, P. (2006). Web-based analysis of the mouse transcriptome using Genevestigator. *BMC Bioinformatics*, *7*(311). https://doi.org/10.1186/1471-2105-7-311

Lee, Y., Rubio, M. C., Alassimone, J., & Geldner, N. (2013). A Mechanism for Localized Lignin Deposition in the Endodermis. *Cell*, *153*(2), 402–412. https://doi.org/https://doi.org/10.1016/j.cell.2013.02.045

Lee, Y., Yoon, T. H., Lee, J., Jeon, S. Y., Lee, J. H., Lee, M. K., … Kwak, J. M. (2018). A Lignin Molecular Brace Controls Precision Processing of Cell Walls Critical for Surface Integrity in

Arabidopsis. *Cell*, *173*(6), 1468–1480. https://doi.org/10.1016/j.cell.2018.03.060

Leple, J.-C., Dauwe, R., Morreel, K., Storme, V., Lapierre, C., Pollet, B., … Boerjan, W. (2007). Downregulation of Cinnamoyl-Coenzyme A Reductase in Poplar: Multiple-Level Phenotyping Reveals Effects on Cell Wall Polymer Metabolism and Structure. *The Plant Cell*, *19*, 3669–3691. https://doi.org/10.1105/tpc.107.054148

Lev-Yadun, S. (1997). Fibres and fibre-sclereids in wild-type Arabidopsis thaliana. *Annals of Botany*, *80*(2), 125–129. https://doi.org/10.1006/anbo.1997.0419

Lev-Yadun, S., & Flaishman, M. A. (2001). The effect of submergence on ontogeny of cambium and secondary xylem and on fiber lignification in inflorescence stems of Arabidopsis. *IAWA Journal*, *22*(2), 159–169. https://doi.org/10.1163/22941932-90000275

Lewis, N. G., & Yamamoto, E. (1990). Lignin: Occurrence, Biogenesis and Biodegradation. *Annual Review of Plant Physiology and Plant Molecular Biology*, *41*(1), 455–496. https://doi.org/10.1146/annurev.pp.41.060190.002323

Li, P., Yu, Q., Gu, X., Xu, C., Qi, S., Wang, H., … Wu, S. (2018). Construction of a Functional Casparian Strip in Non-endodermal Lineages Is Orchestrated by Two Parallel Signaling Systems in Arabidopsis thaliana. *Current Biology*, *28*(17), 2777–2786. https://doi.org/10.1016/j.cub.2018.07.028

Li, Y., Kajita, S., Kawai, S., Katayama, Y., & Morohoshi, N. (2003). Down-regulation of an anionic peroxidase in transgenic aspen and its effect on lignin characteristics. *Journal of Plant Research*, *116*(3), 175–182. https://doi.org/10.1007/s10265-003-0087-5

Lige, B., Ma, S., & Van Huystee, R. B. (2001). The effects of the site-directed removal of N-glycosylation from cationic peanut peroxidase on its function. *Archives of Biochemistry and Biophysics*, *386*(1), 17–24. https://doi.org/10.1006/abbi.2000.2187

Lin, S. Y., & Dence, C. W. (1992). *Methods in lignin chemistry*. Springer, Berlin, Heidelberg. https://doi.org/10.1007/978-3-642-74065-7

Liszkay, A., van der Zalm, E., & Schopfer, P. (2004). Production of Reactive Oxygen Intermediates (O2.- , H2O2 , and OH.) by Maize Roots and Their Role in Wall Loosening and Elongation Growth. *Plant Physiology*, *136*, 3114–3123. https://doi.org/10.1104/pp.104.044784.3114

Little, D., Gouhier-Darimont, C., Bruessow, F., & Reymond, P. (2006). Oviposition by Pierid Butterflies Triggers Defense Responses in Arabidopsis. *Plant Physiology*, *143*, 784–800. https://doi.org/10.1104/pp.106.090837

Livak, K. J., & Schmittgen, T. D. (2001). Analysis of relative gene expression data using real-time quantitative PCR and the 2-ΔΔCT method. *Methods*, *25*(4), 402–408. https://doi.org/10.1006/meth.2001.1262

Lu, S., Li, Q., Wei, H., Chang, M.-J., Tunlaya-Anukit, S., Kim, H., … Chiang, V. L. (2013). Ptr-miR397a is a negative regulator of laccase genes affecting lignin content in Populus trichocarpa. *Proceedings of the National Academy of Sciences*, *110*(26), 10848–10853. https://doi.org/10.1073/pnas.1308936110

Lüthje, S., & Martinez-Cortes, T. (2018). Membrane-Bound Class III Peroxidases: Unexpected Enzymes with Exciting Functions. *International Journal of Molecular Sciences*, *19*(10), 2876. https://doi.org/10.3390/ijms19102876

Maestre-Reyna, M., Liu, W. C., Jeng, W. Y., Lee, C. C., Hsu, C. A., Wen, T. N., … Shyur, L. F. (2015). Structural and functional roles of glycosylation in fungal laccase from Lentinus sp. *PLoS ONE*, *10*(4). https://doi.org/10.1371/journal.pone.0120601

Mahon, E. L., & Mansfield, S. D. (2019). Tailor-made trees: engineering lignin for ease of processing and tomorrow's bioeconomy. *Current Opinion in Biotechnology*, *56*, 147–155. https://doi.org/10.1016/j.copbio.2018.10.014

Mansfield, S. D. (2009). Solutions for dissolution—engineering cell walls for deconstruction. *Current Opinion in Biotechnology*, *20*(3), 286–294. https://doi.org/https://doi.org/10.1016/j.copbio.2009.05.001

Marita, J. M., Ralph, J., Lapierre, C., Jouanin, L., & Boerjan, W. (2001). NMR characterization of lignins from transgenic poplars with suppressed caffeic acid O-methyltransferase activity. *Journal of the Chemical Society, Perkin Transactions*, *1*, 2939–2945. https://doi.org/10.1039/b107219f

Mayer, A. M., & Harel, E. (1979). Polyphenol oxidases in plants. *Phytochemistry*, *18*(2), 193–215. https://doi.org/10.1016/0031-9422(79)80057-6

McCaig, B. C., Meagher, R. B., & Dean, J. F. D. (2005). Gene structure and molecular analysis of

the laccase-like multicopper oxidase (LMCO) gene family in Arabidopsis thaliana. *Planta*, *221*(5), 619–636. https://doi.org/10.1007/s00425-004-1472-6

McCartney, L., Marcus, S. E., & Knox, J. P. (2005). Monoclonal antibodies to plant cell wall xylans and arabinoxylans. *Journal of Histochemistry and Cytochemistry*, *53*(4), 543–546. https://doi.org/10.1369/jhc.4B6578.2005

McFarlane, H. E., Döring, A., & Persson, S. (2014). The Cell Biology of Cellulose Synthesis. *Annual Review of Plant Biology*, *65*, 69–94. https://doi.org/10.1146/annurev-arplant-050213-040240

McFarlane, H. E., Watanabe, Y., Gendre, D., Carruthers, K., Levesque-Tremblay, G., Haughn, G. W., … Samuels, L. (2013). Cell wall polysaccharides are mislocalized to the vacuole in echidna Mutants. *Plant and Cell Physiology*, *54*(11), 1867–1880. https://doi.org/10.1093/pcp/pct129

Meents, M. J., Watanabe, Y., & Samuels, A. L. (2018). The cell biology of secondary cell wall biosynthesis. *Annals of Botany*, *121*(6), 1107–1125. https://doi.org/10.1093/aob/mcy005

Mesulam, M. M. (1978). Tetramethyl benzidine for horseradish peroxidase neurohistochemistry: A non-carcinogenic blue reaction-product with superior sensitivity for visualizing neural afferents and efferents. *Journal of Histochemistry and Cytochemistry*, *26*(2), 106–117. https://doi.org/10.1177/26.2.24068

Miller, A. R. (1986). Oxidation of cell wall polysaccharides by hydrogen peroxide: A potential mechanism for cell wall breakdown in plants. *Biochemical and Biophysical Research Communications*, *141*(1), 238–244. https://doi.org/10.1016/S0006-291X(86)80359-X

Minic, Z., Jamet, E., San-Clemente, H., Pelletier, S., Renou, J.-P., Rihouey, C., … Jouanin, L. (2009). Transcriptomic analysis of Arabidopsis developing stems: a close-up on cell wall genes. *BMC Plant Biology*, *9*(1), 6. https://doi.org/10.1186/1471-2229-9-6

Mohr, P. G., & Cahill, D. M. (2007). Suppression by ABA of salicylic acid and lignin accumulation and the expression of multiple genes, in Arabidopsis infected with Pseudomonas syringae pv. tomato. *Functional and Integrative Genomics*, *7*(3), 181–191. https://doi.org/10.1007/s10142-006-0041-4

Morales, J., Kadota, Y., Zipfel, C., Molina, A., & Torres, M. A. (2016). The Arabidopsis NADPH

oxidases RbohD and RbohF display differential expression patterns and contributions during plant immunity. *Journal of Experimental Botany*, *67*(6), 1663–16736. https://doi.org/10.1093/jxb/erv558

Mottiar, Y., Vanholme, R., Boerjan, W., Ralph, J., & Mansfield, S. D. (2016). Designer lignins: Harnessing the plasticity of lignification. *Current Opinion in Biotechnology*, *37*, 190–200. https://doi.org/10.1016/j.copbio.2015.10.009

Moustacas, A. M., Nari, J., Borel, M., Noat, G., & Ricard, J. (2015). Pectin methylesterase, metal ions and plant cell-wall extension. The role of metal ions in plant cell-wall extension. *Biochemical Journal*, *279*(2), 351–354. https://doi.org/10.1042/bj2790351

Muro-Villanueva, F., Mao, X., & Chapple, C. (2019). Linking phenylpropanoid metabolism, lignin deposition, and plant growth inhibition. *Current Opinion in Biotechnology*, *56*, 202–208. https://doi.org/10.1016/j.copbio.2018.12.008

Naseer, S., Lee, Y., Lapierre, C., Franke, R., Nawrath, C., & Geldner, N. (2012). Casparian strip diffusion barrier in Arabidopsis is made of a lignin polymer without suberin. *Proceedings of the National Academy of Sciences*, *109*(25), 10101–10106. https://doi.org/10.1073/pnas.1205726109

Neill, S. J., Desikan, R., Clarke, A., Hurst, R. D., & Hancock, J. T. (2002). Hydrogen peroxide and nitric oxide as signalling molecules in plants. *Journal of Experimental Botany*, *53*(372), 1237–1247. https://doi.org/10.1093/jxb/53.372.1237

Nishiyama, Y. (2009). Structure and properties of the cellulose microfibril. *Journal of Wood Science*, *55*(4), 241–249. https://doi.org/10.1007/s10086-009-1029-1

Novo-Uzal, E., Fernández-Pérez, F., Herrero, J., Gutiérrez, J., Gómez-Ros, L. V, Bernal, M. Á., … Pedreño, M. Á. (2013). From Zinnia to Arabidopsis: approaching the involvement of peroxidases in lignification. *Journal of Experimental Botany*, *64*(12), 3499–3518. Retrieved from http://dx.doi.org/10.1093/jxb/ert221

Ohashi-Ito, K., Oda, Y., & Fukuda, H. (2010). Arabidopsis VASCULAR-RELATED NAC-DOMAIN6 Directly Regulates the Genes That Govern Programmed Cell Death and Secondary Wall Formation during Xylem Differentiation. *The Plant Cell*, *22*(10), 3461–3473. Retrieved from http://www.plantcell.org/content/22/10/3461.abstract

Onnerud, H. (2002). Polymerization of Monolignols by Redox Shuttle-Mediated Enzymatic Oxidation: A New Model in Lignin Biosynthesis I. *The Plant Cell*, *14*(8), 1953–1962. https://doi.org/10.1105/tpc.001487

Passardi, F., Cosio, C., Penel, C., & Dunand, C. (2005). Peroxidases have more functions than a Swiss army knife. *Plant Cell Reports*, *24*(5), 255–265. https://doi.org/10.1007/s00299-005-0972-6

Passardi, F., Penel, C., & Dunand, C. (2004). Performing the paradoxical: How plant peroxidases modify the cell wall. *Trends in Plant Science*, *9*(11), 534–540. https://doi.org/10.1016/j.tplants.2004.09.002

Patel, R. V., Nahal, H. K., Breit, R., & Provart, N. J. (2012). BAR expressolog identification: Expression profile similarity ranking of homologous genes in plant species. *The Plant Journal*, *71*(6), 1038–1050. https://doi.org/10.1111/j.1365-313X.2012.05055.x

Pelloux, J., Rustérucci, C., & Mellerowicz, E. J. (2007). New insights into pectin methylesterase structure and function. *Trends in Plant Science*, *12*(6), 267–277. https://doi.org/10.1016/j.tplants.2007.04.001

Péret, B., De Rybel, B., Casimiro, I., Benková, E., Swarup, R., Laplaze, L., … Bennett, M. J. (2009). Arabidopsis lateral root development: an emerging story. *Trends in Plant Science*, *14*(7), 399–408. https://doi.org/10.1016/j.tplants.2009.05.002

Perkins, M., Smith, R. A., & Samuels, L. (2019). The transport of monomers during lignification in plants: anything goes but how? *Current Opinion in Biotechnology*, *56*, 69–74. https://doi.org/https://doi.org/10.1016/j.copbio.2018.09.011

Persson, S., Wei, H., Milne, J., Page, G. P., & Somerville, C. R. (2005). Identification of genes required for cellulose synthesis by regression analysis of public microarray data sets. *Proceedings of the National Academy of Sciences*, *102*(24), 8633–8638. https://doi.org/10.1073/pnas.0503392102

Pesquet, E., Zhang, B., Gorzsas, A., Puhakainen, T., Serk, H., Escamez, S., … Tuominen, H. (2013). Non-Cell-Autonomous Postmortem Lignification of Tracheary Elements in Zinnia elegans. *The Plant Cell*, *25*(4), 1314–1328. https://doi.org/10.1105/tpc.113.110593

Pilling, J., Willmitzer, L., Bücking, H., & Fisahn, J. (2004). Inhibition of a ubiquitously expressed

pectin methyl esterase in Solanum tuberosum L. affects plant growth, leaf growth polarity, and ion partitioning. *Planta*, *219*(1), 32–40. https://doi.org/10.1007/s00425-004-1204-y

Pomar, F., Merino, F., & Barceló, A. R. (2002). O-4-linked coniferyl and sinapyl aldehydes in lignifying cell walls are the main targets of the Wiesner (phloroglucinol-HCl) reaction. *Protoplasma*, *220*(1–2), 17–28. https://doi.org/10.1007/s00709-002-0030-y

Pourcel, L., Routaboul, J. M., Kerhoas, L., Caboche, M., Lepiniec, L., & Debeaujon, I. (2005). Transparent Testa10 encodes a laccase-like enzyme involved in oxidative polymerization of flavonoids in Arabidopsis seed coat. *The Plant Cell*, *17*(11), 2966–2980. https://doi.org/10.1105/tpc.105.035154.1

Prats Mateu, B., Hauser, M. T., Heredia, A., & Gierlinger, N. (2016). Waterproofing in Arabidopsis: Following Phenolics and Lipids In situ by Confocal Raman Microscopy. *Frontiers in Chemistry*, *4*(10). https://doi.org/10.3389/fchem.2016.00010

Pumplin, N., Zhang, X., Noar, R. D., & Harrison, M. J. (2012). Polar localization of a symbiosis-specific phosphate transporter is mediated by a transient reorientation of secretion. *Proceedings of the National Academy of Sciences*, *109*(11), E665–E672. https://doi.org/10.1073/pnas.1110215109

Queval, G., Hager, J., Gakière, B., & Noctor, G. (2008). Why are literature data for H2O2 contents so variable? A discussion of potential difficulties in the quantitative assay of leaf extracts. *Journal of Experimental Botany*, *59*(2), 135–146. https://doi.org/10.1093/jxb/erm193

Raggi, S., Ferrarini, A., Delledonne, M., Dunand, C., Ranocha, P., De Lorenzo, G., … Ferrari, S. (2015). The Arabidopsis Class III Peroxidase AtPRX71 Negatively Regulates Growth under Physiological Conditions and in Response to Cell Wall Damage. *Plant Physiology*, *169*(4), 2513–2525. https://doi.org/10.1104/pp.15.01464

Ralph, J., Bunzel, M., Marita, J. M., Hatfield, R. D., Lu, F., Kim, H., … Steinhart, H. (2004). Peroxidase-dependent cross-linking reactions of p-hydroxycinnamates in plant cell walls. *Phytochemistry Reviews*, *3*, 79–96. https://doi.org/10.1023/B:PHYT.0000047811.13837.fb

Ralph, J., Lundquist, K., Brunow, G., Lu, F., Kim, H., Schatz, P. F., … Boerjan, W. (2004). Lignins: Natural polymers from oxidative coupling of 4-hydroxyphenyl- propanoids. *Phytochemistry*

Reviews, *3*(1–2), 29–60. https://doi.org/10.1023/B:PHYT.0000047809.65444.a4

Ralph, J., MacKay, J. J., Hatfield, R. D., O'Malley, D. M., Whetten, R. W., & Sederoff, R. R. (1997). Abnormal lignin in a loblolly pine mutant. *Science*, *277*(5323), 235–239. https://doi.org/10.1126/science.277.5323.235

Ranocha, P., Chabannes, M., Chamayou, S., Danoun, S., Jauneau, A., Boudet, A.-M., & Goffner, D. (2002). Laccase Down-Regulation Causes Alterations in Phenolic Metabolism and Cell Wall Structure in Poplar. *Plant Physiology*, *129*(1), 145–155. Retrieved from http://www.plantphysiol.org/content/129/1/145.abstract

Ren, C., & Kermode, A. R. (2002). An Increase in Pectin Methyl Esterase Activity Accompanies Dormancy Breakage and Germination of Yellow Cedar Seeds. *Plant Physiology*, *124*, 231–242. https://doi.org/10.1104/pp.124.1.231

Ren, L.-L., Liu, Y.-J., Liu, H.-J., Qian, T.-T., Qi, L.-W., Wang, X.-R., & Zeng, Q.-Y. (2014). Subcellular Relocalization and Positive Selection Play Key Roles in the Retention of Duplicate Genes of Populus Class III Peroxidase Family. *The Plant Cell*, *26*(6), 2404–2419. https://doi.org/10.1105/tpc.114.124750

Renault, H., Alber, A., Horst, N. A., Basilio Lopes, A., Fich, E. A., Kriegshauser, L., … Werck-Reichhart, D. (2017). A phenol-enriched cuticle is ancestral to lignin evolution in land plants. *Nature Communications*, *8*(14713). https://doi.org/10.1038/ncomms14713

Rennie, E. A., & Scheller, H. V. (2014). Xylan biosynthesis. *Current Opinion in Biotechnology*, *26*, 100–107. https://doi.org/10.1016/j.copbio.2013.11.013

Roberts, A. W., & Haigler, C. H. (1994). Cell Expansion and Tracheary Element Differentiation Are Regulated by Extracellular pH in Mesophyll Cultures of Zinnia elegans L. *Plant Physiology*, *105*(2), 699–706. https://doi.org/10.1104/pp.105.2.699

Ros-Barceló, A., Gómez-Ros, L. V., Ferrer, M. A., & Hernández, J. A. (2006). The apoplastic antioxidant enzymatic system in the wood-forming tissues of trees. *Trees - Structure and Function*, *20*, 145–156. https://doi.org/10.1007/s00468-005-0020-8

Ros-Barceló, A., Pomar, F., López-Serrano, M., Martínez, P., & Pedreño, M. A. (2002). Developmental regulation of the H2O2-producing system and of a basic peroxidase isoenzyme in the Zinnia elegans lignifying xylem. *Plant Physiology and Biochemistry*, *40*(4),

325–332. https://doi.org/10.1016/S0981-9428(02)01376-1

Ros Barceló, A. (1998). The generation of H2O2 in the xylem of Zinnia elegans is mediated by an NADPH-oxidase-like enzyme. *Planta*, *207*(2), 207–216. https://doi.org/10.1007/s004250050474

Ros Barceló, A. (2005). Xylem parenchyma cells deliver the H2O2 necessary for lignification in differentiating xylem vessels. *Planta*, *220*(5), 747–756. https://doi.org/10.1007/s00425-004-1394-3

Ruel, K., Berrio-Sierra, J., Mir-Derikvand, M., Pollet, B., Thévenin, J., Lapierre, C., … Joseleau, J. P. (2009). Impact of CCR1 silencing on the assembly of lignified secondary walls in Arabidopsis thaliana. *New Phytologist*, *184*, 99–113. https://doi.org/10.1111/j.1469-8137.2009.02951.x

Ruprecht, C., Mutwil, M., Saxe, F., Eder, M., Nikoloski, Z., & Persson, S. (2011). Large-Scale Co-Expression Approach to Dissect Secondary Cell Wall Formation Across Plant Species. *Frontiers in Plant Science*, *2*(23). https://doi.org/10.3389/fpls.2011.00023

Růžička, K., Ursache, R., Hejátko, J., & Helariutta, Y. (2015). Xylem development - from the cradle to the grave. *New Phytologist*, *207*(3), 519–535. https://doi.org/10.1111/nph.13383

Santos, R. B., Capanema, E. A., Balakshin, M. Y., Chang, H. M., & Jameel, H. (2012). Lignin structural variation in hardwood species. *Journal of Agricultural and Food Chemistry*, *60*(19), 4923–4930. https://doi.org/10.1021/jf301276a

Sarkanen, K., & Ludwig, C. (1971). Lignins: Occurrence, formation, structure and reactions. In *Journal of Polymer Science Part B: Polymer Letters*. New York: Wiley-Interscience. https://doi.org/10.1002/pol.1972.110100315

Sasaki, S., Baba, K., Nishida, T., Tsutsumi, Y., & Kondo, R. (2006). The cationic cell-wall-peroxidase having oxidation ability for polymeric substrate participates in the late stage of lignification of Populus alba L. *Plant Molecular Biology*, *62*(6), 797–807. https://doi.org/10.1007/s11103-006-9057-3

Sato, Y., Demura, T., Yamawaki, K., Inoue, Y., Sato, S., Sugiyama, M., & Fukuda, H. (2006). Isolation and characterization of a novel peroxidase gene ZPO-C whose expression and function are closely associated with lignification during tracheary element differentiation.

Plant and Cell Physiology, *47*(4), 493–503. https://doi.org/10.1093/pcp/pcj016

Scheller, H. V., & Ulvskov, P. (2010). Hemicelluloses. *Annual Review of Plant Biology*, *61*, 263–289. https://doi.org/10.1146/annurev-arplant-042809-112315

Schindelin, J., Arganda-Carreras, I., Frise, E., Kaynig, V., Longair, M., Pietzsch, T., … Cardona, A. (2012). Fiji: an open-source platform for biological-image analysis. *Nature Methods*, *9*(7), 676–682. https://doi.org/10.1038/nmeth.2019

Schmid, M., Davison, T. S., Henz, S. R., Pape, U. J., Demar, M., Vingron, M., … Lohmann, J. U. (2005). A gene expression map of Arabidopsis thaliana development. *Nature Genetics*, *37*(5), 501–506. https://doi.org/10.1038/ng1543

Schmittgen, T. D., & Livak, K. J. (2008). Analyzing real-time PCR data by the comparative C(T) method. *Nature Protocols*, *3*, 1101–1108.

Schubert, D. (2004). Silencing in Arabidopsis T-DNA Transformants: The Predominant Role of a Gene-Specific RNA Sensing Mechanism versus Position Effects. *The Plant Cell*, *16*, 2561–2572. https://doi.org/10.1105/tpc.104.024547

Schuetz, M., Benske, A., Smith, R. A., Watanabe, Y., Tobimatsu, Y., Ralph, J., … Samuels, A. L. (2014). Laccases Direct Lignification in the Discrete Secondary Cell Wall Domains of Protoxylem. *Plant Physiology*, *166*(2), 798–807. https://doi.org/10.1104/pp.114.245597

Schuetz, Mathias, Smith, R., & Ellis, B. (2013). Xylem tissue specification, patterning, and differentiation mechanisms. *Journal of Experimental Botany*, *64*(1), 11–31. Retrieved from http://dx.doi.org/10.1093/jxb/ers287

Sederoff, R. R., MacKay, J. J., Ralph, J., & Hatfield, R. D. (1999). Unexpected variation in lignin. *Current Opinion in Plant Biology*, *2*(2), 145–152. https://doi.org/10.1016/S1369-5266(99)80029-6

Shaner, N. C., Campbell, R. E., Steinbach, P. A., Giepmans, B. N. G., Palmer, A. E., & Tsien, R. Y. (2004). Improved monomeric red, orange and yellow fluorescent proteins derived from Discosoma sp. red fluorescent protein. *Nature Biotechnology*, *22*(12), 1567–1572. https://doi.org/10.1038/nbt1037

Shigeto, J., Itoh, Y., Hirao, S., Ohira, K., Fujita, K., & Tsutsumi, Y. (2015). Simultaneously disrupting AtPrx2, AtPrx25 and AtPrx71 alters lignin content and structure in Arabidopsis

stem. *Journal of Integrative Plant Biology*, *57*(4), 349–356. https://doi.org/10.1111/jipb.12334

Shigeto, J., Kiyonaga, Y., Fujita, K., Kondo, R., & Tsutsumi, Y. (2013). Putative cationic cell-wall-bound peroxidase homologues in arabidopsis, AtPrx2, AtPrx25, and AtPrx71, are involved in lignification. *Journal of Agricultural and Food Chemistry*, *61*(16), 3781–3788. https://doi.org/10.1021/jf400426g

Shigeto, J., Nagano, M., Fujita, K., & Tsutsumi, Y. (2014). Catalytic profile of Arabidopsis peroxidases, AtPrx-2, 25 and 71, contributing to stem lignification. *PLoS ONE*, *9*(8). https://doi.org/10.1371/journal.pone.0105332

Shigeto, J., & Tsutsumi, Y. (2016). Diverse functions and reactions of class III peroxidases. *New Phytologist*, *209*(4), 1395–1402. https://doi.org/10.1111/nph.13738

Shukry, N., Fadel, S. M., Agblevor, F. A., & El-Kalyoubi, S. F. (2008). Some physical properties of acetosolv lignins from bagasse. *Journal of Applied Polymer Science*, *109*(1), 434–444. https://doi.org/10.1002/app.28059

Singh, H., Dixit, S., Verma, P. C., & Singh, P. K. (2013). Differential peroxidase activities in three different crops upon insect feeding. *Plant Signaling and Behavior*, *8*(9), e25615. https://doi.org/10.4161/psb.25615

Sinlapadech, T., Stout, J., Ruegger, M. O., Deak, M., & Chapple, C. (2007). The hyper-fluorescent trichome phenotype of the brt1 mutant of Arabidopsis is the result of a defect in a sinapic acid:UDPG glucosyltransferase. *The Plant Journal*, *49*(4), 655–668. https://doi.org/10.1111/j.1365-313X.2006.02984.x

Smith, R. A., Schuetz, M., Karlen, S. D., Bird, D., Tokunaga, N., Sato, Y., … Samuels, A. L. (2017). Defining the Diverse Cell Populations Contributing to Lignification in Arabidopsis Stems. *Plant Physiology*, *174*(2), 1028–1036. https://doi.org/10.1104/pp.17.00434

Smith, R. A., Schuetz, M., Roach, M., Mansfield, S. D., Ellis, B., & Samuels, L. (2013). Neighboring Parenchyma Cells Contribute to Arabidopsis Xylem Lignification, while Lignification of Interfascicular Fibers Is Cell Autonomous. *The Plant Cell*, *25*(10), 3988–3999. https://doi.org/10.1105/tpc.113.117176

Šola, K., Gilchrist, E. J., Ropartz, D., Wang, L., Feussner, I., Mansfield, S. D., … Haughn, G. W.

(2019). RUBY, a Putative Galactose Oxidase, Influences Pectin Properties and Promotes Cell-To-Cell Adhesion in the Seed Coat Epidermis of Arabidopsis. *The Plant Cell*, *31*, 809–831. https://doi.org/10.1105/tpc.18.00954

Somerville, C. (2006). Cellulose Synthesis in Higher Plants. *Annual Review of Cell and Developmental Biology*, *22*, 53–78. https://doi.org/10.1146/annurev.cellbio.22.022206.160206

Spicer, R. (2014). Symplasmic networks in secondary vascular tissues: Parenchyma distribution and activity supporting long-distance transport. *Journal of Experimental Botany*, *65*(7), 1829–1848. https://doi.org/10.1093/jxb/ert459

Sterjiades, R., Dean, J. F. D., & Eriksson, K.-E. L. (1992). Laccase from Sycamore Maple (Acer pseudoplatanus) Polymerizes Monolignols. *Plant Physiology*, *99*(3), 1162–1168. https://doi.org/10.1104/pp.99.3.1162

Sterjiades, R., Dean, J. F. D., Gamble, G., Himmelsbach, D. S., & Eriksson, K. E. L. (1993). Extracellular laccases and peroxidases from sycamore maple (Acer pseudoplatanus) cell-suspension cultures: Reactions with monolignols and lignin model compounds. *Planta*, *190*(1), 75–87. https://doi.org/10.1007/BF00195678

Suh, M., Samuels, A., & Jetter, R. (2005). Cuticular lipid composition, surface structure, and gene expression in Arabidopsis stem epidermis. *Plant Physiology*, *139*, 1649–1665. https://doi.org/10.1104/pp.105.070805.1

Sundell, D., Street, N. R., Kumar, M., Mellerowicz, E. J., Kucukoglu, M., Johnsson, C., … Hvidsten, T. R. (2017). AspWood: High-Spatial-Resolution Transcriptome Profiles Reveal Uncharacterized Modularity of Wood Formation in *Populus tremula*. *The Plant Cell*, *29*(7), 1585–1604. https://doi.org/10.1105/tpc.17.00153

Survila, M., Davidsson, P. R., Pennanen, V., Kariola, T., Broberg, M., Sipari, N., … Palva, E. T. (2016). Peroxidase-Generated Apoplastic ROS Impair Cuticle Integrity and Contribute to DAMP-Elicited Defenses. *Frontiers in Plant Science*, *7*(1945). https://doi.org/10.3389/fpls.2016.01945

Syrjänen, K., & Brunow, G. (2000). Regioselectivity in lignin biosynthesis. The influence of dimerization and cross-coupling. *Journal of the Chemical Society, Perkin Transactions 1*, *2*,

183–187. https://doi.org/10.1039/a907919j

Szychowski, K. A., Rybczyńska-Tkaczyk, K. K., Leja, M. L., Wojtowicz, A. K., & Gmiński, J. (2016). Tetrabromobisphenol A (TBBPA)-stimulated reactive oxygen species (ROS) production in cell-free model using the 2',7'-dichlorodihydrofluorescein diacetate (H2DCFDA) assay—limitations of method. *Environmental Science and Pollution Research*, *23*(12), 12246–12252.

Takenaka, Y., Watanabe, Y., Schuetz, M., Unda, F., Hill, J. L., Phookaew, P., … Demura, T. (2018). Patterned deposition of xylan and lignin is independent from the secondary wall cellulose of Arabidopsis xylem vessels. *The Plant Cell*, *30*, 2663–2676. https://doi.org/10.1105/tpc.18.00292

Taylor, N. G., Scheible, W.-R., Cutler, S., Somerville, C. R., & Turner, S. R. (1999). The irregular xylem3 Locus of Arabidopsis Encodes a Cellulose Synthase Required for Secondary Cell Wall Synthesis. *The Plant Cell*, *11*(5), 769–780. https://doi.org/10.2307/3870813

Terashima, N., & Fukushima, K. (1988). Heterogeneity in formation of lignin-XI: An autoradiographic study of the heterogeneous formation and structure of pine lignin. *Wood Science and Technology*, *22*(3), 259–270. https://doi.org/10.1007/BF00386021

Terashima, N., Yoshida, M., Hafrén, J., Fukushima, K., & Westermark, U. (2012). Proposed supramolecular structure of lignin in softwood tracheid compound middle lamella regions. *Holzforschung*, *66*(8), 907–915. https://doi.org/10.1515/hf-2012-0021

Terrett, O. M., & Dupree, P. (2019). Covalent interactions between lignin and hemicelluloses in plant secondary cell walls. *Current Opinion in Biotechnology*, *56*, 97–104. https://doi.org/10.1016/j.copbio.2018.10.010

Thieme, C. J., Rojas-Triana, M., Stecyk, E., Schudoma, C., Zhang, W., Yang, L., … Kragler, F. (2015). Endogenous Arabidopsis messenger RNAs transported to distant tissues. *Nature Plants*, *15025*. https://doi.org/10.1038/nplants.2015.25

Tobimatsu, Y., & Schuetz, M. (2019). Lignin polymerization: how do plants manage the chemistry so well? *Current Opinion in Biotechnology*, *56*, 75–81. https://doi.org/10.1016/j.copbio.2018.10.001

Tognolli, M., Penel, C., Greppin, H., & Simon, P. (2002). Analysis and expression of the class III

peroxidase large gene family in Arabidopsis thaliana. *Gene*, *288*(1–2), 129–138. https://doi.org/10.1016/S0378-1119(02)00465-1

Torres, M. A., & Dangl, J. L. (2005). Functions of the respiratory burst oxidase in biotic interactions, abiotic stress and development. *Current Opinion in Plant Biology*, *8*(4), 397–403. https://doi.org/10.1016/j.pbi.2005.05.014

Tsai, A. Y.-L., Kunieda, T., Rogalski, J., Foster, L. J., Ellis, B. E., & Haughn, G. W. (2017). Identification and Characterization of Arabidopsis Seed Coat Mucilage Proteins. *Plant Physiology*, *173*(1), 1053–1074. https://doi.org/10.1104/pp.16.01600

Turlapati, P. V, Kim, K.-W., Davin, L. B., & Lewis, N. G. (2011). The laccase multigene family in Arabidopsis thaliana: towards addressing the mystery of their gene function(s). *Planta*, *233*(3), 439–470. https://doi.org/10.1007/s00425-010-1298-3

Ursache, R., Andersen, T. G., Marhavý, P., & Geldner, N. (2018). A protocol for combining fluorescent proteins with histological stains for diverse cell wall components. *The Plant Journal*, *93*(2), 399–412. https://doi.org/10.1111/tpj.13784

Valério, L., De Meyer, M., Penel, C., & Dunand, C. (2004). Expression analysis of the Arabidopsis peroxidase multigenic family. *Phytochemistry*, *65*(10), 1331–1342. https://doi.org/10.1016/j.phytochem.2004.04.017

van de Meene, A. M. L., Doblin, M. S., & Bacic, A. (2017). The plant secretory pathway seen through the lens of the cell wall. *Protoplasma*, *254*(1), 75–94. https://doi.org/10.1007/s00709-016-0952-4

Vanholme, R., Demedts, B., Morreel, K., Ralph, J., & Boerjan, W. (2010). Lignin Biosynthesis and Structure. *Plant Physiology*, *153*(3), 895–905. https://doi.org/10.1104/pp.110.155119

Vazquez-Cooz, I., & Meyer, R. W. (2002). A differential staining method to identify lignified and unlignified tissues. *Biotechnic & Histochemistry*, *77*, 277–282. https://doi.org/10.1080/bih.77.5-6.277.282

Veljovic-Jovanovic, S., Noctor, G., & Foyer, C. H. (2002). Are leaf hydrogen peroxide concentrations commonly overestimated? The potential influence of artefactual interference by tissue phenolics and ascorbate. *Plant Physiology and Biochemistry*, *40*(6–8), 501–507. https://doi.org/10.1016/S0981-9428(02)01417-1

Verhertbruggen, Y., Marcus, S. E., Haeger, A., Ordaz-Ortiz, J. J., & Knox, J. P. (2009). An extended set of monoclonal antibodies to pectic homogalacturonan. *Carbohydrate Research*, *344*(14), 1858–1862. https://doi.org/10.1016/j.carres.2008.11.010

Voxeur, A., Wang, Y., & Sibout, R. (2015). Lignification: different mechanisms for a versatile polymer. *Current Opinion in Plant Biology*, *23*, 83–90. https://doi.org/https://doi.org/10.1016/j.pbi.2014.11.006

Vukašinović, N., Oda, Y., Pejchar, P., Synek, L., Pečenková, T., Rawat, A., … Žárský, V. (2017). Microtubule-dependent targeting of the exocyst complex is necessary for xylem development in Arabidopsis. *New Phytologist*, *213*(3), 1052–1067. https://doi.org/10.1111/nph.14267

Waese, J., Fan, J., Pasha, A., Yu, H., Fucile, G., Shi, R., … Provart, N. J. (2017). ePlant: Visualizing and Exploring Multiple Levels of Data for Hypothesis Generation in Plant Biology. *The Plant Cell*, *29*, 1086–1821. https://doi.org/10.1105/tpc.17.00073

Walz, C., Juenger, M., Schad, M., & Kehr, J. (2002). Evidence for the presence and activity of a complete antioxidant defence system in mature sieve tubes. *The Plant Journal*, *31*(2), 189–197. https://doi.org/10.1046/j.1365-313X.2002.01348.x

Wang, C. Y., Zhang, S., Yu, Y., Luo, Y. C., Liu, Q., Ju, C., … Chen, Y. Q. (2014). MiR397b regulates both lignin content and seed number in Arabidopsis via modulating a laccase involved in lignin biosynthesis. *Plant Biotechnology Journal*, *12*(8), 1132–1142. https://doi.org/10.1111/pbi.12222

Wang, J., Feng, J., Jia, W., Chang, S., Li, S., & Li, Y. (2015). Lignin engineering through laccase modification: A promising field for energy plant improvement. *Biotechnology for Biofuels*, *8*(145). https://doi.org/10.1186/s13068-015-0331-y

Wang, Y., Bouchabke-Coussa, O., Lebris, P., Antelme, S., Soulhat, C., Gineau, E., … Sibout, R. (2015). LACCASE5 Is Required for Lignification of the Brachypodium distachyon Culm. *Plant Physiology*, *168*(1), 192–204. Retrieved from http://www.plantphysiol.org/content/168/1/192.abstract

Wang, Y., Chantreau, M., Sibout, R., & Hawkins, S. (2013). Plant cell wall lignification and monolignol metabolism. *Frontiers in Plant Science*, *4*(220).

https://doi.org/10.3389/fpls.2013.00220

Warinowski, T., Koutaniemi, S., Kärkönen, A., Sundberg, I., Toikka, M., Simola, L. K., … Teeri, T. H. (2016). Peroxidases Bound to the Growing Lignin Polymer Produce Natural Like Extracellular Lignin in a Cell Culture of Norway Spruce. *Frontiers in Plant Science*, *7*(1523). https://doi.org/10.3389/fpls.2016.01523

Wei, D., Houtman, C. J., Kapich, A. N., Hunt, C. G., Cullen, D., & Hammel, K. E. (2010). Laccase and its role in production of extracellular reactive oxygen species during wood decay by the brown rot basidiomycete Postia placenta. *Applied and Environmental Microbiology*, *76*(7), 2091–2097. https://doi.org/10.1128/AEM.02929-09

Welinder, K. G., Justesen, A. F., Kjærsgård, I. V. H., Jensen, R. B., Rasmussen, S. K., Jespersen, H. M., & Duroux, L. (2002). Structural diversity and transcription of class III peroxidases from Arabidopsis thaliana. *European Journal of Biochemistry*, *269*(24), 6063–6081. https://doi.org/10.1046/j.1432-1033.2002.03311.x

Weng, J. K., & Chapple, C. (2010). The origin and evolution of lignin biosynthesis. *New Phytologist*, *187*(2), 273–285. https://doi.org/10.1111/j.1469-8137.2010.03327.x

Westermark, U. (1982). Calcium promoted phenolic coupling by superoxide radical -a possible lignification reaction in wood. *Wood Science and Technology*, *16*(1), 71–78. https://doi.org/10.1007/BF00351376

Wi, S. G., Singh, A. P., Lee, K. H., & Kim, Y. S. (2005). The pattern of distribution of pectin, peroxidase and lignin in the middle lamella of secondary xylem fibres in alfalfa (Medicago sativa). *Annals of Botany*, *95*(5), 863–868. https://doi.org/10.1093/aob/mci092

Wightman, R., & Turner, S. R. (2008). The roles of the cytoskeleton during cellulose deposition at the secondary cell wall. *The Plant Journal*, *54*(5), 794–805. https://doi.org/10.1111/j.1365-313X.2008.03444.x

Willats, W. G. T., Mccartney, L., Mackie, W., & Knox, J. P. (2001). Pectin: Cell biology and prospects for functional analysis. *Plant Molecular Biology*, *47*, 9–27. https://doi.org/10.1023/A:1010662911148

Winterbourn, C. C. (2014). The challenges of using fluorescent probes to detect and quantify specific reactive oxygen species in living cells. *Biochimica et Biophysica Acta - General*

Subjects, *1840*(2), 730–738. https://doi.org/10.1016/j.bbagen.2013.05.004

Xia, Y., Suzuki, H., Borevitz, J., Blount, J., Guo, Z., Patel, K., … Lamb, C. (2004). An extracellular aspartic protease functions in Arabidopsis disease resistance signaling. *EMBO Journal*, *23*(4), 980–988. https://doi.org/10.1038/sj.emboj.7600086

Xiong, J., Yang, Y., Fu, G., & Tao, L. (2015). Novel roles of hydrogen peroxide (H2O2) in regulating pectin synthesis and demethylesterification in the cell wall of rice (Oryza sativa) root tips. *New Phytologist*, *206*(1), 118–126. https://doi.org/10.1111/nph.13285

Yamaguchi, M., Goue, N., Igarashi, H., Ohtani, M., Nakano, Y., Mortimer, J. C., … Demura, T. (2010). VASCULAR-RELATED NAC-DOMAIN6 and VASCULAR-RELATED NAC-DOMAIN7 Effectively Induce Transdifferentiation into Xylem Vessel Elements under Control of an Induction System. *Plant Physiology*, *153*(3), 906–914. https://doi.org/10.1104/pp.110.154013

Yamaguchi, M., Mitsuda, N., Ohtani, M., Ohme-Takagi, M., Kato, K., & Demura, T. (2011). VASCULAR-RELATED NAC-DOMAIN 7 directly regulates the expression of a broad range of genes for xylem vessel formation. *The Plant Journal*, *66*(4), 579–590. https://doi.org/10.1111/j.1365-313X.2011.04514.x

Ye, Z.-H. (2002). Vascular tissue differentiation and pattern formation in plants. *Annual Review of Plant Biology*, *53*(1), 183–202. https://doi.org/10.1146/annurev.arplant.53.100301.135245

Zamil, M. S., & Geitmann, A. (2017). The middle lamella—more than a glue. *Physical Biology*, *14*(1), 15004. https://doi.org/10.1088/1478-3975/aa5ba5

Zeng, J., Dong, Z., Wu, H., Tian, Z., & Zhao, Z. (2017). Redox regulation of plant stem cell fate. *The EMBO Journal*, *36*, 2844–2855. https://doi.org/10.15252/embj.201695955

Zhang, Y., Liu, C. M., Emons, A. M. C., & Ketelaar, T. (2010). The plant exocyst. *Journal of Integrative Plant Biology*, *52*(2), 138–146. https://doi.org/10.1111/j.1744-7909.2010.00929.x

Zhao, Q. (2016). Lignification: Flexibility, Biosynthesis and Regulation. *Trends in Plant Science*, *21*(8), 713–721. https://doi.org/10.1016/j.tplants.2016.04.006

Zhao, Q., Nakashima, J., Chen, F., Yin, Y., Fu, C., Yun, J., … Dixon, R. A. (2013). LACCASE Is

Necessary and Nonredundant with PEROXIDASE for Lignin Polymerization during Vascular Development in Arabidopsis. *The Plant Cell*, *25*(10), 3976–3987. https://doi.org/10.1105/tpc.113.117770

Zhong, R., Burk, D. H., & Ye, Z.-H. (2001). Fibers. A Model for Studying Cell Differentiation, Cell Elongation, and Cell Wall Biosynthesis. *Plant Physiology*, *126*(2), 477–479. Retrieved from http://www.plantphysiol.org/content/126/2/477.abstract

Zhong, R., Demura, T., & Ye, Z.-H. (2006). SND1, a NAC Domain Transcription Factor, Is a Key Regulator of Secondary Wall Synthesis in Fibers of Arabidopsis. *The Plant Cell*, *18*(11), 3158–2170. https://doi.org/10.1105/tpc.106.047399

Zhong, R., Ripperger, A., & Ye, Z.-H. (2000). Ectopic Deposition of Lignin in the Pith of Stems of Two Arabidopsis Mutants. *Plant Physiology*, *123*, 59–69. https://doi.org/10.1104/pp.123.1.59

Zhong, R., Taylor, J. J., & Ye, Z. H. (1997). Disruption of interfascicular fiber differentiation in an Arabidopsis mutant. *The Plant Cell*, *9*(12), 2159–2170. https://doi.org/10.1105/tpc.9.12.2159

Zhong, R., & Ye, Z.-H. (2015). Secondary cell walls: Biosynthesis, patterned deposition and transcriptional regulation. *Plant and Cell Physiology*, *56*(2), 195–214. https://doi.org/10.1093/pcp/pcu140

Appendix

Localization-guided phenotyping of *prx64* null mutants

Despite having the highest expression of any PRX in stem tissues, little is known about the functional role of AtPRX64 in stem lignification. Previous unpublished work by Zhao (2016) noted that *prx64* T-DNA insertion mutants had no observable changes to stem lignin content or composition (Zhao, 2016). Given the localization of AtPRX64-mCherry to the cell corners of interfascicular fibers (Chou et al., 2018), I used confocal microscopy techniques to test whether there was a specific defect in morphology or lignification of cell corners in the fibers of a *AtPRX64* T-DNA insertion line.

Homozygous *prx64* null (SALK_203548) T-DNA insertion seeds were obtained from Dr. Zhao Qiao (Tsinghua University, China). T-DNA mapping indicated a putative insertion in the fourth exon, so I performed RT-qPCR to assess whether the T-DNA insertion resulted in reduced expression. Expression data showed *prx64* null plants had negligible *AtPRX64* expression compared with the wild-type Col-0 background, confirming they were knockout lines. *Prx64* null growth and development appeared similar to Col-0 and showed no significant defects in root length after one week or rosette size after four weeks of growth (data not shown).

To test whether loss of *AtPRX64* resulted in alterations to stem lignin, I used UV autofluorescence to study lignin at the base of 17cm-tall stems. Qualitatively, *prx64* null and Col-0 stems had similar lignin deposition in stems. I quantified the intensity of lignin autofluorescence specifically in cell corners and found no significant differences in cell corner autofluorescence of fibers between Col-0 and *prx64* null plants. Therefore, loss of *AtPRX64* did not significantly impact lignification in the cell corners or middle lamella of stem fibers. As the localizations of tagged AtLAC10 and AtPRX71 overlapped with tagged AtPRX64 in the cell corners (Figure 3.6), the lack of a phenotype may reflect redundant functions of one or more of these enzymes. However, this study only looked at UV autofluorescence in stems, so future quantitative analysis on lignin content and structure could confirm the lack of a lignin phenotype.

Previous miRNA-silencing of *AtPRX64* led to impaired development of the Casparian strip in roots (Lee et al. 2013). To evaluate whether *prx64* null plants have abnormal Casparian strip development, I used a propidium iodide (PI) uptake assay (Alassimone et al., 2010). The Casparian

strip forms an apoplastic barrier in roots and is thought to allow selective transfer of nutrients into the vascular tissues (Barberon, 2017). Unlike stem vascular tissues, the endodermal cell layer on which the Casparian strip is deposited does not develop a SCW but instead accumulates lignin and suberin within regions of the PCW (Naseer et al., 2012). Casparian strip integrity can be assessed using the fluorescent dye PI, as a functional Casparian strip will block diffusion of PI into the stele but a defective Casparian strip will be permeable to the dye (Alassimone et al., 2010). In Col-0 plants, PI was consistently restricted from the stele, signifying a functional Casparian strip. In contrast, *prx64* null plants showed diffusion of PI into the stele tissues, indicative of a non-functional Casparian strip. Therefore, *prx64* null plants had defective development of the Casparian strip in roots and showed a similar phenotype to miRNA-silenced plants (Lee et al. 2013). Therefore, these results confirm that AtPRX64 is required for formation of the Casparian strip, but its role in stem lignification is likely masked by the presence of redundant oxidative enzymes, such as AtPRX71 and/or AtLAC10.

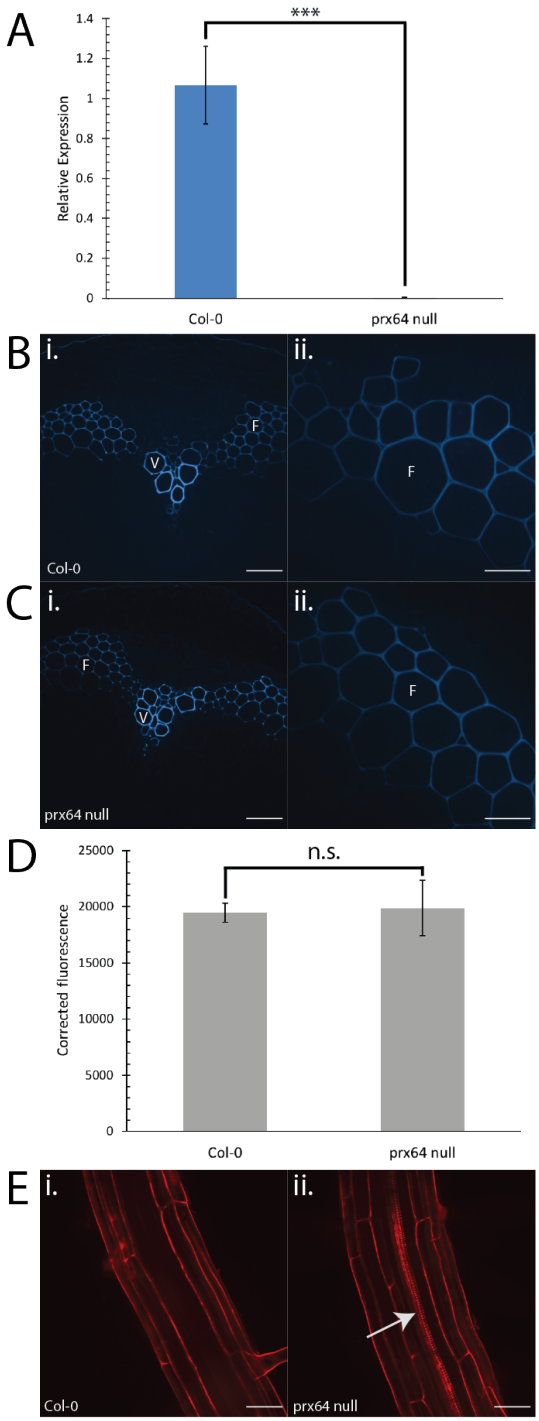

Appendix. AtPRX64 acts redundantly in stem lignification but not in Casparian strip lignification. A) RT-qPCR analysis shows AtPRX64 expression is significantly reduced relative to Col-0 at the base of 17cm-tall prx64 null stems. n=3 biological replicates/line; 2-way t-test ***p<0.001. Bars are SE. B-C) Representative images of UV lignin autofluoresence (blue). V=xylem vessel element; F=fiber. Scale bars are 50µm for i) and 20µm for ii). B) Base of 17cm-tall Col-0 stem at low (i) and high magnification (ii). C) Base of 17cm-tall prx64 null stem at low (i) and high magnification (ii). D) Quantification of corrected fluorescence of lignified cell corners of Col-0 and prx64 null stems. N=50 cell corners from 5 biological replicates; 2-way t-test, p=0.84; n.s.(not significant). Bars are SE. E) Casparian strip integrity was assessed using propidum iodide (PI; Alassimone et al., 2010). Col-0 roots have an intact Casparian strip and PI (red) is restricted from the stele (i) while prx64 null roots have a defective Casparian strip and PI diffuses into the stele (ii). Arrow indicates PI staining of vascular tissue in stele in prx64 null mutants. Scale bars are 50µm.